SEQUENCE-STRATIGRAPHIC CONTROLS ON SANDSTONE DIAGENESIS: AN EXAMPLE FROM THE WILLIAMS FORK FORMATION, PICEANCE BASIN, COLORADO

by

ADEL ABOKTEF

B.A., University of Tripoli, I989

M.S., University of Manchester, I998

A thesis submitted to the

Faculty of the Graduate School of the

University of Colorado in partial fulfillment

of the requirement for the degree of

Doctor of Philosophy

Department of Geological Sciences

2013

This thesis entitled:

Sequence-stratigraphic controls on sandstone diagenesis: an example from the Williams Fork Formation, Piceance Basin, Colorado

written by Adel Aboktef
has been approved for the Department of Geological Sciences

____
David A. Budd, Chair

____
Mary J. Kraus

____
G. Lang Farmer

August 15, 2013

The final copy of this thesis has been examined by the signatories, and we
Find that both the content and the form meet acceptable presentation standards
Of scholarly work in the above mentioned discipline.

Aboktef, Adel (Ph.D., Geological Sciences)

SEQUENCE-STRATIGRAPHIC CONTROLS ON SANDSTONE DIAGENESIS: AN EXAMPLE FROM THE WILLIAMS FORK FORMATION, PICEANCE BASIN, COLORADO

Thesis directed by Professor David A. Budd

ABSTRACT

This study documents the distribution of diagenetic alterations in Williams Fork fluvial sandstones, assess sequence stratigraphic controls on diagenetic features, and addresses diagenetic impacts on porosity. Petrographic point counts of 220 thin sections from six wells forms the database. The near absence of potassium feldspar and volcanic rock fragments in the lower Williams Fork interval and increasing plagioclase content upward represent changes in sediment provenance rather than stratigraphic variability in diagenesis. The lower Williams Fork sands are from sedimentary sources whereas middle and upper Williams Fork sands include input from magmatic arcs and basement uplifts.

Compaction, early and late cementation, dissolution, and replacement by calcite or clay minerals combined to alter Williams Fork sandstones. Infiltration of clays occurred prior to any burial. Chlorite, quartz, non-ferroan calcite, compaction and dissolution features, and kaolinite formed during eo-diagenesis at <70°C. More quartz, compaction and dissolution features, plus albite, illite, mixed-layer illite/smectite, ferroan calcite, and dolomite formed in the meso-diagenetic realm (>70°C). Four of these features show spatial variability with respect to systems tracts. Infiltrated clays are concentrated in

lowstand systems tracts (LST) and highstand systems tracts (HST) because accommodation space rose slow or fell during deposition of those sands, which led to prolonged sand body exposure on floodplain and ample opportunities for downward percolation of mud during flood events. Concentration of pseudomatrix (mud intraclasts) in HST and LST deposits resulted from floodplain erosion when base-level fell with decreasing accommodation space. Authigenic chlorite formed in the HST and transgressive systems tracts (TST) of the upper half of the Williams Fork Formation because volcanic clasts are abundant in that interval. Quartz overgrowths are more likely to exceed 7% in TST deposits for reasons that are unknown. High total clay content (infiltrated, grain coatings, pseudomatrix) does inhibit quartz overgrowths in all systems tracts.

Williams Fork sandstones form low-permeability tight-gas reservoirs. Primary porosity was almost entirely destroyed by compaction and cementation. Reservoir rock resulted from one of two pathways. Eogenetic authigenic chlorite and/or calcite inhibited quartz cementation, minimized compaction and protected some primary porosity. Alternately, dissolution of framework grains or cements created secondary porosity. The later pathway tends to be the more dominant.

Acknowledgements

I would like to express my sincere thanks to my adviser, Dr. David Budd for his support, encouragement and guidance during this work. Words are not enough to thank him for the advice, guidance, and countless revisions that were significant in completion of this thesis. This great experience goes way beyond student-professor relationship. I always felt that I'm so lucky to get his assistance and supervision.

I would like to thank all of my committee members: Dr. David Budd, Dr. G Lang Farmer, Mary J Kraus, Charles R Stern and Harihar Rajaram for their time and input. Dr. Farmer and Dr. Kraus comments and support shaped the final output of my thesis and are highly appreciated. Further thanks and acknowledgement goes to Dr. Gus Gustason and Steve Cumella for their involvement and valuable comments, time and data that they offered. I would like to thank Lesley Evans (Williams E&P) and John Hessenbruch (Oxy) for their advice and support by offering time, data, and technical support. I would like to thank Dr. El-ghali Mohamed for responding to my emails concerning sequence-stratigraphy and diagenesis technical issues and for taking part in thoughtful discussions concerning my research.

I would like to thank Paul Boni, Dan Mitchell and John Drexler for their friendship and great lab and technical support that they offered during this research. I would like to express my greatest gratitude and special thanks to Barbara Amaral, Joanne Brunetti and Carrie Simon for their help and support during my stay at CU.

Many thanks go to my classmates in the Geological Sciences Department at CU Boulder for their collaboration efforts and support throughout this research. I would, also, like to thank Patrick Boulas for his help in the XRD samples preparations and scanning. I would like to thank my friend Auwal Farouk for his support and help during this research.

I would like to thank my daughter Salsabel for her unconditional support and for giving me the joy of life. I would also like to thank my mother Khadija and my father Mohamed for their love, support, advice and encouragement. My thanks go also to my family members in Libya. Brother Ramzi, Abo-Hurira Mohamed (my nephew) and all my sisters and brothers for their support and encouragement.

CONTENTS

List of Tables

List of Figures

CHAPTER ONE: INTRODUCTION

BACKGROUND AND RESEARCH QUESTIONS

For decades geologists studying reservoir quality and heterogeneity of siliciclastic reservoir facies treated diagenesis separately from the sequence-stratigraphic context of the facies. Recently, researchers have begun to examine the link between the spatial and temporal distribution of diagenetic alteration and the sequence-stratigraphic framework of facies. For example, it has been demonstrated that the spatial and temporal distribution of some diagenetic alterations can be closely related to key sequence-stratigraphic surfaces (Figure 1.1) (Taylor et al., 1995; Morad et al., 2000, 2010; Ketzer et al., 2003a, 2003b; Al-Ramadan et al., 2005; El-ghali et al., 2006a, 2006b, 2009a, 2009b; Mansurbeg et al., 2008).

The diagenetic evolution of sandstones is controlled by a number of interrelated parameters, including composition of framework grains, pore-water chemistry, tectonic setting of the basin, and burial-thermal history of the succession (Figure 1.2) (Morad et al., 2000; Stonecipher, 2000). With the exception of burial-thermal history, all of these diagenetic controls also affect, or are affected by, the sequence-stratigraphic position of a unit, thus closely linking diagenesis and sequence stratigraphy.

The compositional variations of sandstone framework grains and pore-water chemistry are broadly influenced by changes in relative sea level, which occur due to eustatic sea-level changes and/or tectonic uplift/subsidence (Morad et al., 2000; El-gahli et al., 2006b, 2009b). Detrital compositional changes, meaning the type and proportion of extrabasinal and intrabasinal material, are controlled by the tectonic setting of the

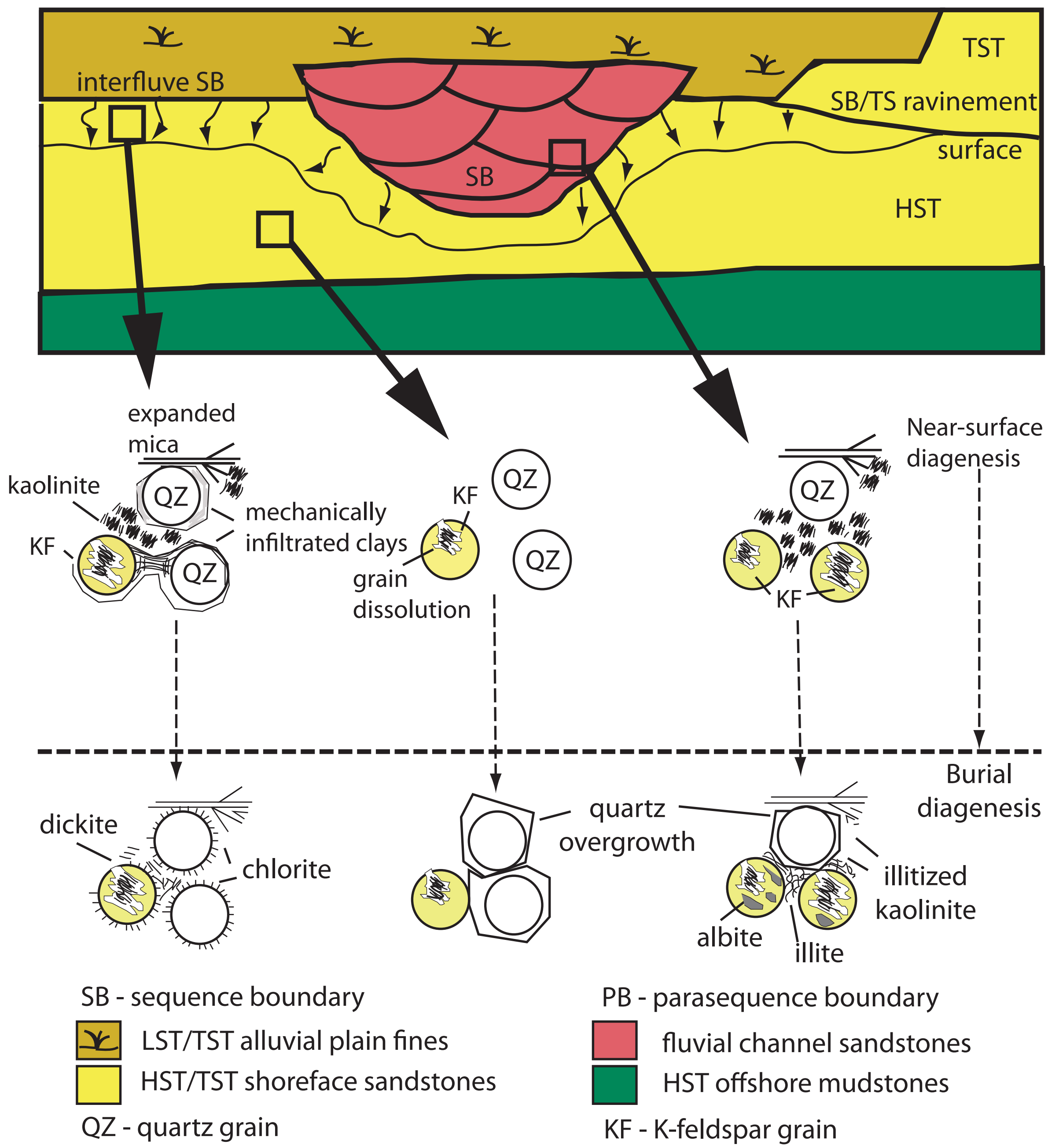

Figure 1.1A - Distribution and evolution of diagenetic alterations in sandstones below sequence boundaries and within incised valleys. Note that the zone with mechanically infiltrated clays is thin (or absent) below the ravinement surface. From Ketzer et al. (2002).

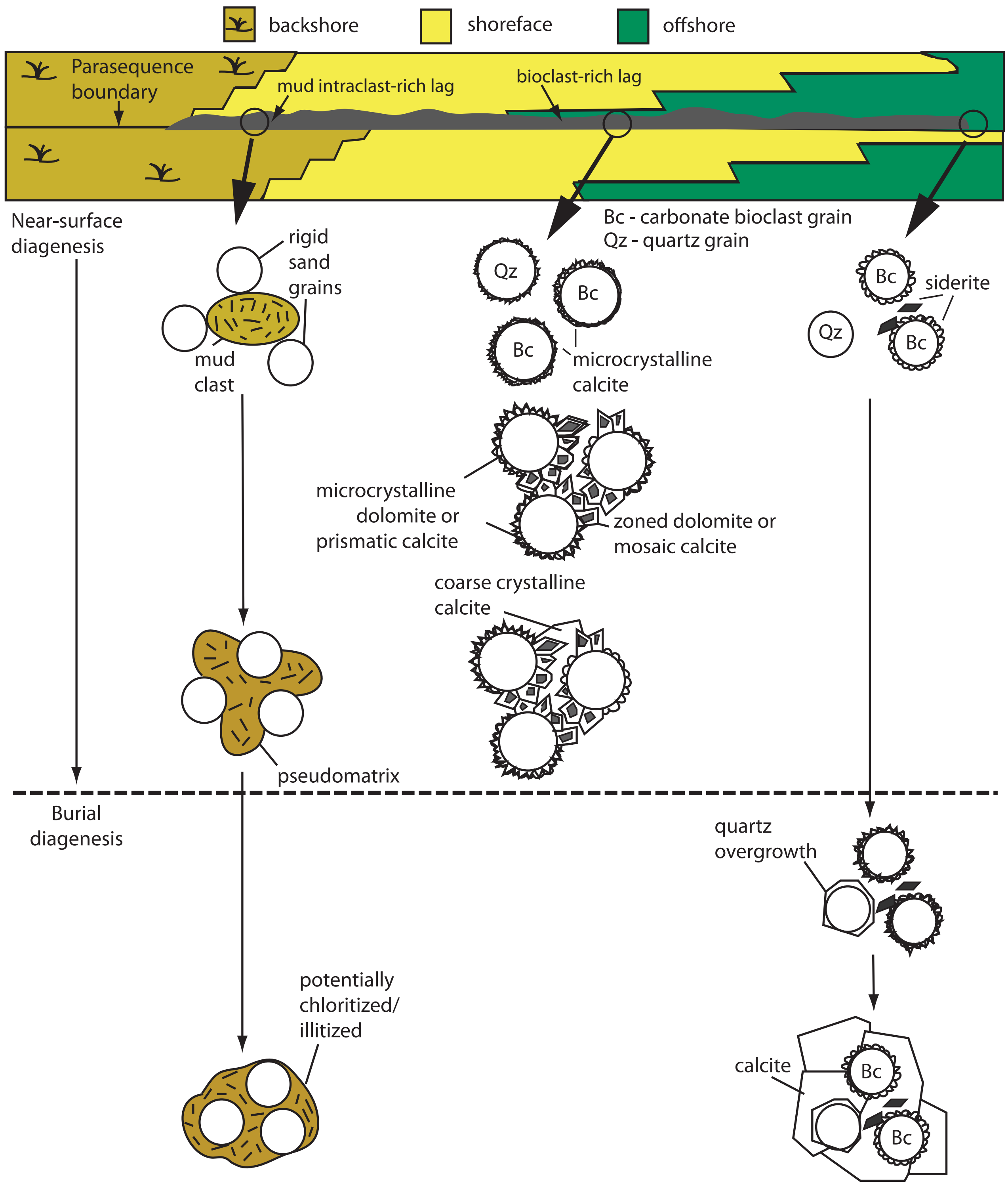

Figure 1.1B - Distribution of diagenetic alterations in lag deposits at parasequence boundaries in proximal, intermediate, and distal locations. From Ketzer et al. (2002).

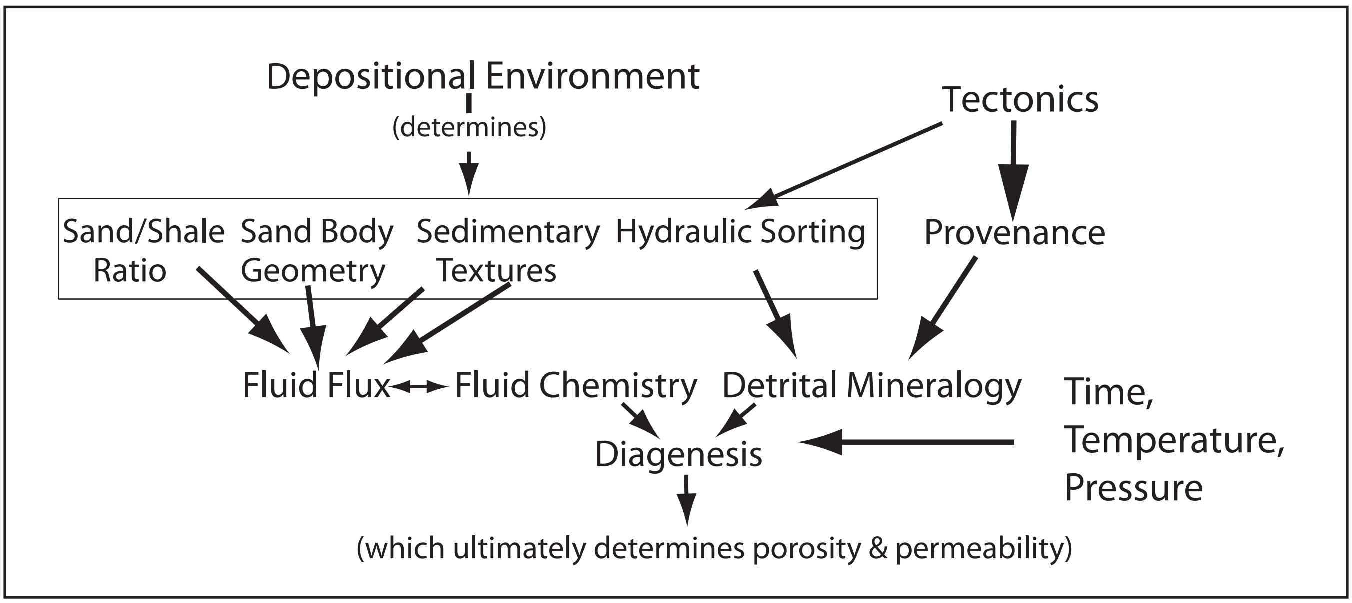

Figure 1.2 - Factors controlling sandstone diagenesis. From Stonecipher et al. (1984)

basin, changes in relative sea level, paleoclimatic conditions, and the sediment source (Amorosi, 1995; Zuffa et al., 1995; Ketzer et al., 2002, 2003b). Pore-water chemistry in many cases is a function of sea-level change and the consequent shifting of meteoric, marine, and brackish fluid compositions (Mckay et al., 1995; Morad et al., 2000). Regression may lead to subaerial exposure of at least part of the shelf and the concomitant flushing of shoreface and deltaic sediments by meteoric waters. Alternatively, transgression causes pore waters to be dominated by marine water and the mixing zone is shifted landward (Figure 1.3) (Morad et al., 2000). These changes in fluid chemistry promote various diagenetic alterations as well as reservoir-quality modifications (Morad et al., 2000; El-ghali et al., 2006b; El-ghali et al., 2009b; Mansurbeg et al., 2008).

Sequence-stratigraphic techniques, which are important for predicting both the spatial and temporal distribution of reservoirs, seals and source rocks in sedimentary basins, are based on relative-sea level changes and changing sediment supply (e.g., Posamentier and Allen, 1999). Facies-controlled porosity and permeability are subject to modification by diagenetic reactions and alterations at near-surface conditions and during progressive sediment burial. Thus, studying diagenesis and sequence stratigraphy as two linked subjects generates a better understanding of diagenetic alteration’s spatial and temporal distribution within sandstone-reservoir facies. This linkage would further enhance our ability to predict reservoir quality evolution in sedimentary basins (Taylor et al., 1995; Dutton and Willis, 1998; Morad et al., 2000; Ketzer et al., 2003a, 2003b; El-ghali et al., 2009a, 2009b).

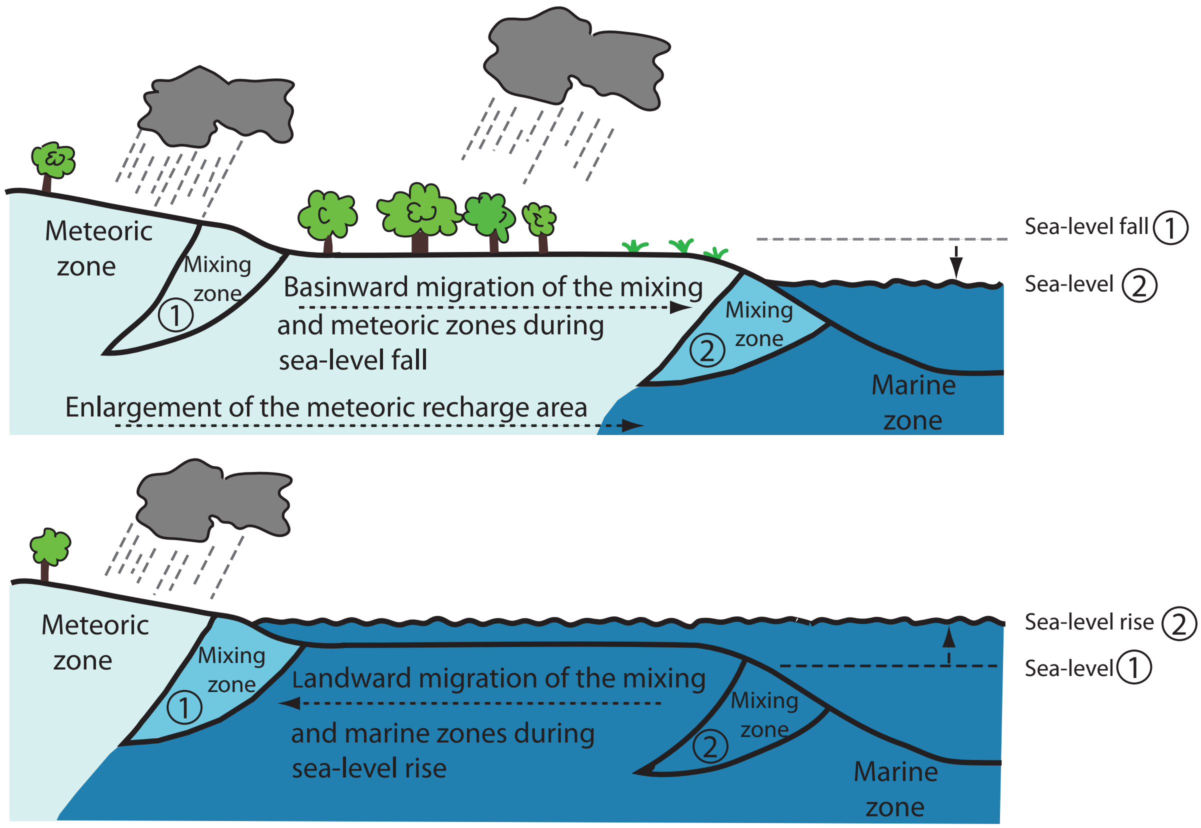

Figure 1.3 - Diagram illustrating how changes in the relative sea level modify the initial pore-water chemistry of near-surface deposits. A fall in relative sea level results in the invasion of meteoric waters and a basinward shift of the mixing zone. When relative sea level rises pore water is dominantly marine and the mixing zone is shifted landward. Modified after Morad et al. (2000) and Ketzer et al. (2003b).

Unraveling diagenetic alteration in a sequence-stratigraphic framework has gained significant interest in recent years, with applications in both carbonate and siliciclastic marine reservoirs (e.g., Read and Horbury, 1993; Tucker, 1993; Moss and Tucker, 1996; Al-Ramadan, et al., 2005; El-ghali et al., 2006a, 2006b; El-ghali et al. 2009a, 2009b; Morad et al., 2010). However, the relationship between diagenetic alterations and changes in relative sea level in continental siliciclastic rocks is more challenging because changes in relative sea level only have an indirect impact on the spatial and temporal distribution of fluvial facies (Blum and Tornqvist, 2000). The application of sequence-stratigraphic techniques to elucidate and predict the response of fluvial style to changes in relative sea level is thus less straightforward when compared with paralic and shallow-marine environments. However, changes of the fluvial style from braided to high-sinuosity meandering (i.e. architecture of fluvial deposits) has been suggested by Wright and Marriott (1993), Shanley and McCabe (1994), Posamentier and Allen (1999), and Blum and Tornqvist (2000) to occur as a consequence of changes in the depositional base level, as controlled by changes in the relative sea level (Figure 1.4). Morad et al. (2000) have built a general model (Figure 1.5) that illustrates what types of early diagenetic reactions might be expected in fluvial sandstones, but how these reactions might vary spatially or temporally between lowstand and highstand sandstones of the same unit has not been explored.

Published case studies documenting links between diagenetic alterations, fluvial depositional facies, and changes in relative sea level are limited. There is still a need to learn more about the direct and indirect relationship between the diagenesis in fluvial deposits and the sequence-stratigraphic framework of continental deposits. Using the

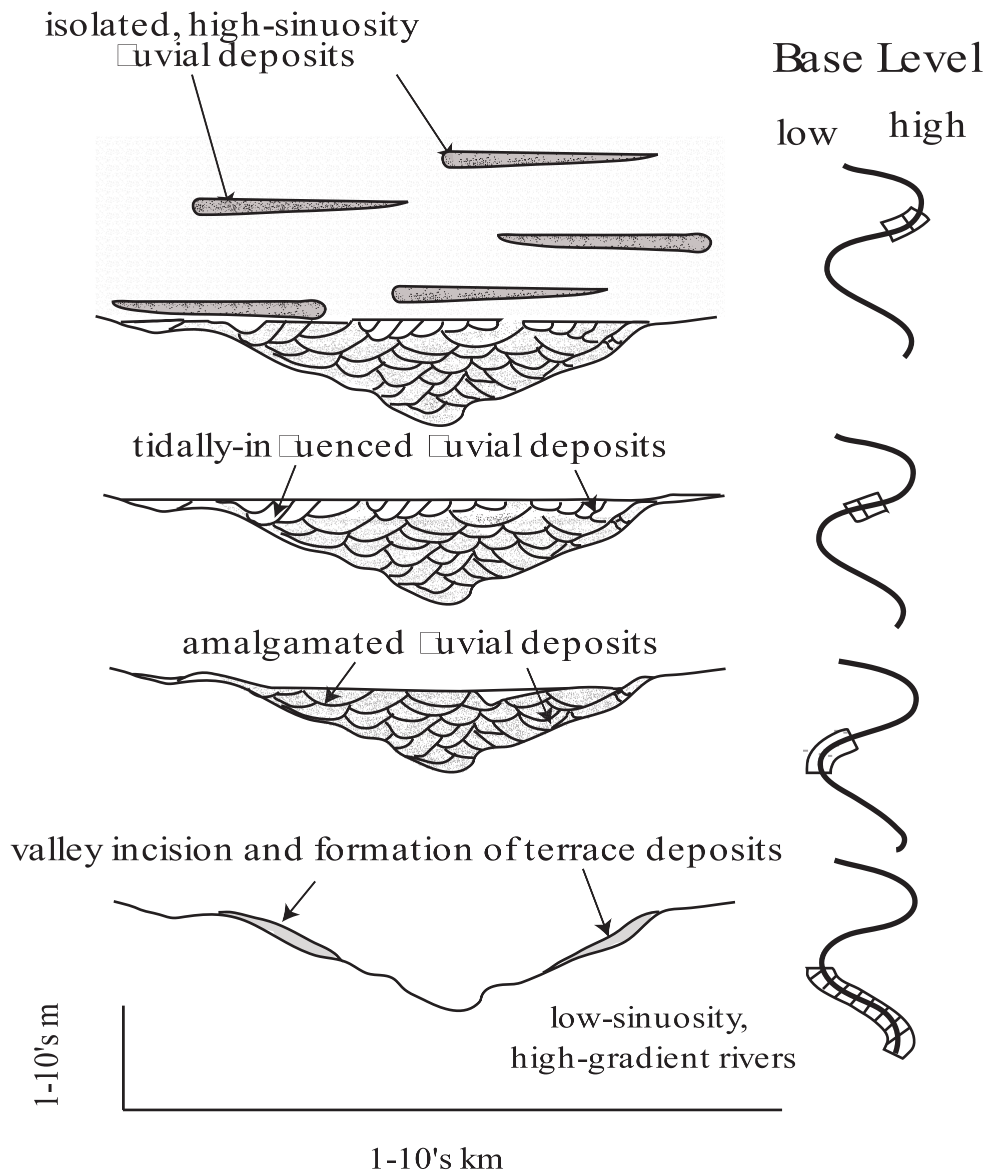

Figure 1.4 - Model from Shanley and McCabe (1994) for evolution of fluvial-coastal-marine strata of the Cretaceous Western Interior basin in response to base-level change. The concept of incision and sediment bypass during base-level fall is illustrated and common to many sequence-stratigraphic models. Valley filling follows, first with amalgamated fluvial deposits, then tidally influenced strata and finally fluvial deposits with a low sand to total thickness ratio. From Blum and Turnqvist (2000).

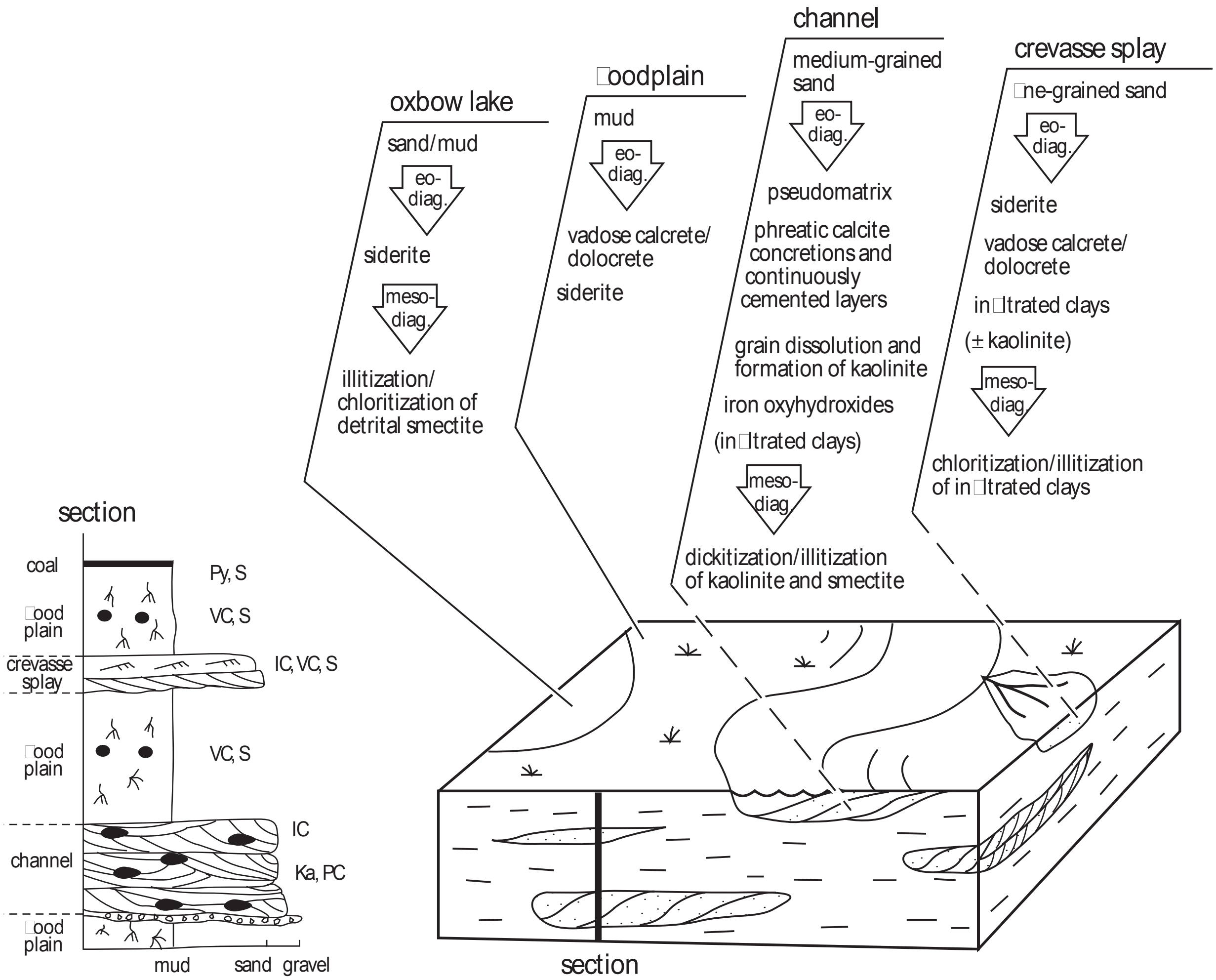

Figure 1.5 - Facies-related spatial distribution of eogenetic diagenetic products in a fluvial meandering depositional system and the influence of those eogenetic products on the mesogenetic alteration of the sediments. S = siderite, IC = infiltrated clays, VC = vadose calcite/dolomite concretions, PC = phreatic calcite concretions, Py = pyrite, and Ka = kaolinite. Modified from Morad et al. (2000).

Williams Fork Formation of the Mesaverde Group in the Piceance Basin as a case study, this research addresses the following question: Is the spatial and temporal distribution of diagenetic alterations in fluvial sandstones related to changes in accommodation potential (relative sea level), and hence predictable within a sequence-stratigraphic framework? Using the existing sequence-stratigraphic framework of the Williams Fork Formation (Patterson et al, 2003; Leibovitz, 2010; Foster, 2010), this research addresses the relationship between the diagenesis (both evolution and distribution of events) and the position and type of sandstone bodies in the Williams Fork Formation. In order to answer the main research question, this study investigates the spatial distribution of detrital and authigenic minerals, creates a detailed paragenetic sequence, identifies the process that is responsible for the recognized authigenic components, and discusses the linkages between depositional and post-depositional diagenetic alteration within a sequence-stratigraphic framework. The impact of the mineralogical (detrital and authigenic) composition on reservoir quality and heterogeneity is also investigated, as well as the timing of different diagenetic alterations.

The Williams Fork Formation was selected for this research because 1) it consists of several lowstand systems tracts (LST), transgressive systems tracts (TST), and highstand systems tracts (HST) (Patterson et al, 2003) and the sandstone diagenetic components can be compared based on their spatial and temporal distribution in the Williams Fork sequence-stratigraphic framework. 2) The Williams Fork Formation in the southern Piceance Basin has been drilled sufficiently and adequate core samples were available for this study (Table 1).

Well #	Well Name	Field	API #	Company / Organization	Core Coverage
1	Plateau Creek BT-202	Plateau Creek	Behind outcrop	CU Boulder	680 ft (207 m)
2	Cascade Creek 967-20-28	Grand Valley	05-045-10477	Oxy USA WTP LP	565 ft (172 m)
3	Puckett/Tosco, PA 424-34	Parachute	05-045-10927	Williams Production	430 ft (131 m)
4	Superior MWX 1	Rulison	05-045-06325	Williams Production	4180 ft (1274 m)
5	Last Dance 43C-3-792	Mamm Creek	05-045-11402	Bill Barrett Corporation	410 ft (125 m)
6	Cactus Valley 1 D111	Cactus Valley	05-045-06221	TRW Exploration & Production	180 ft (55 m)

Table 1. Cores used in the study

STUDY AREA

Data were acquired and analyzed from six cored wells that form a transect from west to east across the southern Piceance Basin (Figure 1.6). The cores come from the following fields or locations: Rulison Field, Parachute Field, Mamm Creek Field, Cactus Valley Field, Grand Valley Field, and Plateau Creek Canyon (a behind-outcrop cored well) (Figure 1.6, Table 1). The cores represent intervals from the lower, middle, and upper Williams Fork Formation. The selected cores are also from parts of the basin that have experienced different burial histories. The cores range in length from 410 to 565 ft (125 to 172 m) and average about 500 ft (152.4 m) in length, except for Cactus Valley #1 and the MWX #1 wells, whose core coverage are 180 ft (55 m) and 2620 ft (1136.5 m), respectively (Table 1).

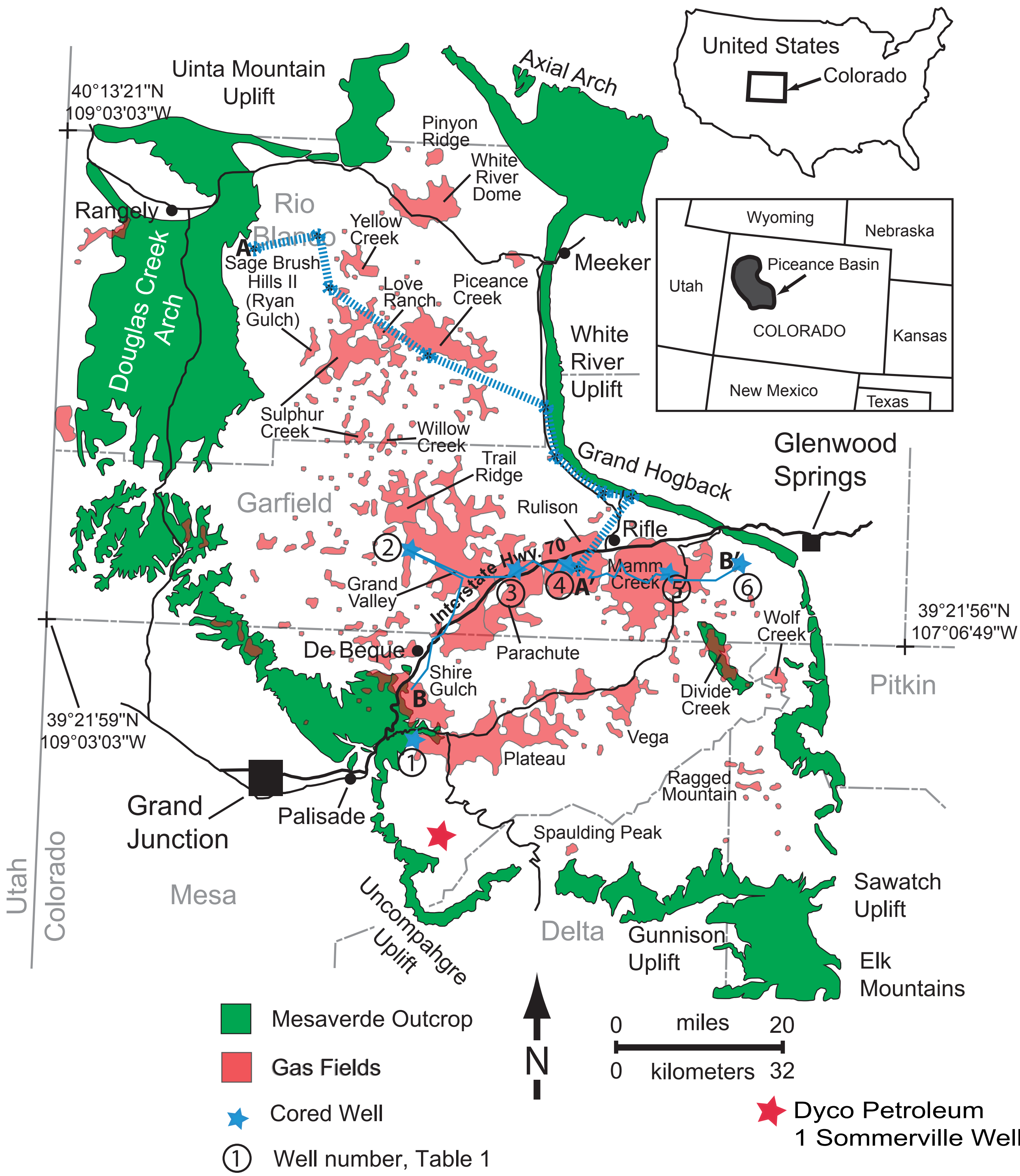

Figure 1.6 - Location map of the Piceance Basin. Mesaverde gas fields are shown in red and outcrops of the Mesaverde Group that occur on the margins of the basin are shown in green. The cored studied wells are shown in blue stars. The location of cross sections A-A' and B-B' (Figures 1-9, 1-13) are shown by blue lines. Modified from Johnson (1989), Tyler and McMurry (1995), Hoak and Klawitter (1997) and Pranter et al. (2009).

GEOLOGICAL SETTING

General Stratigraphy

During the Cretaceous, the Piceance Basin area occupied a part of the western foreland margin of the Western Interior Seaway, an epeiric seaway that covered the central part of North America and extended from the Gulf of Mexico to Canada (Johnson, 1989) (Figure 1.7). The Sevier orogenic belt to the west fed the basin with vast amounts of clastic sediments (Fouch et al., 1983). Several thousand feet of non-marine and shallow-marine sediments were eventually deposited. Initially, the shoreline had a generally north-south orientation, but it gradually shifted to a north-northeast to south-southeast direction (Cole and Cumella, 2003; Hettinger and Kirschbaum, 2002).

The Upper Cretaceous (late Campanian) Mesaverde Group is comprised of the Iles and Williams Fork formations (Figures 1.8, 1.9). The Iles Formation corresponds to the lower part of the Mesaverde Group and includes three regressive marine sandstone cycles. In ascending order these are the Corcoran, Cozzette and Rollins sandstone members. These three members are separated by the marine Mancos Shale and were deposited in inner shelf, deltaic, shoreface, estuarine, and lower coastal-plain settings. These sandstone cycles are laterally continuous and can be correlated across much of the southern and eastern Piceance Basin. Repeated transgressions and regressions of the Western Interior Seaway are recorded within the Iles Formation (Hettinger and Kirschbaum, 2002, 2003).

The middle to upper Campanian Williams Fork Formation conformably overlies the Iles Formation and forms the upper part of the Mesaverde Group, first named by Holmes (1877) in the Four Corners area of the San Juan Basin (Tyler and McMurry,

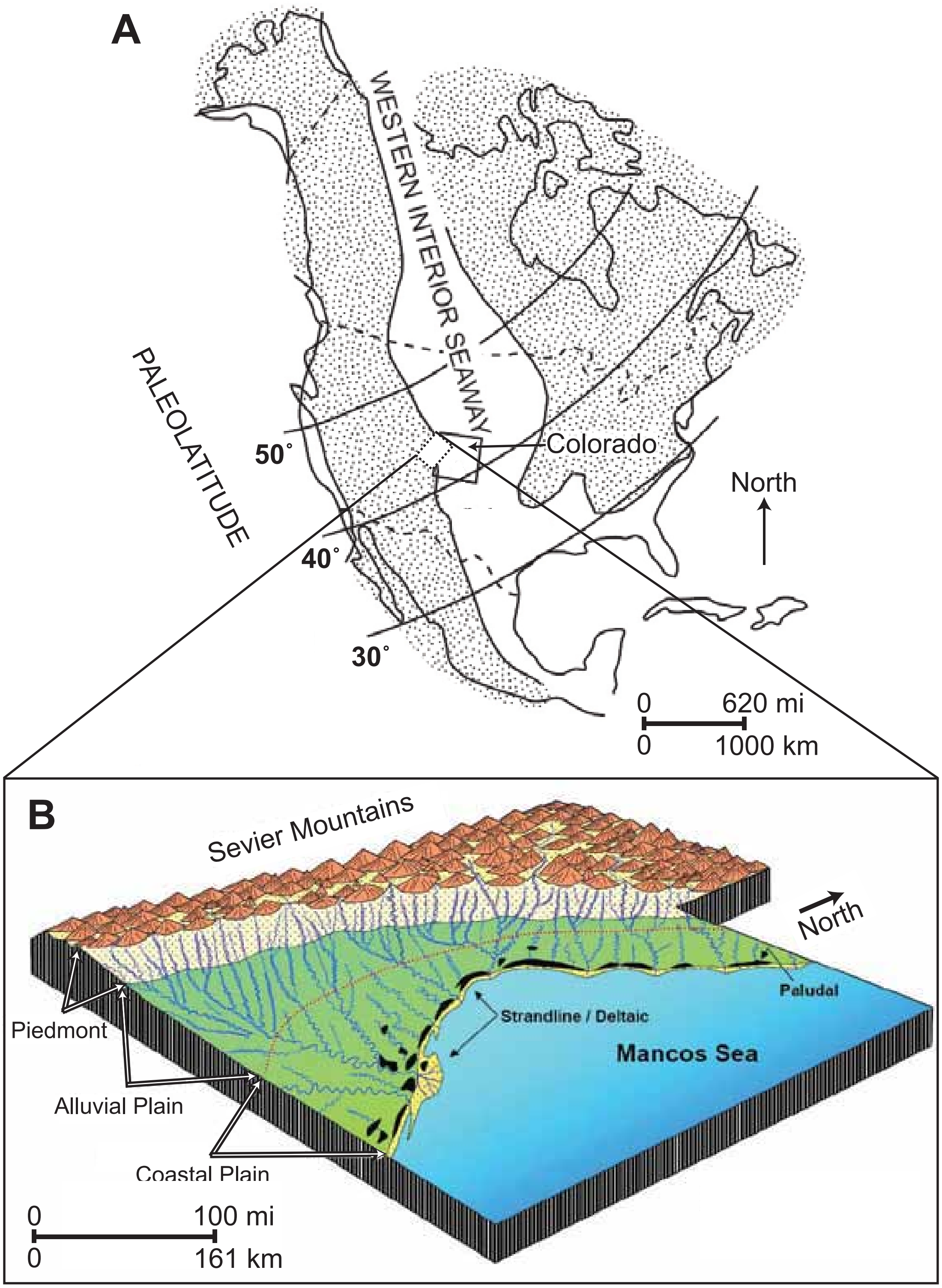

Figure 1.7 - Late Cretaceous paleogeography. (A) Extent of the Western Interior Seaway during the Late Campanian (modified from Johnson and Finn, 1986). (B) Idealized depiction of the Late Cretaceous depositional environments in Utah and western Colorado (modified from Ryer and McPhillips, 1983, and Cole and Cumella, 2003).

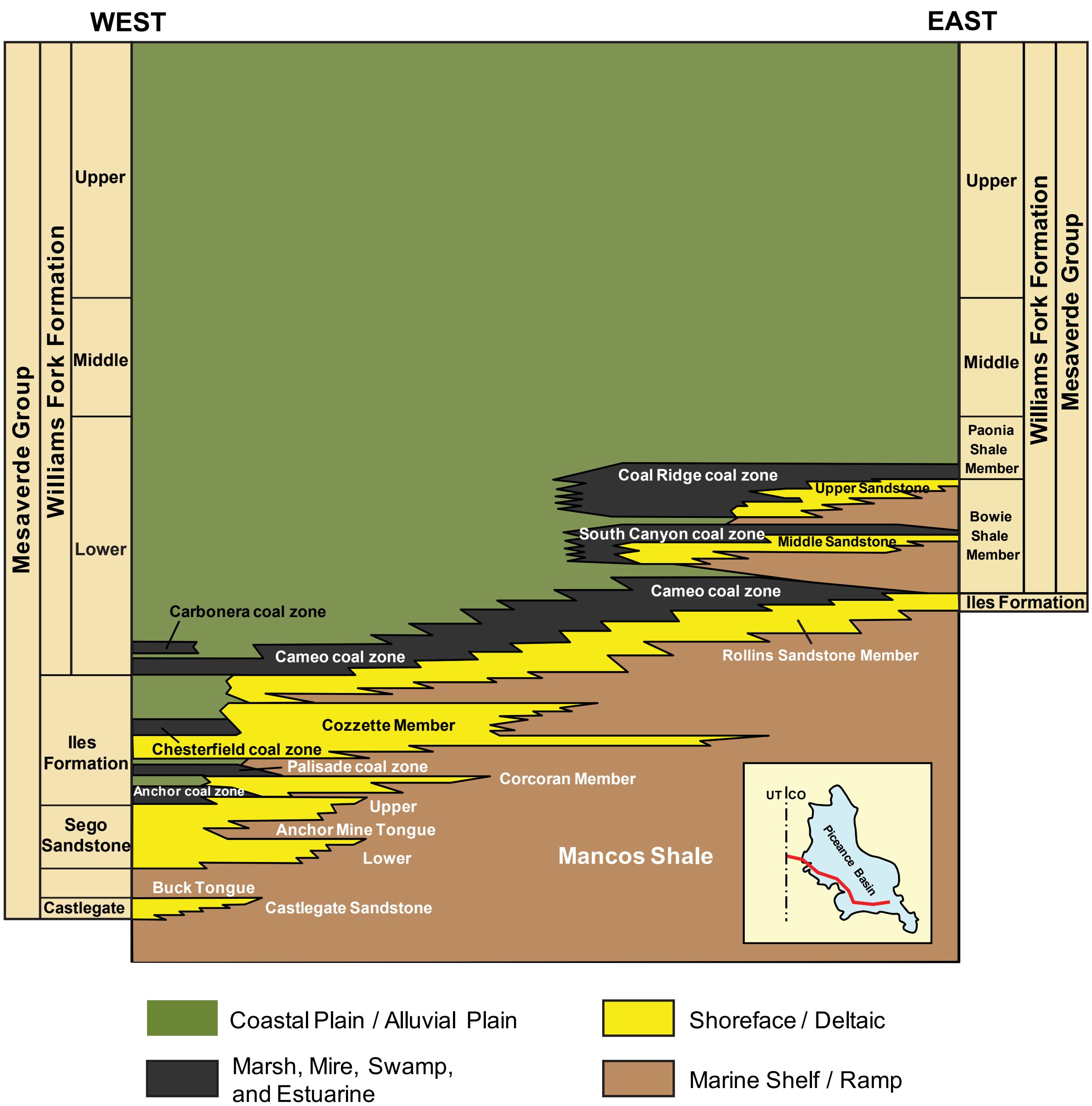

Figure 1.8 - Stratigraphic nomenclature of Upper Cretaceous strata of the southern Piceance Basin. The Williams Fork Formation is divided into lower, middle, and upper intervals in this portion of the basin. Approximate location of transect is shown in map inset. From Carroll et al. (2004).

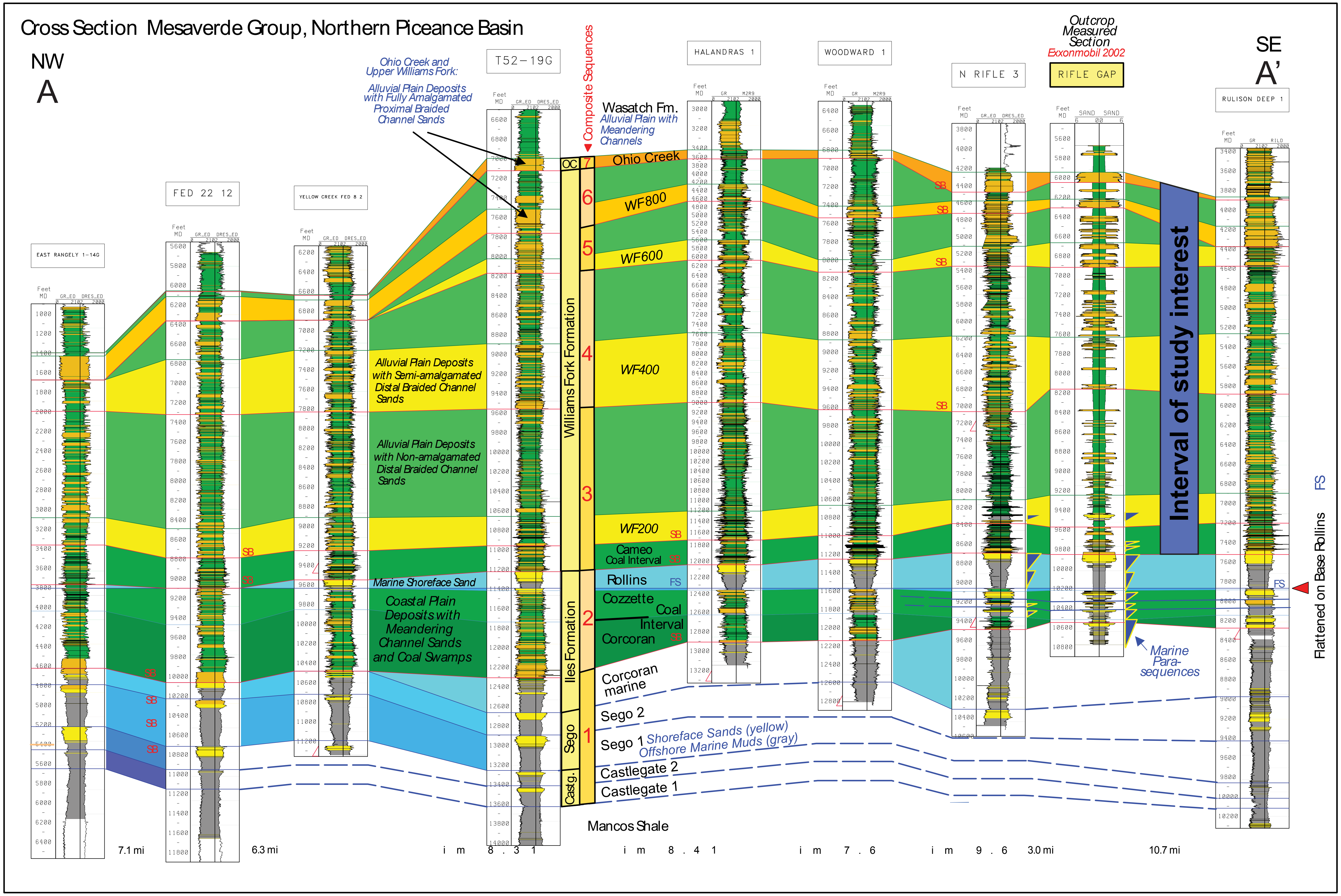

Figure 1.9 -Regional cross section illustrates sequence-stratigraphic framework of the Mesaverde Group and Ohio Creek Conglomerate in central and northern Piceance Basin, Colorado (from Patterson et al., 2003). The interval of interest in this study is shown with a blue bar and corresponds to sequences 3, 4, 5, 6 and 7. See Figure 1-6 for the line of section.

Lowstand systemes Tract deposits   Highstand and Trnsgressive Systems Tracts deposits   Marine Shoreface deposits .

1995). It includes the strata from the Rollins sandstone member up to the unconformity at the Cretaceous-Tertiary boundary (Johnson, 1989). The Upper Cretaceous and Tertiary stratigraphy of the southwestern Piceance Basin is shown in Figures 1.8 and 1.9. Hettinger and Kirschbaum's (2002, 2003) stratigraphic nomenclature is used in this study.

The Williams Fork Formation is informally subdivided into the lower, middle, and upper intervals, and consists of interbedded sandstone, mudrock, and coal, all deposited in alluvial-plain, lower coastal-plain and marginal-marine settings (the latter only in the eastern Piceance Basin) (Johnson, 1989; Hettinger and Kirschbaum, 2002; Patterson et al., 2003; Cole and Cumella, 2005; Shaak, 2010).

The Williams Fork Formation is also divided into a number of genetic depositional sequences that were deposited during episodes of shoreline advance and retreat. These sequences are bounded by low-resistivity shale markers that represent marine flooding surfaces in a basinward direction and non-depositional surfaces in terrestrial facies (Tyler and McMurry 1995). Coal occurrence is controlled by depositional environment; genetic units of the thickest and most continuous coals formed by peat accumulation and preservation on the coastal plain in a setting proximal to the shoreline. The paleoshoreline position within the Piceance Basin during the Late Cretaceous strongly influenced the southeastern basin sediments, which created more marine-influenced sandstone and an abundance of coal (Tyler and McMurry, 1995; Shaak, 2010).

In the western, southwestern, and southern Piceance Basin, the cumulative sandstone thickness (beds greater than 10 ft, or 3.0 m) in the Williams Fork Formation is approximately 1,000 ft (304.8 m), whereas in the northeastern Piceance Basin, the cumulative thickness is nearly 2,000 ft (609.6 m) (Cole and Cumella, 2005). The Williams Fork Formation is approximately 5,155 ft (1,570 m) thick at the Grand Hogback and thins to approximately 1,200 ft (365 m) at the Utah-Colorado state line (Hettinger and Kirschbaum, 2002). Hettinger and Kirschbaum (2002) and Johnson and Roberts (2003) have attributed the westward stratigraphic thinning to the unconformity separating the Williams Fork Formation from the Wasatch Formation and/or variations in subsidence across the Piceance Basin.

In Figure 1.10, the Dyco Petroleum #1 Sommerville well log and a composite-measured section of the lower Williams Fork Formation from Coal Canyon (Cole and Cumella, 2005) show the Iles Formation overlain by the Williams Fork Formation. The three coarsening-upwards marine-shoreface sandstones of the Iles Formation can be recognized through the gamma-ray and resistivity curve changes in the well log. The Williams Fork Formation gamma-ray and resistivity curves show the sandstone-rich strata increasing upward in the Williams Fork Formation (Figure 1.10). The transitional sequences of Mancos-Iles-Williams Fork represent a lowering of the base level during the Late Cretaceous associated with the regression of the now-extinct Western Interior Seaway.

The uppermost portion of the Williams Fork Formation, Ohio Creek Member (Ohio Creek Conglomerate), consists of lowstand, coarse-grained, braided fluvial deposits formed in the Paleocene (Patterson et al., 2003). The base of the Ohio Creek Conglomerate represents a regional unconformity that is attributed to the onset of the Laramide Orogeny (Figure 1.11) (Patterson et al., 2003). Upper Paleocene (~60 ma)

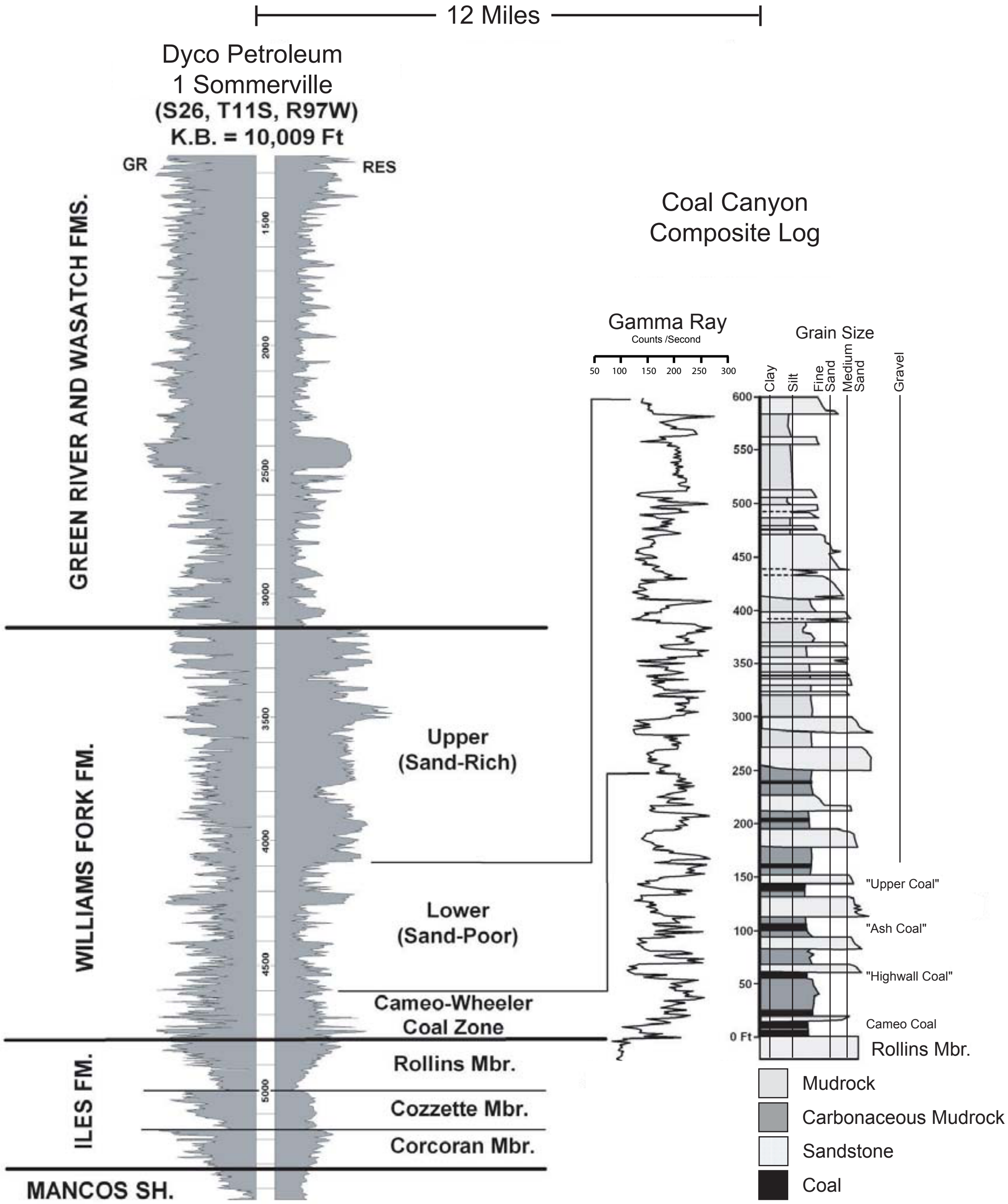

Figure 1.10 - Comparison of the Dyco Petroleum 1 Sommerville well and a composite measured section of the lower Williams Fork Formation in Coal Canyon. Well-log data for the Dyco Petroleum 1 Sommerville well are from Hettinger and Kirschbaum (2002, 2003). Coal Canyon composite measured section data are from Cole and Cumella (2003, 2005). The thickness of the composite measured section corresponds to the study interval. Modified from Cole and Cumella (2005) and Pranter et al. (2007). See Figure 1-6 for wel location.

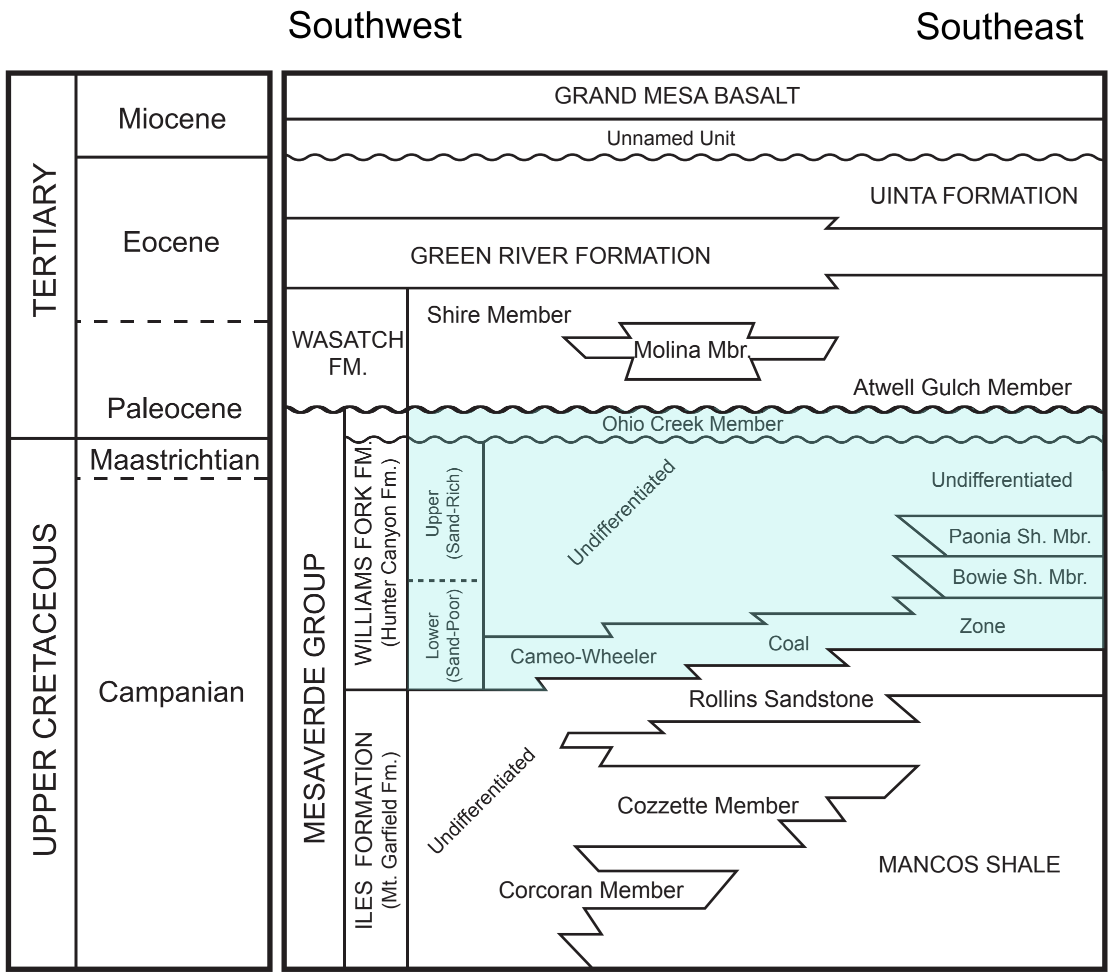

Figure 1.11 - Upper Cretaceous and younger stratigraphic nomenclature for the southern Piceance Basin. The Williams Fork Formation is divided into lower and upper members based on a marked difference in sandstone content. The interval of interest in this study is shaded blue. The Ohio Creek Member of the Williams Fork Formation is placed within the Paleocene. Modified from Collins (1976), Hettinger and Kirschbaum (2002), Cole and Cumella (2003, 2005), Hettinger et al. (2003), Johnson and Roberts (2003), Patterson et al. (2003), German (2006), Burger (2007), and Pranter et al. (2009).

vertebrate fossils from the Ohio Creek Conglomerate have been described by Burger (2007). The Wasatch Formation unconformably overlies the Ohio Creek Conglomerate. This low net-to-gross fluvial unit shows some sandstone-rich horizons such as the Molina Member (Johnson, 1989; Johnson and Flores, 2003).

In the southeastern Piceance Basin, the Williams Fork Formation is subdivided into lower and upper intervals based on net-to-gross sandstone ratio (Cole and Cumella, 2005). The lower Williams Fork Formation is a relatively low net-to-gross ratio (< 50%) succession of approximately 500 to 700 ft (152 – 213 m) as exposed in outcrop in Coal Canyon on the southwestern margin of the Piceance Basin. It consists of fluvial channel-fill sandstones, crevasse splays, floodplain mudrock, and subordinate coal. The depositional environment of these rocks has been interpreted as a highly sinuous meandering river system in a coastal-plain setting (Cole and Cumella, 2005; German, 2006; Patterson et al., 2003; Pranter et al., 2007, 2009). The upper Williams Fork Formation, including the Ohio Creek Conglomerate, has net-to-gross sandstone ratios between 50-80% (Patterson et al., 2003; Cole and Cumella, 2005; German, 2006; Pranter et al., 2007, 2009).

The Cameo-Wheeler coal zone overlying the Rollins sandstone (Figure 1.11) generally consists of shale, interbedded with sandstone and numerous coal beds ranging in net thickness from 20 ft (6 m) in the southeastern part of the basin to more than 60 ft (18 m) in the east-central part of the basin (Lorenz 1983, 1989; Johnson 1989). Cameo-Wheeler coal was deposited in peat bogs and mires (muddy marshes), forming laterally continuous and correlatable coal beds. These numerous coal seams alternate with sandstones and carbonaceous shale. Thin crevasse-splay sandstones commonly overlie coal beds. Interbedded thicker lenticular sandstones that are isolated within mudstones are interpreted to be fluvial point-bar deposits, typical of all other sandstone bodies within the lower Williams Fork interval, and having a limited lateral extent (Lorenz 1983, 1989; Johnson 1989; Cumella and Ostby 2003, Carroll et al 2004).

Collins (1976, 1977) investigated the outcrop exposures along the eastern margin of the Piceance Basin and the Coal Basin areas to describe and analyze the stratigraphic and depositional environment of the Williams Fork Formation, with a focus on the middle and upper marine sandstones and coal resources in the lower Williams Fork interval. In addition to the detailed description of the stratigraphic relationships between formation thicknesses and rock units, Collins (1976, 1977) reported that the Mesaverde Group was deposited by a south-southeastward prograding deltaic complex in the Coal Basin area. The study concluded that this depositional setting comprises three cycles of marine shale, delta-front sand, and lower delta plain sediments, including economic coal beds that were deposited in fresh-water swamps. Collins (1976, 1977) also indicated that these sequences were compacted and were subject to deformation. The Bowie Shale Member and Paonia Shale Member (Figure 1.8) were interpreted to be deposited as a shoreface, offshore, and coal-bearing coastal-plain environments (Collins, 1976 1977). Collins (1976) also interpreted the “undifferentiated” part of the Williams Fork Formation as fluvial in origin.

In the eastern and southeastern Piceance Basin, the Williams Fork Formation is subdivided into a Bowie Shale Member, Paonia Shale Member, and an undifferentiated middle and upper members (Figures 1.8 and 1.11). The Bowie Shale Member is about 600 to 1,000 ft (180 to 300 m) thick in the southeastern portion of the Piceance Basin and was deposited in coastal-plain to shallow-marine settings (Johnson, 1989; Tyler and McMurry, 1995; Hettinger and Kirschbaum, 2002; Shaak, 2010).

The lower Williams Fork Formation in the southeastern Piceance Basin represents a transition from coastal-plain to shallow-marine environments of deposition (Shaak, 2010). Parasequences of the lower Williams Fork Formation in the southeastern Piceance Basin are composed of wave-dominated shoreface sandstones that transition landward into paludal (marsh) environments. Overlaying environments of deposition are characterized by coastal-plain deposits containing isolated channel sandstones and floodplain strata. Tidally influenced deposits and brackish-water fauna also formed landward of the marine shorelines and reflect fluctuating fresh-water and marine influence in the lower coastal plain. The presence of bays behind transgressive shoreline deposits have also been recognized (Shaak 2010).

Two transgressive-regressive cycles have been identified within the lower Williams Fork Formation, through which each marine sandstone and associated coal zone records a retrogradational to progradational stacking pattern of parasequences (Shaak, 2010).

Fossils of *Teredolites*-bored logs have been observed in the Cameo-Wheeler coal zone in Coal Canyon, at the top of the middle Williams Fork Formation in Plateau Creek Canyon, and near the top of the Mesaverde Group near Rifle Gap. These observations suggest marine influence within the Williams Fork Formation. It is believed that high-frequency eustatic sea-level changes might have influenced the Williams Fork depositional setting. In general, the marine influence is believed to have been minor on the western basin margin but more significant eastward (Lorenz, 1982, 1987; Johnson, 1989; Cole and Cumella, 2005). *Teredolites* might also be associated with salt-water wedges that invade coastal river systems during periods of low flow (Johnson, 1989).

The middle-to-upper portion of the Williams Fork formation is generally undifferentiated and characterized by transition to more sandstone-rich (~50-80% net-to-gross ratio) deposition within alluvial-plain settings (Johnson, 1989; Patterson et al., 2003; Cole and Cumella, 2003, 2005; German, 2006). Integrated outcrop and subsurface data (high-resolution aerial lidar, digital orthophotographs, photomosaics, behind-outcrop cores, nearby well-logs, and field measurements) from Plateau Creek Canyon suggest that the middle-to-upper Williams Fork sandstone deposits were deposited in a low-sinuosity, sand-dominated, braided alluvial-plain setting. This low-sinuosity braided-river system was a response to changes in topographic gradient, accommodation space, and depositional environment that caused paleostreams to gradually change from high-sinuosity meandering streams to low-sinuosity braided streams (Cole and Cumella, 2005; Patterson et al., 2003; German, 2006; Pranter et al., 2009). The braided river depositional environments resulted in more continuous sheet-like sandstone bodies (Patterson et al., 2003; German, 2006; Pranter et al., 2009).

A large-scale sequence-keyed framework for the Mesaverde Group, which proposes a non-marine sequence-stratigraphic architecture for the alluvial strata of the Williams Fork Formation in the Piceance basin, was constructed by Patterson et al. (2003). Other studies (Tyler and McMurry, 1995; Kirschbaum and Hettinger, 2004) have also contributed by elucidating the sequence-stratigraphic context of the Mesaverde Group.

Sequence Stratigraphy

Patterson et al. (2003) integrated detailed measured outcrop sections and subsurface data (facies analyses of cored intervals, well-log correlations, biostratigraphy of well cuttings, and 2-D seismic interpretations) into a facies architecture and sequence-stratigraphic framework for the Mesaverde Group and the Ohio Creek Conglomerate in the central and northern Piceance Basin. According to Patterson et al. (2003), the Upper Cretaceous Mesaverde strata largely represent progradational shoreline successions reflecting both regression of the Cretaceous Western Interior Seaway and subsequent basement-involved tectonic events of the Laramide orogeny.

Patterson et al. (2003) defined seven composite, third order sequences, which define a larger-scale alluvial architectural framework for the Williams Fork and Ohio Creek strata in the Piceance Basin (Figure 1.12). The lowstand deposits form the thick and laterally-extensive sandstone-prone intervals, whereas the transgressive and highstand deposits are comprised of isolated channel elements within the mudstone-prone intervals overlying each of the Williams Fork lowstand deposits (Figures 1.9, 1.13). The lower three composite sequences of the Williams Fork Formation represent alluvial plain deposits within moderate accommodation periods. Dissimilarly, the uppermost composite sequence of the Williams Fork Formation and the composite sequence of the Ohio Creek Conglomerate were deposited during low accommodation potential attributed to the onset of the Laramide uplift, and are characterized by the more amalgamated channel and channel-complex elements within the lowstand strata.

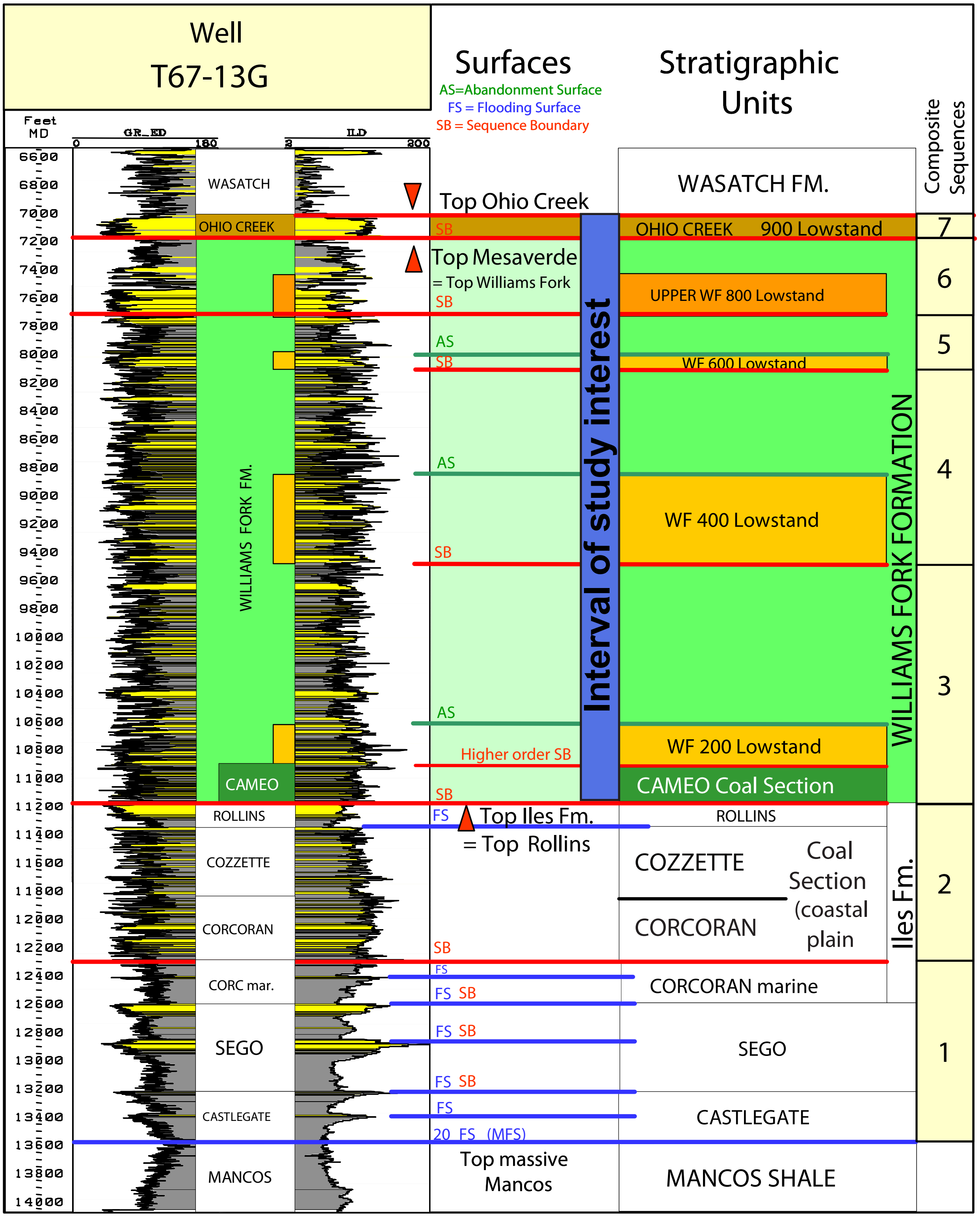

Figure 1.12 - Type log of the Mesaverde Group and Ohio Creek Conglomerate showing the sequence-stratigraphic framework of the Williams Fork Formation (from Patterson et al., 2003). The area of interest in this study is shown with a blue bar and corresponds to sequences 3, 4, 5, 6 and 7. Lowstand systems tract deposits Highstand and trannsgressive systems tracts deposits

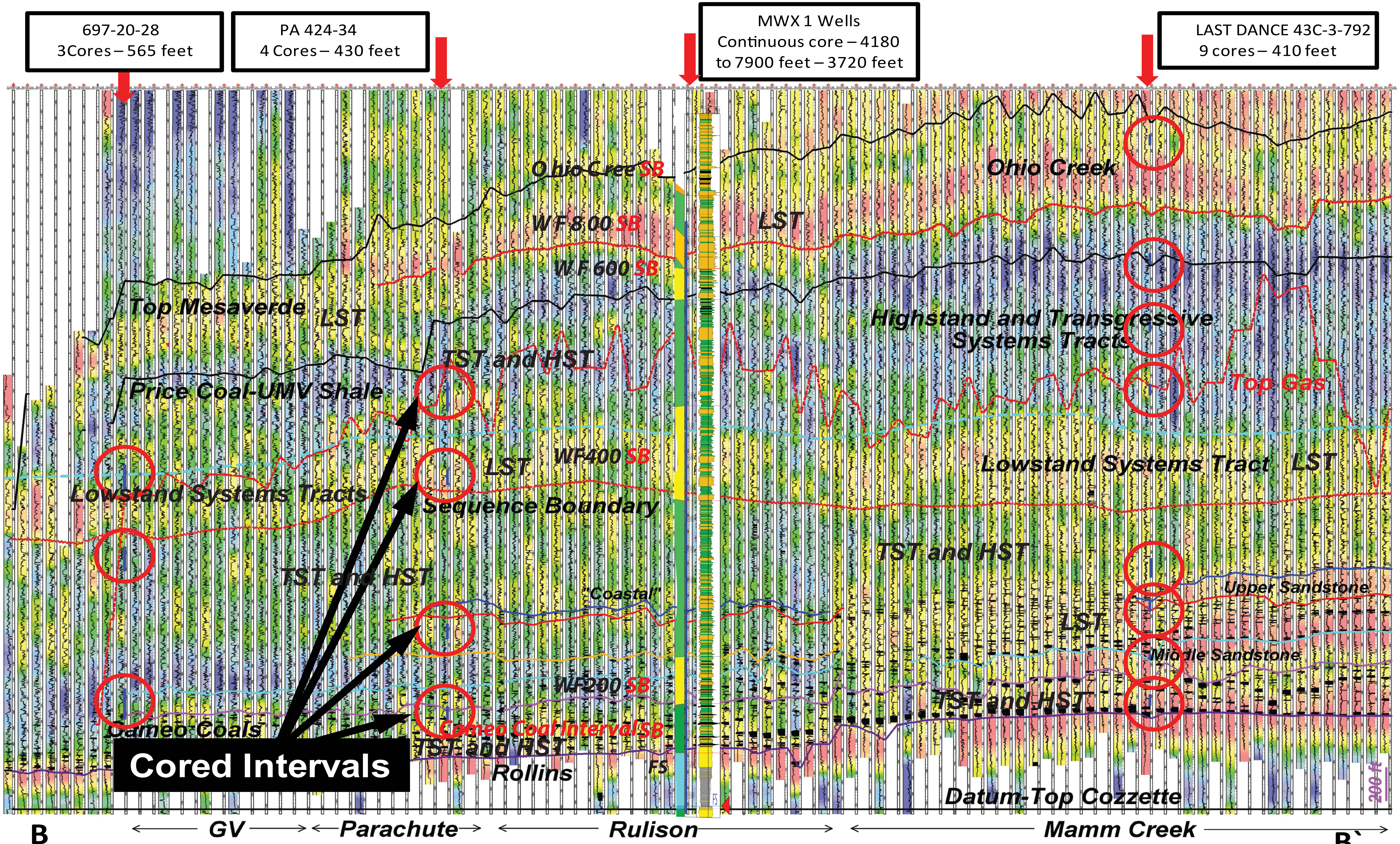

Figure 1.13 - Smoothed gamma-ray regional cross section illustrating the sequence-stratigraphic framework of the Williams Fork and Ohio Creek Conglomerate in southern Piceance Basin, Colorado (based on Patterson et al., 2003). The cored intervals are shown in red bars and circles. Modified from (Patterson et al., 2003; and Cumella, Personal contact). See Figure 1-6 for line of section.

Structural Setting

The Piceance Basin, located in northwestern Colorado, is one of several Rocky Mountain basins formed by Laramide tectonism during the Late Cretaceous through Paleocene (Johnson, 1989). Prior to the Laramide Orogeny, the Piceance Basin was a part of the Rocky Mountain Foreland Basin that was created by the Sevier Orogeny. Laramide uplifts transformed the Colorado Plateau region into a mosaic of basins and created today's existing uplifts (Johnson and Flores, 2003; DeCelles, 2004). The Piceance Basin is bounded by the Uinta Mountain uplift and the Axial Arch on the north, the White River uplift on the east, the Douglas Creek Arch on the west, and the Uncompahgre, Gunnison, and Sawatch uplifts on the south (Figure 1.14).

The Piceance Basin is highly asymmetrical and shows gently dipping western and southwestern flanks and a sharply upturned eastern flank (Grand Hogback), which is believed to be underlain by a deep-seated west-vergent thrust fault (Gries 1983; Johnson 1989). The northern-most part of the basin is almost separated from the rest of the basin by the White River Dome, which is a southeast-plunging anticline in the northern part of the basin. South and west of the White River Dome, there is another southeast-plunging anticline, the Rangely Anticline, which forms the northern terminus of the Douglas Creek Arch (Johnson, 1989). Three large anticlines in the southern Piceance (the Divide Creek, Wolf Creek, and Coal Basin anticlines) are believed to be underlain by deep-seated west- and southwest-thrusting reverse or thrust faults related to the major thrust fault beneath the Grand Hogback (Gries, 1983) (Figure 1.14). The formation of the Divide Creek Anticline is believed to be a result of a high-angle reverse

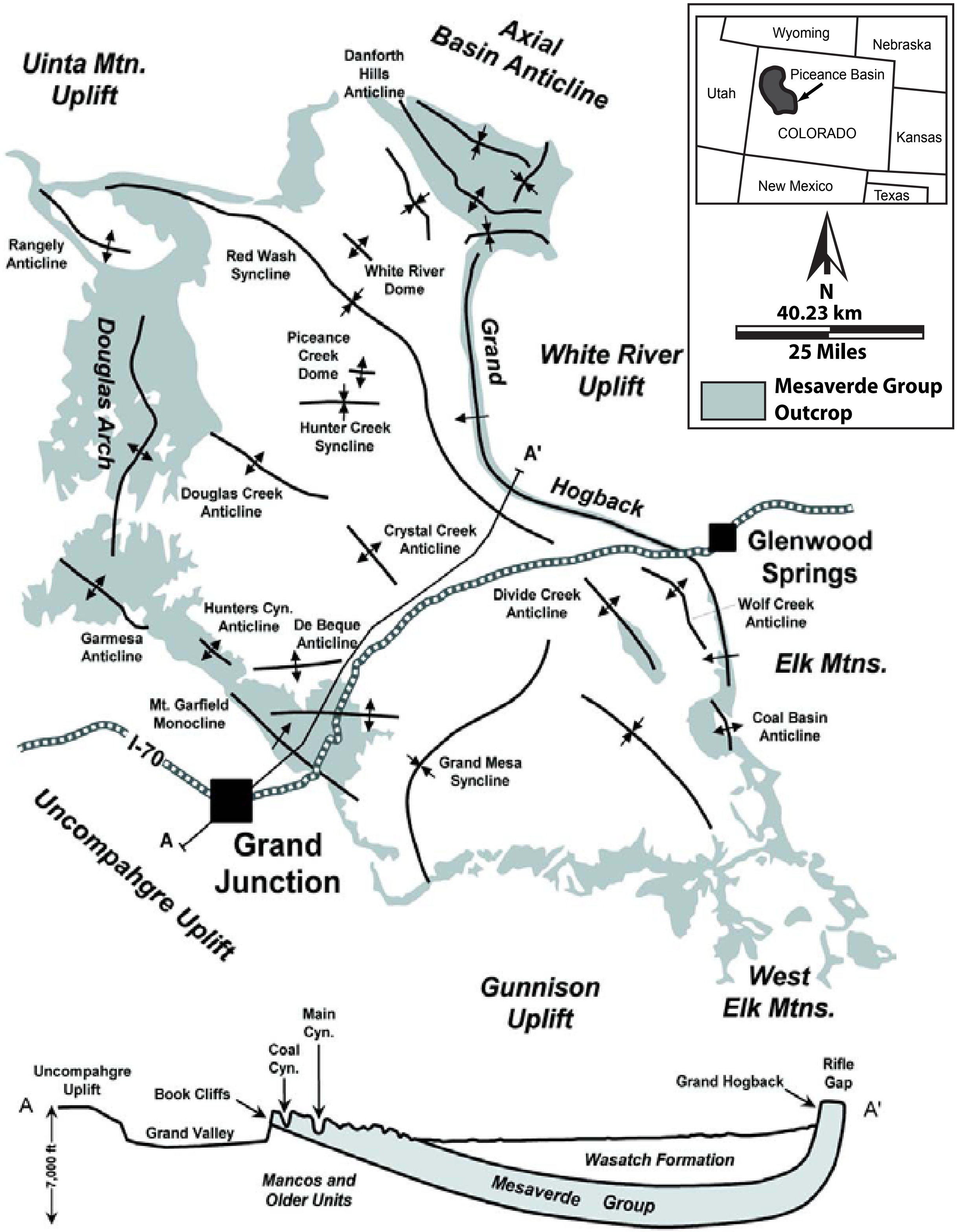

Figure 1.14 - Map illustrating the structural elements of the Piceance Basin. The structural cross section is diagrammatic. Modified from Cole and Cumella (2003).

fault with a displacement varying from 210-900 ft (64-274 m) and extending in a NW-SE direction for over 8 mi (13 km) (Berry, 1959).

There is a dominant fracture system in Mesaverde Group rocks along the Grand Hogback, and possibly in the subsurface, along a hogback system in the eastern part of the basin. This older hogback fracture system developed in rocks of the Mesaverde Group prior to uplift along the Grand Hogback and consists of well-defined fracture sets trending N80W and approximately due north. A younger fracture system is the dominant system in the Tertiary rocks throughout the basin. It consists of several sets of fractures with a dominant fracture orientation of west-northwest to north-northeast in the Eocene Green River Formation. There is yet another set of fractures oriented north-northwest to north-northeast. The west-northwest system, which is almost parallel with the Hogback system of the N80W fracture set, is comprised of two sets with totally different ages (Verbeek and Grout 1984). The west-northwest fracture set is almost parallel with the dominant fault orientation in the basin. These sets are common to both the Grand Hogback and the younger Piceance fracture systems. The Piceance Basin faulting system is almost exclusively oriented north-to-west-northwest and has shown limited spread throughout the basin (Verbeek and Grout 1984).

Petrography

Efforts to understand the reservoir quality and what controls porosity and permeability within the Williams Fork Formation reservoirs have resulted in a number of petrographic and diagenetic studies (e.g., Pitman et al., 1989; Laubach et al., 2006; Ozkan 2010). These petrological studies provide valuable mineralogical and petrophysical data for understanding the factors controlling the reservoir characteristics of low permeability rocks in these complex marine and non-marine fluvial depositional systems. Pitman et al. (1989) and Laubach et al. (2006) revealed that the Mesaverde Group reservoirs in the east-central Piceance Basin MWX wells have rock types ranging from feldspathic litharenite to lithic arkoses and litharenites. Pitman et al. (1989) and Ozkan (2010) describe a mineral assemblage consists of a framework of quartz, feldspar, volcanic and sedimentary lithic grains, authigenic carbonate minerals including calcite, dolomite and ankerite, and a variety of clays including kaolinite, illite, chlorite and illite-smectite. The abundance, distribution, and grain density of these minerals all significantly affect the quality of the reservoir sandstone.

Due to diagenetic alterations, including extensive cementation by authigenic clays, the reservoir quality of these sandstones is extremely low (Pitman et al., 1989), with matrix permeability on the order of microdarcies. Natural fractures significantly increase reservoir permeability, but massive multistage artificial fracturing is required for commercial production. Diagenesis plays a critical role in the capacity of fractures to conduct fluid in these tight reservoirs (Pitman et al., 1989; Laubach et al., 2006; Cumella and Sheevel, 2008).

The effect of diagenesis on the fracture cementation in Mesaverde sandstones was examined by Laubach et al. (2006). They reported that Mesaverde fractures are frequently cemented by quartz, dolomite, ankerite, and calcite, with quartz often forming the first cement, and calcite, where present, forming a late post-kinematic cement. Reconstructions of pore and fracture cement sequences suggest the fracture cementation closely follows the burial diagenetic sequence of pore-filling cement.

Quartz either completely occludes fractures or forms cement linings along walls of otherwise uncemented fractures. In several occurrences, Laubach et al. (2006) report fractures lined with quartz cement contain quartz cement bridges, with fractures between bridges either remaining uncemented and thus available for fluid movement, or occluded by later carbonate cement. Crack-seal textures of quartz cement bridges indicate syn-kinematic cement growth, i.e., cement precipitation concurrent with the fracture opening (Laubach et al., 2006). Fractures in the Mesaverde Group in the Piceance Basin are primarily opening-mode fractures; some of these “extension fractures or joints” had gone through several episodes of repeatedly opening, cementation, then opening again (Cumella and Scheevel, 2008).

Ozkan (2010) described the influence of Williams Fork cementation history on fracture patterns. At the microscale, Ozkan (2010) argued that diagenetic processes impose fabric heterogeneities (i.e., cement/grain, cement/pore, and cement/cement boundaries) that control the growth of fractures. Her study provides a tool to predict fracture behavior at different times in the burial history, and concludes that modern rock properties at the present state of stress do not always yield information that is useful for understanding fracture patterns in the subsurface. Ozkan et al. (2011) correlated lithofacies to log responses in order to predict the reservoir quality directly from well logs. Sandstone with low bulk density log values have no or very low carbonate cement and were identified as the best reservoir quality intervals. Clay matrix- and mica-rich samples that have high gamma-ray and bulk density values were identified as poor reservoir quality facies.

Petroleum System

Gas was discovered in the Piceance basin in the 1890s in the Wasatch and Green River formations, and since then many other discoveries were made. However, significant volumes of commercial gas production did not start until mid-1980s because most of the gas in the basin was trapped in the tight, low permeability sandstones of the Mesaverde Group. The breakthrough occurred when Barrett Resources established commercial production at Grand Valley, Parachute, and Rulison fields with development of new well completion and recovery techniques (Yuewicz et al., 2006; Cumella and Scheevel, 2008).

The gas production in the Piceance Basin is primarily from a large, basin-centered gas accumulation of an unconventional petroleum system. The amount of generated gas and the ability of the Mesaverde Group sandstones to transmit and/or trap and retain gas appear to control the distribution of gas (Yurewicz et al., 2003, 2008; Cumella and Scheevel, 2008). The entire petroleum system covers about 20,000 mi^2 (52,000 km^2) across the Piceance Basin with thicknesses ranging from 1,500 ft (460 m) on the western margin at the Douglas Arch to more than 10,000 ft (3,050 m) in the center of the basin (Johnson and Roberts, 2003).

Reservoir Rocks. - The reservoir includes sandstone, siltstone, shale, and coal deposits associated with a fluvial depositional system (Pitman et al., 1989; Cumella and Ostby, 2003; Pranter et al. 2007; Cumella and Scheevel, 2008; Pranter et al. 2009; Pranter and Sommer 2011). These fluvial deposits consist of isolated and stacked point-bar deposits, crevasse splays and overbank (floodplain) mudrock interbedded with shales and coals (Pranter et al., 2008). Sandstones include single-story channel bodies and crevasse splays that form isolated sandstone bodies and amalgamated multistory channel bodies and channel complexes (Hewlett, 2010). The main reservoir sandstones include point-bar deposits which are highly lenticular with typical lateral extents of 500-800 ft (152-244 m) and very low-permeability (Cumella and Ostby, 2003). Bedding and scour surfaces are present, forming common internal permeability barriers (Cumella and Ostby, 2003). Reservoir rocks are typically low porosity (< 13%), low permeability (<0.1 md) (Pitman et al., 1989; Cumella, 2006; Yurewicz et al., 2008). Open natural fractures and hydraulic-fracturing methods make these tight sandstones commercial gas producers (Pitman et al., 1989; Yurewicz et al., 2008). Gas is produced at abnormal reservoir pressures where discontinuous fluvial sandstones of the Williams Fork Formation are continuously gas-saturated and form productive intervals that can reach total thicknesses of about 3000 ft (900 m) (Cumella and Scheevel, 2008). The Williams Fork Formation gas-saturated interval dramatically thins close to the basin margins (Cumella and Scheevel, 2008). The reservoir productivity and ultimate recovery are very much controlled by the distribution and connectivity of the fluvial sandstones. The large-scale stratigraphic variability due to vertical stacking patterns and the structural heterogeneities associated with faults are what create lateral and reverse offsets and highly-impacted reservoir fluid flow (Pranter et al., 2008).

Source Rocks. - The hydrocarbon source is primarily the Cameo-Wheeler coal zone deposits that include coals and organic-rich shales and siltstones of the Upper Cretaceous Mesaverde Group (Johnson and Roberts, 2003). Coal deposits in this zone are 20 to 80 ft (6 to 24 m) thick across the basin (Johnson and Roberts, 2003). Increasing thermal maturity in the coal beds made the generation greatest in or near the deep axis of the basin (Yurewicz et al., 2003, 2008). Although the organic-rich continental shales in the overlying Williams Fork Formation are thick and extensive, these source rocks have low hydrogen indices and thus have generated relatively small volumes of gas. The marine shales at the base of the Cretaceous section have higher hydrogen indices than the continental shales within the Mesaverde Group, but have also generated much less gas than that generated by the coals (Yurewicz et al., 2003, 2008).

Gas Generation and Trapping. - Johnson and Roberts (2003) argued that the Mesaverde hydrocarbon system began generating gas around 55 million years ago (early Eocene) with peak gas generation between 47 and 39 million years ago. In contrast, Payne et al. (2000) concluded that gas generation within the Mesaverde petroleum system in the Piceance Basin coincided with maximum burial of the Williams Fork Formation during Oligocene time (33.7 to 23.8 Ma). As of 2006, it was confirmed that the southern Piceance Basin contained an estimated 31.5 trillion ft^3 (892 billion m^3) of recoverable gas and the northern Piceance Basin held 11.0 trillion ft^3 (311.5 billion m^3) of recoverable gas (Kuuskraa, 2007). Capillary seal, or water block, and some structural trapping are the causes of the sealing and trapping of the gas (Law, 2002; Johnson and Roberts, 2003).

METHODS

Detailed sedimentologic core descriptions were made in terms of lithology, grain size, sedimentary structures, bounding surfaces, and ichnofacies. Facies and facies associations were interpreted from these observations.

Petrographic analysis was used to differentiate between detrital and diagenetic phases, understand their relationships, and quantify mineral and pore-type abundance. Modal analyses were done by counting 400 points in each of 220 thin sections. The 400 counts per slide provide representative data of the major and minor mineralogical constituents (detrital and authigenic) and diagenetic features. Samples for thin sections were chosen based on vertical and lateral changes in texture, color, and sedimentary structures, and/or based on their position within the sequence-stratigraphic framework (i.e., focusing on systems tracts and key sequence stratigraphic surfaces). Most thin-sections were provided by the cores' owners. Twenty five new thin sections made by first impregnating rock samples with blue dye epoxy in order to color the pore space and to help in the evaluation of porosity under the microscope. Standard 4 cm x 1.5 cm x 30 µm polished thin sections were made. Alizarin Red S and potassium ferricyanide were applied as staining agents to assist carbonate mineral identification. Sodium cobalt nitrite and barium chloride staining solution was used for distinguishing potassium and plagioclase feldspars.

Electron microscopy of a subset of samples was used to examine the details of mineral morphology, grain-cement relationships, and porosity, especially microporosity. Back-scattered-electron imaging (BSEI) was used to analyze a representative selection of polished and carbon-coated thin sections. Small pieces of unpolished rock from the same samples were also examined using scanning electron microscopy (SEM). These rock fragments were about 10 mm x 10 mm x 5 mm. Only freshly broken surfaces were chosen and glued to SEM pin stubs and then gold coated.

X-ray diffraction (XRD) was used to identify different types of clay minerals and to confirm the clay mineralogies determined by petrographic analysis. All XRD analyses utilized a Phillips goniometer with Ni-filters and a copper kα radiation (l = 1.5418A), 40.0 kV, 25.1 mA, continuous scan mode, and a scan rate of 2 degrees per minute. Results were automatically saved on a computer disk as RD files. Mineralogical compositions were determined by peak analysis using a Siemans analysis package. Whole-rock XRD analyses used approximately 10 g of rock from petrographically studied samples. This material was dry-milled and the resultant powder was packed onto glass slides and scanned from 2 to 65 degrees 2Ɵ.

For clay mineral analysis, oriented samples were prepared from the same rock samples used for all other techniques. Clays were size separated using the procedure of Tucker (1988). Rock samples were disaggregated using an agate mortar and pestle with a calgon solution. Suspended clays, silt, and sand were then transferred to a glass tube, topped up with calgon solution, agitated and then centrifuged at 1000 rpm for about 4 minutes to drop out the coarse fraction. The suspended portion was decanted into a clean centrifuge tube, and spun at high speed (10,000 rpm) for 20 minutes to settle all but the < 5 µm fraction. A drop from the supernatant containing the < 5 µm clay fraction was smeared on a glass slide of about 2.7 x 4.6 cm by using a micro pipette. The slides were dried at room temperature and then then scanned from 2 to 40 degrees 2θ. The clay smear slide was then glycolated in a container to enlarge expandable clay layers and then x-rayed a second time, to discriminate expandable smectite clays. The samples were then heated to 350°C and x-rayed again, and heated to 550°C and x-rayed yet again in order to facilitate the identification of the various clay minerals (Tucker, 1988).

CHAPTER TWO: FACIES AND FACIES ASSOCIATIONS

INTRODUCTION

Sedimentological core descriptions were performed for the following five cored wells, Plateau Creek BT-202, Cascade Creek # 697-20-28, Puckett/Tosco PA 424-34, Last Dance 43C-3-792 and Cactus Valley 1 D111. An existing description of the Superior MWX 1 core (Lorenz, 1987, 1988, 1989, 1990) was reviewed with the actual core. Approximately 4,465 ft (1361 m) of slabbed cores from the Williams Fork Formation were studied (Table 1, Figure 1.13). Sedimentological core descriptions were used to define lithofacies and facies associations. Lithofacies were described based on lithology, sedimentary structures, grain size, bioturbation, bed thickness, and bed contacts. Facies is a body of rock characterized by a particular combination of lithology, and physical and biological structures that is different from the rock intervals above, below, and laterally adjacent (Walker, 1992). Facies associations are groups of facies genetically related to one another that represent a succession of rock units deposited within a certain depositional environment and which have some environmental significance (Collinson, 1969; Walker, 1992). Facies associations are defined based on facies analysis data, facies stacking patterns, and stratigraphic relationships.

LITHOFACIES

Twelve geologically distinct Williams Fork lithofacies were defined based on core analysis (Table 2).

Color	Name (Code)	Sedimentary Structures & Comments	Depositional Process	Image
	Coal (C)	Cleating, fractures, associated with carbonaceous mudstone and (occasionally) rooted mudstone. Thickness range from 0.5 to 10 ft (15.2 cm to 3 m)	Swamps, marsh, mires, probably deposited in well drained swamps and mire	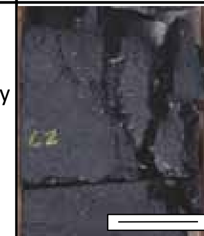
	Carbonaceous mudstone (Mc)	Massive, with fractures, root traces, woody materials and coal stringers in some intervals. Thickness < 1 ft to 8 ft (< 0.30 m to 2.4 m)	Peat and organic-rich sediment deposited in floodplain and shallow swamps and wetlands.	
	Ripple cross-laminated sandstone (Sr)	Very fine-to-fine grained, asymmetrical ripple cross lamination, climbing ripples may exist. Thickness 1 to 3 ft (30 cm to 0.91 m)	Traction transport in ripple bedforms.	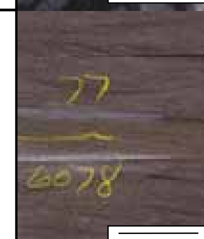
	Interbedded siltstone and mudstone (STMs)	Wavy, planar, and lenticular bedding. Mudstone, silty-mudstone, siltstone, occasionally very fine -grained sandstone. Maybe bioturbated and/or rooted. Thickness 0.5 to 2.5 ft (15 to 76 cm)	Alternating traction transport of silts and suspension settling of muds imply relatively low energy currents	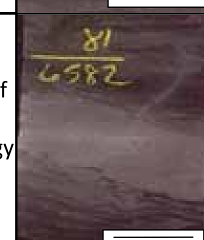

Bar scale = 1 in (2.5 cm)

Color	Name (Code)	Sedimentary Structures & Comments	Depositional Process	Image
	Wavy, lenticular, flaser bedded Sandstone (Sw)	Wavy, lenticular, and flaser bedding. Very fine grained, abundant silt content in some facies. Soft-sediment deformation maybe present. Thickness 2 to 5 ft (0.6 to 1.5 m)	Variable current velocities with traction transport of sands in small bedforms and suspension settling of fines as currents wane.	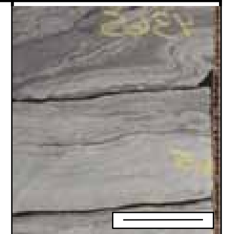
	Conglomeratic "mud chip" sandstone (Cgm)	Very fine-to-medium grained with intraformational mudclast rip-ups. Overlies scoured surfaces and erosive beds . Thickness , 1 to 6.5 ft (< 30 cm to 2 m)	High energy current, scoured surfaces, erosional, rapid deposition	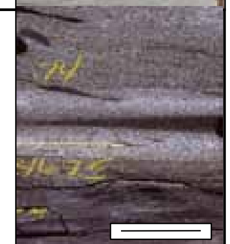
	Siltstone (ST)	Massive, contorted, laminated. Interbedded with mudstones and/or very fine grained sandstone. Maybe bioturbated or rooted . Thickness 0.3 to 4 ft (9 cm to 1.2 m)	Moderate to low energy	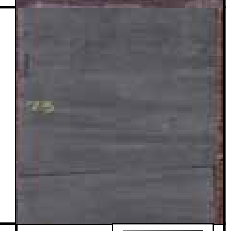
	Horizontal laminated sandstone (Shl)	Horizontal laminations. Very fine-to-medium grained well-to-moderately sorted. Thickness 1 to 8 ft (30.5 cm to 2.4 m), associated locally with ripple laminated facies and/or low-angle cross laminated sandstone facies	Mostly deposited at toes of straight-crested sand waves with rest of bedform (with angled cross laminations) not preserved. Some thinner intervals may represent her upper flow regime plane bed deposition.	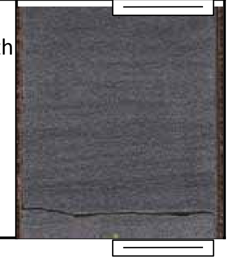

Bar scale = 1 in (2.5 cm)

Color	Name (Code)	Sedimentary Structures & Comments	Depositional Process	Image
	Low-angle cross bedded sandstone (Sla)	Low-angle(<10 degrees) cross lamination. Very fine-to-medium grained and well sorted. Thickness 4 to 20 ft (1.2 m to 6 m).	Lower flow regime traction transport of bed load in sand waves.	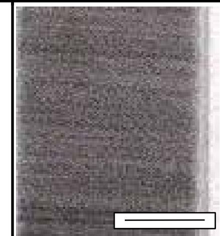
	High-angle cross bedded sandstone (Sha)	High-angle (>10 degrees) cross lamination, well- to moderately sorted, lower very fine-to-medium grained, trough and tabular cross bedding. Thickness 1 to 16 ft (0.3 to 4.9 m)	Lower flow regime traction transport of bed load in sand waves.	
	Mudstone (Ms)	Horizontal, wavy, and contorted lamination. Root traces, and soft-sediment deformation is common. Fractures and siderite concretions exist in some facies. Thickness 0.2 to 12 ft (6 cm to 3.65 m)	Suspension settling from flood waters on floodplain.	
	Structureless sandstone (Ss)	Featureless, mostly due to bioturbation, very fine-to-coarse grained, well-to-moderately sorted. Thickness 0.4 to 8 ft (12 cm to 2.4 m)	Deposition in lower flow regime bedform, with destruction of cross bedding or ripple lamina by subsequent bioturbation	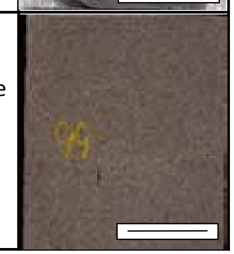

Table 2. Summary of facies described in Williams Fork cores. Bar scale = 1 in (2.5 cm).

Coal (C)

Coal is a distinctive lithofacies in the lower interval of the Williams Fork Formation. It is an important feature identifying the base of the formation, forming an important part of the Cameo-Wheeler zone. Coal beds facilitate subsurface correlation due to their lateral extent and ease of identification. Coal seams range from 0.5 to 10 ft (15.2 cm to 3 m), exhibit cleating, and are associated with carbonaceous mudstone and (occasionally) rooted mudstone. The coal was deposited in freshwater swamps and mires, contains mainly woody plant material, and is predominantly low sulfur coal (Collins, 1976, 1977). Alternating with sandstones and carbonaceous mudstones coal is important as a gas source rock in the Piceance Basin. Along the eastern part of the basin, the deepest coal near the Cameo-Wheeler base is a high-volatile bituminous to semi-anthracite (Collins, 1976, 1977).

Carbonaceous Mudstone (Mc)

Carbonaceous mudstone is mainly associated with coal, mudstone, and rooted mudstone at the top of upward-fining successions, and it overlies siltstone and/or mudstone. The carbonaceous mudstone is dark brown-to-black-to-dark gray in color and frequently contains woody and/or organic matter, coal stringers, and fractures. Bed thickness ranges from < 1 ft to 8 ft (less than 0.30 m to 2.4 m). Carbonaceous mudstone was deposited in swamp and floodplain settings, close to other peat-accumulating depositional settings. It could also represent a part of a lake or abandoned channel-fill depositional setting.

Ripple Cross-laminated Sandstone (Sr)

Rippled sandstone is typically light gray to gray, very fine-to fine-grained, asymmetrical ripple-laminated sandstone that commonly exhibits climbing ripples. This lithofacies exists within the uppermost intervals of channel fills. It ranges from 1 to 3 ft (30 cm to 0.91 m) thick, and caps the horizontal, low angle and/or trough laminated channel sandstone lithofacies. Rippled sandstone is typically overlain by finer silty mudstones and is locally bioturbated (e.g., *Arenicolites*). The very fine-grained ripple-laminated sandstone is also common within thin (0.5 to 2.5 ft thick (15.24 cm to 76.2 cm)) sandstone units of the crevasse splay sandstones, which are commonly separated by mudstone and isolated in floodplain deposits.

In general, sets of ripple laminae are 1 to 3 in (2.5 to 7. 6 cm) thick, with thin mudstone drapes < 0.08 in (< 2 mm) occasionally present between sets. Other minor structures associated with the rippled sandstone lithofacies include cm-scale horizontal and very low-angle laminations. Ripple cross-laminated sandstone lithofacies are interpreted to have formed from low-energy currents in channel settings, crevasse splays, and possibly any other setting dominated by low-energy currents.

Interbedded Siltstone and Mudstone (STMs)

Interbedded siltstone and mudstone lithofacies is typically made of mudstone, silty mudstone and siltstone, and is occasionally associated with rippled sandstone. This lithofacies is white-to-light gray-to greenish gray with some reddish light brown, thinly interbedded (0.25 to 1 ft; 7.6 to 30.5 cm), and typically 0.5 to 2.5 ft (15 to 76 cm) in thickness. It may or may not be bioturbated. This lithofacies is interpreted to have been deposited in a fluctuating current within a floodplain and crevasse-splay setting.

Wavy, Lenticular and Flaser Sandstone (Sw)

Wavy, lenticular and flaser sandstone is a very fine grained sandstone with abundant silt in some samples. This lithofacies is light gray-to-greenish gray, rarely white, with thin beds of < 1 ft (< 30 cm) composed of alternating thin laminations. There is limited bioturbation in this lithofacies, but when present consists of discrete burrows and cryptic bioturbation. The wavy, lenticular and flaser sandstone lithofacies is an indicator of a low-energy depositional setting which, due to changing current strengths, led to alternations between bedload and suspension deposition in the floodplain and crevasse-splay setting.

Conglomeratic Mud-Chip Sandstone (Scg)

The conglomeratic mud-chip sandstone is a very distinctive lithofacies that occurs over scoured surfaces and erosive beds. The matrix is very fine-to-medium sandstone. Clasts are intraformational mudstone. These angular-to-sub-angular mudstone clasts range in diameter from 0.03 to 0.6 in (0.07 cm to 1.5 cm). This lithofacies ranges in thickness from < 1 ft to 6.5 ft (< 30 cm to 2 m). The sandstone is typically light gray-to-light greenish gray, with noticeable common dark carbonaceous debris when it overlies carbonaceous or coal-rich intervals.

The conglomeratic “mud chip" sandstone is interpreted to be high-energy deposit associated with erosional scour processes. Erosion occurred at the base of fluvial channels as result of incision and/or lateral migration of the channel into previously existing floodplain deposits.

Siltstone (ST)

Siltstone is yellowish white-to-light gray, changing to dark gray in some intervals, and is moderately-to-well cemented. The siltstone lithofacies is not commonly thick in the studied cores; and ranges from 0.3 to 4 ft (9.1 cm to 1.2 m) thick. It occurs as massive, contorted and laminated siltstone, and is occasionally bioturbated. These siltstones represent low-energy lithofacies, are typically interbedded with mudstones and/or very fine sandstone, and occur on the top of channel-fill successions as a part of fining-upward fluvial packages.

Horizontal Laminated Sandstone (Shl)

Horizontal laminated, very fine-to-medium grained sandstone is typically light gray, well to moderately sorted, well cemented, sometimes argillaceous, and locally bioturbated. The sandstone is 1 to 8 ft (30.5 cm to 2.4 m) thick, is interbedded sometimes with siltstone and mudstone, and associated locally with rippled and/or low-angle sandstone lithofacies. Horizontal laminae are interpreted to be the down-current toes of migrating sand waves in which the bulk of the sand wave was not preserved. In the studied core, this lithofacies is interpreted to have been deposited in channel fill, crevasse splay, and floodplain settings.

Low-Angle Cross-bedded Sandstone (Sla)

Low-angle (< 10°) cross-bedded sandstone is commonly made up of light gray, greenish gray-to-yellowish white, very fine-to-medium grained, well sorted sandstone that is frequently well cemented and shows low-angle planar cross-bedding. It ranges in thickness from 4 to 20 ft (1.22 to 6 m), and sometimes is associated with slumped bedding and organic carbonaceous coal debris. This lithofacies is interpreted to represent the down current toes of trough cross-bedded sand waves. The low-angle cross-bedded sandstone forms the thick part of many Williams Fork channel-fill deposits and normally overlies conglomeratic mud-chip sandstone. It is also interpreted to also occur in some crevasse-channel deposits.

High-Angle Cross-bedded Sandstone (Sha)

The high-angle (>10°) cross-bedded sandstone is well to moderately sorted, lower very fine to medium-grained, mostly gray to very light gray, and well-cemented. Thickness ranges from 1 to 16 ft (0.3 to 4.9 m). The high-angle laminations are interpreted to represent trough and tabular cross bedding. This sandstone occurs within the lower part of the channel-fill deposits. It overlies conglomeratic mud-chip sandstone and commonly gradually changes upward to low-angle and rippled sandstone.

Mudstone (Ms)

Mudstone lithofacies are common within the studied cores; especially within the low net-to-gross sandstone interval of the lower Williams Fork Formation. Mudstones are light gray-to-black and are occasionally associated and/or interbedded with siltstone. Mudstones range from 0.2 to 12 ft (6 cm to 3.65 m) thick and separate sandstones of crevasses splay and channel-fill lithofacies. Some mudstone intervals are massive and bioturbated, but with minor horizontal and contorted laminations, (0.04 to 0.08 in (1 to 2 mm)). Root structures, soft-sediment deformation, fractures, and siderite concretions are common. This lithofacies commonly overlies fining-upward successions and represents quiet-energy settings of the floodplain, overbank, and levees.

Structureless Sandstone (Ss)

Structureless sandstone does not show lamination or any other sedimentary structure. This dominantly fine- to medium-grained sandstone changes upward to lower coarse-grained sandstone in some intervals (e.g., BT 202 core). It is well cemented, well to moderately sorted, light gray to yellowish white, and measures 0.4 to 8 ft (12 cm to 2.4 m) in bed thickness. The lack of sedimentary structures is interpreted to be caused by pervasive bioturbation. Millimeter-scale circles occur in this sandstone and are interpreted to be very subtle, non-discrete biogenic structures. They are presumed to cryptic bioturbation features generated by meiofaunal activity. This lithofacies is interpreted to have formed in channel-fill and crevasse-splay units.

FACIES ASSOCIATIONS

The twelve Lithofacies have been assigned to three main facies associations: Fluvial Channel (FC), Crevasse Splay (CS) and Floodplain and Swamp (FLS). Each association represents a distinctive environment of deposition based on: 1) lithofacies occurrence, 2) lithofacies stacking patterns, 3) deposit thickness, 4) percentage of sandstone, and 5) organic content.

Fluvial Channel (FC)

Within the Williams Fork Formation, there are stratigraphic intervals with sandstone bodies that exhibit lithofacies successions that commonly include in ascending order: conglomeratic mud-chip sandstone (Scg), high-angle cross-bedded sandstone (Sha), low-angle cross-bedded sandstone (Sla), horizontal laminated sandstone (Shl), structureless very fine-to-coarse grained sandstone (Ss), and ripple cross-laminated sandstone lithofacies (Sr). These sandstone-rich intervals are commonly bounded by erosional basal contacts that truncate underlying beds (Figures 2.1, 2.2, 2.3). Conglomeratic mud-chip sandstones (Scg) and reworked plant and wood fragments often overly the erosional surfaces. Grain size and bedding thickness decrease upward and create a distinct, fining-upward characteristic of the succession.

Collectively the vertical succession of grain size, sedimentary structures, and lithofacies in the sandstone bodies are interpreted to indicate deposition in fluvial channels with an upward decrease in the strength of depositional currents through time. Relatively higher energy currents created the low-to-high angle cross-bedded sandstones. Relatively lower current energy is represented by ripple-laminated sandstones (Sr) in the upper part of the package.

The thickness and amalgamation of the fluvial channel sandstone bodies vary widely depending on stratigraphic position. In the lower Williams Fork, where the fluvial channel sandstone bodies are typically < 16 ft thick (< 4.8 m) and isolated in fine-grained sediments (Figure 2.1). Where amalgamated in the middle and upper Williams

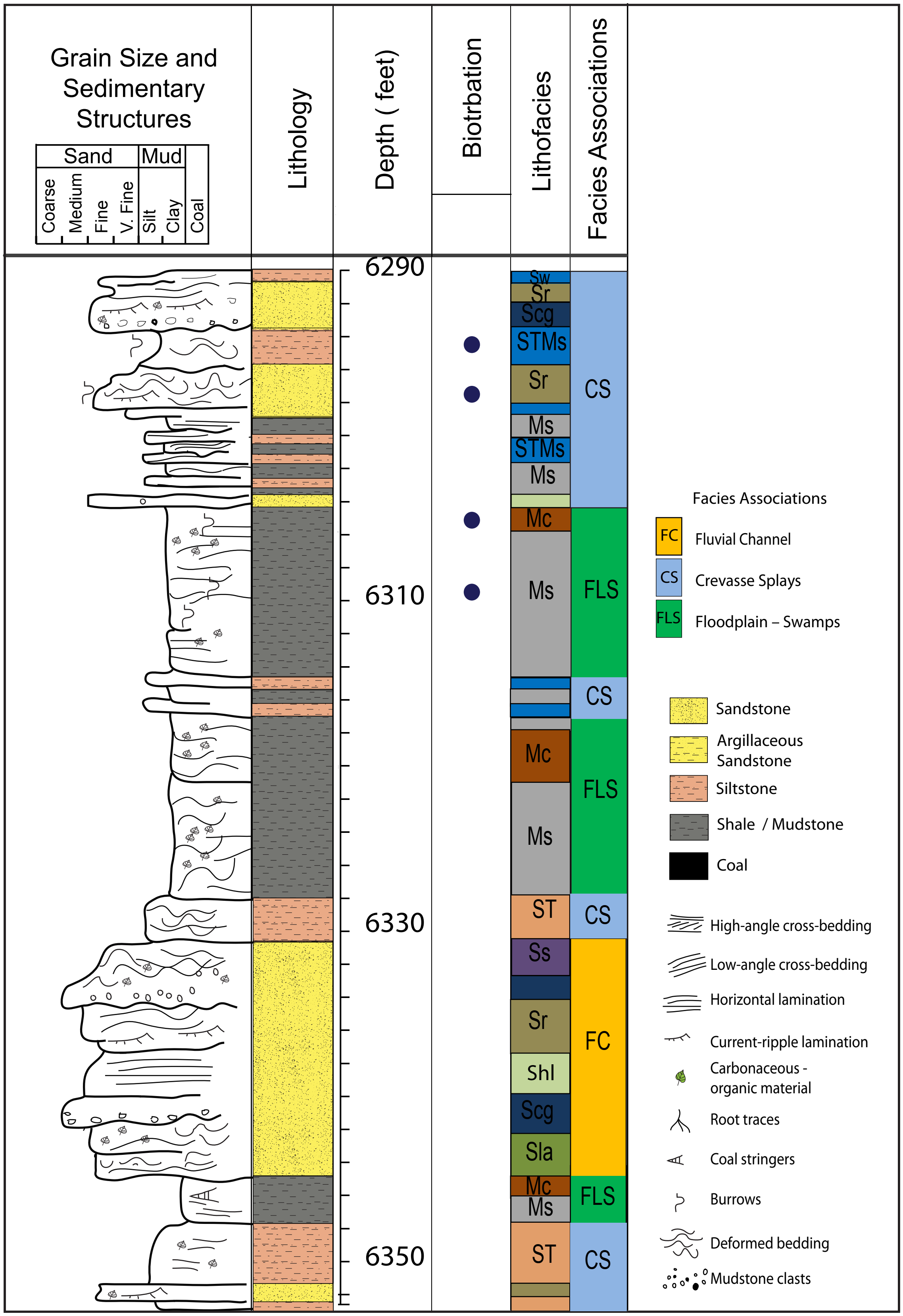
Grain Size and Sedimentary Structures
Sand
Mud
Coarse
Medium
Fine
V. Fine
Silt
Clay
Coal
Lithology
Depth (feet)
Biotrbation
Lithofacies
Facies Associations
6290
6310
6330
6350
Sw
Sr
Scg
STMs
Sr
Ms
STMs
Ms
Mc
Ms
Mc
Ms
ST
Ss
Sr
Shl
Scg
Sla
Mc
Ms
ST
CS
FLS
CS
FLS
CS
FC
FLS
CS
Facies Associations
FC Fluvial Channel
CS Crevasse Splays
FLS Floodplain – Swamps
Sandstone
Argillaceous Sandstone
Siltstone
Shale / Mudstone
Coal
High-angle cross-bedding
Low-angle cross-bedding
Horizontal lamination
Current-ripple lamination
Carbonaceous - organic material
Root traces
Coal stringers
Burrows
Deformed bedding
Mudstone clasts

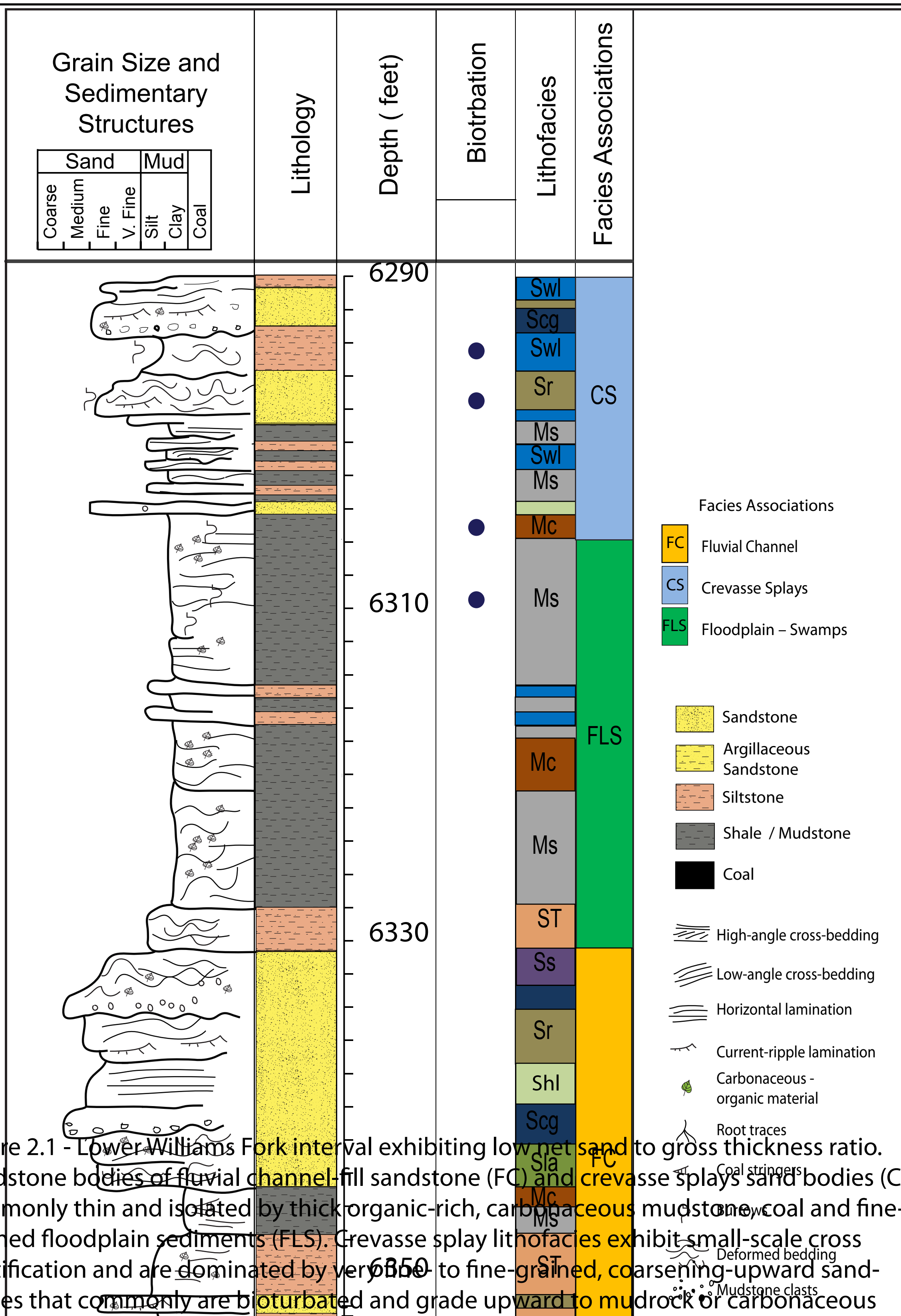

Figure 2.1 - Lower Williams Fork interval exhibiting low net sand to gross thickness ratio. Sandstone bodies of fluvial channel-fill sandstone (FC) and crevasse splays sand bodies (CS) commonly thin and isolated by thick organic-rich, carbonaceous mudstone, coal and fine-grained floodplain sediments (FLS). Crevasse splay lithofacies exhibit small-scale cross stratification and are dominated by very fine- to fine-grained, coarsening-upward sandstones that commonly are bioturbated and grade upward to mudrock or carbonaceous mudstones. Last Dance 43C-3-792 core. See Table 2 for lithofacies codes.

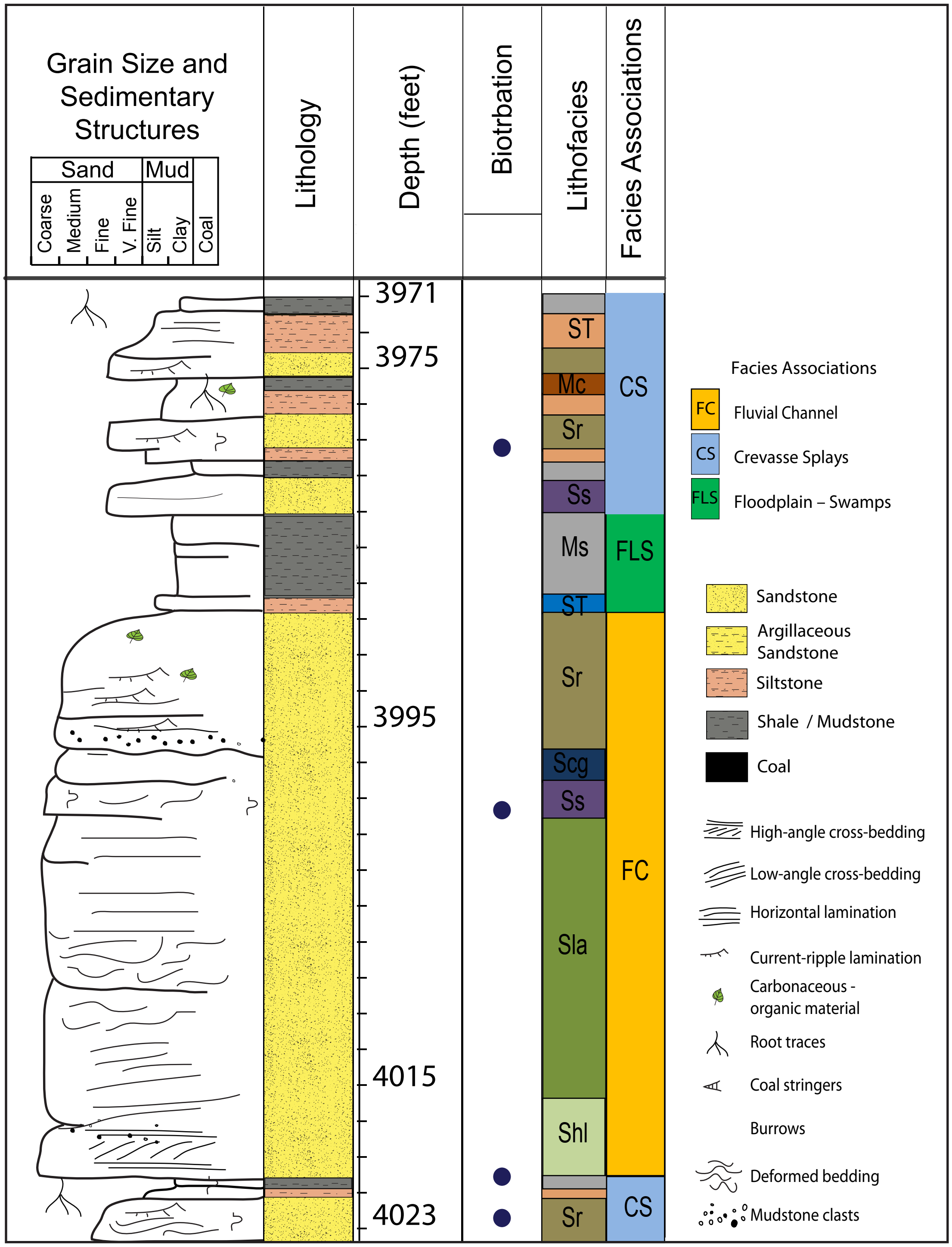

Figure 2.2 – Fining-upward succession of fluvial channel deposits from the middle Williams Fork interval. High-energy fluvial channels (FC) contain abundant cross-stratified sandstone. Lag deposits and an erosional base mark the bottom of the channel succession. The channel-fill sandstones exhibit upper-flow regime sedimentary structures that gradually change upward to lower-energy rippled sediments. The succession is capped by organic-rich, rooted and mudstone-rich floodplain sediments (FLS). Last Dance 43C-3-792 core. See Table 2 for lithofacies codes.

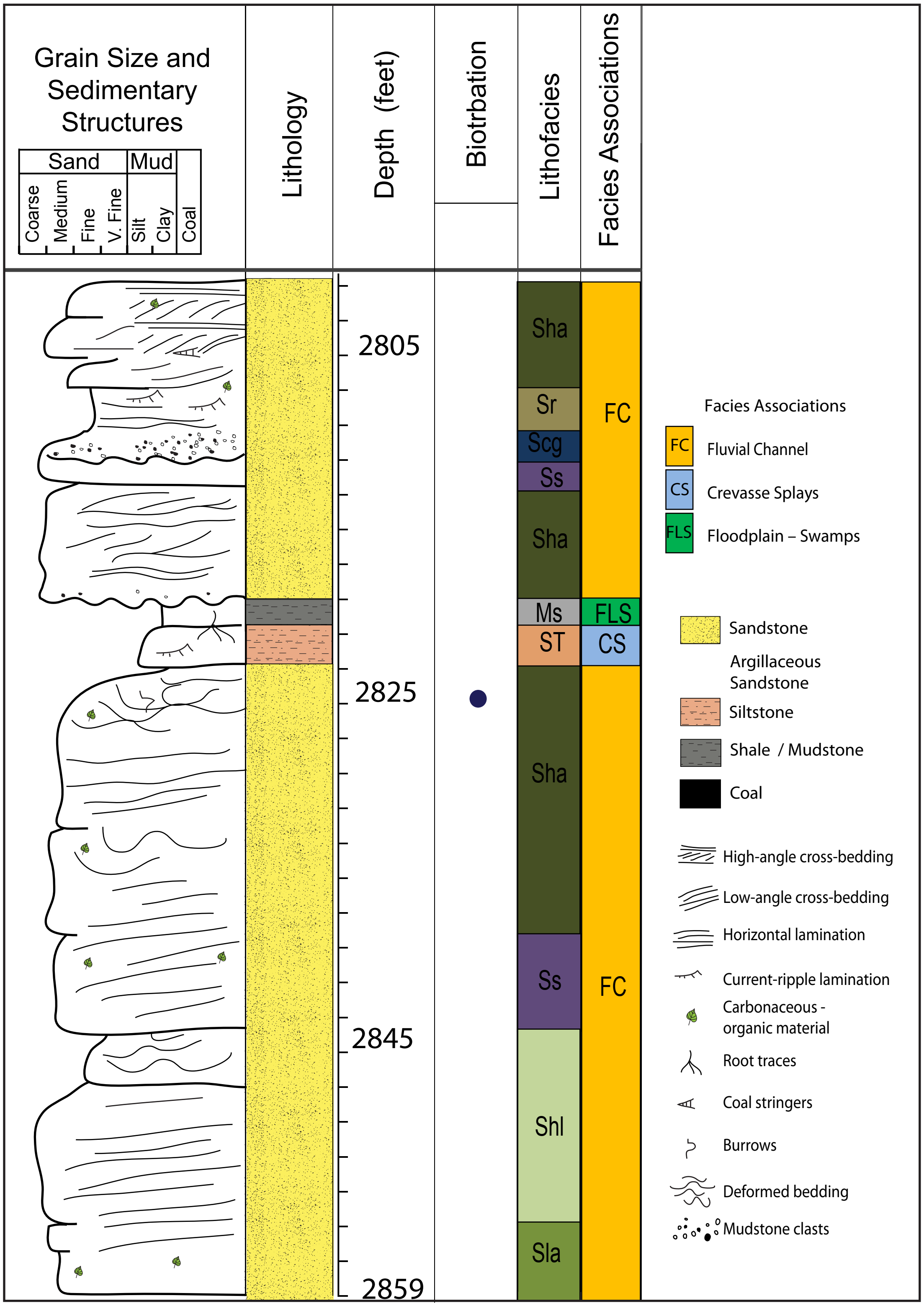

Figure 2.3 - Upper Williams Fork amalgamated sandstones showing repeated fining-upward successions. The sand bodies are commonly bounded by conglomeratic mud-chip sandstone (Scg that overlies an erosional basal contact. Last Dance 43C-3-792 core. See Table 2 for lithofacies codes.

Fork intervals, the channel sandstones form bodies that are up to 42 ft (12.8 m) in thickness (Figure 2.3).

The net-to-gross sandstone ratio is much less in the lower stratigraphic interval than the middle to upper Williams Fork intervals. The cored lower Williams Fork Formation net sandstone to gross thickness ratio ranges from 15 to 35%. For comparison, the lower Williams Fork Formation as exposed in Coal Canyon has an average net sandstone to gross thickness ratio of 15% (Pranter et al., 2007, 2009) and is interpreted to have been deposited by anastomosing to meandering rivers in a coastal-plain setting (Lorenz, 1987; Johnson, 1989; Cole and Cumella, 2005; Patterson et al., 2003; Pranter et al., 2007, 2009). In the cores, amalgamated sandstones of the middle to upper Williams Fork Formation exhibit a net sandstone to gross thickness of 72% to 83%. These sandstone bodies have been interpreted to be deposited within a low-to-moderate sinuosity braided-fluvial system (Lorenz et al., 1985; Johnson, 1989; Cole and Cumella, 2005; German, 2006). The depositional setting differences between the lower and upper Williams Fork formations are most probably caused by changing basin subsidence rates and relative sea-level changes, which combined to control accommodation space during the Late Cretaceous in the Piceance Basin. Higher net-to-gross sandstone ratios were deposited under low accommodation conditions and the lower net-to-gross ratio intervals were deposited under higher accommodation conditions (Patterson et al., 2003).

Crevasse Splay (CS)

The Williams Fork Formation consists of some intervals that exhibit lithofacies successions dominated by mudstone, siltstone, and very fine-to-medium grained sandstones. These successions range from 1 to 4.5 ft (30.5 cm to 1.4 m) in thickness and have an average net-to-gross ratio of 25%. All have fining-upward grain size trends and a number of facies can occur in this association. In ascending order, these include low-angle cross-bedded sandstone (Sla), horizontal-laminated sandstone (Shl), ripple cross-laminated sandstone (Sr), interbedded siltstone and mudstone (STMs), wavy, lenticular and flaser sandstone (Sw), siltstone (ST), mudstone (Ms), and carbonaceous mudstone (Mc) that exhibits high amount of organic matter, including plant fragments and occasionally coal. Some of these lithofacies successions have basal scours and sharp grain-size changes at those surfaces. Most of these lithofacies are not present in any one example as illustrated in Figure 2.1 where ripple cross-laminated sandstone (Sr) are isolated in alternating thin beds of interbedded siltstone and mudstone (STMS) at the top of the displayed interval.

These successions are interpreted to be crevasse splay deposits based on their sharp bases, very fine- to fine-grained sand sizes, and intercalations of siltstone and mudstone. They formed by sediment deposition as a consequence of a breach in the river channel when the fluvial system was at flood stage.

Similar descriptions of an exposed lithofacies succession within the Williams Fork Formation in Coal Canyon were given by Cole and Cumella (2005). They interpreted the very fine-to-fine grained sandstone bodies to be crevasse splays. The thickness of these sandstone bodies ranged from 0.5 to 6.5 ft (15 cm to 2 m) with an average of 2.8

ft (85 cm), while the width-to-thickness ratio ranged from 22 to 464 and averaged 119 (Cole and Cumella, 2005). Pranter and others (2009) measured 279 sandstone bodies in the same location that they also interpreted to be crevasse splays. They found a mean width-to-thickness ratio of 94.6, and range in thickness from 0.5 to 15.0 ft (0.2 to 4.6 m), and 40 to 844 ft (12.2 to 257 m). Recently, Harper (2011) described similar facies within the lower Williams Fork Formation of the Douglas Creek Arch, Colorado. There, the crevasse splay sandstone bodies have apparent widths ranging from 7.4 to 67.5 ft (2.3 to 20.6 m) and maximum thicknesses between 0.3 and 4 ft (0.1 to 1.2 m). The mean value of apparent width is 30.6 (9.3 m) and a maximum thickness of 1.1 ft (0.3 m) (Harper, 2011). In another related description of similar facies successions within the Upper Campanian strata of the Neslen and Mount Garfield Formations, Kirschbaum and Hettinger (2004) reported crevasse splays that are sharp based, ripple laminated, up to 15 ft (4.5 m) thick, and characterized by slightly inclined bounding surfaces.

Floodplain – Swamp (FLS)

Lithofacies successions dominated by mudstone and organic-rich bioturbated fine-grained sediment include the following facies: carbonaceous mudstone (Mc), coal (C), wavy, lenticular and, flaser-laminated sandstone (Sw), siltstone (ST), horizontally laminated sandstone (Shl), mudstone (Ms), and interbedded siltstone and mudstone (STMs). Of these, the mudstone (MS) dominate (Figure 2.1), representing from 40 to 70% of the lower Williams Fork Formation and between 20% and 50% of the middle and upper Williams Fork interval. When present, coals exhibit sharp contacts.

Carbonaceous mudstone and mudstones of these lithofacies successions commonly cap coarser sediment of crevasse splays (CS) and/or fluvial channel facies associations (FC) and form the top of fining-upward facies succession.

Mudstone-rich stratigraphic intervals range from <1 ft and up to 50 ft (< 0.3 m to 15 m) in thickness, and are heavily bioturbated. There is limited siltstone and sandstone associated with this mudstone-dominated facies succession, but when present they are thin and argillaceous. Some mudstone and silty mudstone facies show high organic content that include roots, plant debris, and woody fragments.

The mudstone-rich lithofacies successions are attributed to be floodplain deposits; coal and carbonaceous mudstone are interpreted to have formed in swamps and marshes on the floodplain. Deposition of suspended sediments in flood waters formed the mudstone. Such deposits typically form in areas with low relief and slow rates of accumulation (Davies, 1983). Cole and Cumella (2005) also identified eight mudstone-rich lithofacies based on thickness, mudrock lithology, color-and-organic content and bioturbation within the Williams Fork Formation in Coal Canyon. They too interpreted these mudrock facies to have formed within floodplain, marsh, and swamp settings. The thin and intercalated argillaceous sandstones and siltstones probably represent distal or small crevasse splay deposits, but are grouped in the floodplain association due to their isolation in the mudstones.

CHAPTER THREE: DETRITAL COMPONENTS OF WILLIAMS FORK SANDSTONES

INTRODUCTION

The petrographic study of the Williams Fork Formation is based on the petrographic analysis and point counts of 220 thin sections (400 point counts per slide). In addition, 30 samples were analyzed by scanning electron microscopy and bulk and clay fraction XRD analysis were done on 20 samples. The numerical and statistical results of the thin-section petrography are tabulated in Appendix 1.

Sample selection criteria for thin-section analysis were (1) insure coverage of each facies, (2) include sandstones from the entire stratigraphic framework, and (3) cover the range of porosity and permeability values observed. Thin section selections were made to ensure that all sequence stratigraphic components were covered so that observations could be compared across depositional and sequence-stratigraphic settings, e.g. highstand sandstone compared to other highstand sandstones. The results are presented according to the three main stratigraphic divisions: lower Williams Fork paludal zone (coastal plain sandstones), middle Williams Fork fluvial zone, and upper Williams Fork fluvial zone.

SANDSTONE CLASSIFICATION

The main detrital minerals in Williams Fork sandstones are quartz, feldspar and lithic fragments. Main authigenic components (Chapter 4) include quartz, clay (illite, illite/smectite mixed-layer, chlorite and kaolinite), carbonates (including calcite, ferroan calcite, dolomite, and ferroan dolomite), and albite (Appendix 1). These findings are consistent with previous studies (e.g. Pitman et al., 1989). The sandstones are not homogeneous mineralogically and texturally but have variations in detrital composition that are controlled by stratigraphic zonation.

Using the classification scheme of Folk (1980), the Williams Fork sandstones range from lithic arkose to litharenite (Figure 3.1). Changes in feldspar and lithic fragment contents are what produce different sandstone types. Upper and middle Williams Fork intervals are relatively more feldspar rich, whereas the lower Williams Fork interval is lithic-rich. Specifically, the paludal sandstones of the lower Williams Fork Formation are litharenites and feldspathic litharenites. Very few samples are sublitharenites. The fluvial intervals of the middle Williams Fork sandstone are feldspathic litharenite and lithic arkose. The fluvial interval of the upper Williams Fork and Ohio Creek formations is mostly feldspathic litharenite with a limited number of samples being either litharenite or lithic arkose (Figure 3.1).

TEXTURE

Textural variations in Williams Fork sandstones are a function of facies, not stratigraphic zonation. Overall the Williams Fork sandstones are mostly very fine- to fine-grained sands with some medium-grained sands at the base of channel fills, particularly in the upper Williams Fork interval. Sorting varies greatly and ranges from well to poorly sorted (Figure 3.2). Sorting is a function of facies and depositional setting, with mostly well-sorted sands in channel fills and thicker (proximal) crevasse splays. Thinner splay sandstones that probably formed farther from the channels are moderately argillaceous (Figure 3.3 A), with some forming wackes rather than arenites.

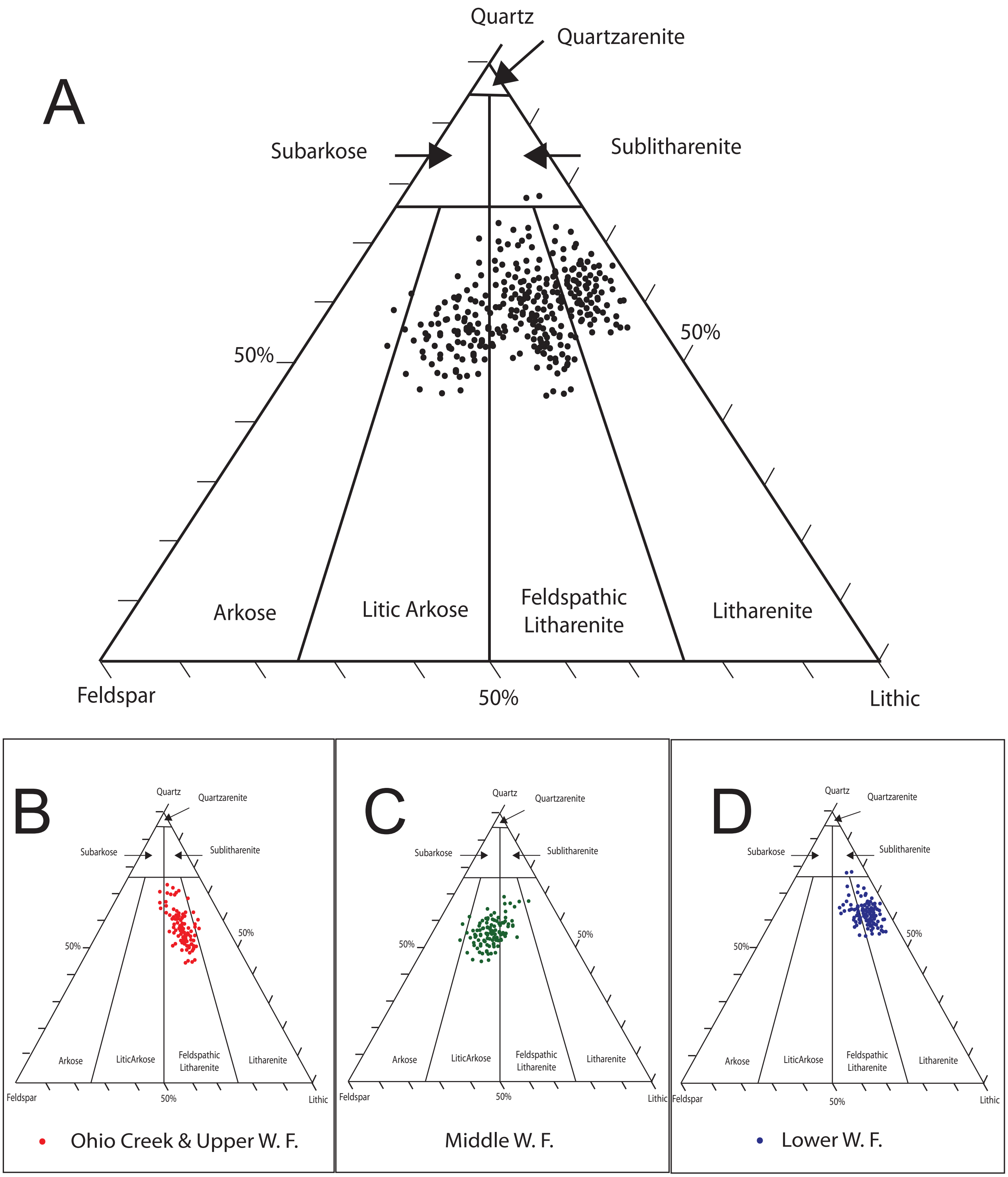

Figure 3.1 - A) Classification of the detrital mineralogy of all Williams Fork sandstones based on the scheme of Folk (1980). B, C and D) Detrital mineralogical composition of lower Williams Fork, middle Williams Fork and Ohio Creek and upper Williams Fork intervals, respectively.

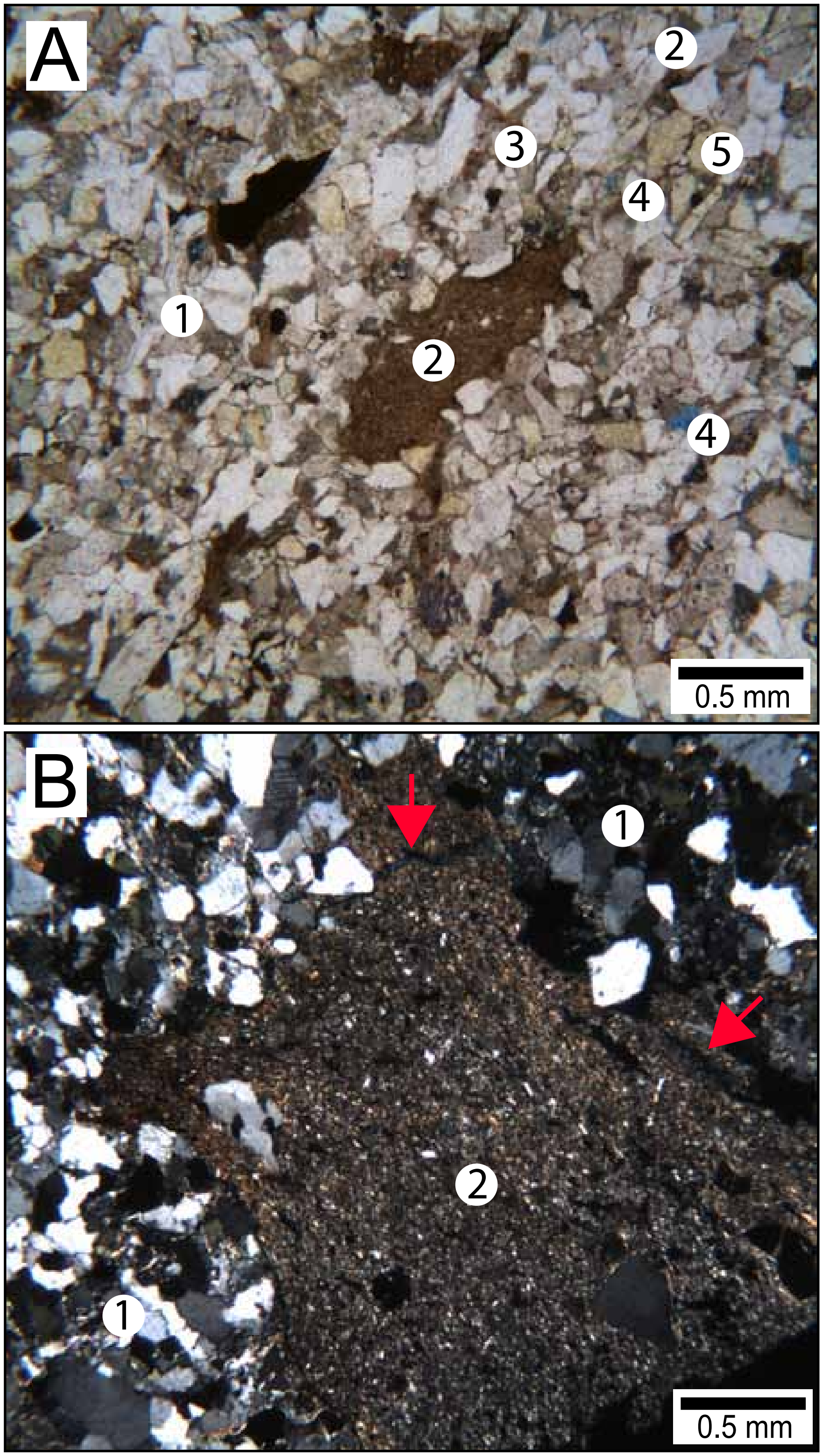
A
2
3
5
4
1
2
4
0.5 mm
B
1
2
1
0.5 mm

Figure 3.2 - Thin-section photomicrographs (A) Parachute 4644', plane light, and (B) Parachute 4575', cross nicols, showing sandstone textural examples. (A) Moderate to poorly sorted and sub-rounded to sub-angular grains. The sandstone is highly compacted (1). Pseudomatrix (2) formed from compacted mud clasts and infiltrated clay (3) in primary pores. The porosity in the samples is secondary due to micro fractures (arrows) and dissolution of K-feldspar (4), some of which remains (5). Note the bimodal texture of the sandstone in (B) due to the presence of a coarse-grained detrital mudstone clast.

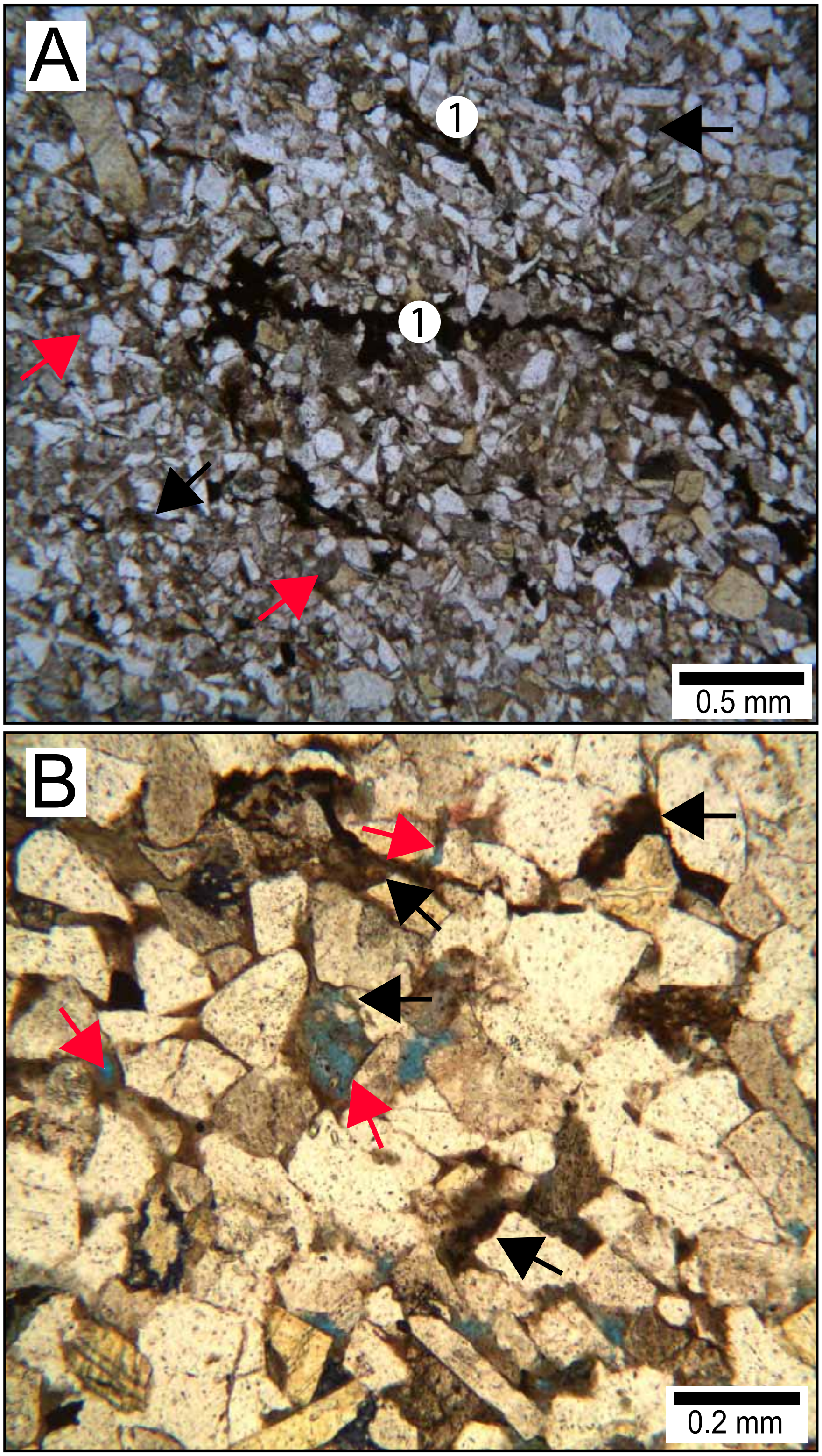

Figure 3.3 - Thin-section photomicrographs (A) Parachute 4631', plane light, and (B) Parachute 6452', plane light, showing sub-angular to sub-round argillaceous sandstone. Pseudomatrix of compacted mud clasts and detrital clay minerals (black arrows) occlude most of the inter-granular porosity. Because of pervasive compaction and interstitial clay minerals, the secondary pores (red arrows) lack well-developed interconnections. (A) Insoluble clays and organic matter are concentrated in stylolite seams (1).

Grains are sub-rounded to sub-angular. With the exception of the behind outcrop BT202 core samples, all analyzed sandstones are moderately-to-highly compacted, as evidenced by abundant long, concave-convex, and sutured grain contacts (Figure 3.4). The BT 202 core exhibits little sandstone compaction as indicated by the predominance of point contacts between grains (Figure 3.5).

FRAMEWORK GRAINS

Quartz

The principal detrital grain in the Williams Fork sandstones is quartz. Both strained and unstrained quartz is present, and many grains display undulatory-to-straight extinction. Monocrystalline quartz is the most common, as very few polycrystalline quartz grains were noted in all intervals (Figure 3.6). In the context of each rocks' entire mineralogy (detrital and authigenic), quartz ranges from 10 to 65% of a sample (Figure 3.7) and averages 40.9% $\pm$ 9.0% (1σ). The range of quartz abundance varies between the upper (28-62%), middle (10-58%), and lower Williams Fork (30-56%) intervals, but mean and median values are similar for all intervals. In the context of just detrital components, quartz is more common in the lower Williams Fork sandstones and least abundant in middle Williams Fork sands (Figure 3.1).

Feldspar

Detrital feldspar in the Williams Fork Formation includes both plagioclase (twinned and untwinned) and potassium feldspars, and can be either fresh or altered. The fresh grains are mostly angular-to-subangular and show twinning. The altered

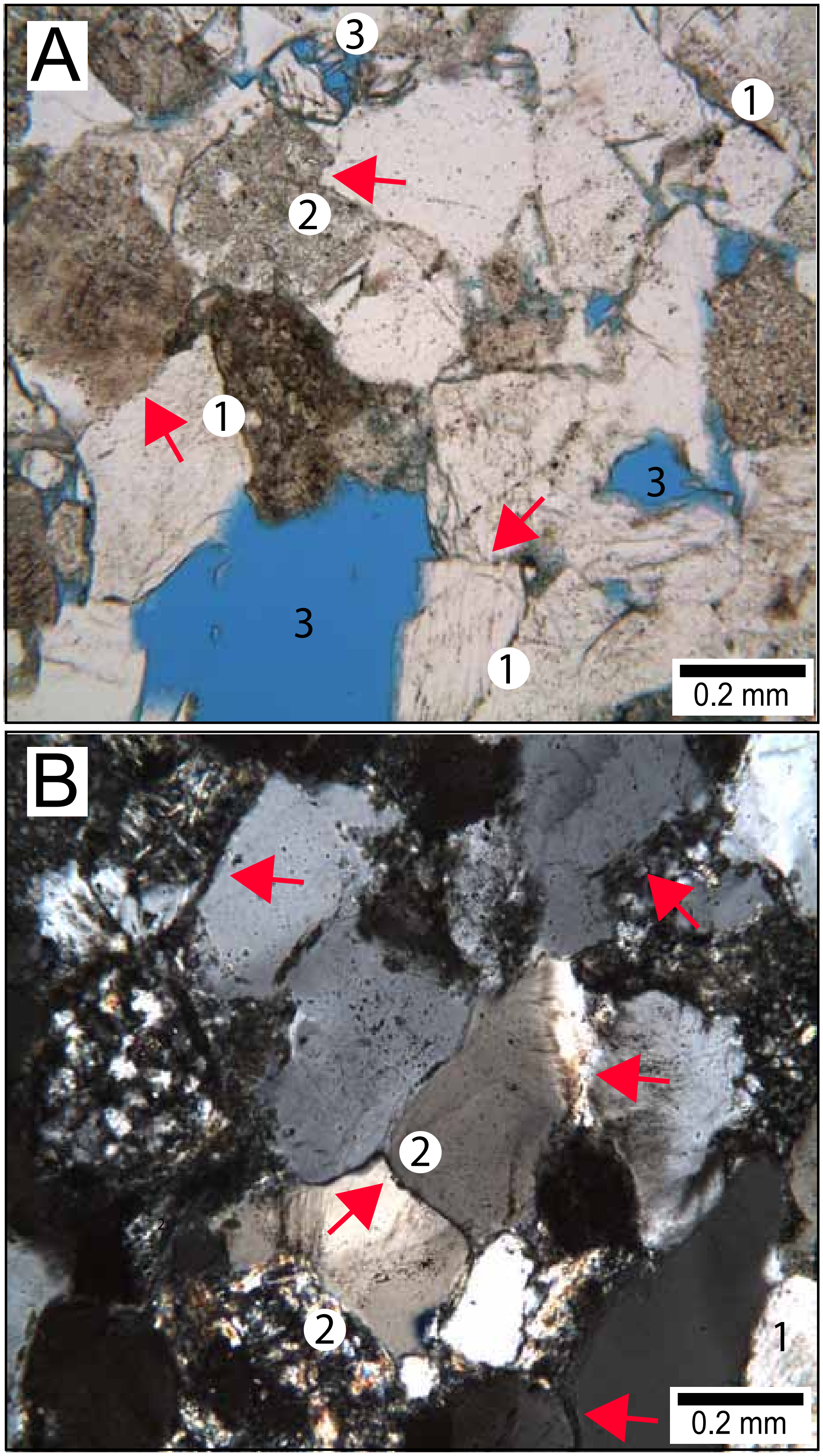

Figure 3.4 - Thin-section photomicrographs (A) Last Dance 3556', plane light, and (B) Last Dance 3995', cross nicols, showing compaction effects. Grains commonly have long contacts (1), but sutured and concave-convex contacts also exist (2). Note the pressure solution resulted from grains dissolve at contact points (red arrows). All initial primary porosity is lost to compaction and cementation. The present porosity (3) is secondary due to dissolution, most likely of feldspars.

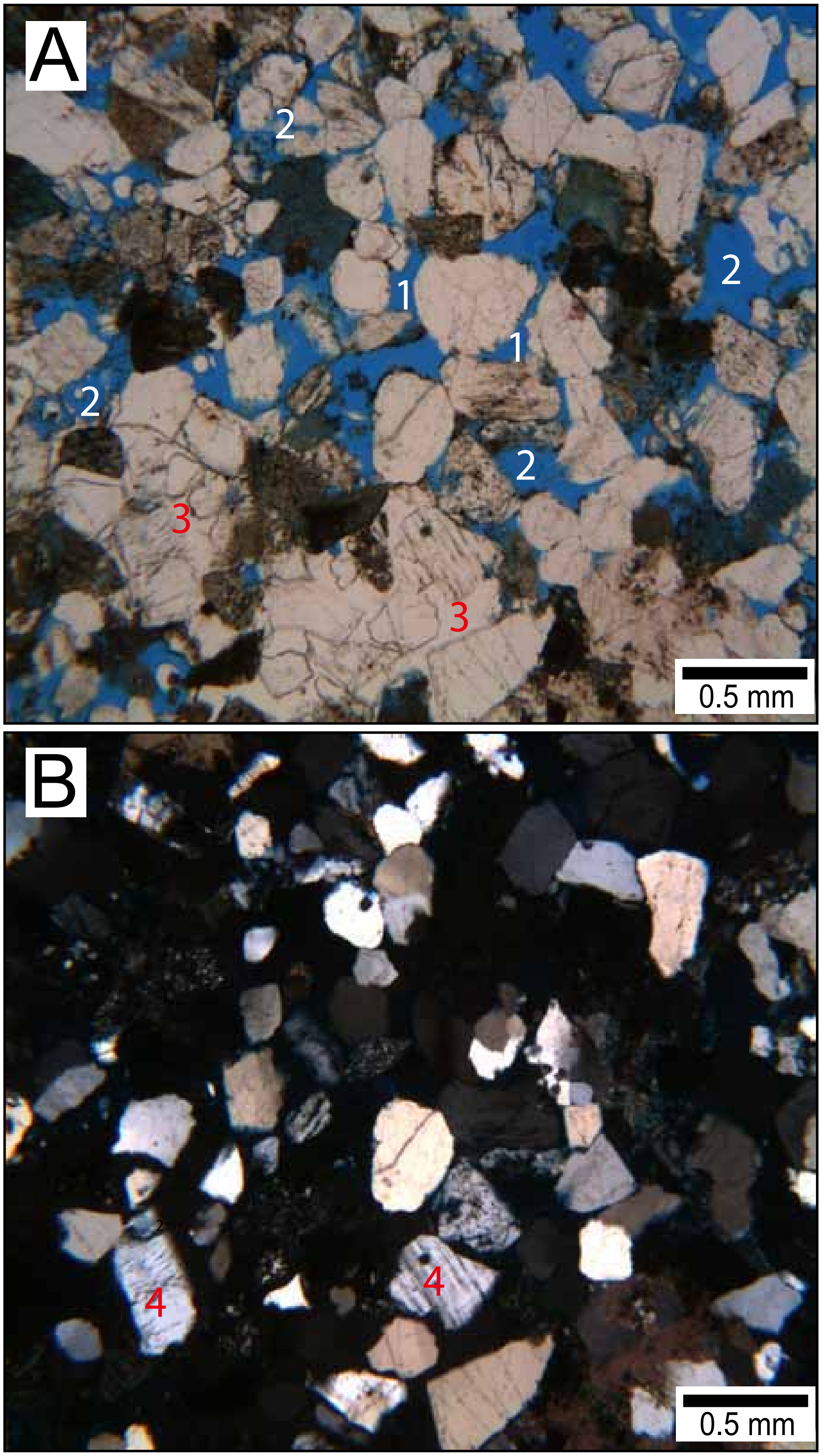

Figure 3.5 - BT 202 130’ in plane light (A) and (B) cross nicols. This is a highly porous sandstone due to dissolution of cement (1) and grains (2) . Note floating grains and predominance of point contacts between grains. Compaction was prevented by early cementation (3). Feldspar grains (4) look fresh where isolated by cement but are partly to totally dissolved (2) when not surrounded by cement.

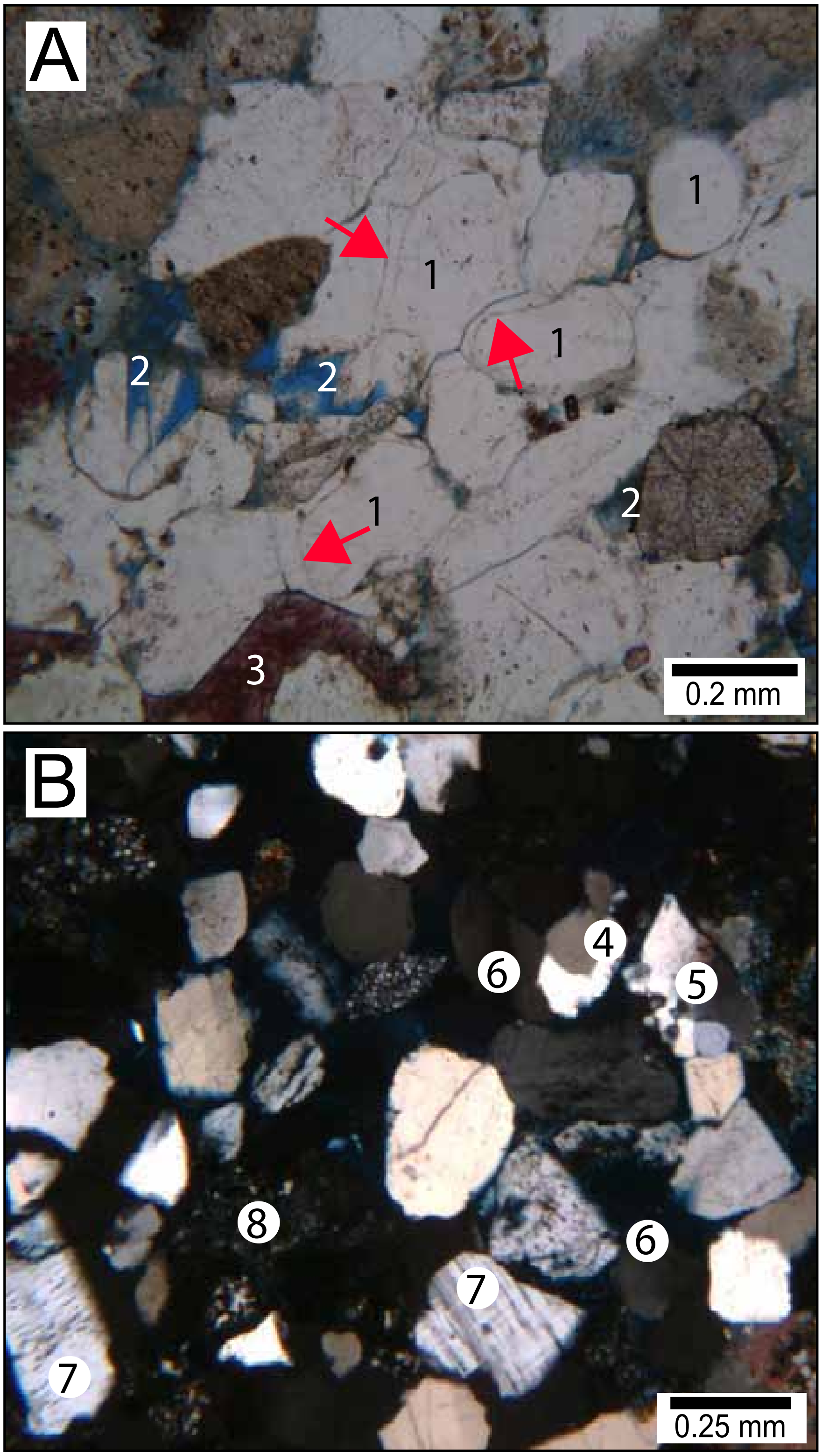
A
1
1
1
1
2
2
2
3
0.2 mm
B
4
5
6
6
7
7
8
0.25 mm

Figure 3.6 - Thin-section photomicrographs (A) Oxy 5331’, plane light, and (B) BT 202 130’, cross nicols, showing monocrystalline and polycrystalline quartz grains. (A) Sandstone dominated by monocrystalline quartz grains (1) and cemented by quartz overgrowths (arrow). Some grains and silica overgrowth were dissolved and increased secondary porosity (2). Ferroan calcite as late cement (3) replaces earlier silica cement and fills intergranular pores. (B) Polycrystalline quartz consists of two sub grains (4) and polycrystalline quartz consists of more than two sub grains (5). Note undulose monocrystalline quartz (6), feldspar (7), and chert (8).

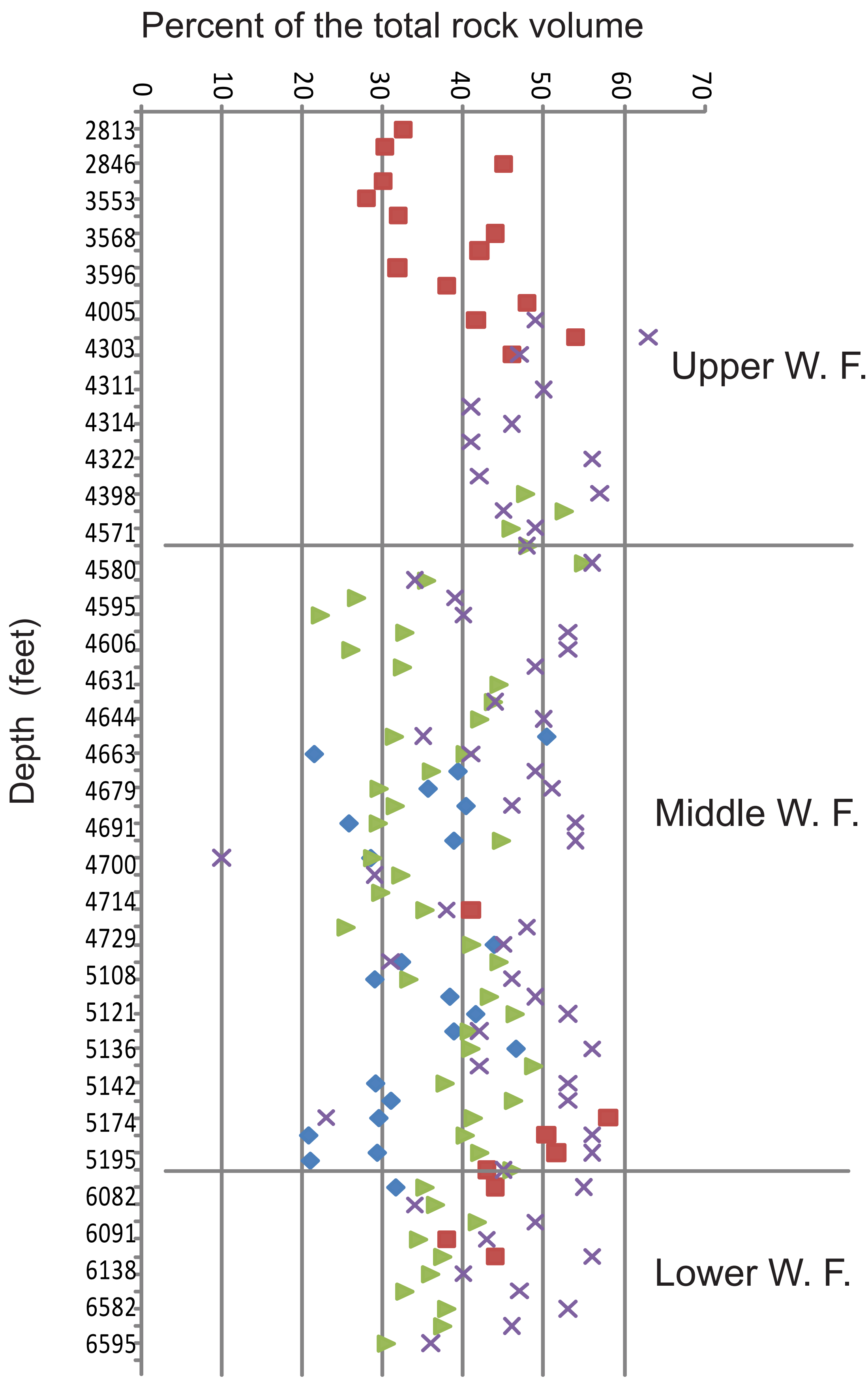
Percent of the total rock volume
0
10
20
30
40
50
60
70
Depth (feet)
2813
2846
3553
3568
3596
4005
4303
4311
4314
4322
4398
4571
4580
4595
4606
4631
4644
4663
4679
4691
4700
4714
4729
5108
5121
5136
5142
5174
5195
6082
6091
6138
6582
6595
Upper W. F.
Middle W. F.
Lower W. F.

Figure 3.7 - Abundance of quartz within the Cascade Creek # 697-20-28 (Oxy), Last Dance # 43C-3-792 (LD), PA 424-34 Parachute (PA), and MWX1 wells. Core depths of individual samples are plotted, thus depth scale is not continuous.

grains, which are common and appear cloudy, are typically altered to clays (Figure 3.8) or replaced by carbonates (Figures 3.9, 3.10). In addition, many detrital feldspars are affected by dissolution (Figure 3.11) or albitization (Chapter 4).

The relative abundance of both plagioclase and potassium feldspar varies with depth in the Williams Fork Formation, as illustrated in Figure 3.12 for the PA 424—34 core. For all cores of the upper Williams Fork interval, plagioclase is 4-25% of the rock- and potassium feldspar is 2 to 11 percent of the rock. In the middle Williams Fork interval, plagioclase feldspar ranges from <1% to 22% of the rock volume whereas potassium feldspar is <1% to 21%. In the lower Williams Fork interval, the feldspars are mostly plagioclase (0-11%) with potassium feldspar being less than 2% and typically nonexistent. The downward decrease in the abundance of potassium feldspar actually begins in the lower half of the middle Williams Fork interval (Figure 3.12). At depth, some original feldspar grain structure and/or very limited patches of potassium feldspar can still be seen, but authigenic carbonate almost totally replaces the original grains (Figure 3.9).

Lithic Rock Fragments

Lithic fragments compose 15-40% of all detrital grains in the Williams Fork sandstones (Figure 3.1) and are primarily sedimentary rock fragments (Figure 3.13). Chert is the dominant rock fragment and makes up to 16 percent of the rock volume in some samples. Other sedimentary rock fragments are shale, mudstone, siltstone, limestone, and dolomite (Figures 3.2, 3.14). Commonly the mudstone and shale clasts have been compacted and deformed into pseudomatrix (Figures 3.2, 3.3, 3.15, 3.16,

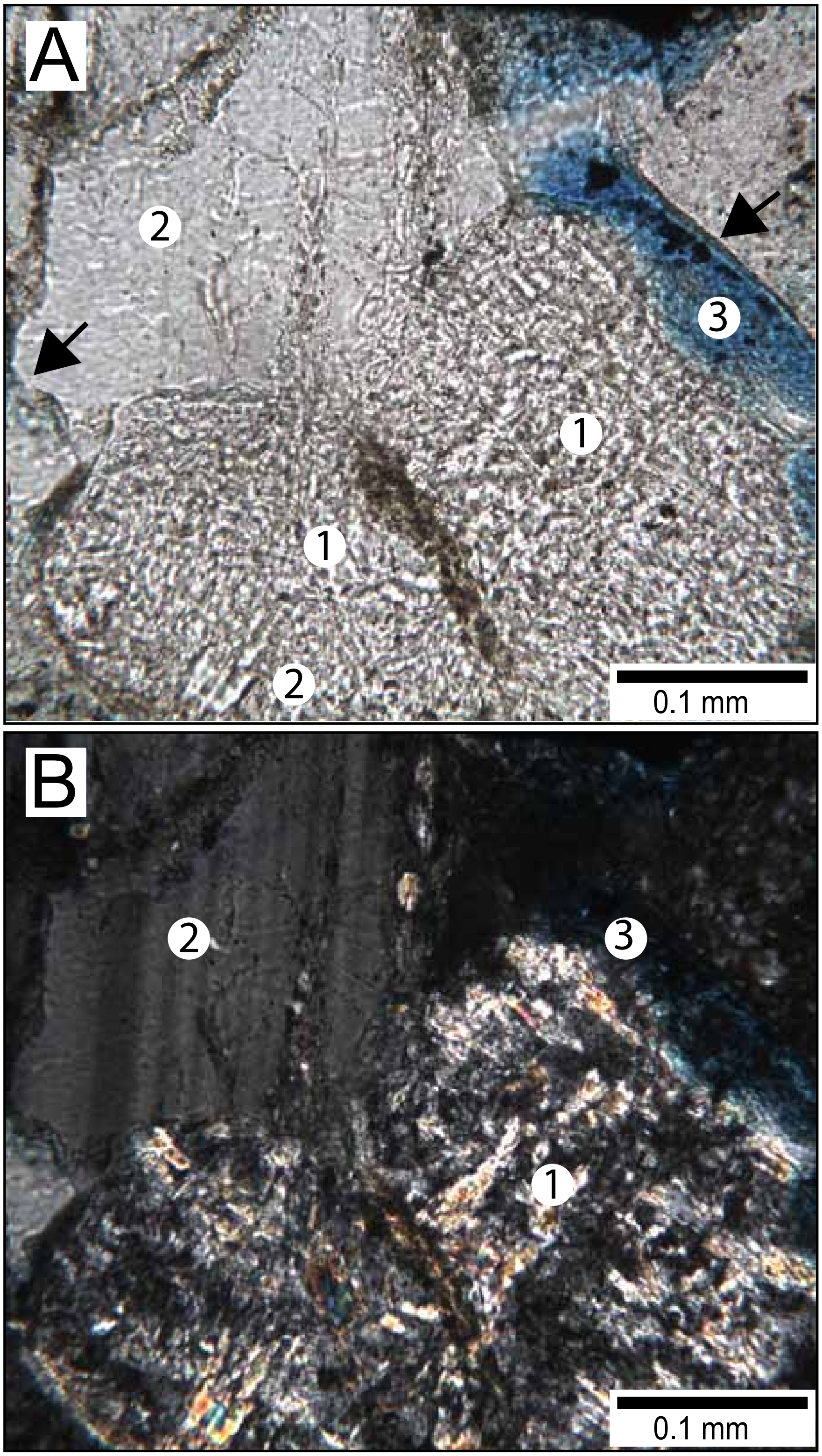

Figure 3.8 - Thin-section photomicrographs Oxy 4834', (A) plane light and (B) cross nicols. Highly altered feldspar grain (1) replaced by authigenic clay. Plagioclase grain (2) exibits very little clay replacement. Partly dissolved edge of the clay-replaced grain enhances secondary porosity (3). Late authigenic clay occurs on grain boundaries in secondary pores (arrows).

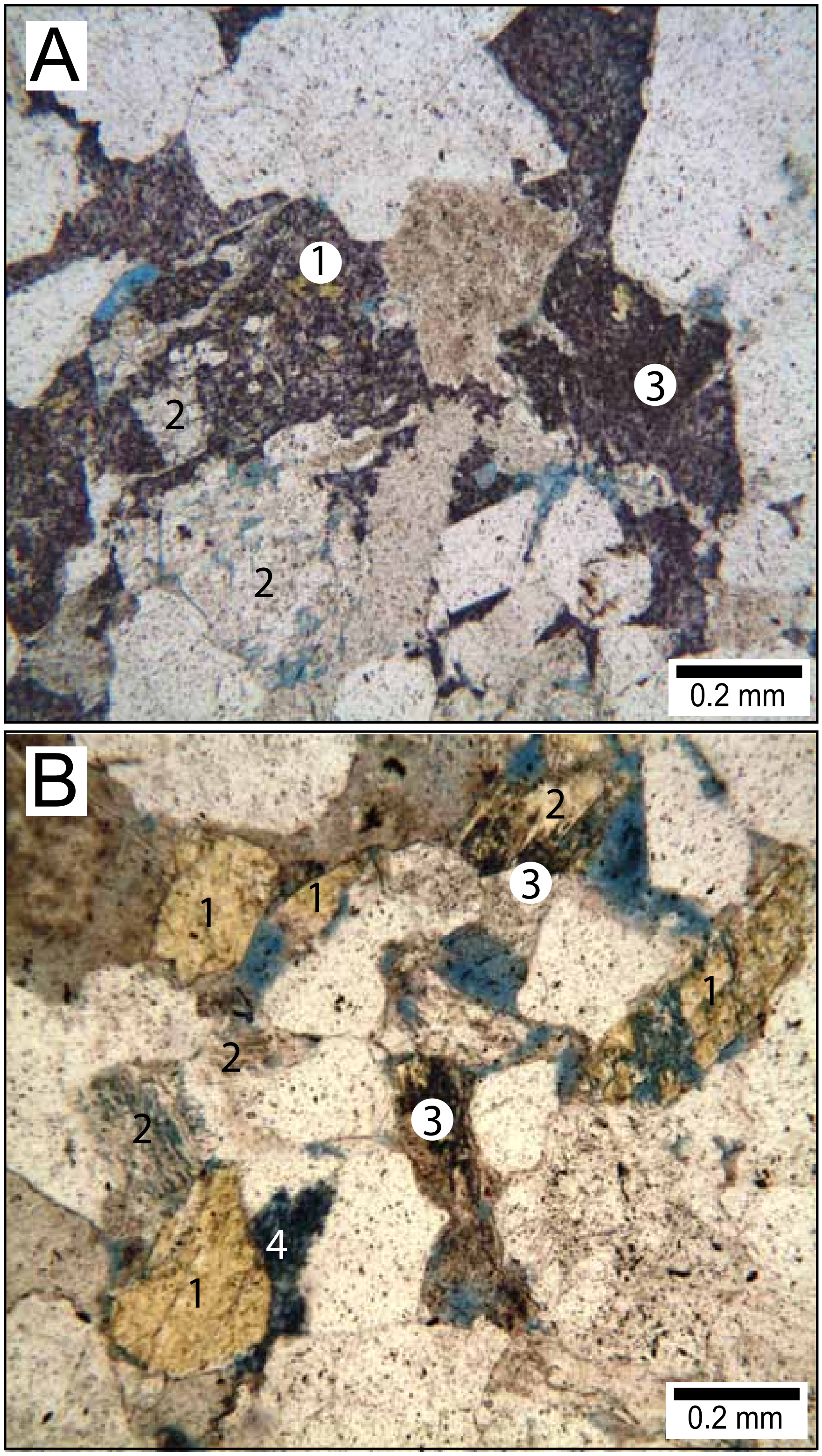
A
1
2
3
2
0.2 mm
B
2
3
1
1
1
2
2
3
4
1
0.2 mm

Figure 3.9 - Thin-section photomicrographs (A) Parachute 4586’, plane light and (B) Parachute 4580’, plane light, showing potassium feldspar (1) and plagioclase (2) grains that are partly dissolved and partly replaced by carbonates. (A) Potassium feldspar and plagioclase grains are replaced by ferroan calcite (3). Note that only limited patches of yellow-stained potassium feldspar can still be seen. (B) Some feldspar grains are selectively replaced by ferroan calcite (3) or ferroan dolomite (4). Porosity (blue) is secondary due to dissolution.

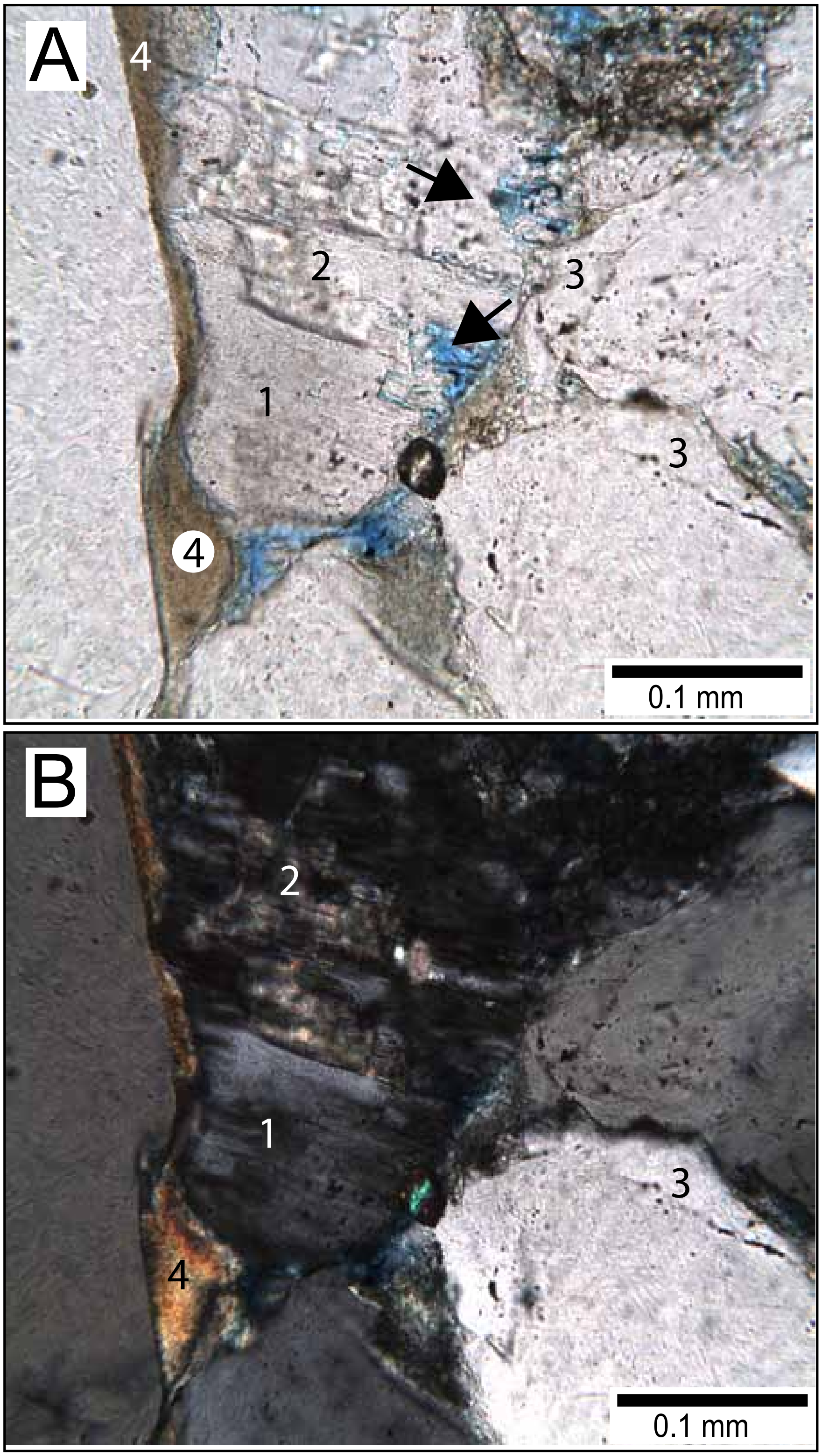

Figure 3.10 - Thin-section photomicrographs Oxy 4809', (A) plane light and (B) cross nicols. Plagioclase grain (1) is partly replaced by calcite (2). The feldspar also partly dissolved (black arrows) forming secondary porosity. Silica cement (3) and infiltrated clays (4) occupy initial porosity.

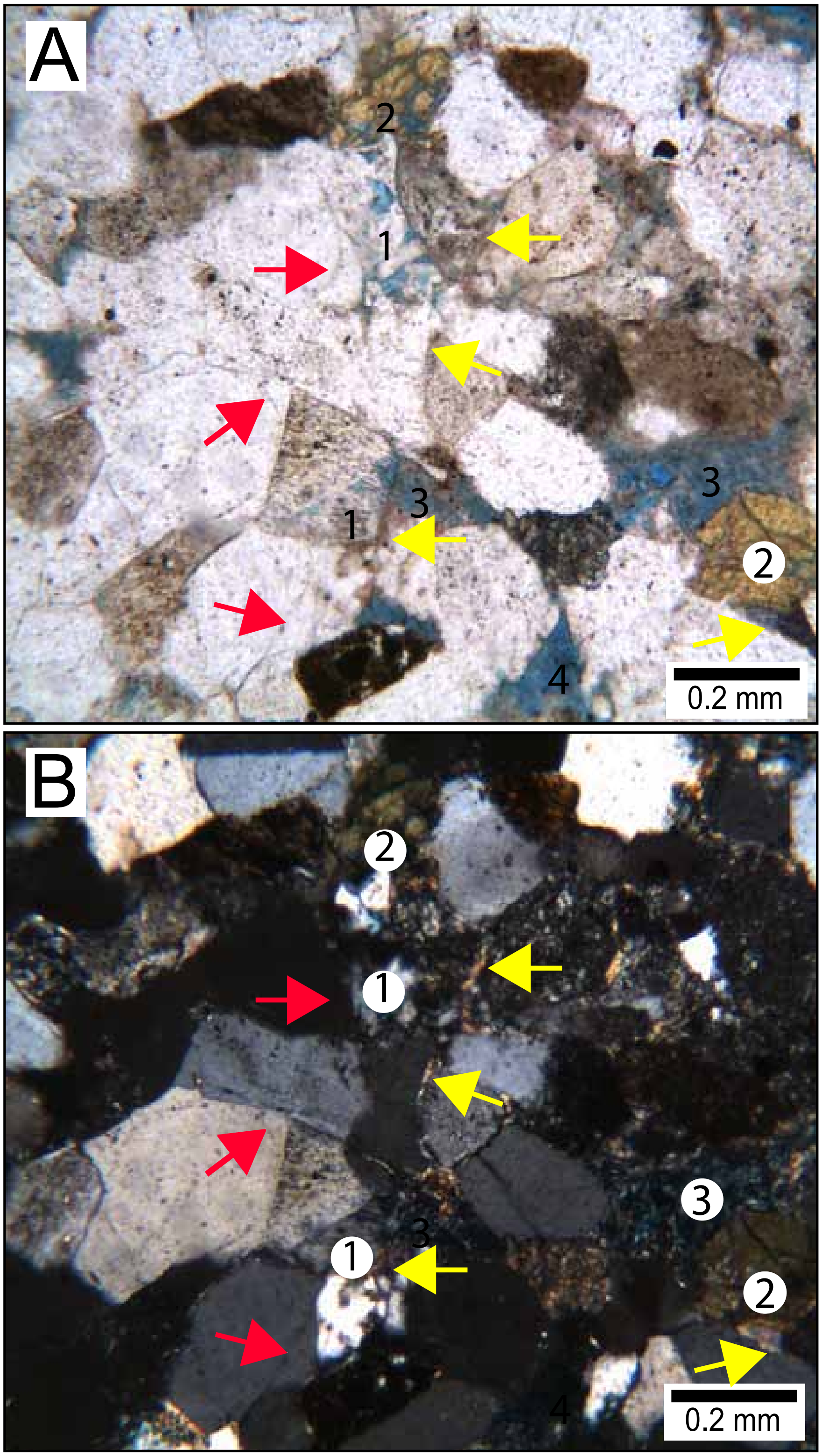

Figure 3.11 - Thin-section photomicrographs Parachute 5195’, (A) plane light and (B) cross nicols, showing partly dissolved plagioclase (1) and potassium feldspar (2). Silica overgrowth (red arrows) and carbonate cement (yellow arrows) occupy initial porosity. Intergranular porosity (3) and intragranular porosity (4) are secondary due to feldspar dissolution.

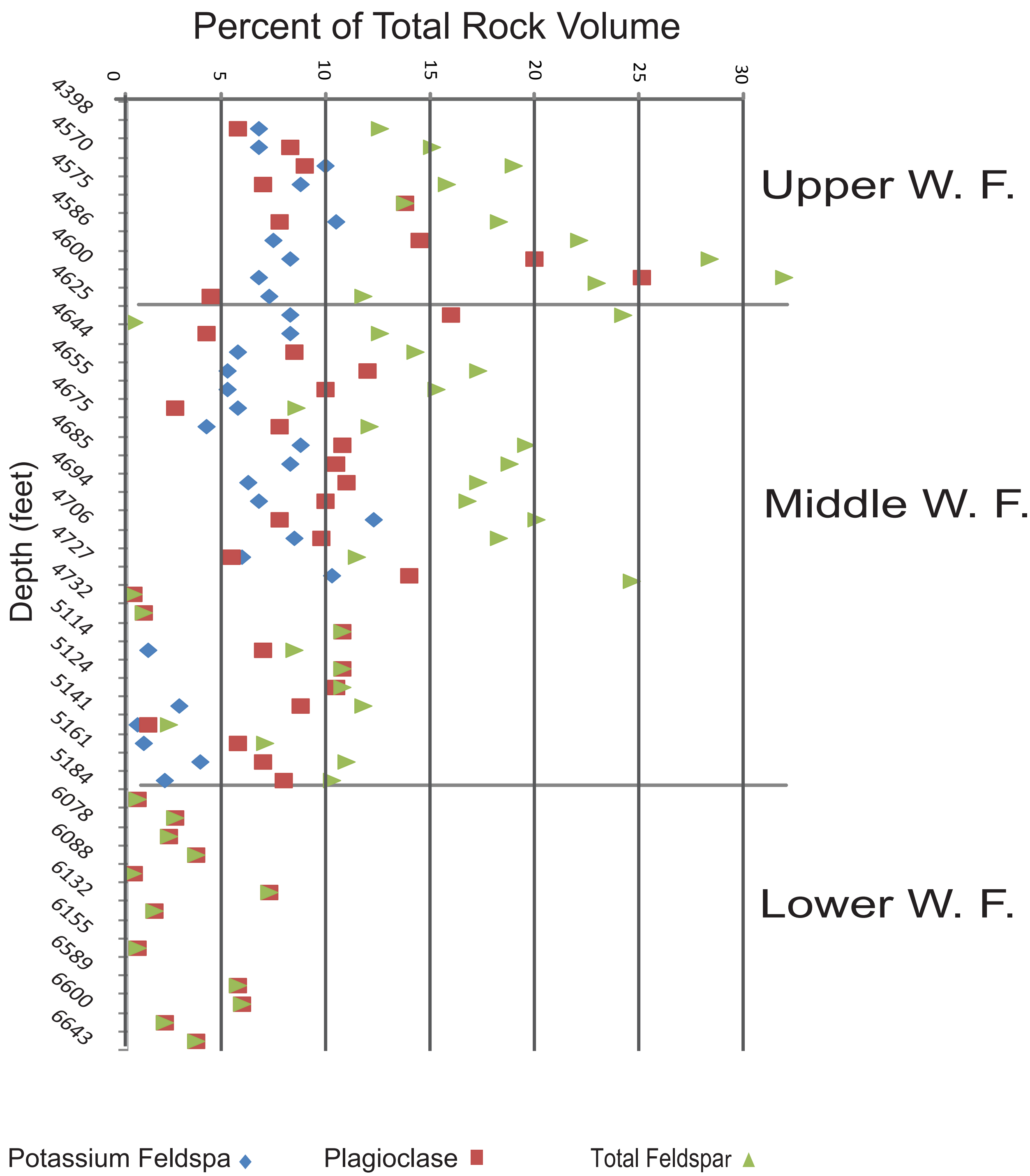

Figure 3.12 - Feldspar abundance with depth in the Parachute 424-34 cores illustrating the decline with depth in total feldspar content. Note also that plagioclase is more abundant than potassium feldspar in most Williams Fork intervals. Potassium feldspar dramatically declines in abundance beginning in the lower half of the middle Williams Fork section and is <1% of the rocks by volume in many samples from the lower half of the Williams Fork Formation.

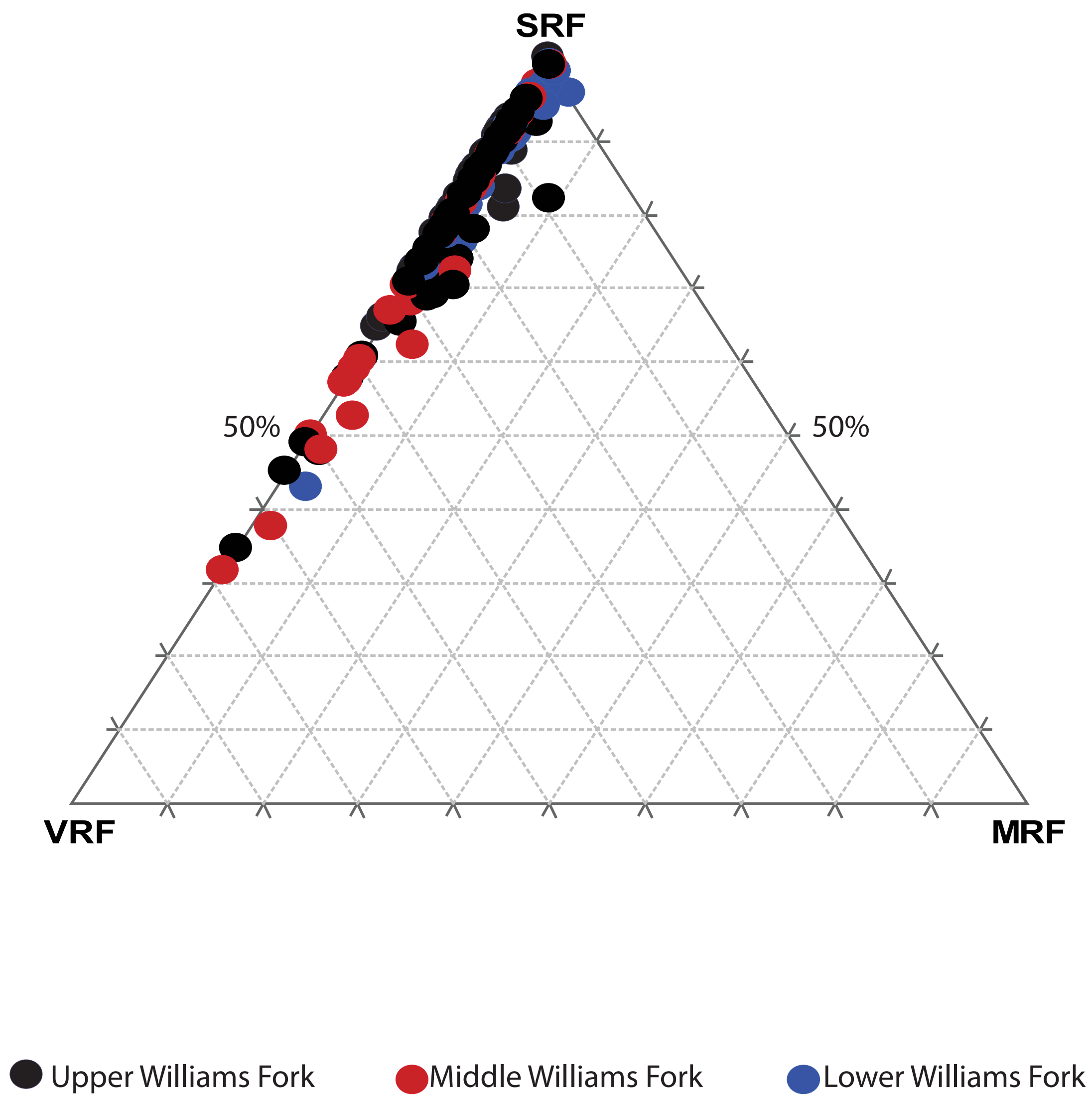

Figure 3.13 - Ternary diagram showing the relative abundance of sedimentary, volcanic, and metamorphic rock fragments in the Williams Fork Formation. Data from the Cascade Creek # 697-20-28, Parachute 424-34, Last Dance # 43C-3-792 and MWX1 cores. Sedimentary rock fragments (SRF) are the most common lithic within all three intervals, followed by volcanic rock fragments (VRF). Metamorphic rock fragments (MRF) are rare and in fact absent from most samples. The abundance of VRF is distinctly less in the lower Williams Fork.

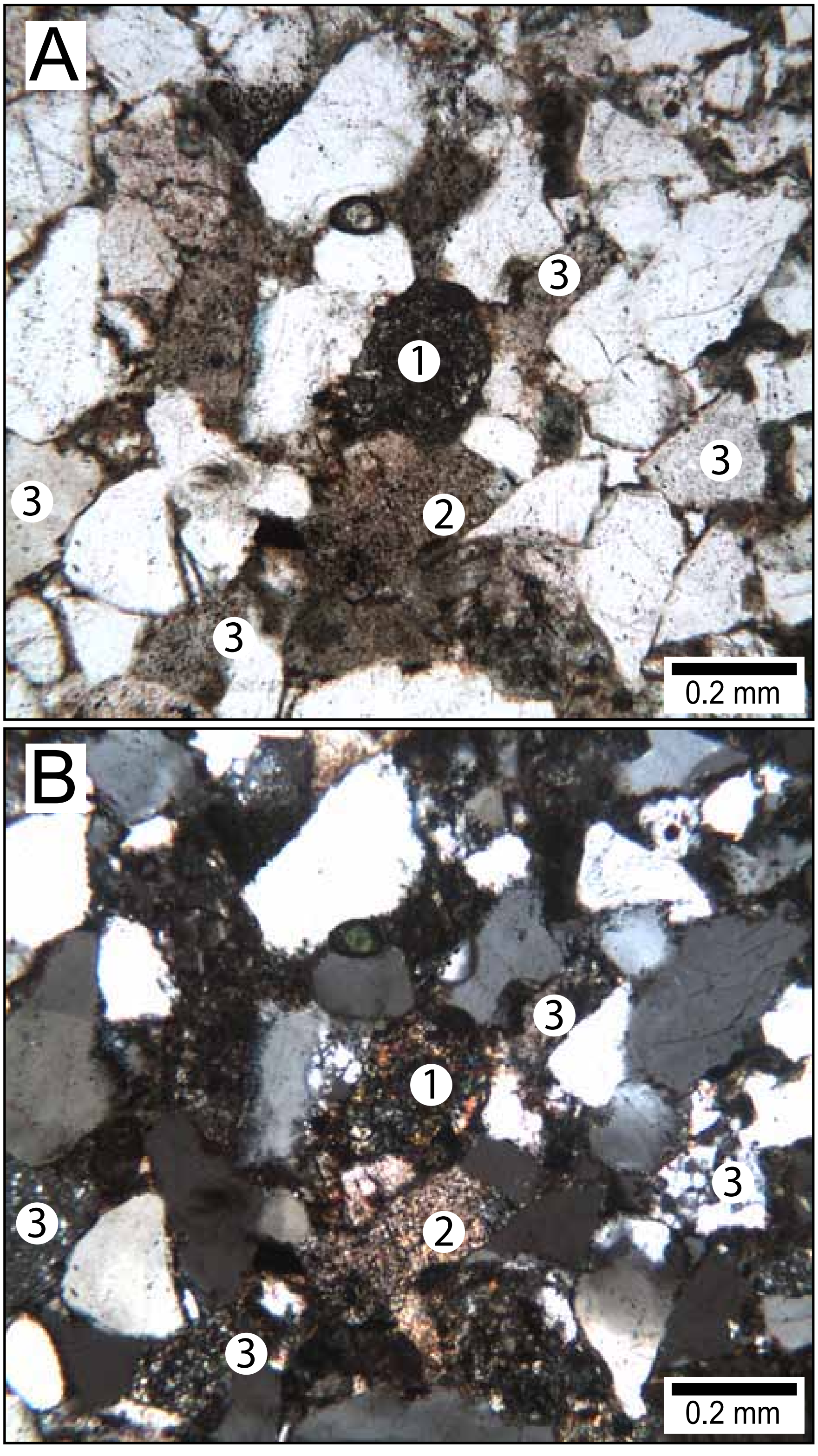

Figure 3.14 - Thin-section photomicrographs Last Dance 3995', (A) plane light and (B) cross nicols, showing detrital rock fragments of dolomite (1), limestone (2), and chert (3).

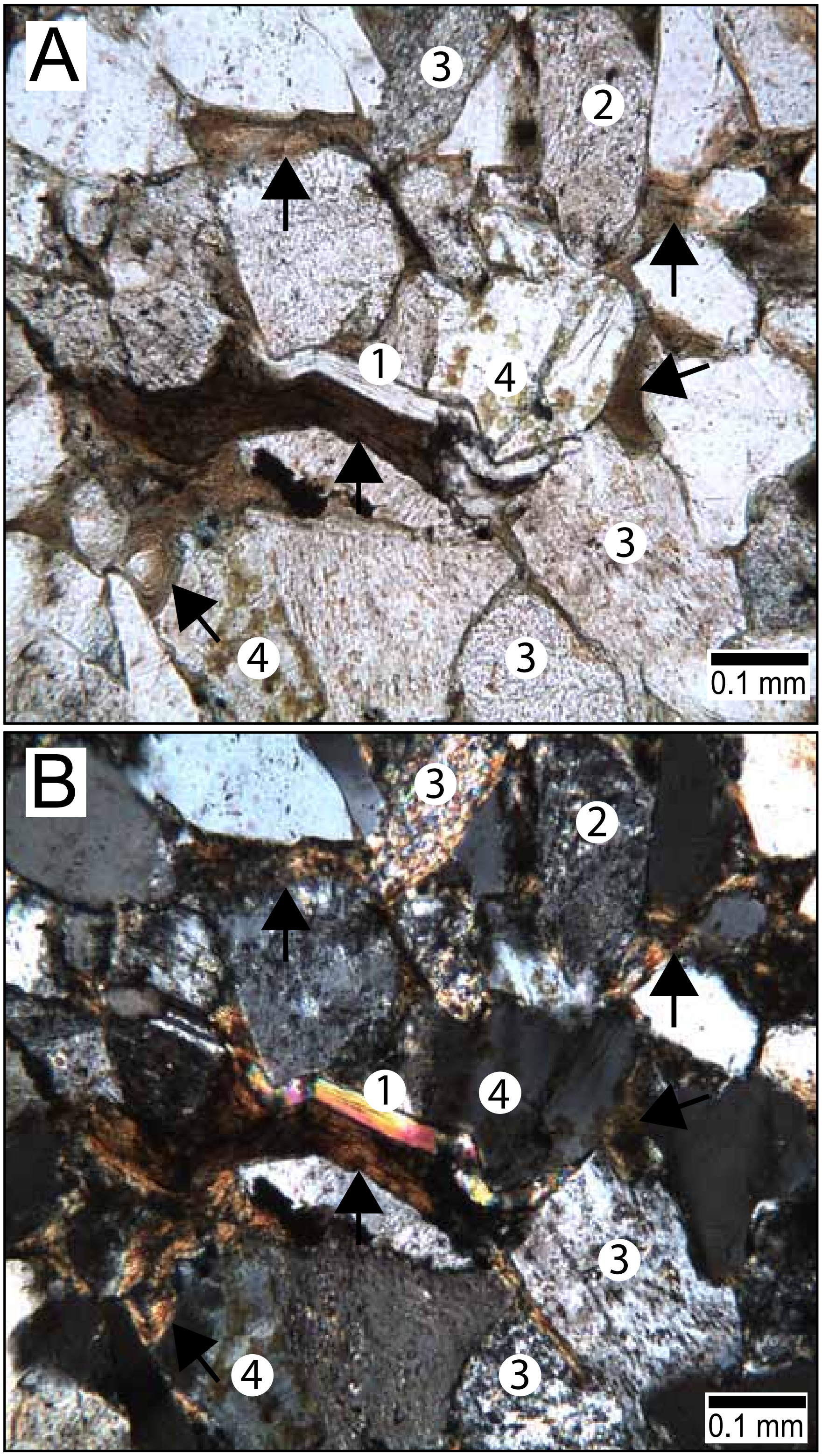

Figure 3.15 - Thin-section photomicrographs Last Dance 3583’, (A) plane light and (B) cross nicols, showing examples of clear unaltered chert (2) and chert partly replaced by clays (3). Pseudomatrix (arrows) formed by compaction of infiltrated clays, siltstone and mudstone clasts between detrital grains. Compaction also deformed a mica grain (1) and fractured a potassium feldspar grain (4).

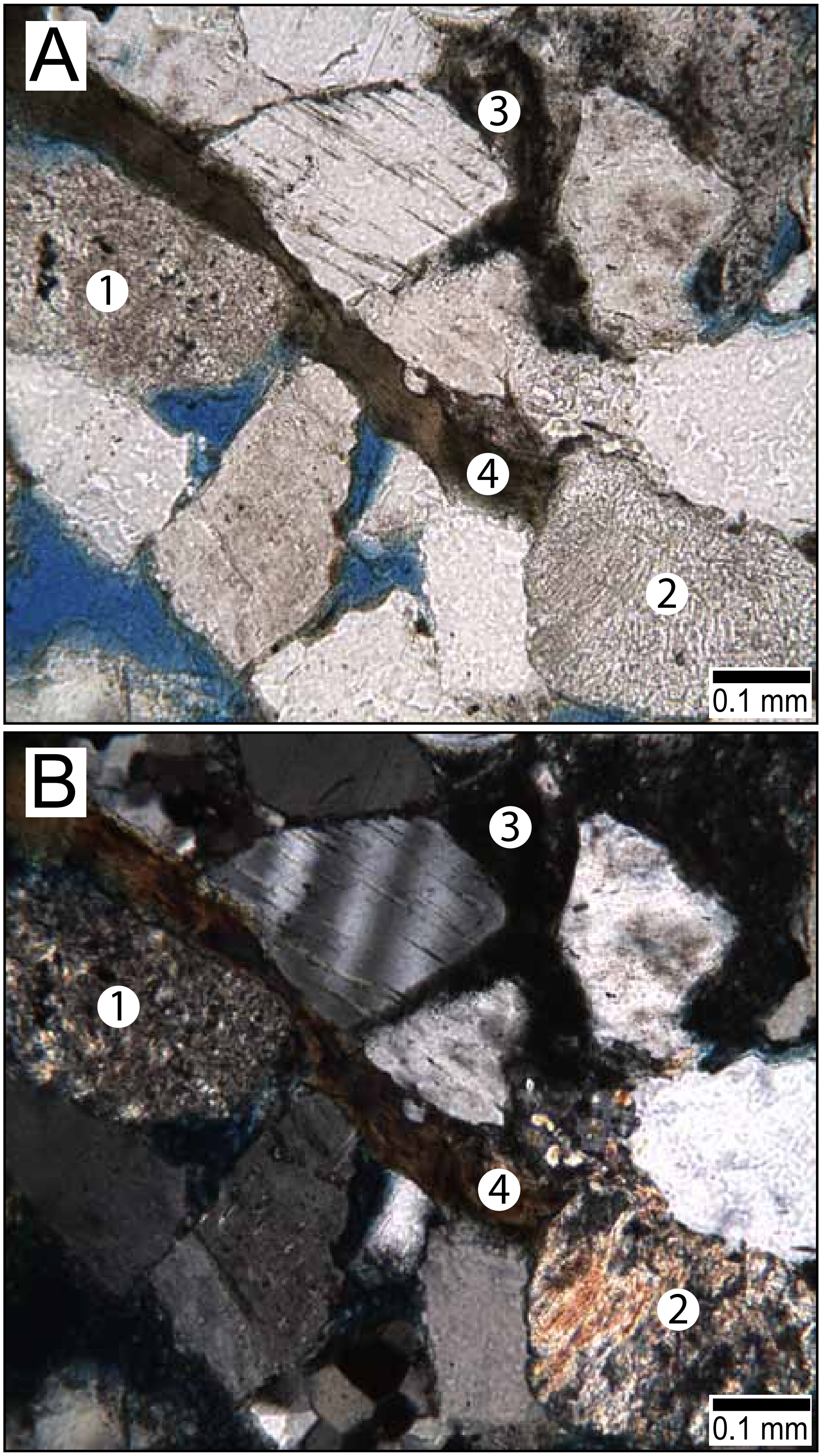

Figure 3.16 - Thin-section photomicrographs Oxy 4834’, (A) plane light and (B) cross nicols, showing examples of unaltered chert (1) and chert altered to clays (2). Pseudomatrix (3) resulted from compaction of an organic-rich mudstone clast and a mica grain (4).

3.17). Chert grains, commonly formed of cryptocrystalline quartz, range from being unaltered to extensively altered to authigenic clays (Figures 3.15, 3.16). Coal fragments and woody material were also observed in in some lower Williams Fork horizons (Figure 3.18).

Volcanic rock fragments are the second most abundant type of lithic fragments; they generally constitute up to 30% of all rock fragments and up to 6% of the rock by volume. Volcanic fragments are commonly sericitized and altered to clays and are difficult to identify in some thin sections (Figure 3.17). Volcanic fragments are noticeably less abundant in the lower Williams Fork sandstones (Figure 3.13).

Clays

Detrital clays in the Williams Fork sandstones occur as matrix (Figure 3.18) and as siltstone, mudstone and clay-rich lithic fragments. X-ray diffraction analysis of sandstones rich in detrital clay indicate that the clays are dominated by illite/smectite and illite/mica. However, the illitic mineralogy is likely the result of illitization during late diagenesis (Chapter 4). Smectite clays dominate most Cretaceous shales of the western US and thus smectitic clays should have dominated the detrital clays within these fluvial sandstones (Keller, 1970; Morad et al., 2000).

Mechanically infiltrated interstitial clays are another form of clay in the Williams Fork sandstones (Figures 3.10, 3.19, 3.20). Mechanical infiltration occurred where porous sands allowed muddy waters to infiltrate through the pore spaces, concentrating clays between detrital grains (Crone, 1975; Walker, 1976). These clays form ridges and bridge in pores and loose aggregate textures (Figure 3.20).

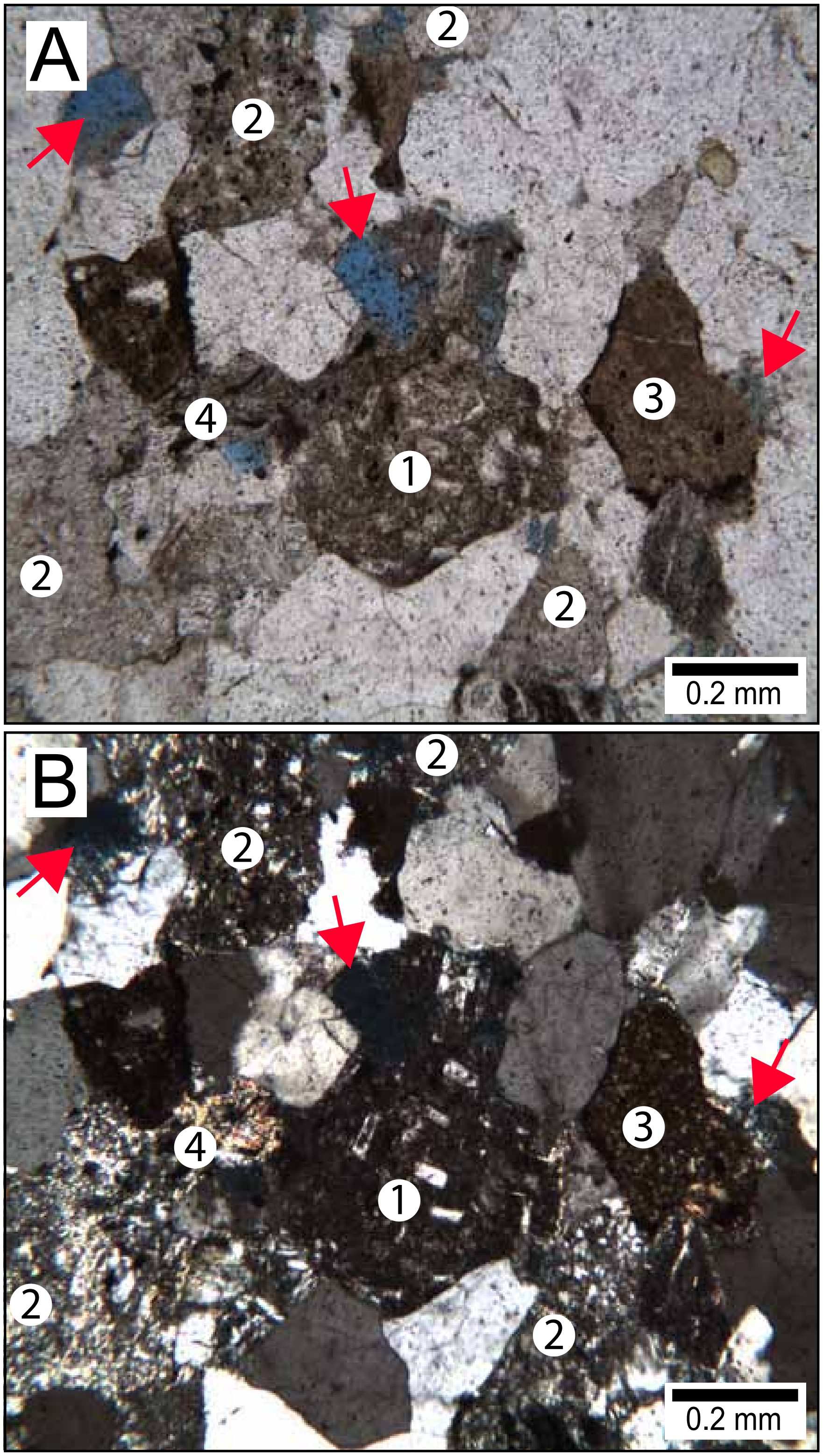

Figure 3.17 - Thin-section photomicrographs Last Dance 3583’, (A) plane light and (B) cross nicols, showing an example of volcanic lithic fragment (1) that is identifiable by the laths of plagioclase feldspar in fine-grained groundmass of the fragment. Other rock fragments include clay-altered (2) and unaltered chert (3), and compacted mudstone (4). Blue is secondary porosity (arrows) formed as result of grain dissolution.

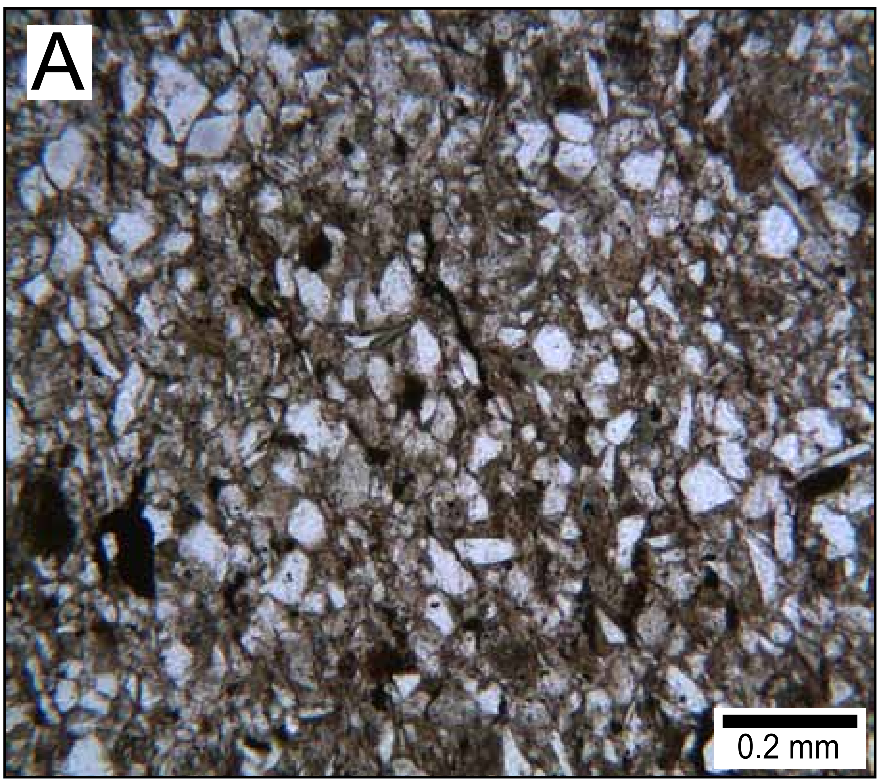

Figure 3.18 - Thin-section photomicrograph of Oxy 4752’, plane light, showing an example of sandstone containing considerable amount of detrital clay matrix. Dark and black grains are coal fragments and organic-rich matter.

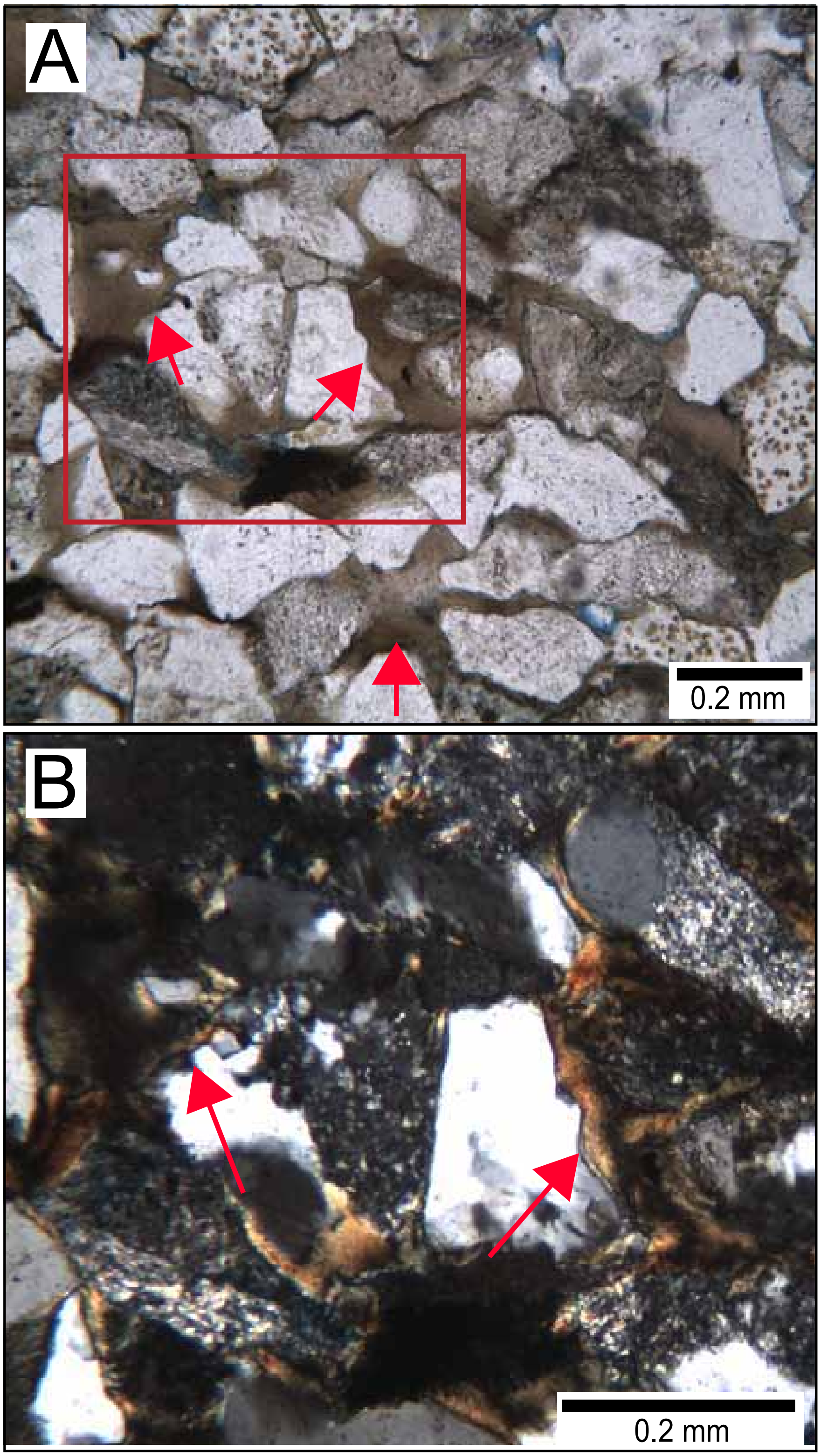

Figure 3.19 - Thin-section photomicrograph Oxy 4809', (A) plane light and (B) cross nicols, showing sandstone's framework grains surrounded by detrital clay particles (red arrows) interpreted as the product of clay infiltration. In cross nicols, the alignment of clay minerals tangential to the grain surfaces is clear, which indicates that the clays are infiltrated and not authigenic.

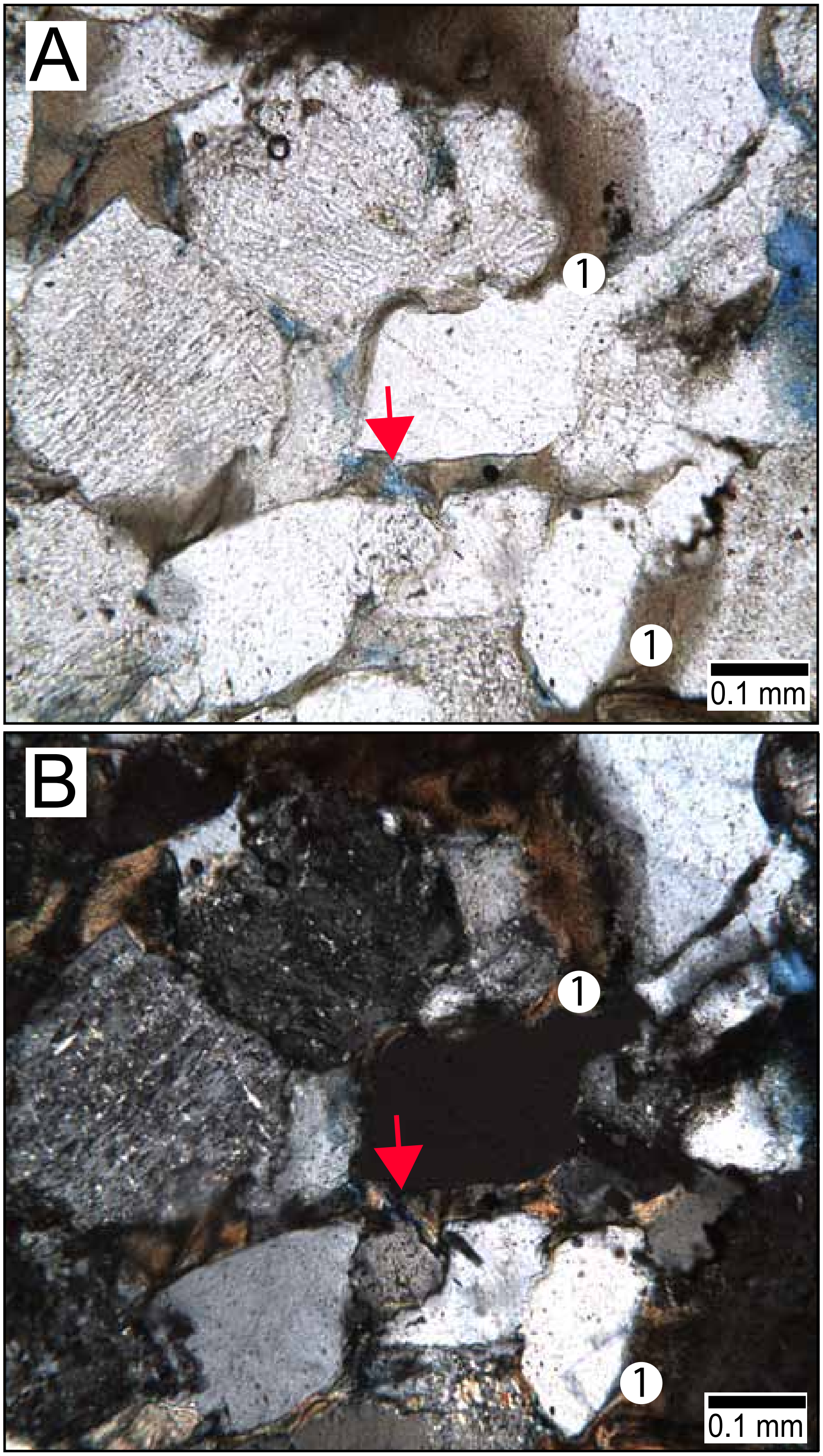

Figure 3.20 - Thin-section photomicrograph Oxy 4809', (A) plane light and (B) cross nicols, showing clay ridges (1) and clay bridges (arrow) across pores, which indicate a mechanically infiltrated origin for the clays.

DISCUSSION – PROVENANCE OR DIAGENESIS

The detrital mineralogy of the Williams Fork sandstones exhibits two major stratigraphic differences: a near absence of potassium feldspar and volcanic rock fragments in the lower Williams Fork interval (Figures 3.12 and 3.13), and an increasing plagioclase content (and hence total feldspar content) upward throughout the upper middle and upper Williams Fork Formation (Figure 3.12). The stratigraphic variability in feldspar mineralogy has been noted by prior workers (Pitman et al., 1989), but it has never been resolved as to whether the difference reflected a change in sediment provenance, diagenesis, or both factors. Certainly there is ample evidence for feldspar replacements and dissolution (Figures 3.9, 3.10, 3.11) and those types of alterations can overprint the detrital mineralogy. However, the point counts performed for this study were done so that any remnant mineralogy in altered feldspar was recorded (e.g., the partially dissolved or replaced feldspars in Figures 3.2, 3.5, 3.8, 3.10, and 3.11), thus detrital mineralogy was determined for all feldspars except those completely dissolved or completely replaced with no inclusions or remnants. This approach meant that provenance determinations were still possible.

Provenance discriminations are based on the schemes of Dickinson et al. (1983) and use a QmFLt ternary plot. A QmFLt plot considers only monocrystalline quartz and places chert in the lithics category. On the QmFLt diagrams (Figure 3.21), the upper Williams Fork sandstones indicate very diverse source areas including recycled sandstone, dissected arc, basement uplifts and mixtures of all four. The middle Williams Fork interval differs only in that it lacks the basement signal. However, the lower Williams Fork is dramatically different in that its source is indicated to be exclusively recycled sandstones.

Dickinson and Gehrels (2008), using U-Pb dating techniques, also noted that recycled orogenic sandstones, characterized by a broad range of Precambrian-aged zircons, were the main sediment source in Cretaceous fluvial sandstones of the Colorado plateau. However, in Late Cretaceous rocks, they also found evidence for increasing input of sands containing detritus from the Mesozoic-aged Cordilleran magmatic arc and Yavapai-Mazatzal-aged basement rocks exposed in the Mogollan highlands to the south (Dickinson and Gehrels (2008).

The provenance changes noted herein and supported by the work of Dickinson and Gehrels (2008) can be explained by a combination of expanding drainages areas and/or migration of the magmatic arc. During deposition of the lower Williams Fork Formation, drainage only extended westward into exposed Mesozoic and Paleozoic sedimentary rocks. The addition of volcanic lithics during middle Williams Fork deposition meant influx from the Cordilleran magmatic arc, which could have occurred by either a westward expansion of drainage areas or the easterly migration of the magmatic arc. By upper Williams Fork time, the introduction of sands from the basement rocks in the Mogollan highlands (Dickinson and Gehrels, 2008) requires the southerly expansion of drainage areas and initiation of longitudinal transport into the Piceance Basin.

The provenance differences (Figure 3.21) and the dissimilarity in lithic types (Figure 3.13) between the three Williams Fork intervals suggests that the near absence of potassium feldspar in the lower Williams Fork section and the progressive increase in

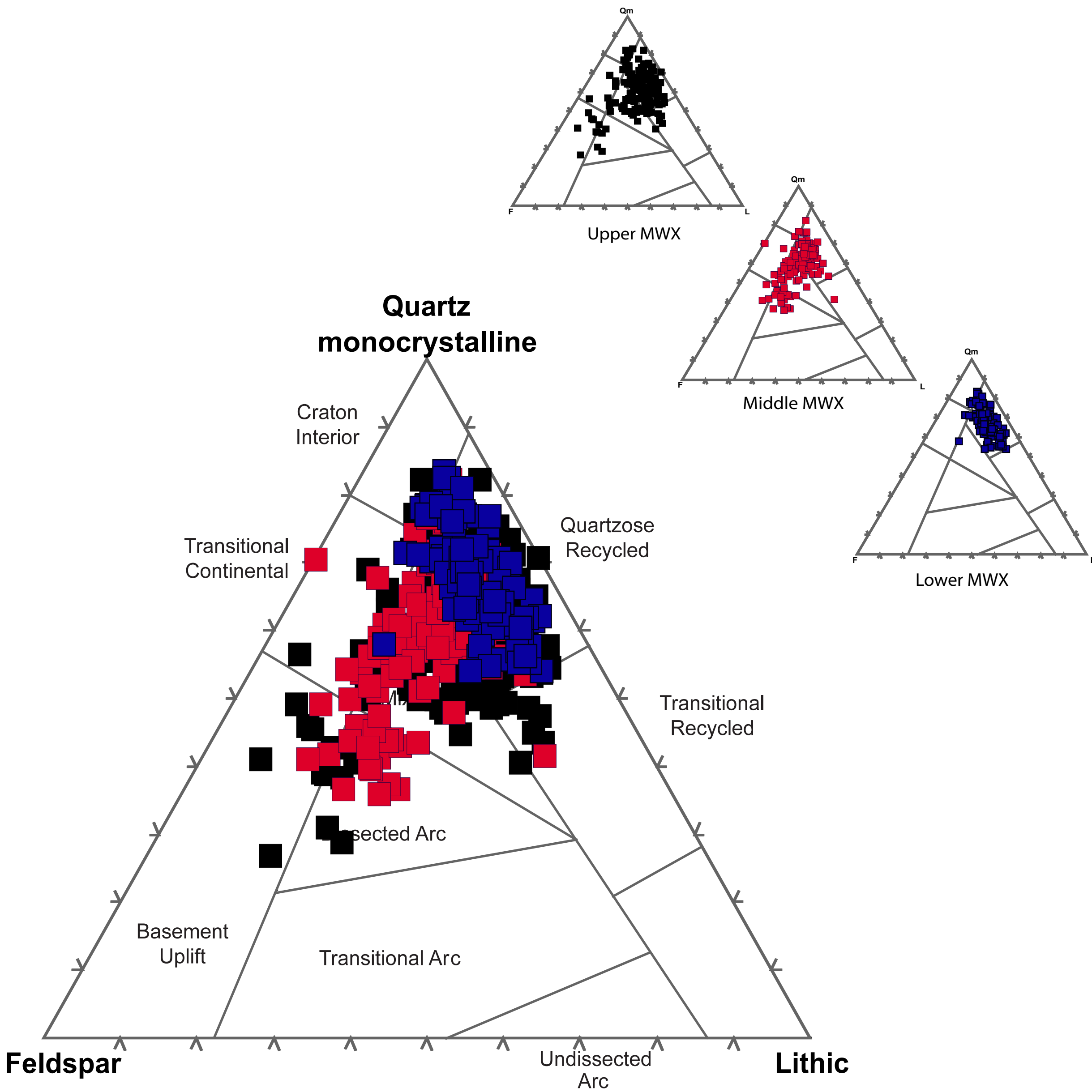

Figure 3.21 - QmFLt ternary diagrams of sandstone composition and inferred provenance for the Williams Fork Formation. The diagram plots only monocrystalline quartz on the quartz pole; chert is plotted in the lithics category. Inferred provenance is from Dickinson (1985).

total feldspar upwards, is primarily due to provenance not diagenesis. The lack of any trend in the abundance of secondary porosity from grain dissolution (Figure 3.22) also supports provenance as the cause of stratigraphic variability in feldspars and volcanic rock fragments. As will be shown in Chapter 4, compaction is pervasive throughout the Williams Fork Formation and preceded the formation of secondary pores, thus compaction did not destroy secondary pores. That in turn means that if the feldspar trends were due to diagenesis, then the decrease in feldspar abundance should be mimicked by an increase in secondary pores from grain dissolution. Such a trend was not observed (Figure 3.22), making the provenance differences documented herein the dominant driver of feldspar variability.

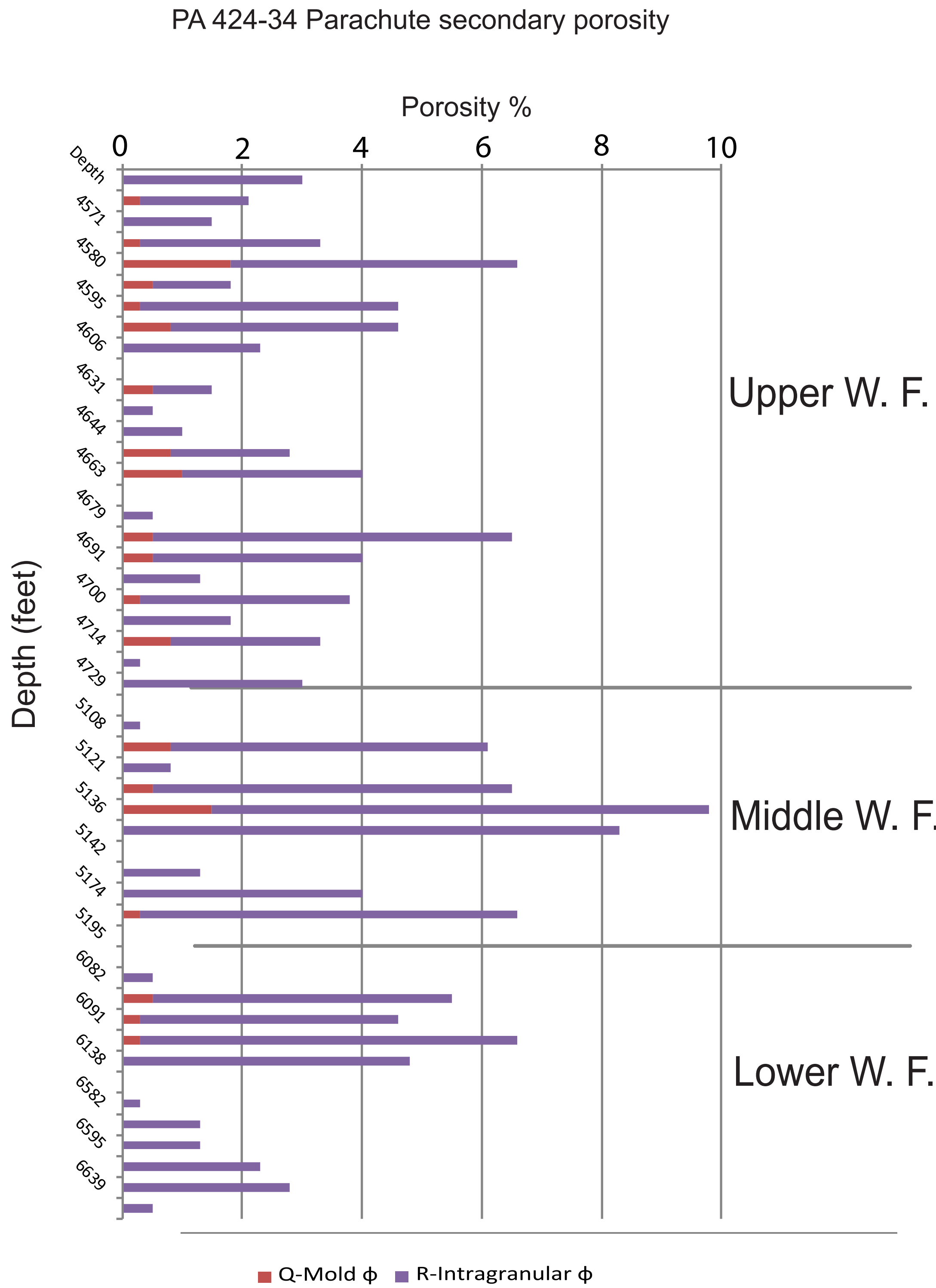

Figure 3.22 - Stratigraphic distribution of secondary pores formed by grain dissolution (primarily of feldspars). Data from the Parachute 424-34 core. Vertical scale depicts sample footages in descending order; it is not a true vertical scale.

CHAPTER FOUR: WILLIAMS FORK DIAGENESIS

INTRODUCTION

Diagenesis represents all processes that affect sandstones after their deposition. It occurs as a result of physical, chemical and biological processes, and can affect the texture, mineralogy and fluid-flow properties of sedimentary rocks. The processes and products of diagenesis have an enormous effect on the evolution of sedimentary basins, and have practical implications for the analysis and interpretation of any sandstone. Selective removal of feldspars and/or rock fragments by intrastratal solution can severely affect the provenance interpretation of a sandstone. Authigenic clay minerals can convert originally matrix-free sandstones to diagenetic wackes (muddy sandstones). Strong post-depositional porosity loss during diagenesis results from compaction and/or cementation; porosity enhancement occurs with dissolution of framework grains and cements. As a result, diagenesis is of great significance to the petroleum industry's understanding of any siliciclastic sedimentary basin. A full understanding of the economic value of any sandstone with regard to its potential as a hydrocarbon reservoir rock can only be reached by addressing the diagenetic history of that sandstone (Boggs, 2009).

In this study, diagenesis has been divided into eo- and meso-diagenesis (Figure 4.1). As noted by others (e.g., Choquette and Pray, 1970; Schmidt and McDonald, 1979; Morad et al., 2000), the boundary between eo- and meso-diagenesis is not precise in terms of burial depths and temperatures. In this thesis, eo-diagenesis is considered modifications by early, low temperature (< 70°C) diagenetic process in pore

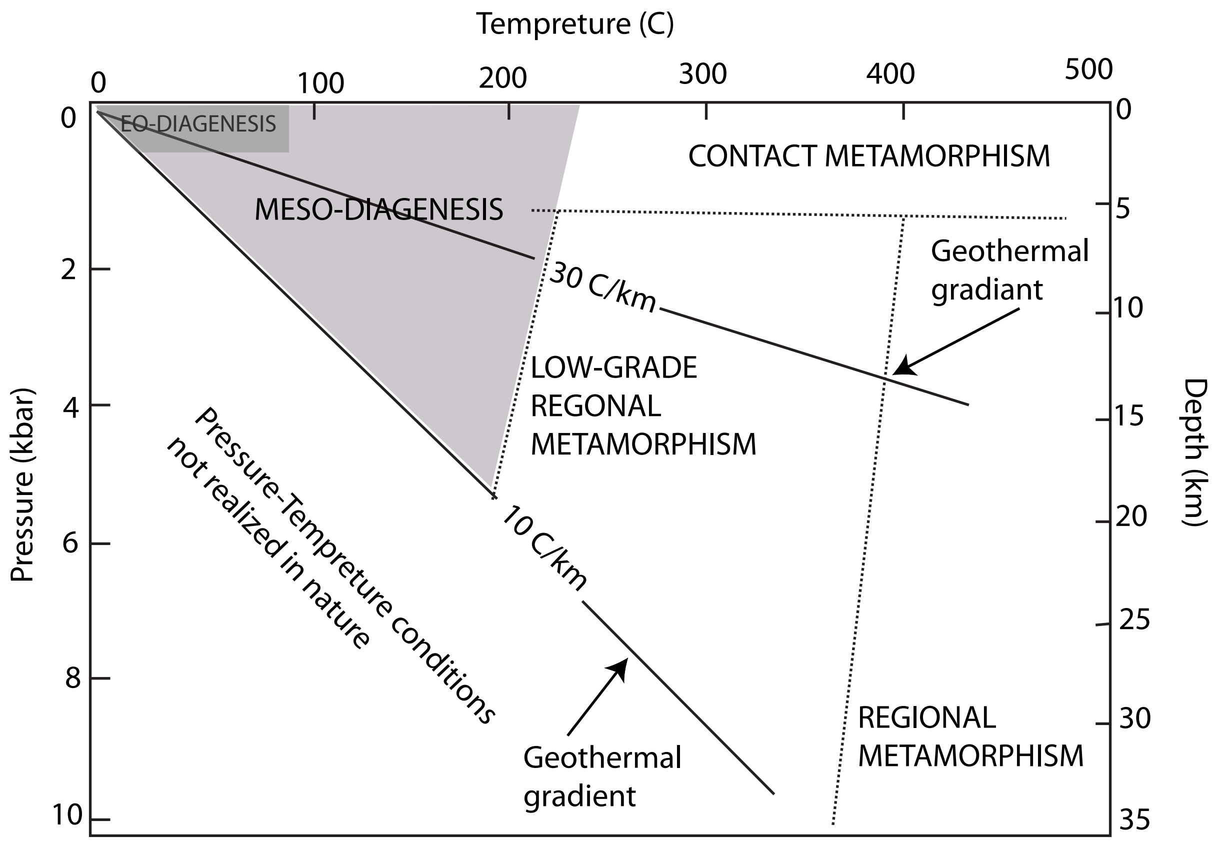

Figure 4.1 - Pressure-temperature diagram relating diagenesis to eo- and meso-diagenetic realms, as well as metamorphic regimes. Modified from Worden and Burly (2009).

water whose chemistry is controlled by meteoric- or marine-derived surface water. Meso-diagenesis refers to diagenetic alterations that take place in evolved formation water at higher (> 70°C) temperatures (Morad et al., 2000). A temperature of 70°C is the boundary because chemical compaction, clay-mineral transformation reactions, substantial thermal alteration of organic matter, and burial quartz cementation all typically initiate at about 70°C (Morad et al., 2000).

The results presented herein reveal that the Williams Fork tight sandstones were subject to intense mechanical compaction and chemical alteration. The chemical changes include cementation, mineral replacements, and dissolution. A variety of different minerals form cements and replacements, and both detrital and authigenic phases are replaced and dissolved. The evidence for each diagenetic event observed in the Williams Fork sandstones is presented below and then integrated into a composite paragenetic sequence.

COMPACTION

Compaction refers to the combined effects of physical compaction (grain rearrangement and deformation) and chemical compaction (pressure solution). It includes rotation, translation, fracturing, and elastic deformation of sandstone grains. Compaction leads to loss of porosity, and in many types of sandstone it is the dominant mechanism of porosity loss and bulk density increase (Pettijohn et al, 1987; Lundegard, 1992). These effects directly influence a sandstone's fluid pressure and fluid-low patterns, as well as the bulk thermal conductivity (Gretener, 198l).

With the exception of the behind outcrop BT202 samples and early silica and/or carbonate cemented sandstones, long, concave-convex and sutured-grain contacts are common in Williams Fork sandstones (Figure 3.4). These features attest to the extent of mechanical (long contacts) and pressure solution (sutured-grain contacts). Many quartz grains show undulatory extinction, which may be a product of crystal deformation due to compaction (Connolly, 1965). The influence of compaction is seen most effectively within highly ductile argillaceous and mica-rich sandstones (Figure 3.15) where sedimentary lithic fragments (mudstones) form pseudomatrix (Figure 3.3) and mica grains broke and deformed. As a result of the abundance of all compaction features, the studied sandstone intervals of the Williams Fork Formation are moderately-to-highly compacted.

Thin-section point-count data were used to quantify the impact of compaction and cementation on porosity loss within Williams Fork sandstones. As per Lundegard (1992), the sum of total thin section porosity (Po) and percentage of pore-filling cement (C) yields the intergranular volume (PMC for minus-cement porosity). Intergranular volume and estimated depositional porosity (P_i) are then used to calculate compactional porosity loss (COPL) as a percentage of the original bulk volume:

$$COPL = P_i - (((100 - Pi) \times PMC)/(100 - PMC)) \quad (1)$$

Cementational porosity loss (CEPL) is then given by:

$$CEPL = (P_i - COPL) \times (C/PMC) \quad (2)$$

Following Lundegrad (1992), an initial porosity value (Pi) of 45% was assumed for all samples. It is important to note that these equations account for the rock volume changes that occur with compaction (Lundegard, 1992), whereas petrographic percentages of cement and grain volume alone do not account for volume changes.

A compaction index (ICOMPACT) that is useful for comparing different sandstone data sets is derived from the fractional ratio of compactional porosity loss (COPL) to the sum of compactional (COPL) and cementational (CEPL) porosity loss:

$$ICOMPACT = COPL/(COPL + CEPL) \qquad (3)$$

Porosity loss is solely due to compaction when ICOMPACT equals one. A value of zero for ICOMPACT means porosity loss is due to cementation only.

The calculated COPL and CEPL data (Figure 4.2) show that compaction is the main mechanism of porosity loss in the Williams Fork sandstones. In all intervals, the amount of porosity loss due to compaction is much greater than porosity loss due to cementation. Fractional ratios of compactional porosity loss (ICOMPACT) range from 0.53 to 0.98 (average 0.83), which also illustrates the dominance of compaction relative to cementation.

CEMENTATION AND MINERAL REPLACEMENTS

Overview

Cementation and mineral replacements within the Williams Fork sandstones changed the mineralogical composition and lithified the sediments. These changes were driven in large part by interaction between pore fluids and solid mineral grains, especially unstable minerals (e.g., feldspars) and lithic fragments. The ions needed for cementation were generated, secondary porosity was created, and significant grain alterations and mineral replacements occurred. These chemical alterations, and

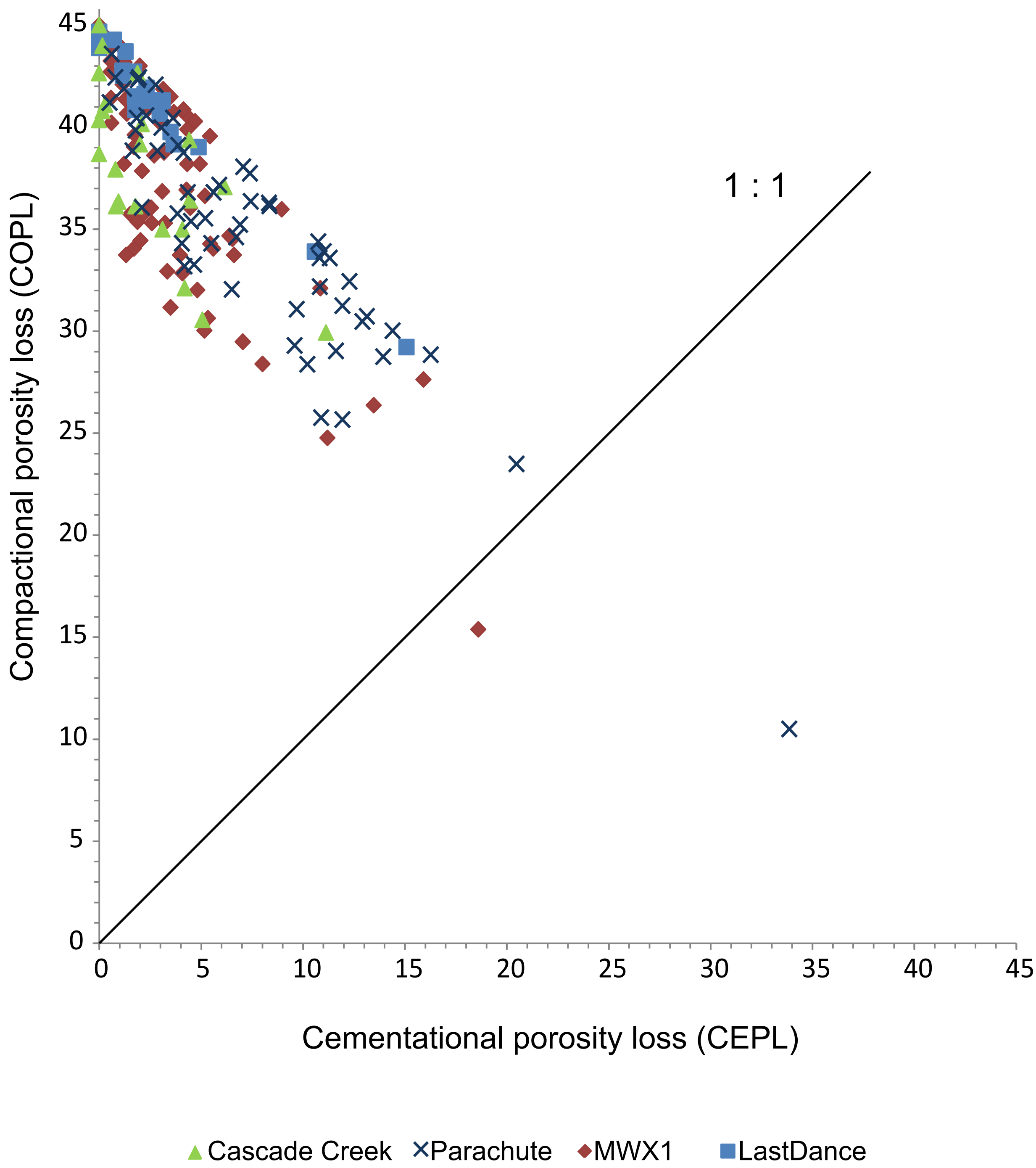

Figure 4.2 - Cross plot of compactional porosity loss versus cementational porosity loss for Williams Fork sandstones cores. Diagonal line is line of equal porosity loss by compaction and cementation. The data show that sandstone throughout the Williams Fork Formation are highly compacted and have lost significantly more porosity by compaction than by cementation.

especially the cements, provide useful information on the history and environment of diagenesis (e.g., Longstaffe 1989; Lundegard 1989).

Cements in the Williams Fork sandstones are mainly the result of chemical precipitation of a binding agent or the chemical welding of adjacent detrital grains. Quartz overgrowths, ferroan and nonferroan calcite, ferroan dolomite and clay minerals are the main cement types. Non-ferroan dolomite is present in minor amounts, with ankerite, albite and zeolite cements were rarely observed and then in just trace amounts.

Alteration by mineral replacement is also common within all three Williams Fork intervals. Potassium feldspar, plagioclase, chert and micas are altered to authigenic kaolinite, illite, or illite/smectite. Calcite, dolomite and, to a much lesser extent, albite replaces some detrital feldspar, chert and, to a lesser extent, detrital quartz and early quartz cement.

Quartz

Quartz overgrowths are common in almost all intervals in the upper and middle Williams Fork Formation, but less common in the lower Williams Fork sandstones. It is the second most abundant type of cement, and forms 1 to 17 percent of the total rock volume. Authigenic quartz nucleated on detrital quartz grains and grew as syntaxial overgrowths into the neighboring pore space, and totally to partly fills those intergranular pores (Figures 3.6, 4.3). If present, inclusions within detrital grains and/or dust rims on the grain surfaces help distinguish the boundary between detrital grain and overgrowth. In other cases, overgrowths lack any distinction with their host but are

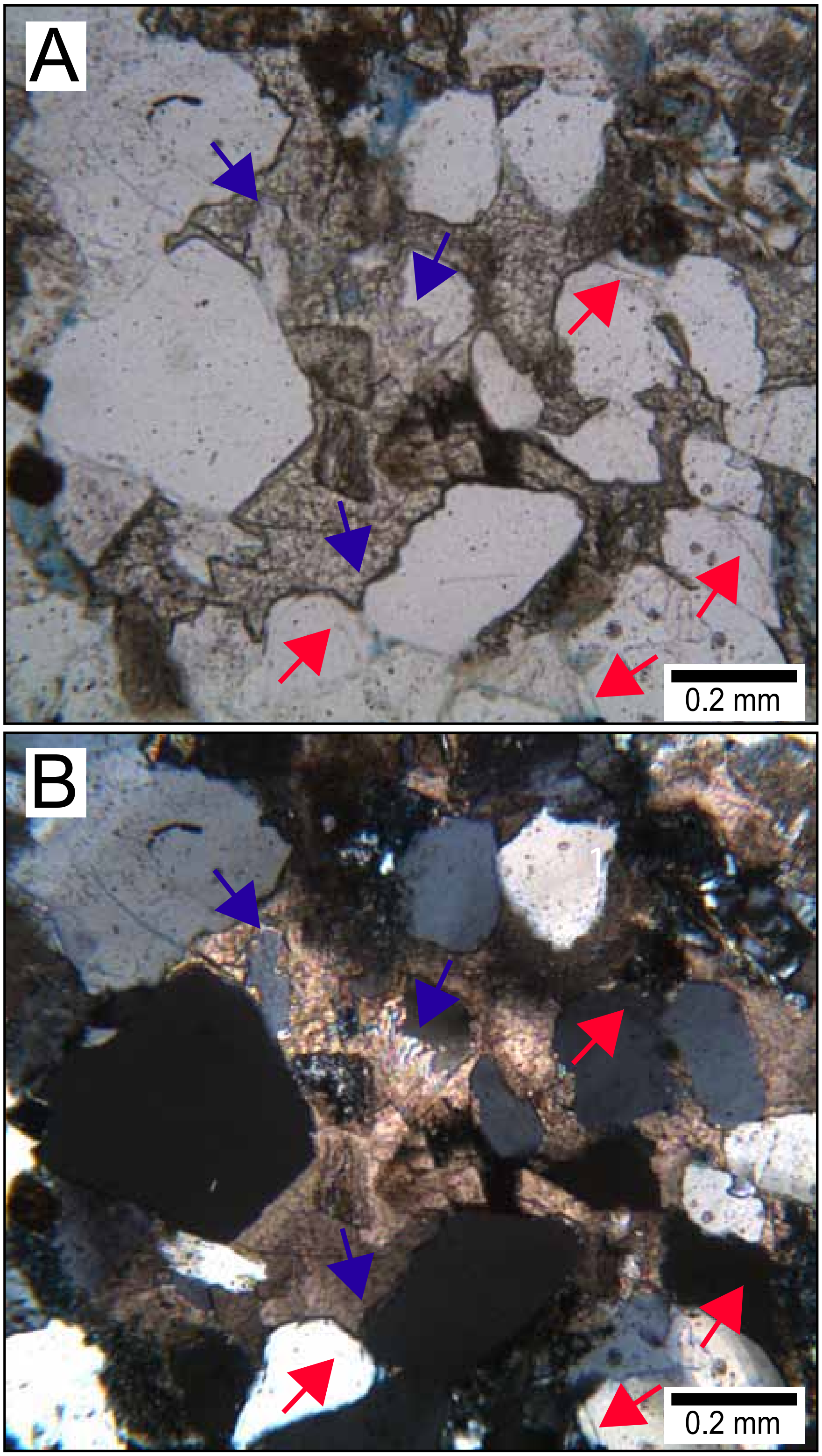

Figure 4.3 - Thin-section photomicrographs Cascade Creek Oxy 6761', (A) plane light and (B) cross nicols. Sample is extensively cemented. Early quartz overgrowths (red arrows) are overlain by calcite cement. The boundary between some quartz overgrowths and detrital grains is marked by a prominent dust-rim. Poikilotopic calcite cement (blue arrows) replaces grains, fills intergranular pore spaces, and partially replaces early silica cement.

recognized by the presence of euhedral prismatic crystal faces in former pores (Figure 3.11).

Quartz cement distribution is a function of facies and early clay diagenesis. It does not exist in sandstones rich in detrital clay, in pseudomatrix-rich facies, and where early authigenic clays coated quartz grains (Figure 4.4). In the last case, continuous clay coats effectively isolated quartz grains, caused a lack of quartz nucleation sites and thus disallowed overgrowth formation. Where clay coats were breached, small prismatic crystals of quartz can extend through the gaps in the coatings (Figure 4.5).

There is also evidence that quartz cementation is multi-generational. As already noted, quartz cement is typically the first generation of cement on detrital quartz grains (Figure 4.6), indicating a relatively early origin for that authigenic quartz. However, there is also quartz cement that post-dates compaction and dissolution as evidenced by authigenic quartz filling secondary intragranular pores (Figure 4.6), intergranular space generated by dissolution of earlier cement, macro and micro fractures that cut across the rock, and compaction-induced microfractures within individual detrital quartz grains.

Carbonates

Carbonate cements occur throughout the Williams Fork Formation (Figure 4.7). Authigenic carbonates comprises up to 48% percent of the total rock volume in some samples, and typically range from trace amounts to less than 25% of the rock volume. The relative proportion of calcite to total carbonate ranges from 0 to 100%. The dominate phases are ferroan calcite in the upper and middle Williams Fork intervals and non-ferroan calcite and dolomite in the lower Williams Fork section (Figure 4.7).

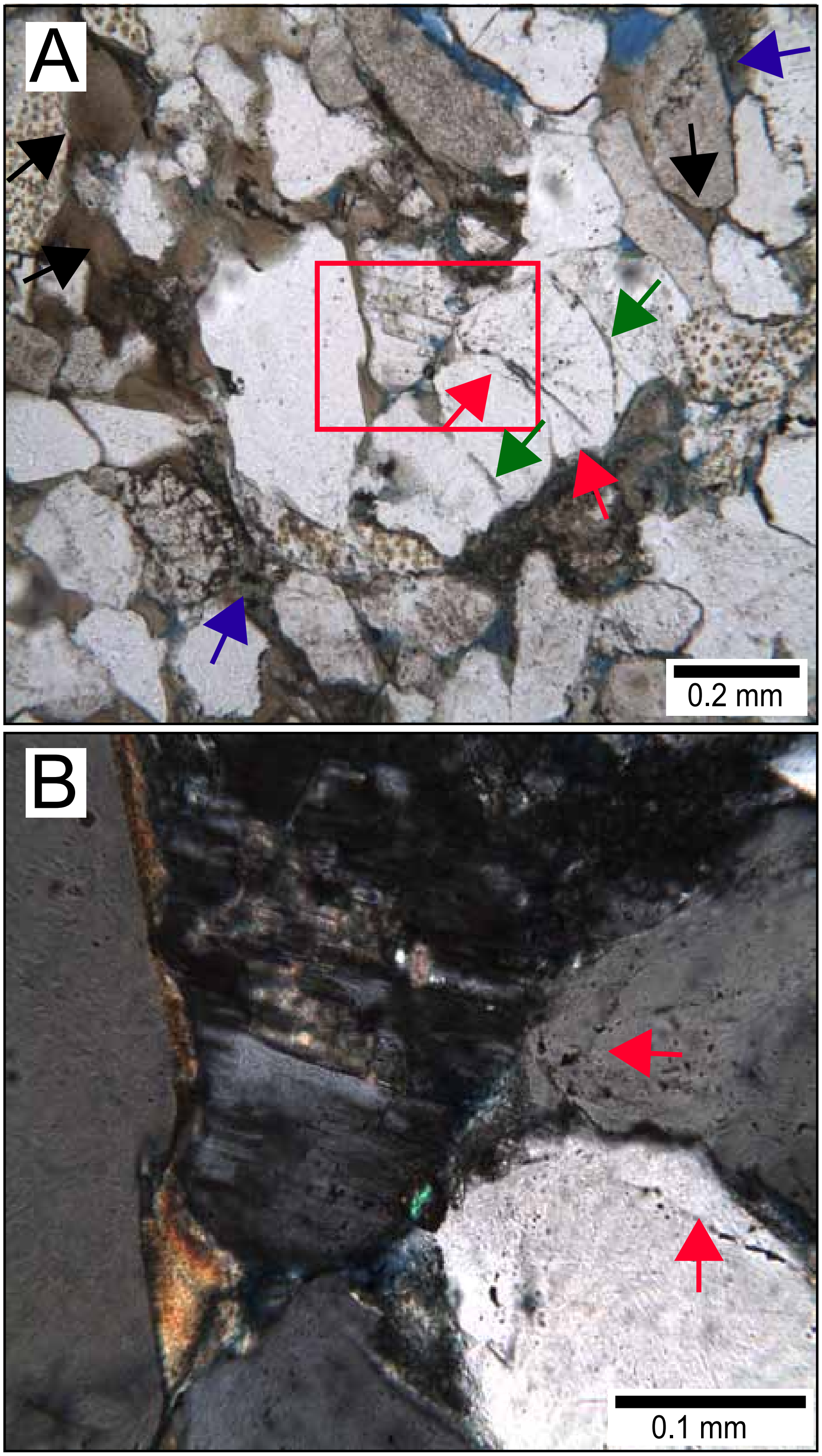
A
0.2 mm
B
0.1 mm

Figure 4.4 - Thin-section photomicrograph Oxy 4809’, (A) plane light, and (B) close-up of outlined area in (A) in cross nicols, showing how an occurrence of clay matrix controlled the distribution of quartz cement. The clay coats quartz grains and prevented nucleation of quartz cement. This sample illustrates high clay content due to detrital (blue arrows), infiltrated (black arrows), and authigenic clays (green arrows). Silica cement (red arrows) developed where no clay lined grain surfaces or filled pore spaces (black arrows).

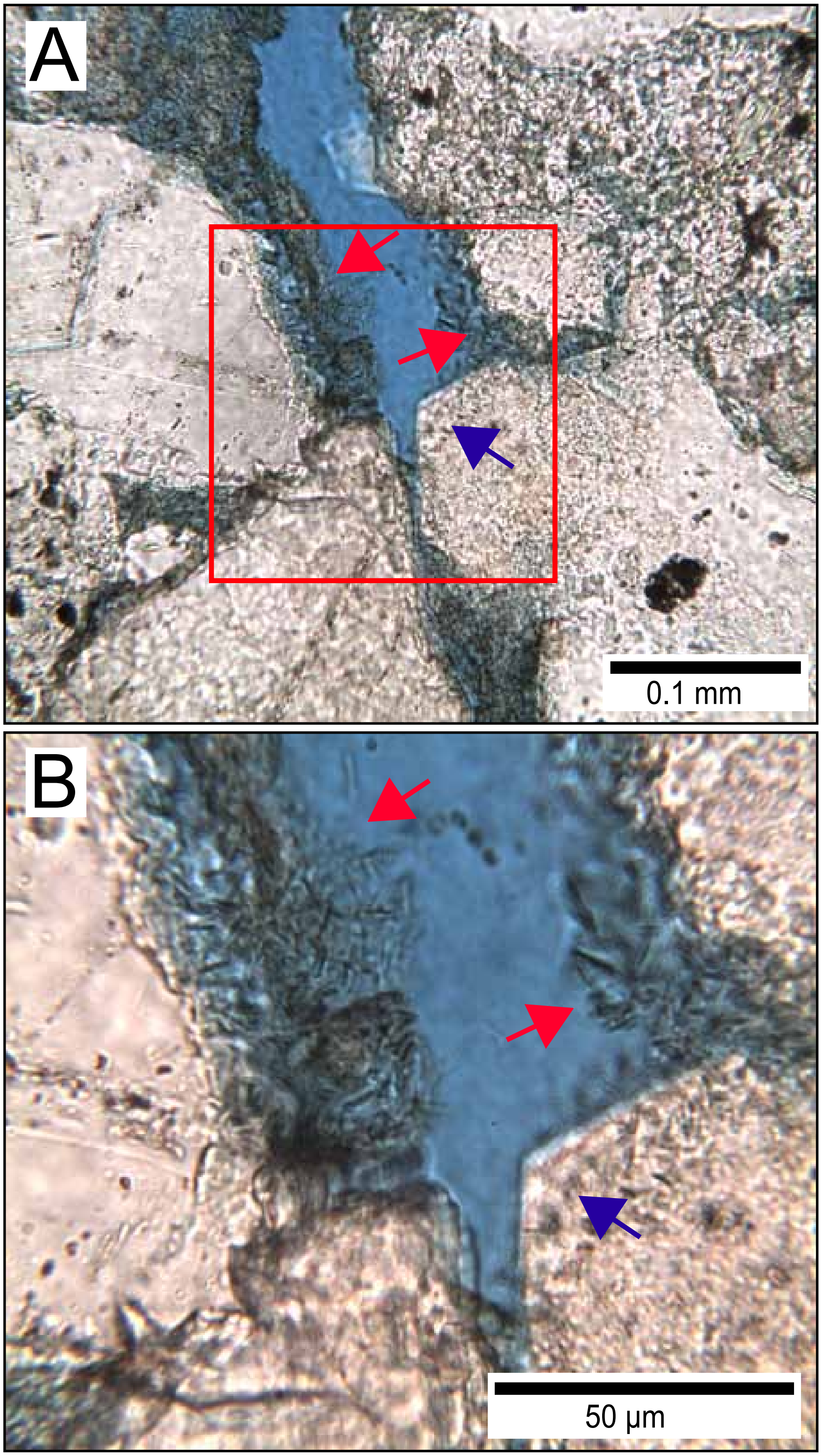

Figure 4.5 - Thin-section photomicrographs Cascade Creek Oxy 4752', plane light. (A) Quartz overgrowth forms a small prismatic crystal through a gap in the clay coat (red arrow). (B) Close up of outlined area in (A). Continuous authigenic clay coats (red arrows) inhibited precipitation of silica overgrowths on other grain surfaces Clays also partially replace the quartz grain surfaces, as evidenced by carries into the grain and an uneven grain surface.

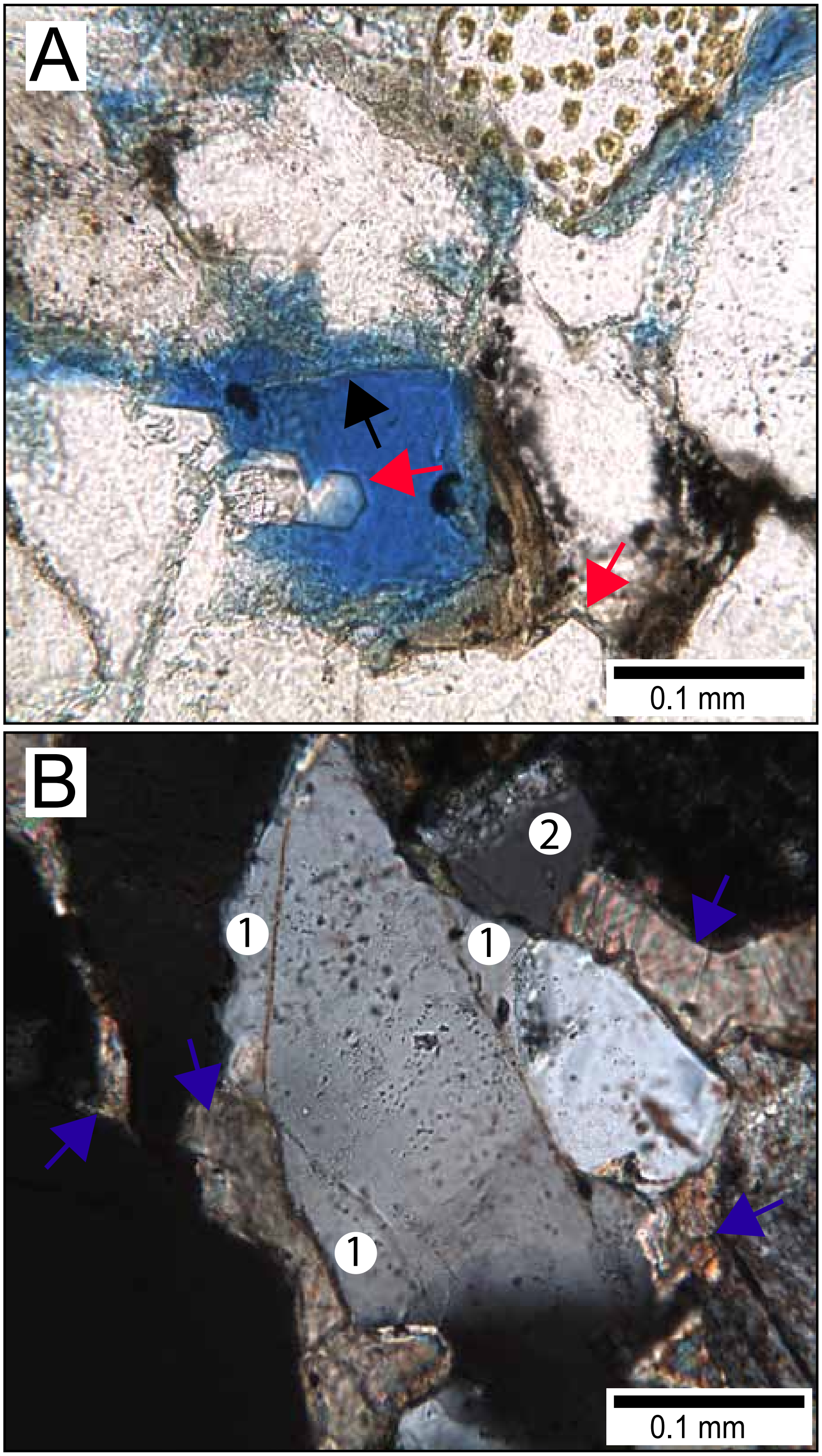
A
0.1 mm
B
1
1
1
2
0.1 mm

Figure 4.6 - Thin-section photomicrographs (A) Cascade Creek Oxy 4809’, plane light, and (B) Last Dance 3563’, cross nicols, showing quartz overgrowth as early and late cement. (A) Late silica cement (red arrow) partly fills secondary dissolution pore. The late silica cement clearly postdates moldic pore formation that resulted from unstable detrital grain dissolution. The moldic pore is outlined by clay minerals (black arrow). Yellow squares on grain to upper right are an artifact of feldspar staining. (B) Silica overgrowth is an initial, hence early, cement (1) that grows into intergranular pores. Authigenic calcite (blue arrows) and albite (2) postdate silica cement and replace both grains and the early quartz and cement.

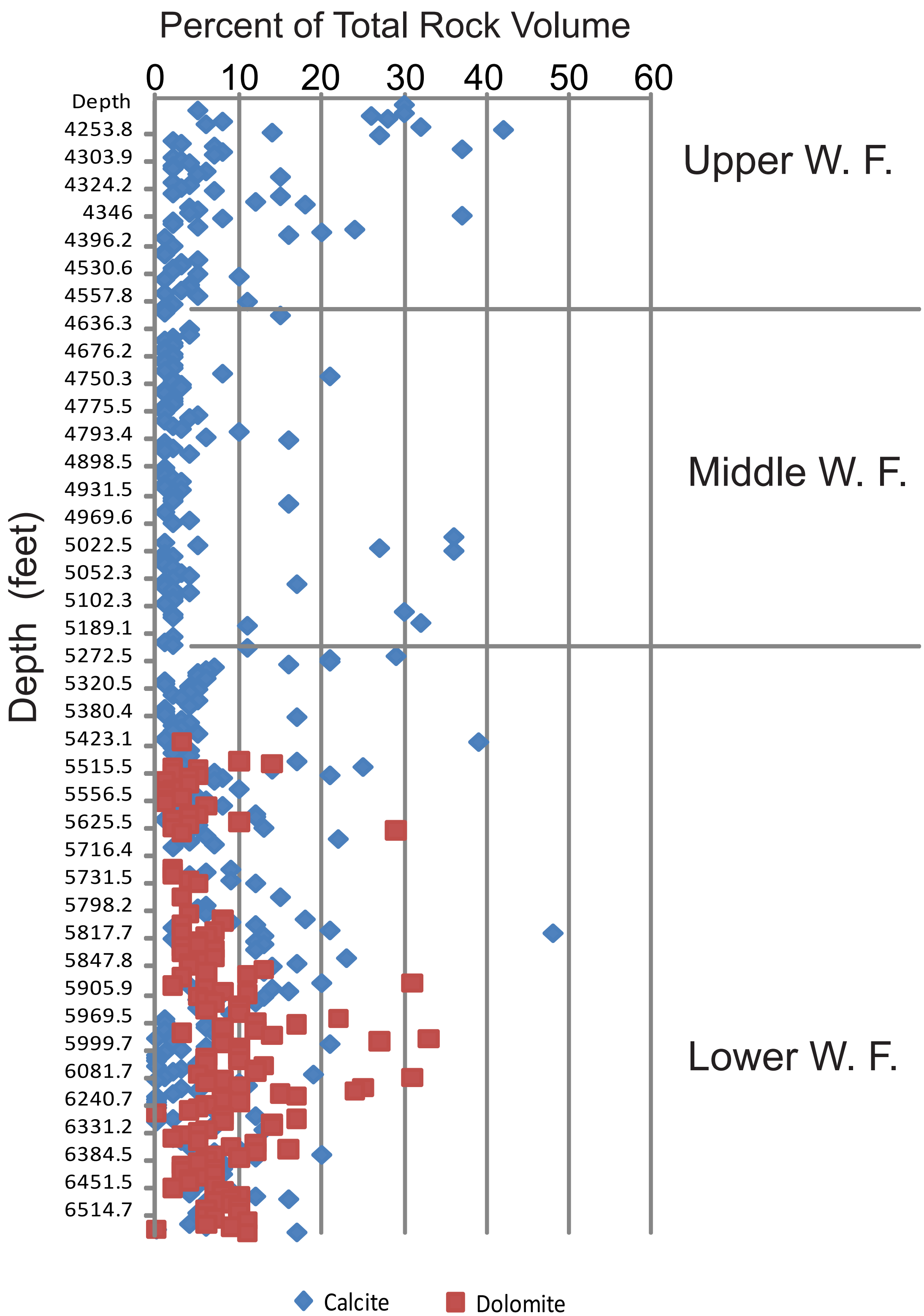

Figure 4.7 - Distribution of authigenic carbonate cements within the MWX1 core. Vertical scale depicts sample footages in descending order; it is not a true vertical scale. Calcite dominants the upper and middle intervals and dolomite is concentrated in the lower Williams Fork sandstones.

Carbonate occurs in microcrystalline to coarse-crystalline poikilotopic textures and in rhombic dolomite crystal-form. Large crystals occur as both a pore filling cement (Figures 4.3, 4.6, 4.8B) and as a replacement (Figure 4.3). Many framework grains, quartz overgrowths, and clay matrix were etched and partly or completely replaced by calcite (Figure 4.6). Some calcite replacements selectively targeted feldspars (Figures 4.9A, 4.10A) with some replacements preferentially initiated along crystal cleavage planes (Figure 4.8A). In some sandstones early quartz cements were selectively targeted by calcite replacement (Figures 4.3, 4.10B, 4.11).

Two generations of calcite precipitation are distinguished based on their relative iron contents, distribution, and texture. The first generation consists of larger calcite crystals (80 to 450 μm) and is typically contains less iron than the later generation. The early non-ferroan calcite partially to completely replaces both detrital feldspar and quartz grains, and fills intergranular pore-spaces. It almost always overlies quartz cements and is commonly overlain or cross cut by late ferroan calcite, dolomite and recognized under authigenic clays (illite/smectite and kaolinite). Some exceptions were observed where early carbonate cement inhibited quartz cement formation. Like the quartz cement, early carbonate cements limited the effect of compaction and preserved some intergranular porosity.

The later ferroan calcite not only has smaller crystals than the early non-ferroan calcite, but also may appear cloudy due to inclusions of precursor detrital grains replaced by the calcite. The ferroan calcite also fills pore-spaces, may replace earlier diagenetic features such as quartz and calcite cements, and fill micro fractures (Figure

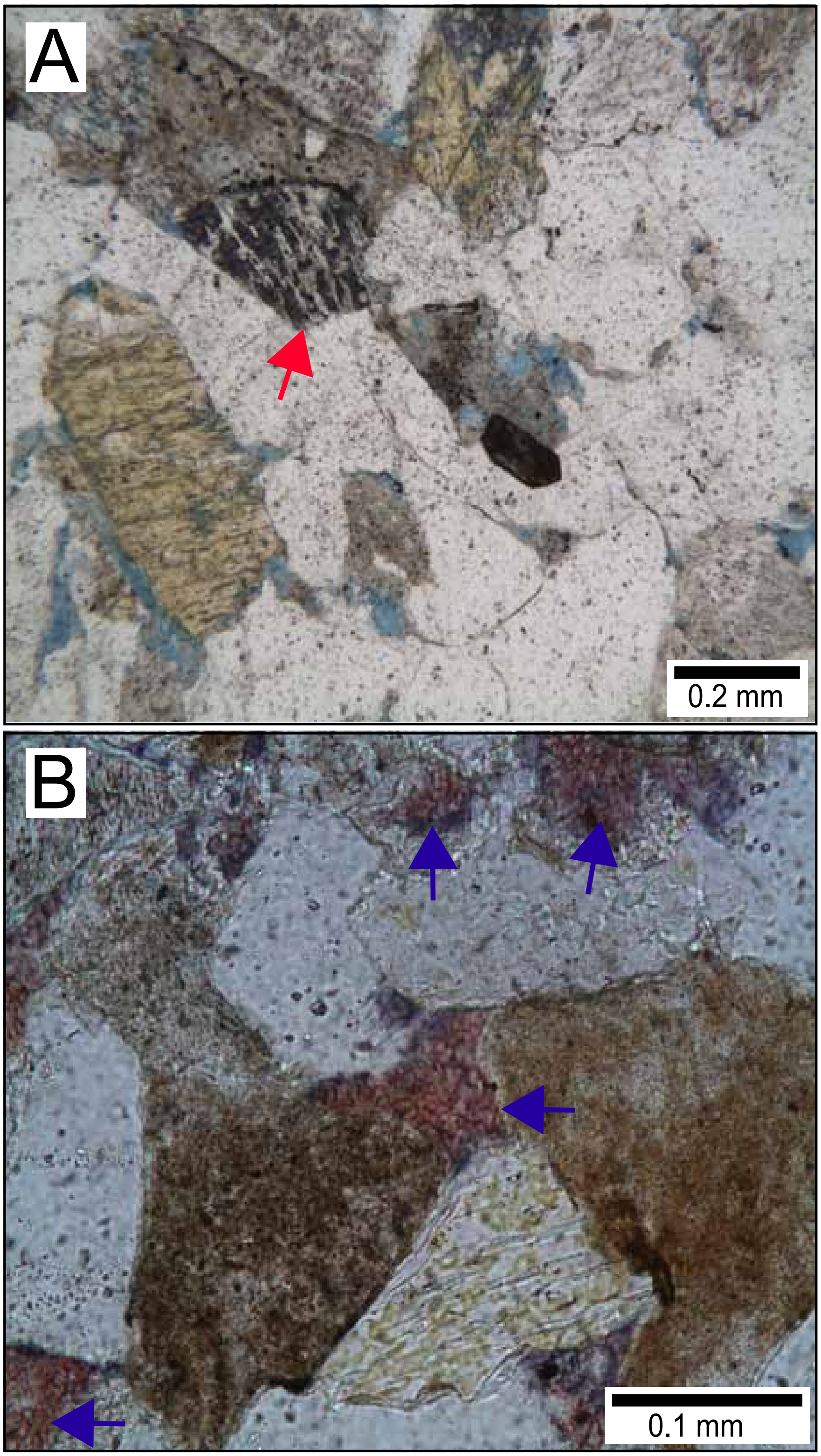

Figure 4.8 - Thin-section photomicrographs (A) Parachute 4580', plane light, and (B) Parachute 4679', plane light, showing non-ferroan and ferroan calcite cements. (A) Ferroan calcite preferentially replaces feldspar along crystal cleavage planes (red arrow). (B) Non-ferroan calcite cement fills intergranular pores (blue arrows).

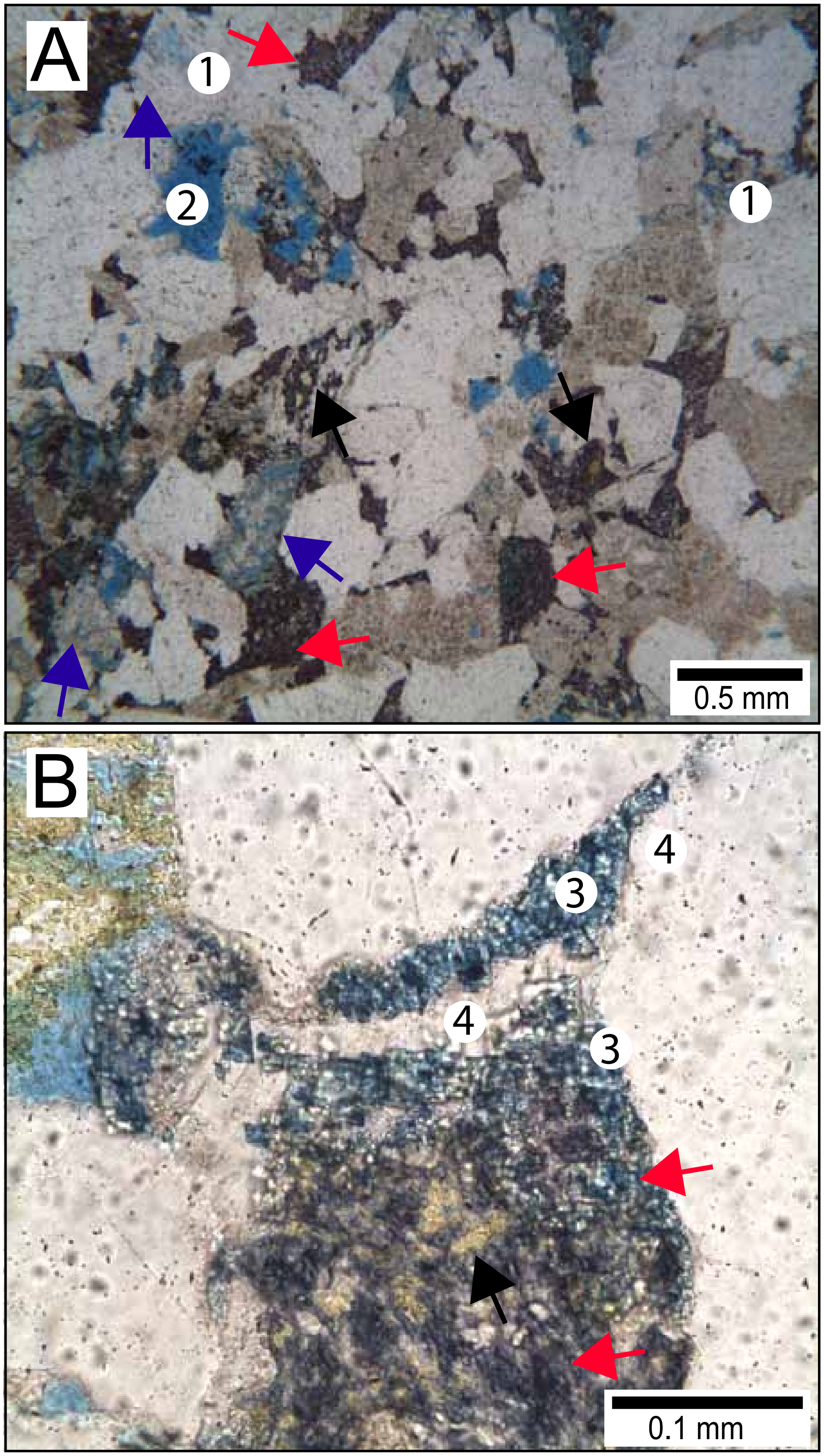
A
1
2
1
0.5 mm
B
4
3
4
3
0.1 mm

Figure 4.9 - Thin-section photomicrographs (A) Parachute 4586’, plane light, and (B) Parachute 4580’, plane light, showing authigenic calcite and dolomite. (A) Ferroan calcite (red arrows) selectively replaces potassium feldspar, as evidenced by tiny yellow-stained remnants of feldspar within the calcite (black arrow). Note plagioclases grains (blue arrow) are not targeted by calcite replacement. Secondary intragranular (1) and moldic (2) porosity resulted from dissolution. (B) Ferroan dolomite (3) replaces the earlier-formed ferroan calcite (red arrow) and the initial cement, quartz overgrowth (4).

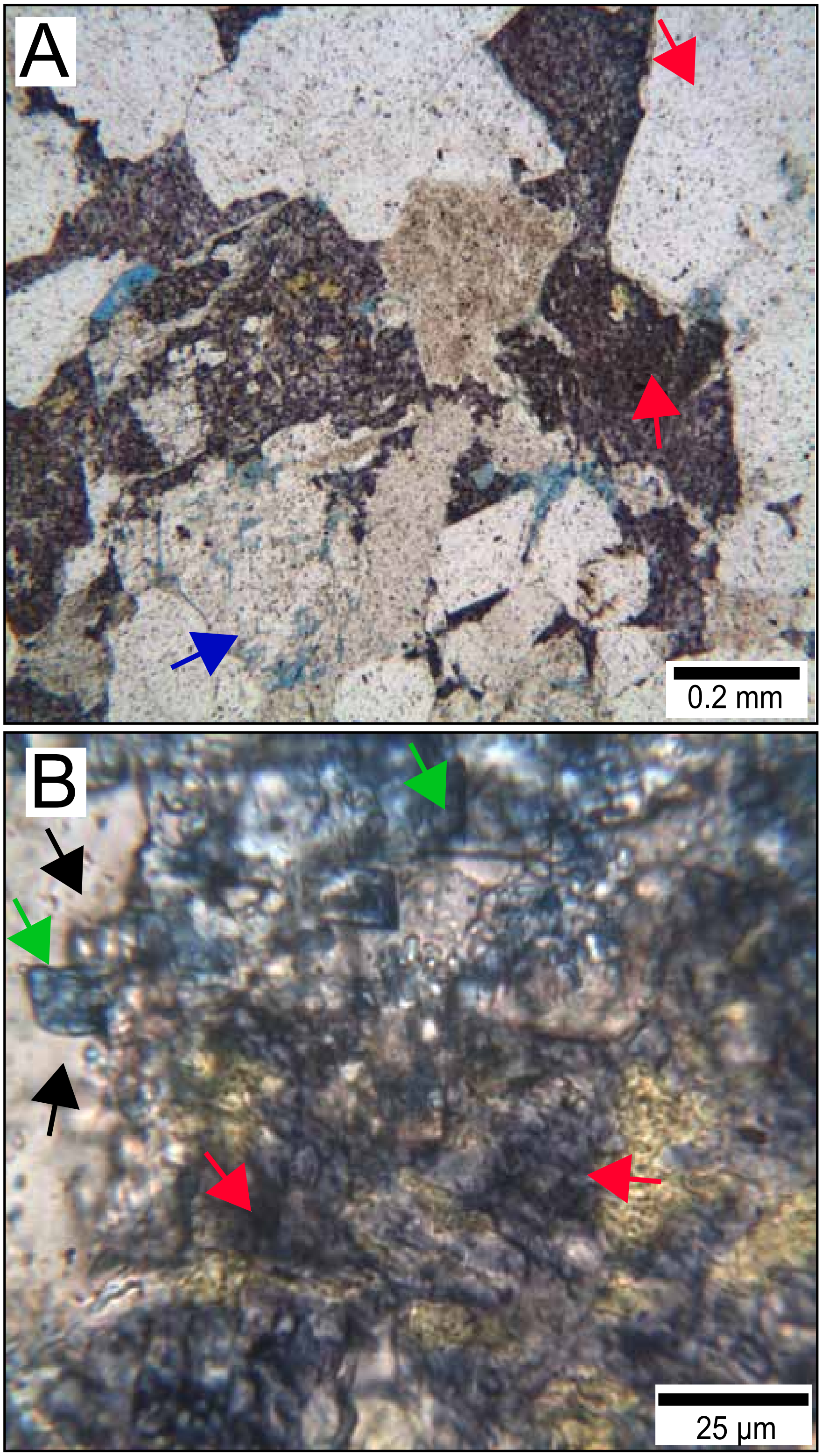

Figure 4.10 - Thin-section photomicrographs (A) Parachute 4586', plane light, and (B) Parachute 4580', plane light, showing ferroan calcite (red arrow) selectively replacing K-feldspar (yellow). (A) Almost all K-feldspar is replaced. Plagioclase (blue arrow) is subject to dissolution that enhances porosity, but not to carbonate replacement in this sample. (B) Ferroan dolomite (red arrows) and ferroan calcite (green arrows) replace quartz (grain and overgrowth at black arrows).

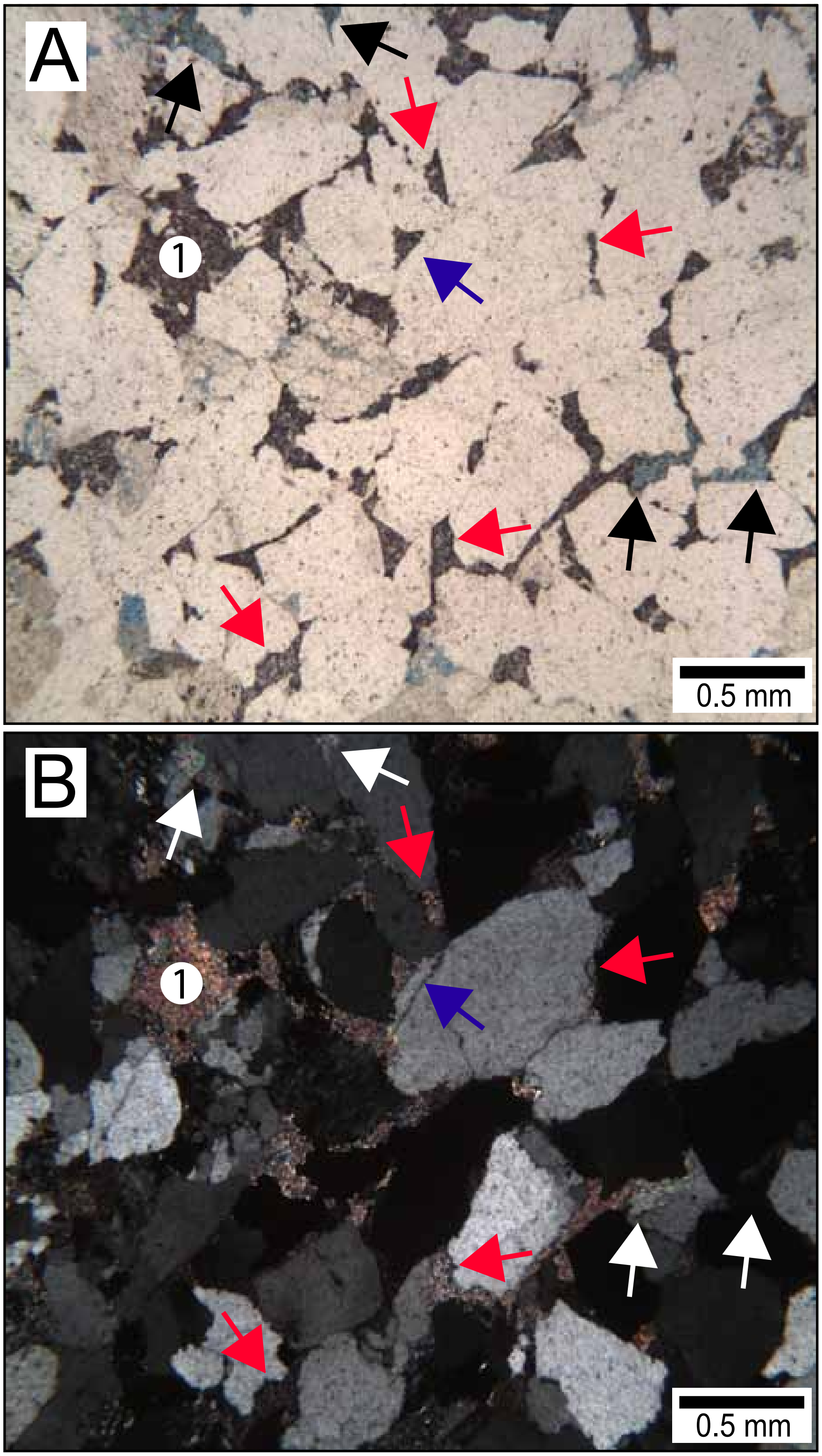

Figure 4.11 - Thin-section photomicrographs Parachute 4586’, (A) plane light, and (B) cross nicols, showing intergranular carbonate selectively replacing earlier cement. Ferroan calcite (red arrows) and ferroan dolomite (black and white arrows) selectively replace earlier quartz overgrowths, some of which can be seen (blue arrow in B). Few grains are targeted by ferroan calcite replacement (1). Blue epoxy in A is in secondary porosity.

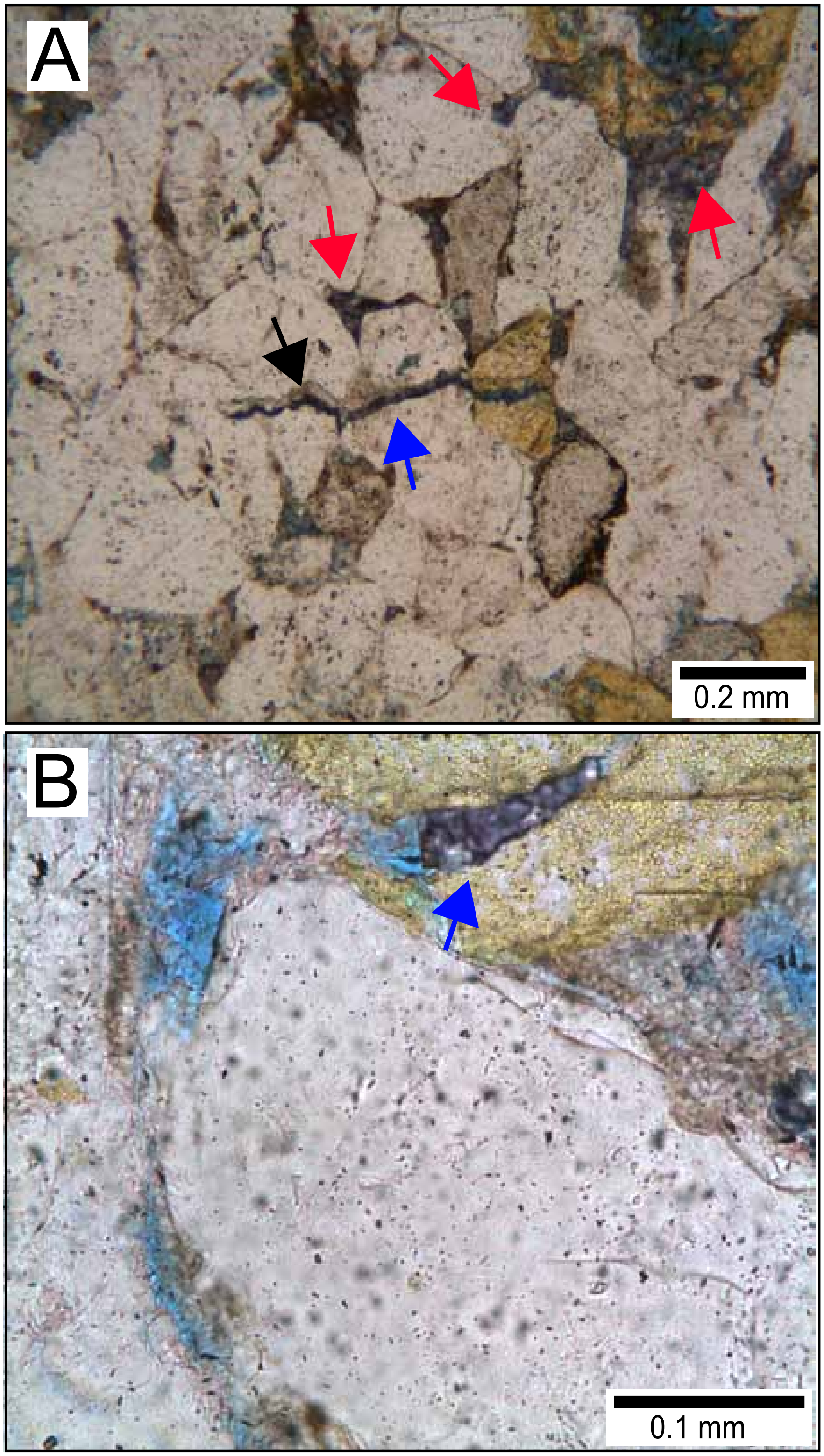
A
0.2 mm
B
0.1 mm

Figure 4.12 - Thin-section photomicrographs (A) Parachute 4571’, plane light, and (B) Parachute 4651’, plane light, showing late calcite cements that fill micro fractures and secondary dissolution pores. (A) Ferroan calcite and dolomite fill micro fracture that postdates early cementation. Note that the non-ferroan dolomite in the upper half of the microfracture shows no staining (black arrow) while the dolomite in the lower side of the fill is purple-stained ferroan-calcite (blue arrow). Ferroan calcite also partly replaces grains and early cements (red arrows). (B) Late ferroan calcite fills micro fracture that resulted from K-feldspar grain breakage during compaction (blue arrow).

4.12) and macro fractures (Figure 4.13B). Locally these late carbonate precipitates post-date formation of authigenic clays (Figures 4.13A, 4.14).

Dolomite is the main carbonate in the lower Williams Fork Formation, occurring as an anhedral pore fill and replacement mineral (Figures 4.9B, 4.10B, 4.15). It is made up mostly of poikilotopic and rhombic crystals of ferroan dolomite, and forms up to 32 percent of the rock volume in some sandstones. In lesser abundance, non-ferroan dolomite also exists in the lowermost interval of the lower Williams Fork Formation. Dolomite exhibits its greatest abundance in facies that have detrital dolostone fragments that formed nuclei for the authigenic dolomite growth. These detrital carbonates are distinctive because of their sub-to-well rounded shapes and their cleavage-like features (Figure 4.15).

Clays

Four types of diagenetic clay minerals were observed within Williams Fork sandstones: chlorite, mixed-layer illite/smectite (I/S), illite, and kaolinite. These authigenic clays occur as grain coatings, pore linings, pore fillings, pseudomorphic replacements, and fracture fillings. An authigenic origin for these clays is based on clay morphology, purity of composition, heterogeneous distribution within samples, and sandstone textural properties. The fragility of the clay morphologies and pore lining fabrics argue against a depositional origin.

Authigenic chlorite occurs as grain coatings, diffuse intergranular chlorite masses, and pore linings. It is common in the fluvial intervals of the middle and upper Williams Fork Formation (Figures 4.16, 4.17) and concentrated in the upper Williams

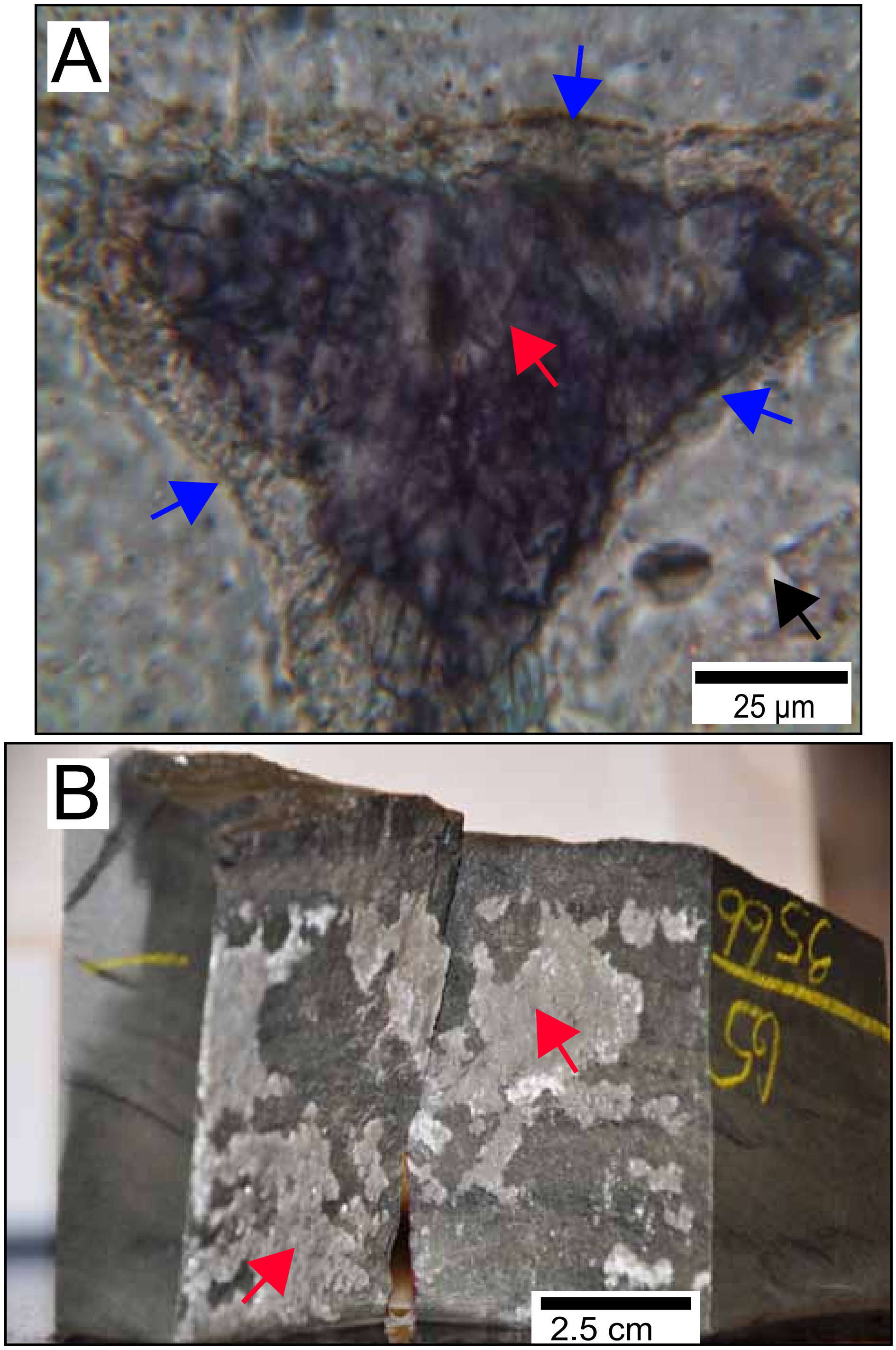

Figure 4.13 - (A) Thin-section photomicrograph Parachute 4651’, plane light showing ferroan calcite that postdates authigenic clay formation. Ferroan calcite (red arrow) fills intergranular pore space that is lined by fibrous authigenic clay (blue arrows). (B) Last Dance core sample, 3566’, showing calcite cements along a fracture wall (red arrows). Natural fractures lined with calcite crystals ranged from partly open to totally sealed within the studied sandstones.

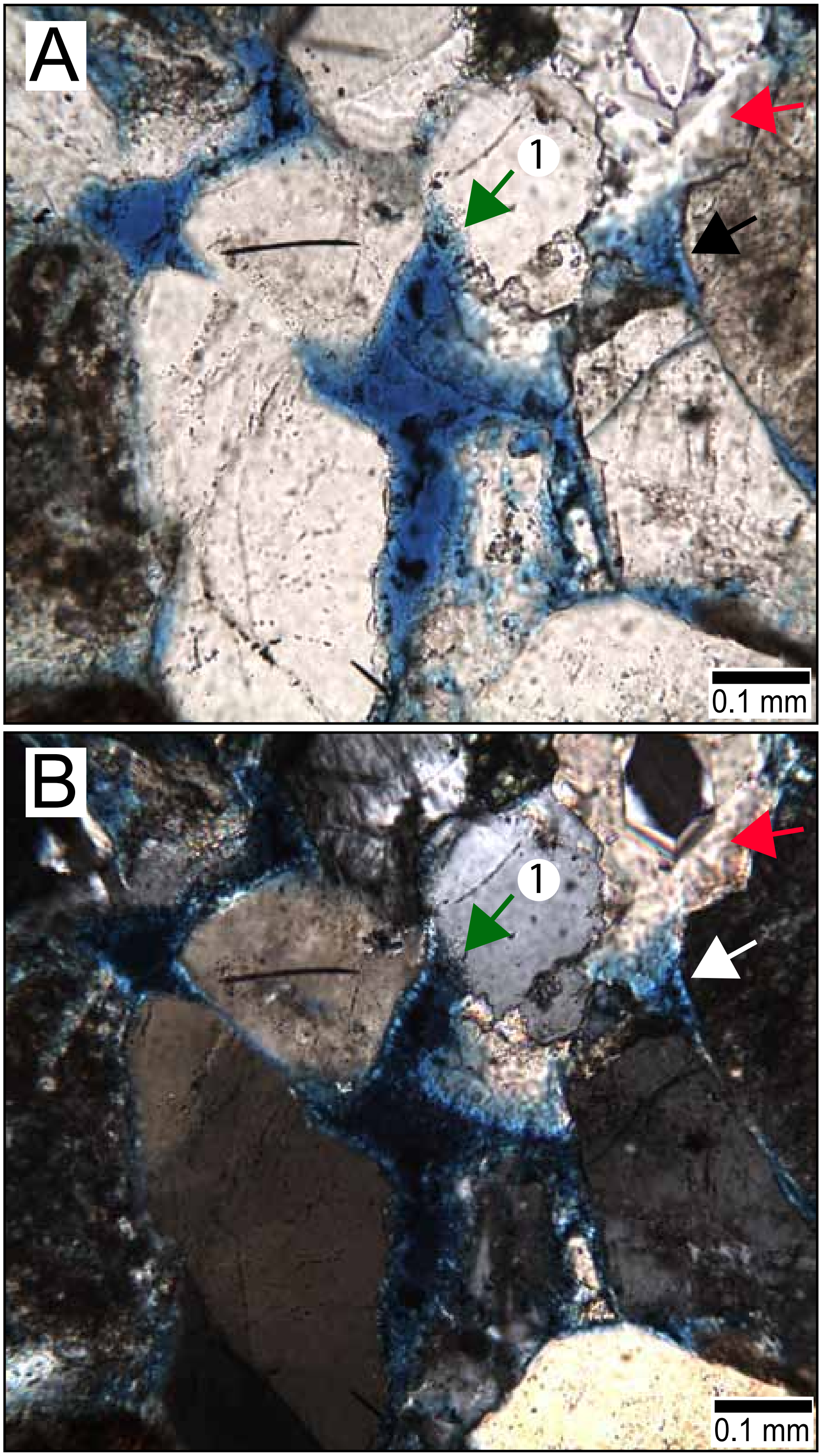
A
1
0.1 mm
B
1
0.1 mm

Figure 4.14 - Thin-section photomicrographs Last Dance 4019’, (A) plane light and (B) cross nicols, showing authigenic calcite “replacement” (red arrows) that postdates all diagenetic events in the sample. Compaction, quartz overgrowth, and authigenic clay formation as well as grains and early cement dissolution are digenetic events predated by the late calcite. Note the partly dissolved quartz grain (1) has authigenic clay lining the outer grain boundary on the side that is not attacked by calcite (green arrow). The late calcite partially fills the secondary pore (white-black arrow) that was lined by fibrous authigenic clay, some of which can be seen at the tip of the white arrows.

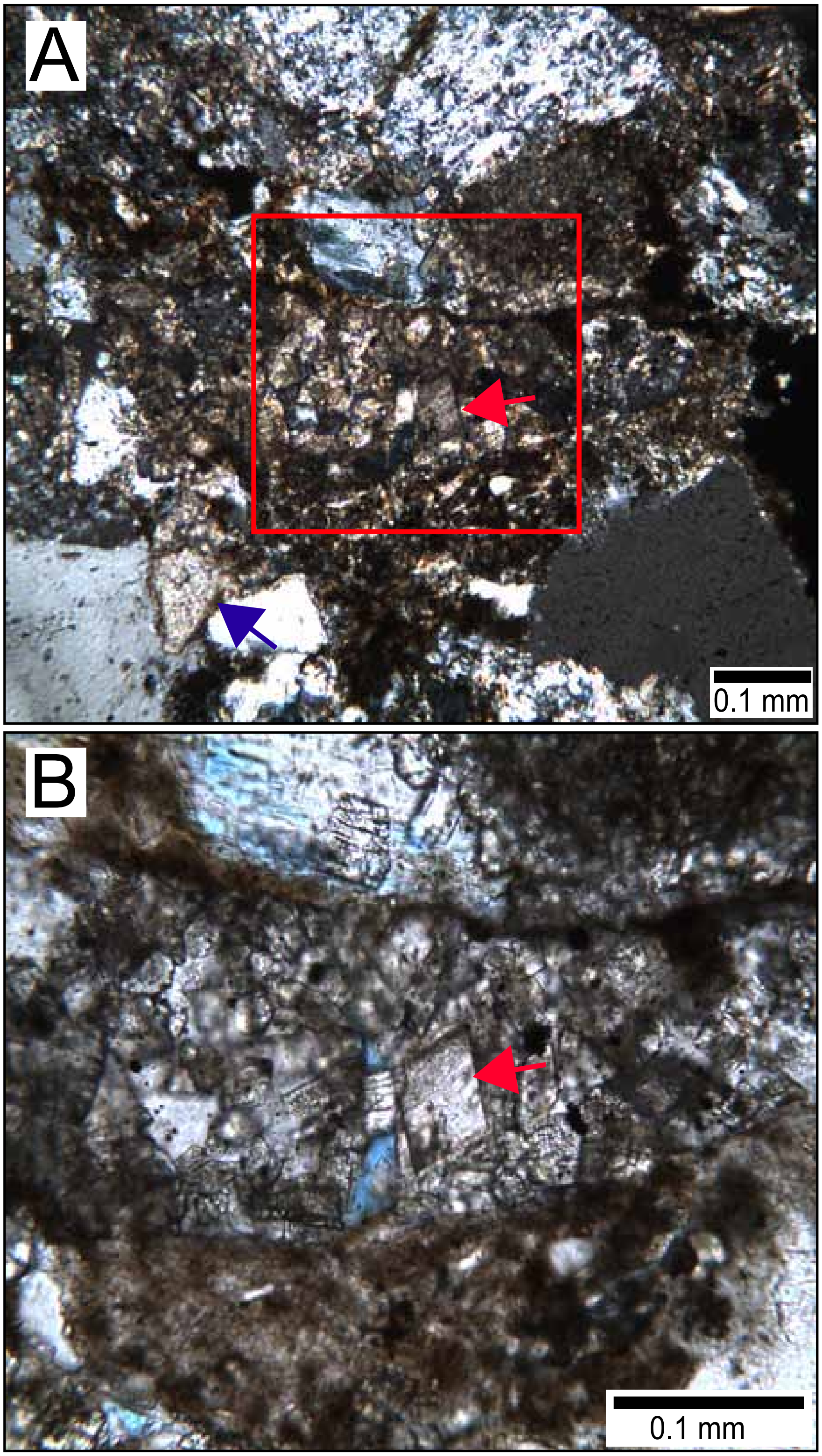

Figure 4.15 - Thin-section photomicrographs (A) Cascade Creek Oxy 4752’, cross nicols, and (B) plane light close-up of outlined area in (A). Authigenic dolomite occurs as pore-fill cement and a replacement, recognizable by its euhedral, rhombic crystal outlines and lack of twinning. Detrital dolostone fragments, like the detrital grain with blue arrow in (A), form nuclei for the authigenic dolomite.

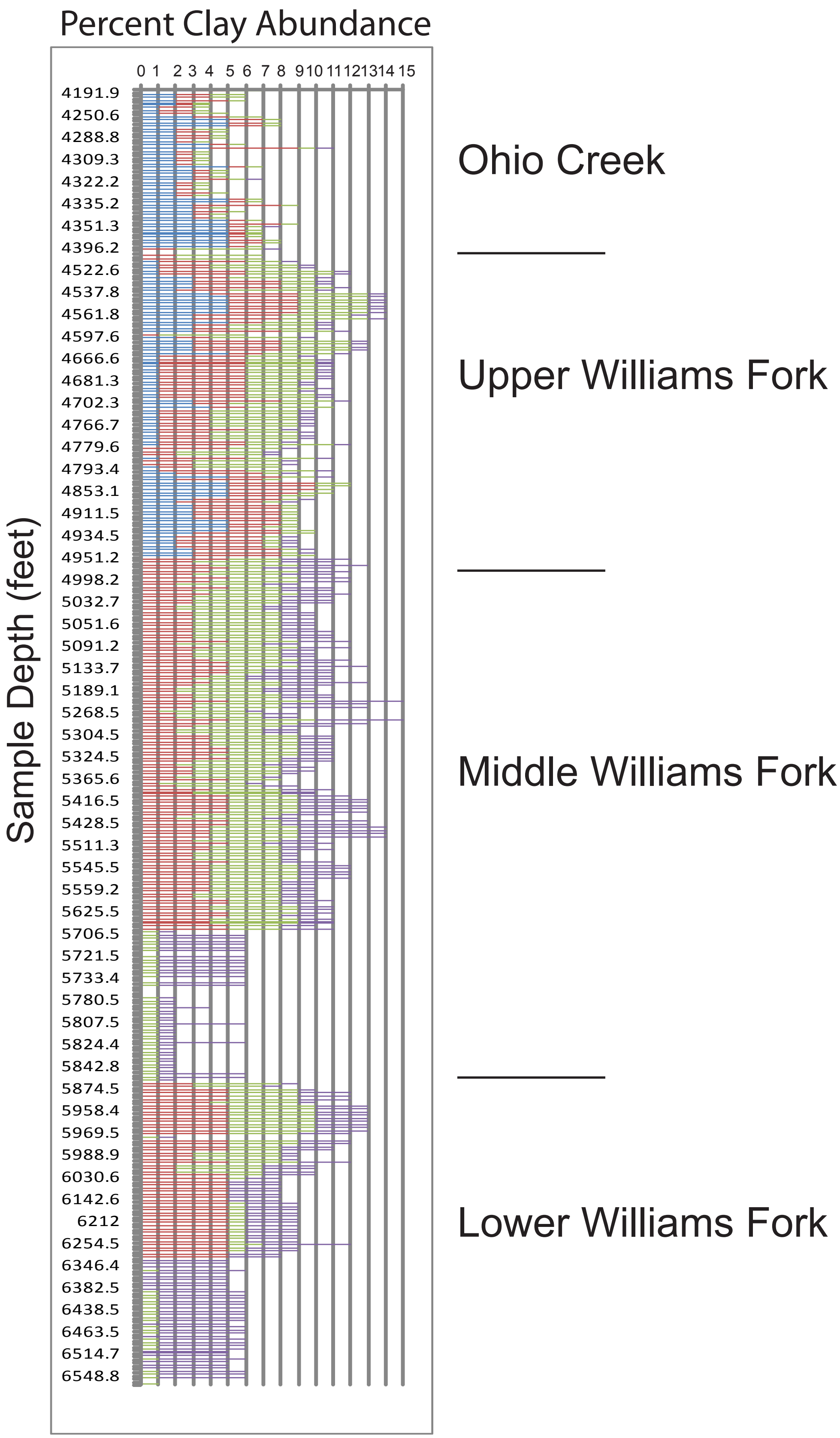
Percent Clay Abundance
0 1 2 3 4 5 6 7 8 9 10 11 12 13 14 15
Sample Depth (feet)
4191.9
4250.6
4288.8
4309.3
4322.2
4335.2
4351.3
4396.2
4522.6
4537.8
4561.8
4597.6
4666.6
4681.3
4702.3
4766.7
4779.6
4793.4
4853.1
4911.5
4934.5
4951.2
4998.2
5032.7
5051.6
5091.2
5133.7
5189.1
5268.5
5304.5
5324.5
5365.6
5416.5
5428.5
5511.3
5545.5
5559.2
5625.5
5706.5
5721.5
5733.4
5780.5
5807.5
5824.4
5842.8
5874.5
5958.4
5969.5
5988.9
6030.6
6142.6
6212
6254.5
6346.4
6382.5
6438.5
6463.5
6514.7
6548.8
Ohio Creek
Upper Williams Fork
Middle Williams Fork
Lower Williams Fork

Figure 4.16 - Clay minerals distribution within sandstones of the MWX1core. Vertical scale depicts sample footages in descending order; it is not a true vertical scale. Illite exists almost throughout the whole interval, chlorite is concentrated in the upper and middle Williams Fork, and mixed-layer clays prevail in the middle and lower intervals. Kaolinite is present only in the upper Williams Fork interval. Data provided by Williams Companies, Inc.

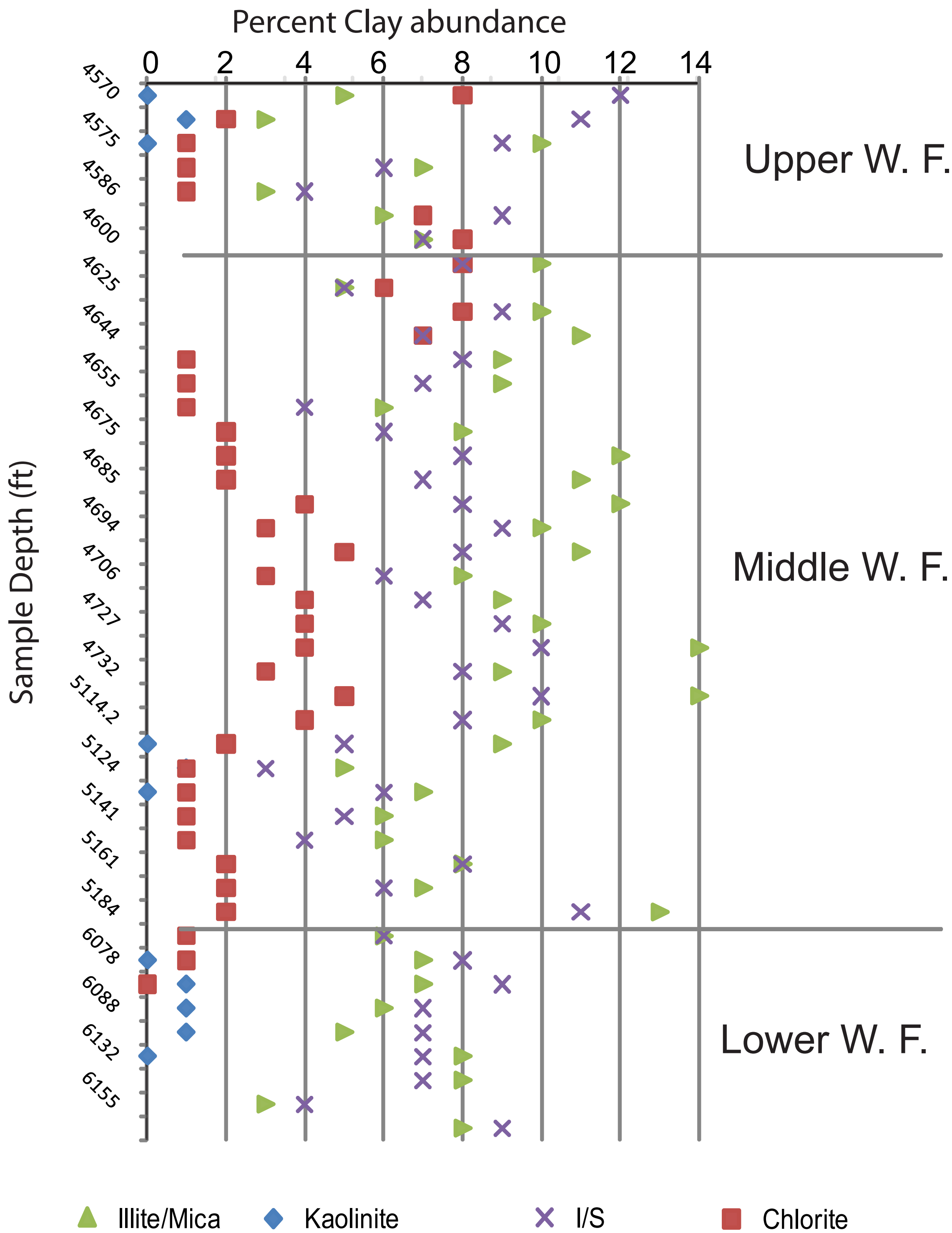

Figure 4.17 - Clay mineral distribution within sandstones of the PA 424-34 Parachute core. Vertical scale depicts sample footages in descending order; it is not a true vertical scale. Illite and mixed-layer illite/smectite (I/S) occur almost throughout the whole section with higher concentration in the middle Williams Fork interval. Chlorite is concentrated in the upper interval and decreases with depth. XRD data provided by Williams Companies, Inc.

Fork section where it may be the main clay component. It is recognizable in core by the distinctive greenish tint it imparts to sandstones. In thin sections, authigenic chlorite presents greenish platelets growing perpendicular to the grain surface, forming thin, uniform green rims around the detrital grains (Figures 4.18, 4.19). Small stacks of face-to-face chlorite plates and/or fan-shaped chlorite plates that partly fill pores are also present. These green rims consist of 2 to 30 micron crystals, commonly are oriented on edge with faces perpendicular to the detrital grain surfaces, and have euhedral, pseudo hexagonal crystal forms. Chlorite masses show high microporosity under SEM.

Numerous studies have reported that chlorite grain coats prohibit silica overgrowths in sandstones, (e.g., Ehrenberg, 1993; Pittman et al., 1989, 1992; Bloch et al., 2002; Berger et al., 2009; Pe-Piper and Weir-Murphy, 2008; Anjos et al., 2009; Taylor et al., 2010). Chlorite in the Williams Fork sandstone is an effective clay coating that prevented the development of silica overgrowth. Quartz grains completely covered by thick and uniformly developed chlorite coatings are usually free of quartz overgrowths and syntaxial quartz cement hardly ever exists if quartz grains are surrounded by chlorite (Figure 4.19). However, quartz grains with thin and patchy (irregular) chlorite coatings may show syntaxial quartz overgrowths (Figure 4.5).

XRD results from <5 μm fractions reveal sharp and symmetrical basal diffractions, suggesting well-crystallized 14 Å chlorite (Figure 4.20). Chlorite peaks showed no change as a result of glycolation, and in some samples heating the sample to 550°C for 1 hour strongly increased the intensity of the 001 14 Å spacing. The XRD results also revealed that the intensity of the even-order basal spacings is much more than the odd-order diffractions, suggesting a high Fe/[Fe+Mg] ratio in the octahedral site

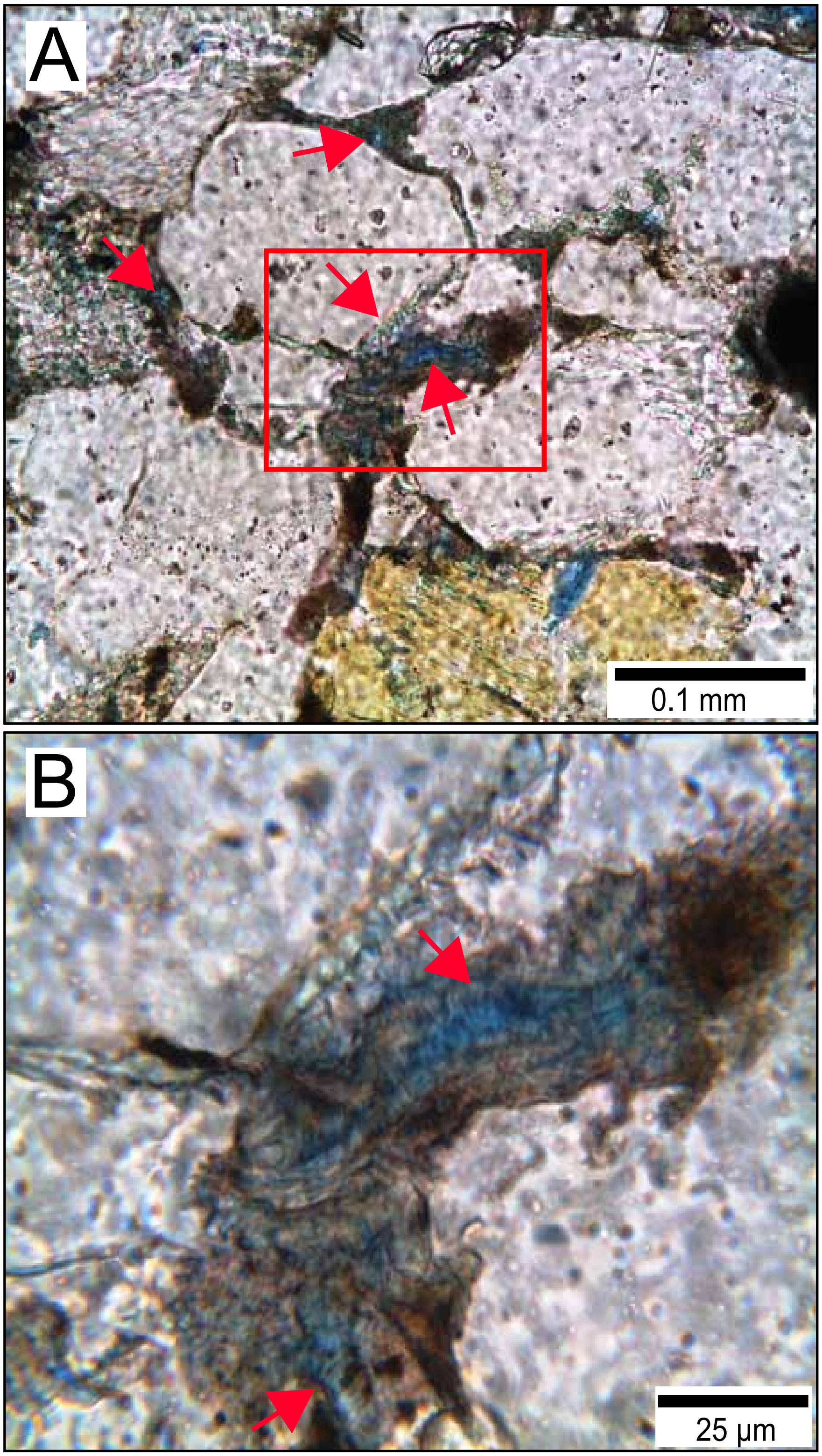

Figure 4.18 - Thin-section photomicrograph Parachute 4625', (A) and (B) plane light showing chlorite-lined intergranular pores. Pore-lining chlorite cement consists of a continuous rim that covers detrital grains and early cement. Note that individual chlorite crystals are oriented on edge, with faces perpendicular to the pore surface. (B) Enlarged view of the outlined area in (A) showing chlorite cements.

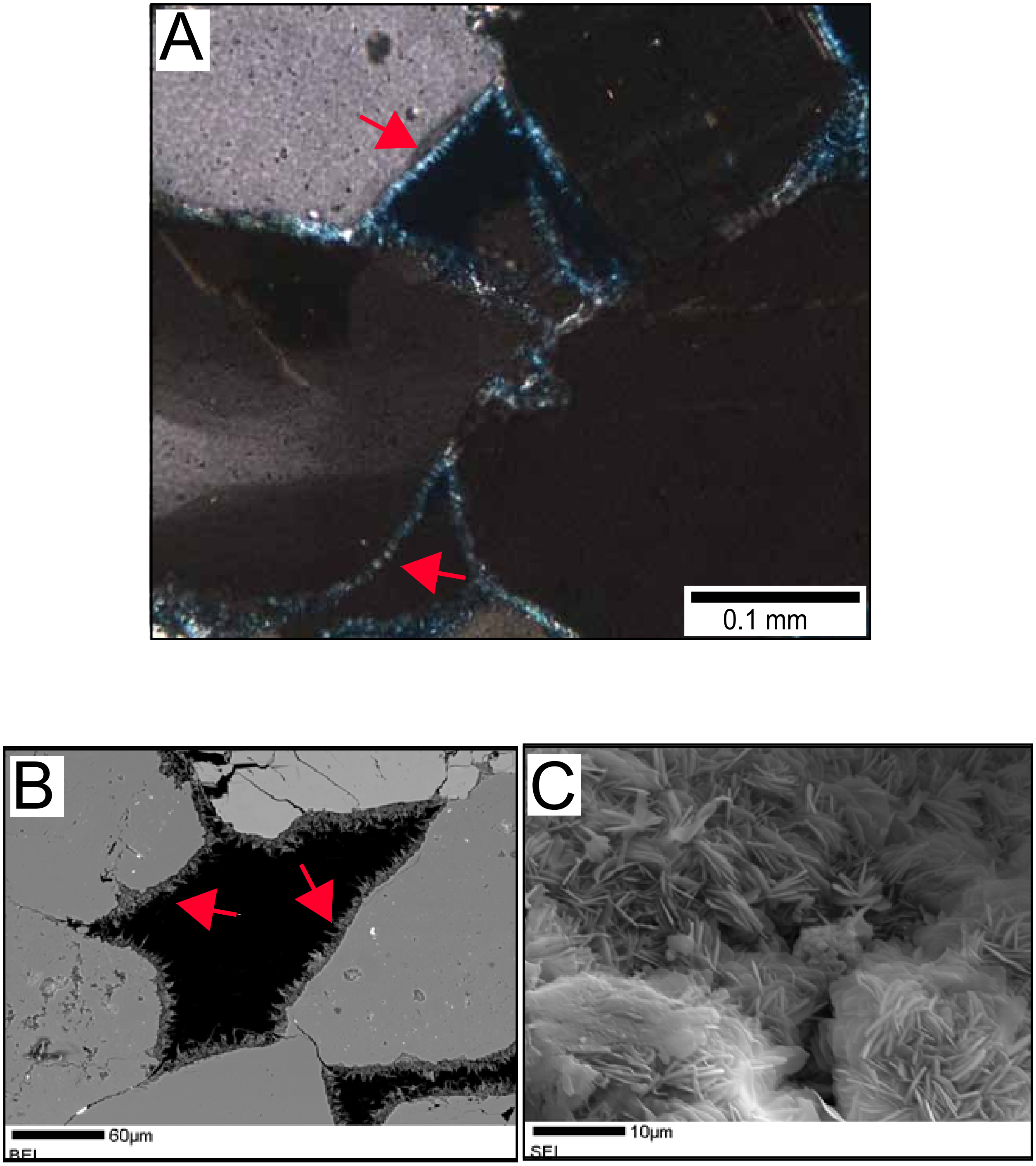

Figure 4.19 - (A) Thin-section photomicrographs Last Dance 2859’, cross nicols, and (B) Last Dance 4010’, backscattered electron photomicrograph showing detrital quartz grains surrounded by thick rims of isopachous grain-coating chlorite cement (red arrows). Note that the sandstone has no silica cement surrounding the chlorite-coated grains. (C) Last Dance 2859’, secondary electron photomicrograph showing authigenic chlorite in rosette pattern that coats quartz grains and lines pores.

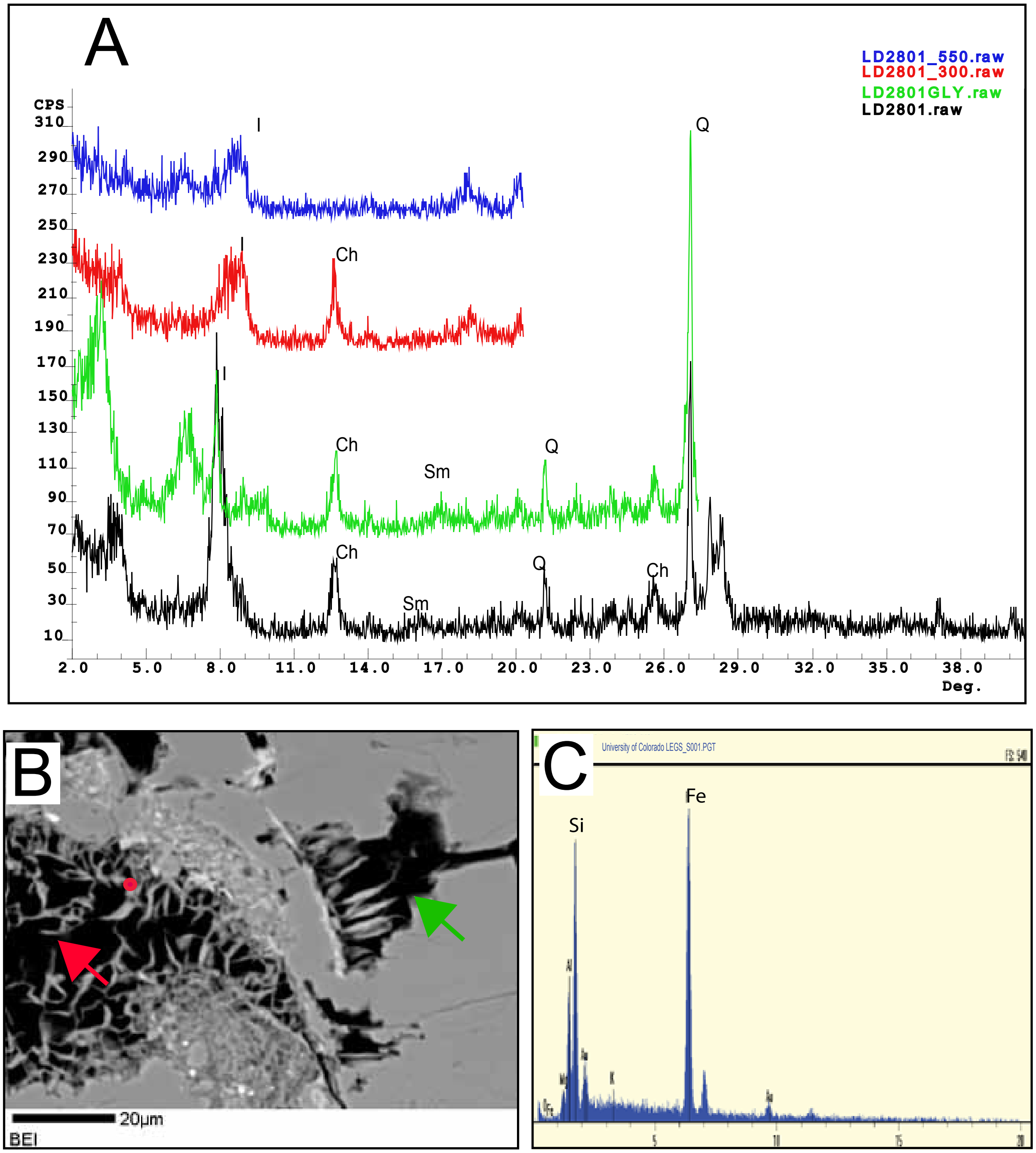

Figure 4.20 - (A) X-Ray diffraction patterns of clay-separated sample from Last Dance 2801'. Diffraction patterns are oriented and air dried (black), glycolated (green), heated to 300°C (red), and heated to 550°C (blue). Labeled peaks are: I= illite, Q= quartz, I/S= illite-smectite, Ch= chlorite Sm= smectite. (B) Backscattered electron photomicro-graph Last Dance 4019' showing authigenic chlorite lining intergranular pore (red arrow) and secondary intragranular pore (green arrow). (C) Energy dispersive X-ray spectrum analysis of red spot in (B) indicates an iron-rich chlorite.

of the chlorite (Spoet et al., 1994). The general ratio of large, even peaks (002) (004) to odd peaks (001) (003) has been interpreted by Moore and Reynolds (1997) to indicate a high iron concentration, which was observed in EDX analysis (Figure 4.20).

Based on SEM and XRD results, the Williams Fork chlorite includes both the Ib and IIb polytypes of Kogure and Banfield (1998). The Ib type is common in low temperature (<150°C) digenetic settings, but the IIb is typical of higher temperature (150°-200°C) environments (Odin, 1990). In SEM, the dominant Ib polytype chlorite crystals are thin, euhedral, pseudohexagonal plates forming a "house-of-cards" texture. These crystals are typically small in diameter relative to the IIb chlorite. These Ib plates are typically characterized by their thinness, which rarely exceeds 0.2 µm. The thicker plates-to-blocky crystals of the IIb chlorite exist in smaller amounts within the Williams Fork samples. They occur in sandstones characterized by higher mechanical and chemical compaction, which caused much lower intergranular volume, and exist as pore fillings rather than grain coatings. The IIb chlorites occasionally post-date early carbonate and/or quartz cement. The Ib and IIb chlorite types form mixtures in many studied samples. It is highly possible that type Ib recrystallized to type IIb with increased burial temperature and pressure (Liu et al., 1998; Peng et al., 2009).

Mixed-layer clays consisting of vertically stacked and mixed layers of illite and smectite (I/S) exist almost throughout the entire Williams Fork Formation, with highest concentration in the middle Williams Fork interval (Figures 4.16, 4.17). Authigenic Illite/smectite coats detrital grains, lines and fills primary and secondary pores (Figures 4.21, 4.22, 4.23A), and forms bridges between pores. In the I/S-rich sandstone intervals, authigenic I/S clays that coat detrital quartz occasionally inhibited the

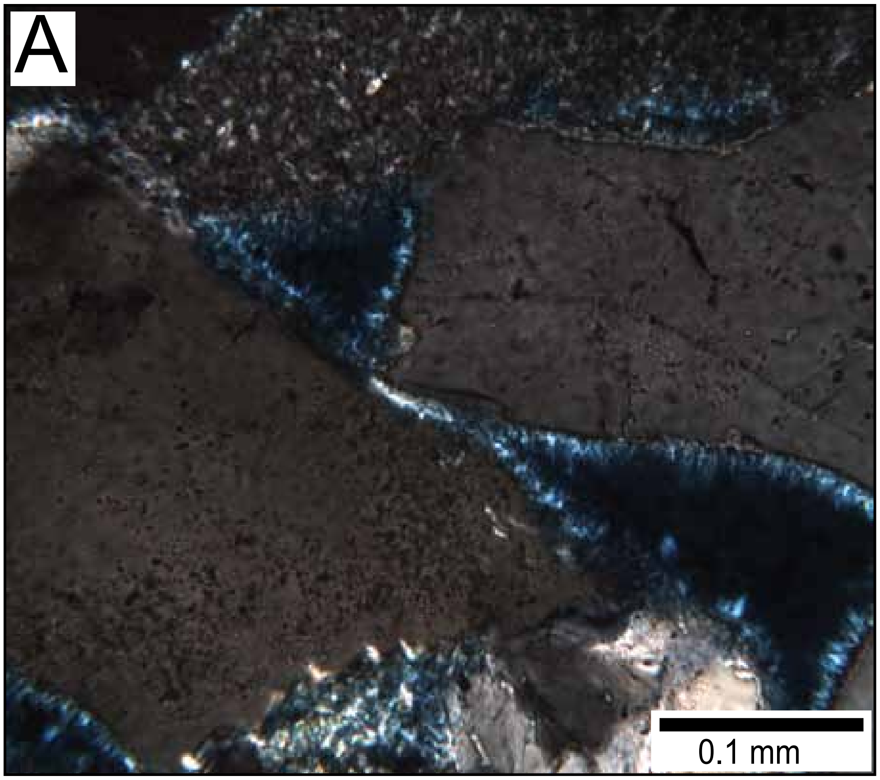

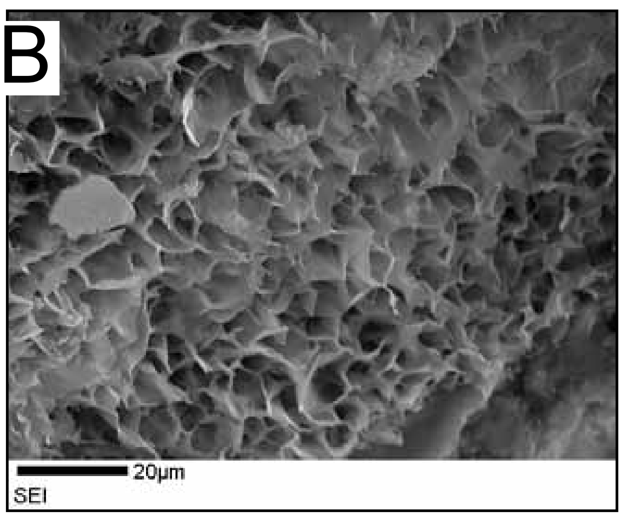

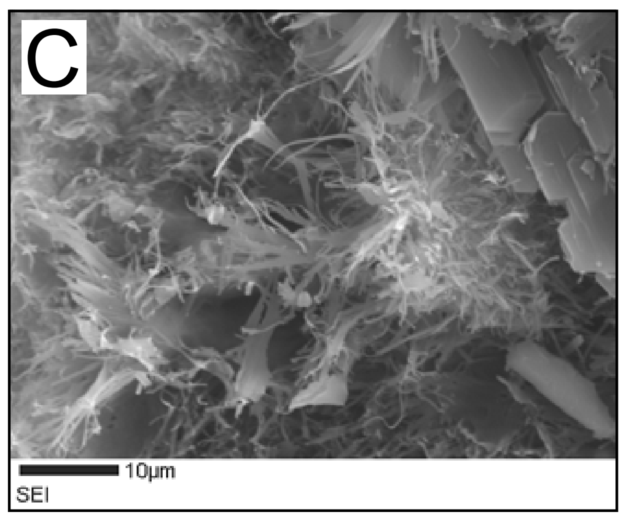

Figure 4.21 - (A) Thin-section photomicrograph Cascade Creek Oxy 4809', cross nicols, showing illite and illite/smectite platelets growing perpendicular to the grain surfaces and forming fibrous-isopachous rims around the detrital grains. (B, C) Secondary electron photomicrographs from Last Dance 5728' and 4010' showing illite and illite/smectite mixed-layer clays. (B) Webby crystal habit morphology of smectite grows on sandstone grains. (C) Illitic ribbons.

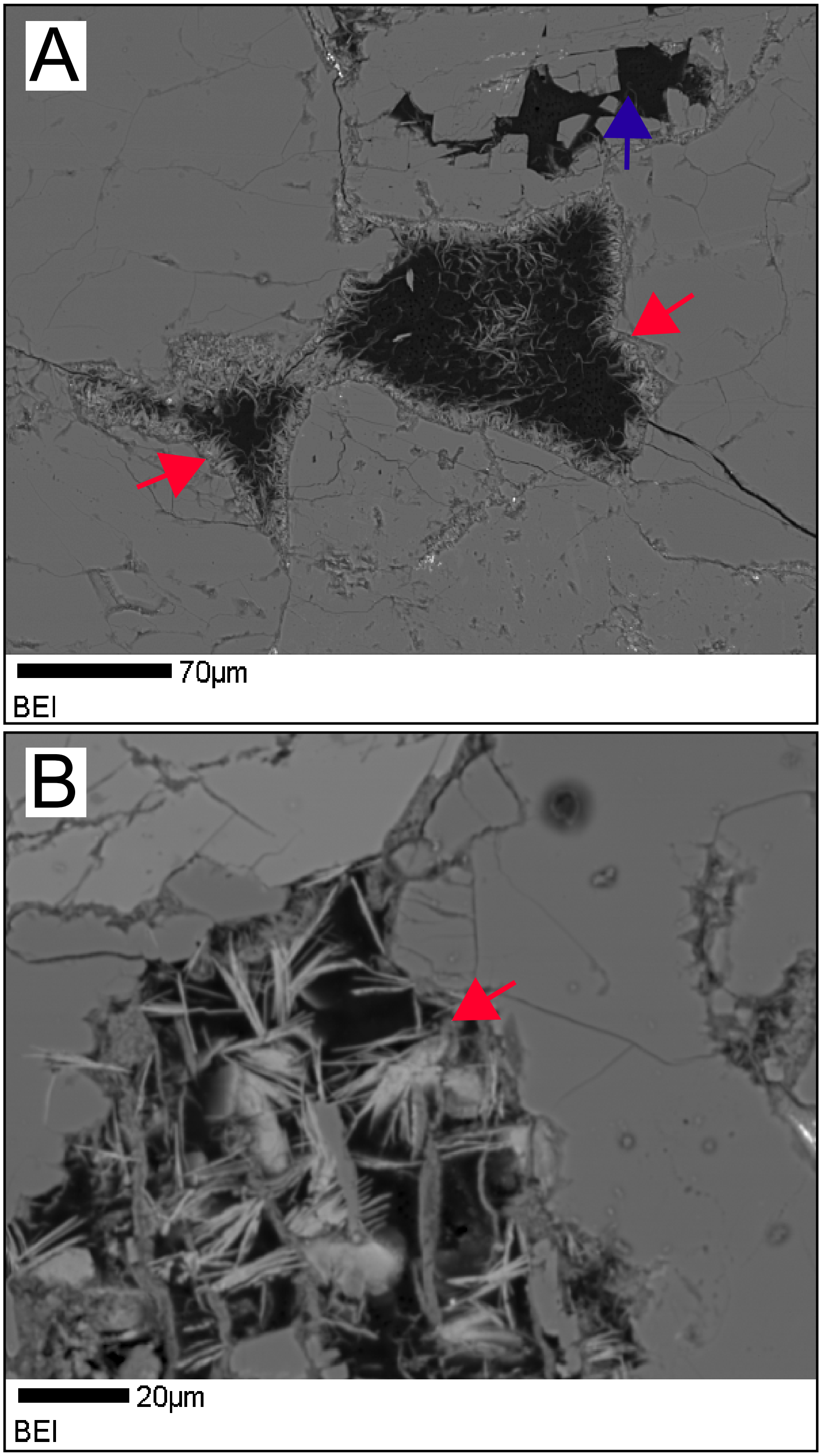
A
70µm
BEI
B
20µm
BEI

Figure 4.22 - Backscattered electron photomicrographs Parachute 4691’ (A) and 4577’ (B), showing illite and illite/smectite authigenic clays that line and fill pores. (A) Illite rims grains and extends perpendicular to the grains surfaces into intergranular pores. It is also replacing some of the original grains (red arrows). Yet illite is essentially absent in the secondary intragranular dissolution pore (blue arrow) that contains rhombs of carbonate cement. (B) Well developed authigenic illite and illite/smectite platelets growing together in a complex morphology and filling an intergranular pore.

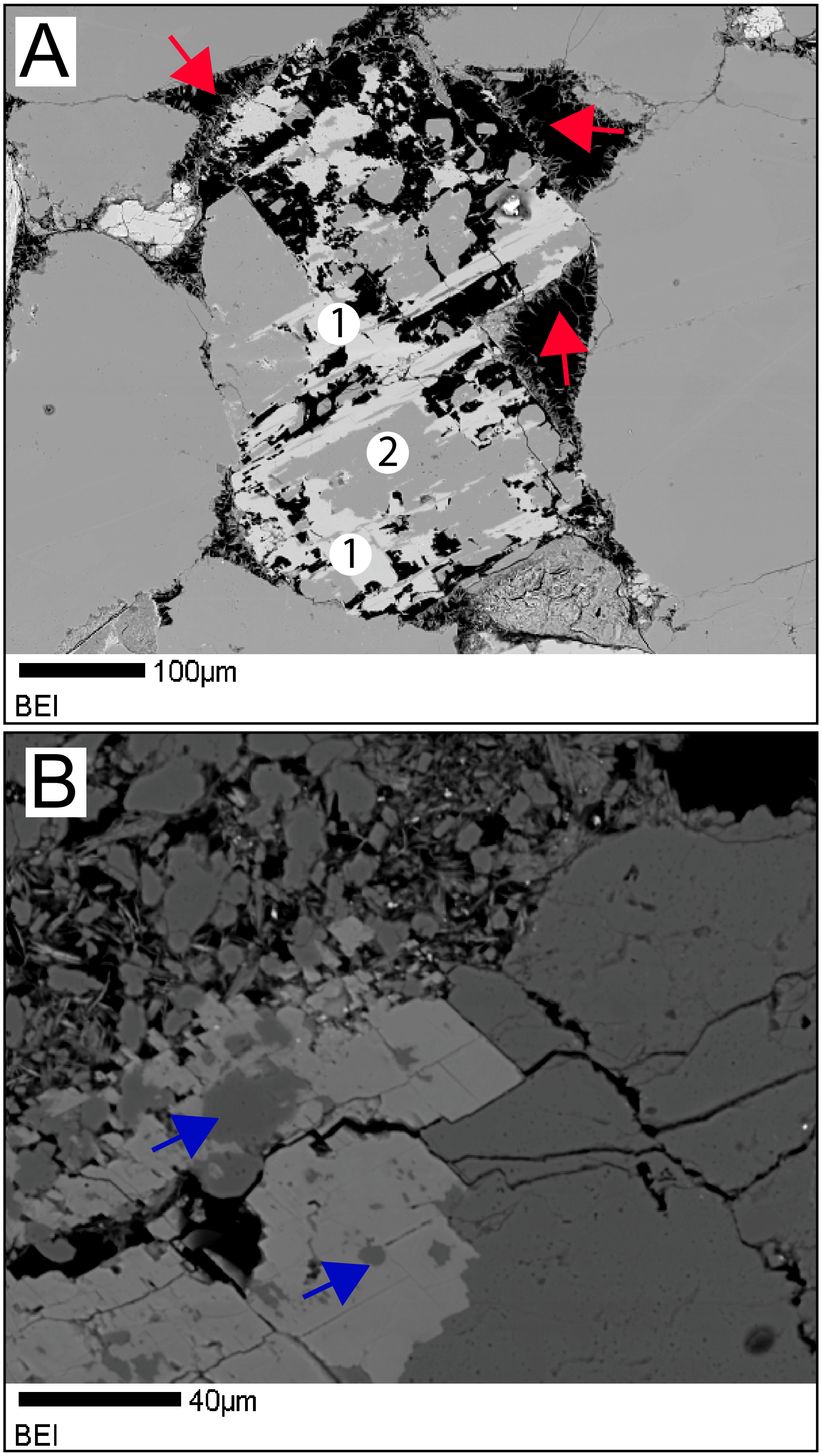

Figure 4.23 - Backscattered electron photomicrographs, (A) Last Dance 4019', and (B) Parachute 4585'. (A) Ferroan calcite (1) replaces albite (2). The feldspar grain is partly dissolved, and the intragranular secondary pores are lined by late authigenic illite and illite/smectite fibers clays (red arrows). (B) Albite (blue arrows) partly replaces potassium feldspar grain.

formation of silica overgrowths (Figure 4.21A). Authigenic Illite occurs as delicate fibers and laths that grows perpendicular to grain surfaces and pore walls (Figures 4.22, 4.24), or may form bridges within pores and across pore-throats. Both authigenic illite and I/S also replace chert and micas.

However, not all illite and I/S is authigenic. Alterations of illite and mixed layer I/S clays were observed at magnifications of 1000x in the polarizing microscope and >1000x in SEM in detrital components including mudstone clasts. These detrital clays typically fill the intergranular spaces and show very thin and faint laminations and/or infiltrated clay micro-structures in thin section.

In X-ray diffractograms, illite was easily identified by its first and second basal reflections at 10, 5 and 3.3 Å on X-ray diffractograms of air-dried and EG-treated specimens. Mixed-layer illite smectite basal reflections occurred at 10 to 14 Å and at 5.2 and 5.1 Å. These reflections expand to higher spacings after samples are treated with ethylene glycol (EG) , and reflections collapse to around 10 Å when heated to 300°C and 550°C. XRD spectra pattern analysis of the first and second basal reflections indicates that I/S are R1 (~ 80% illite) and R3 (> 90% illite). Because of the overlap in illite and I/S basal reflections peaks, which is due to the high illite ratio in the I/S clays, SEM analysis was critical in evaluating the total illite volume within the studied samples.

Kaolinite, where it exists, occurs as a replacement of highly altered feldspar grains or as a pore filling (Figure 4.25). It exists locally within relatively porous facies, occludes secondary dissolution voids, and/or forms pore bridges. The kaolinite demonstrates well-crystallized booklets of stacked hexagonal crystals (Figure 4.26). Some of the kaolinite was assumed to be dickite due to well-developed crystals that are

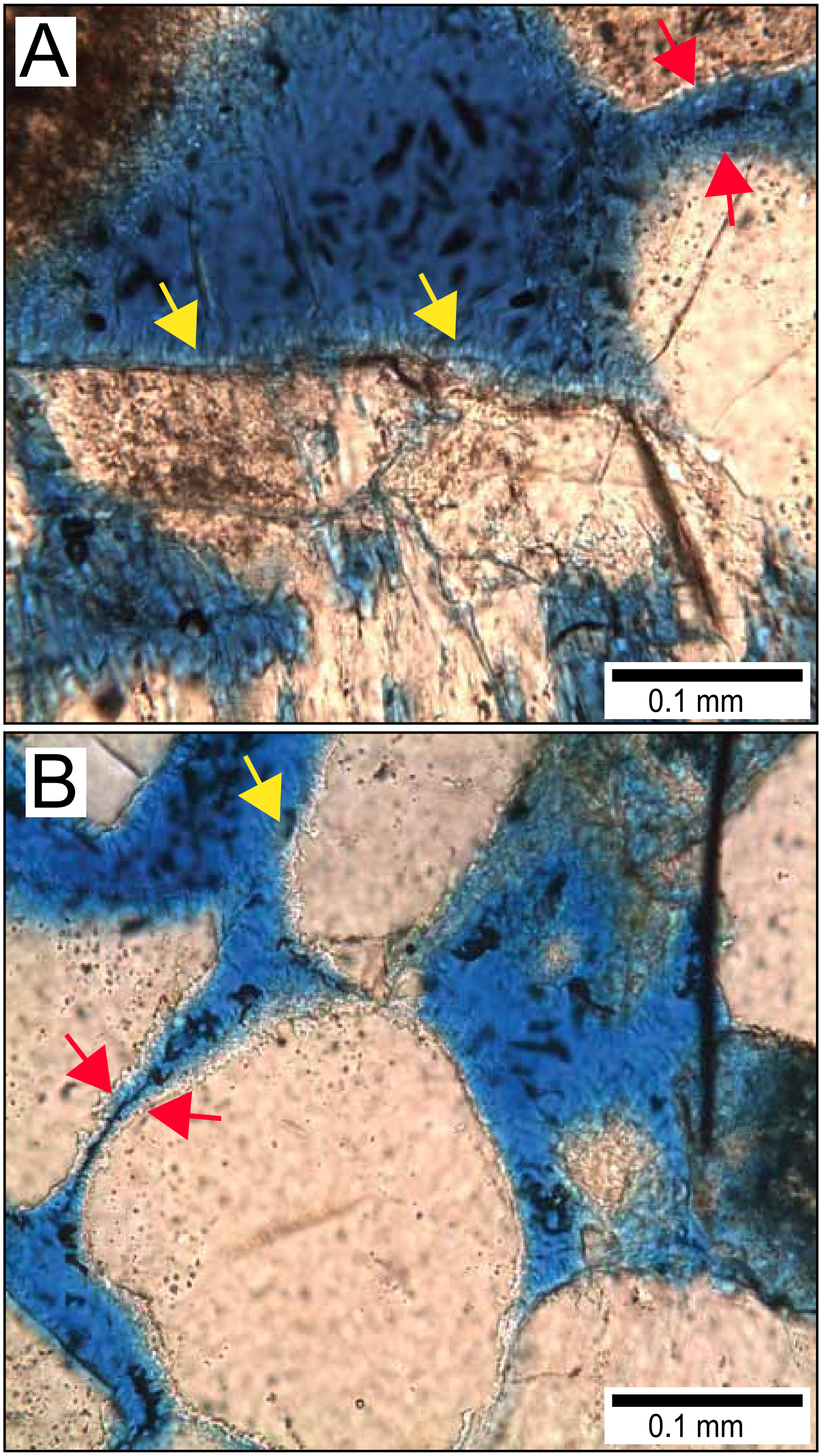

Figure 4.24 -Thin-section photomicrographs (A) Last Dance 4019', plane light and (B) Last Dance 4010', plane light, showing authigenic illite lining pores (yellow arrows) and pore-throats (red arrows). Note skeletal texture of the partly dissolved feldspar grain in A.

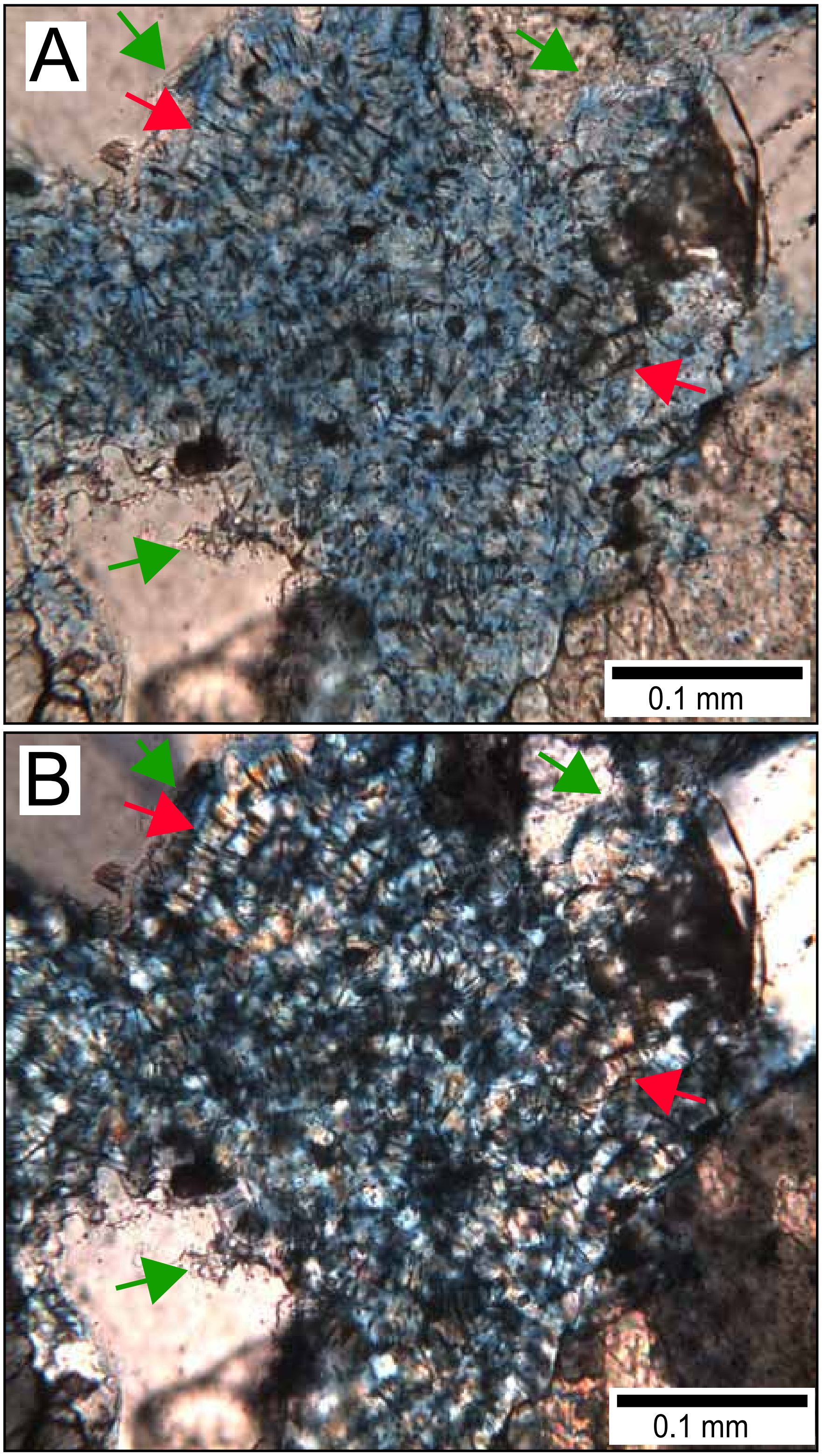
A
0.1 mm
B
0.1 mm

Figure 4.25 - Thin-section photomicrographs Last Dance 4010, (A) plane light, and (B) cross nicols, showing authigenic kaolinite filling intergranular space. Red arrows point to well-developed booklet morphology characteristic of kaolinite. Kaolinite inhabits a framework grain-size area, which might indicate direct replacement of an unstable grain rather than formation as pore-filling cement. This could also be kaolinite in secondary pore space that resulted from aggressive grain and cement dissolution (note the dissolution traces on the grains remains at green arrows).

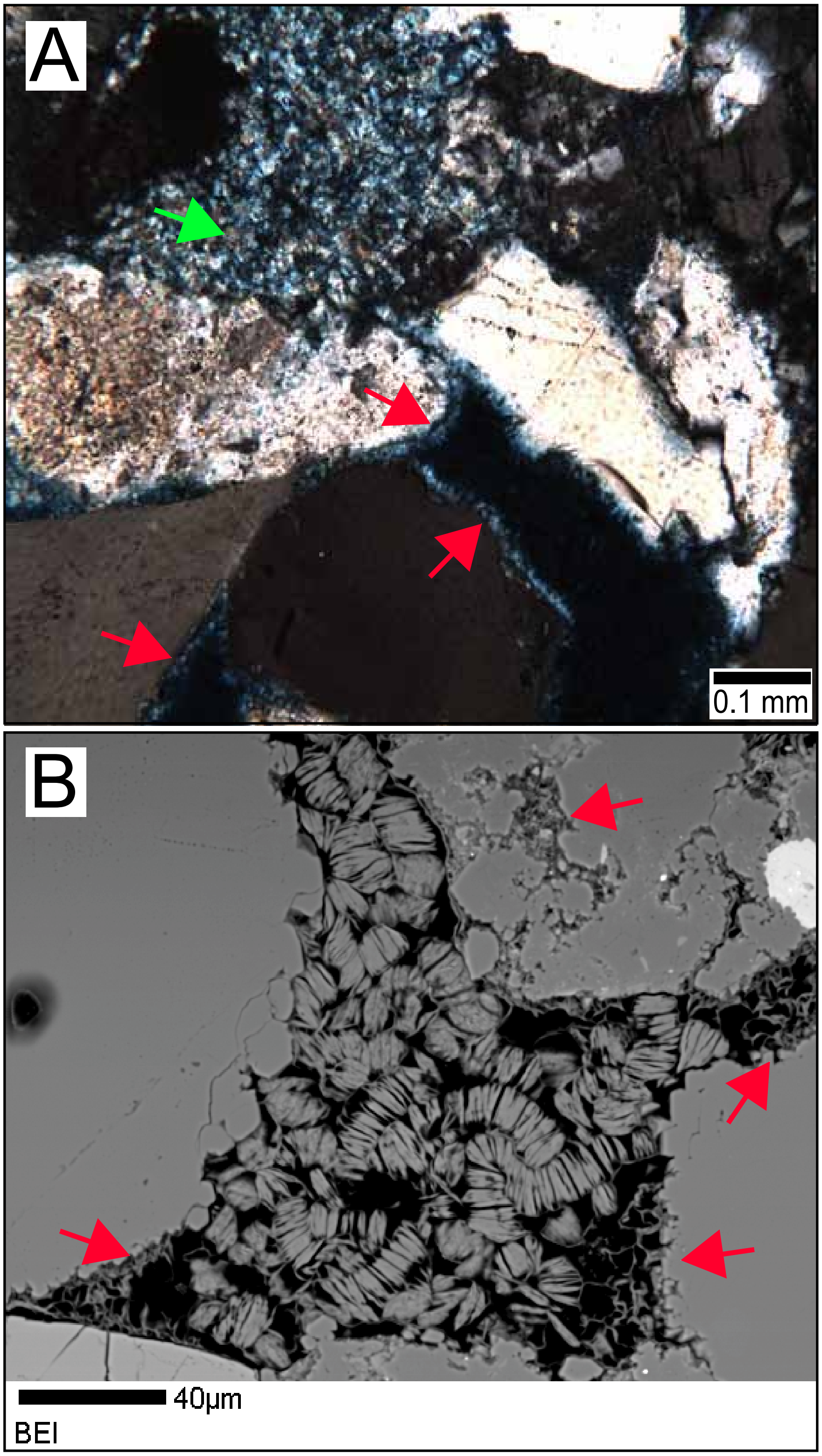
A
0.1 mm
B
40μm
BEI

Figure 4.26 - Last Dance 4010, (A) thin-section photomicrograph, cross nicols, and (B) backscattered electron photomicrograph. (A) A mass of authigenic kaolinite (green arrow) occurs in one pore space, whereas authigenic illite and illite/smectite occur in separate pores as a grain coating cement. The difference in distributions suggests that kaolinite replaced an unstable detrital grain and is not a pore-filling cement. In the backscattered electron photomicrograph (B), illite and kaolinite share an intergranular pore, which indicate direct cement precipitation. Note that illite and illite/smectite are concentrated near pore throats and line grain surfaces (red arrows), indicating this phase preceded precipitation of the kaolinite.

30 to 40 microns in size. Kaolinite exists with illite and mixed layer I/S, and is the least common clay in the Williams Fork samples (Figures 4.16, 4.17).

In the MWX well, the highest kaolinite percentages of kaolinite were observed within the upper Williams Fork fluvial interval (Figure 4.16), whereas in the PA 424-34 well, kaolinite is far less abundant and it is most common in the lower Williams Fork interval (Figure 4.17) and it exists in much lesser amounts in the lower Williams Fork sandstones. Its paucity in the lower Williams Fork Formation might be due to illitization of kaolinite, which is an important reaction in sandstones during burial diagenesis (Hancock and Taylor, 1978; Sommer, 1978; Seemann, 1979; Dutta and Suttner, 1986). Paucity of kaolinite might also be due to the fact that there was not much feldspar within the lower Williams Fork to be subjected to kaolinite formation (Figure 3.12). Carbonate replacement of feldspars is another possible reason for the limited amount of kaolinite in the entire Williams Fork Formation.

Albite

Authigenic albite occurs as a replacement (Figure 4.23B) and as a minor overgrowth (Figure 4.6B) within some Williams Fork feldspar-rich sandstones. Albitization of feldspars, typically plagioclases, ranges from limited patchy spots to complete grain replacements. The albite may exhibit a euhedral crystal shape and replacive albite is darker gray in polarized light than the adjacent non-replaced feldspar grain (Figure 4.23B). Most albitized grains are untwined. Albite comprises < 3% of the total cement and replacement phases within Williams Fork sandstones.

DISSOLUTION

Dissolution is pervasive throughout the Williams Fork Formation (Figure 4.27) as evidenced by the presence of moldic and intragranular porosity. Dissolution of unstable feldspars and some lithics is evidenced by partially dissolved grains (Figures 4.23A, 4.28) and grain-sized pores in otherwise well-compacted sandstones (Figures 3.4, 4.28). In the latter case, such pores would not have survived through compaction; they must have originated by post-compaction dissolution. Dissolved feldspar is the most common origin for most of the secondary dissolution porosity. Some carbonate and silica that replaced detrital grains and/or filled intergranular pores were also subject to dissolution (Figures 3.5, 3.6, 4.28).

PARAGENETIC SEQUENCE

The paragenesis of the William Fork sandstones (Figure 4.29) is established using textural and cross-cutting relationships between diagenetic minerals, although it is not possible to determine the precise timing of every diagenetic alteration. The paragenetic events are generalized relative to the burial history of the Williams Fork Formation in the study area (Figure 4.30) and divided into early (eo-diagenesis) and late (meso-diagenesis).

Eo-diagenetic events are defined are those that likely occurred at the Earth's surface during or shortly after deposition and continuing through burial to a temperature ≤70°C. A temperature of 70°C was chosen as the limit of eo-diagenesis because it generally coincides with the initiation of chemical compaction, reactions of clay-mineral transformation, substantial thermal alteration of organic matter and burial quartz

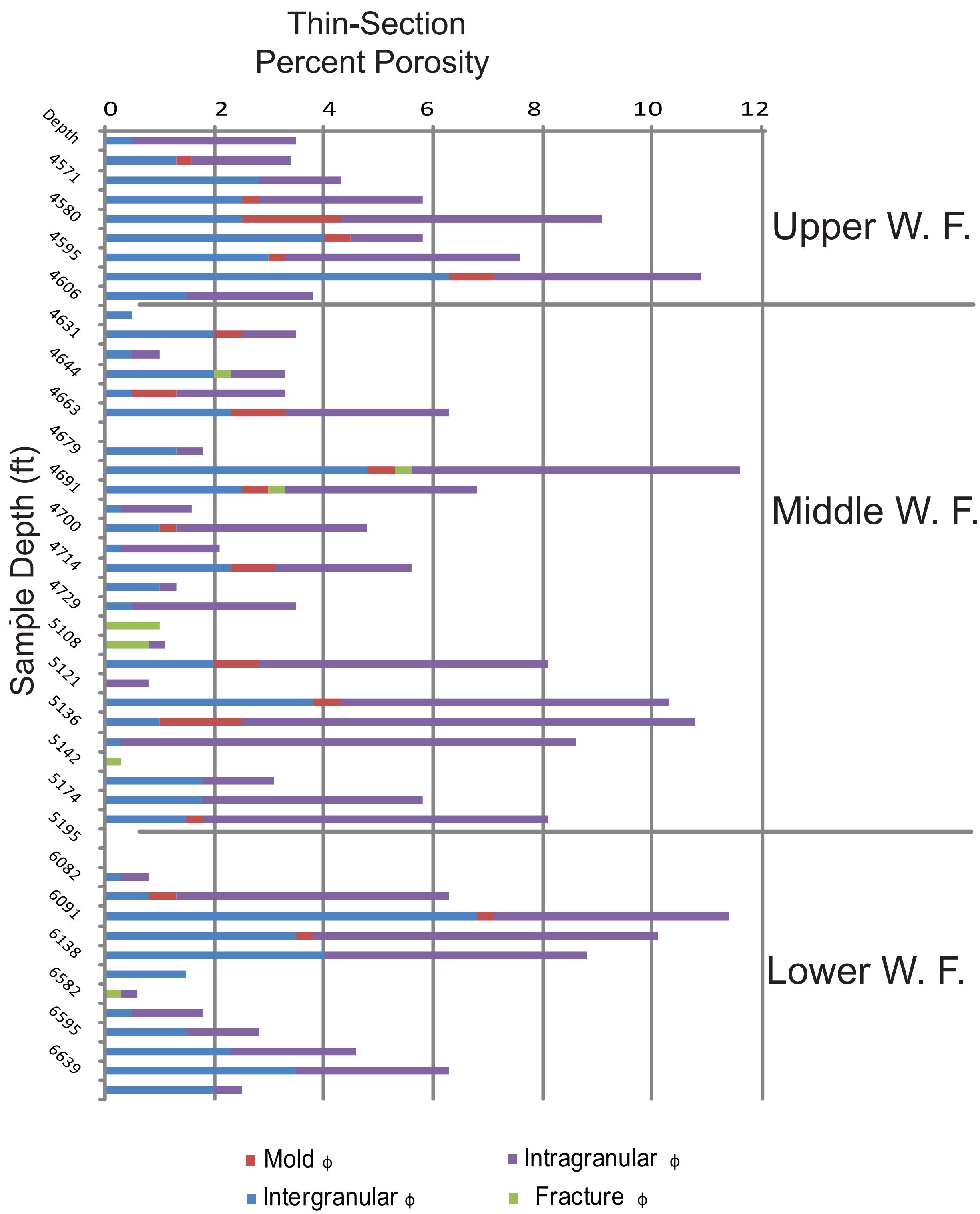

Figure 4.27 - Distribution of pore types in the PA 424-34 Parachute core. Pore type abundance is depicted as a relative fraction of total thin-section porosity. Vertical scale depicts sample footages in descending order; it is not a true vertical scale. Note that moldic porosity shows no depth-related trend. Intergranular and intragranular pore types exist throughout all Williams Fork intervals.

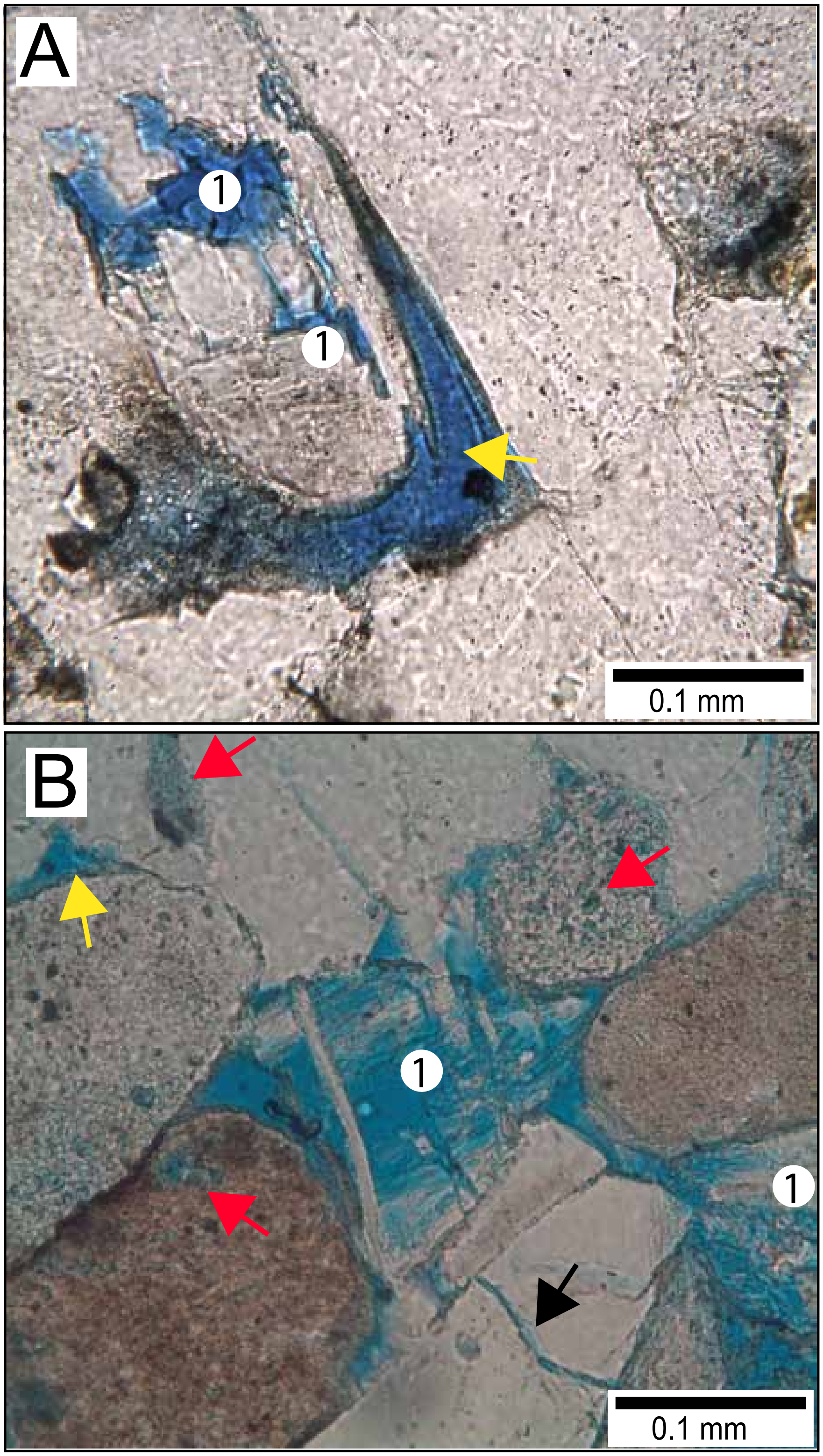

Figure 4.28 - Thin-section photomicrographs Cascade Creek Oxy, plane light (A) 4834', and (B) 4580', showing secondary porosity. Original porosity is completely occluded by early compaction and cementation. Dissolution of feldspar (1) created intragranular secondary porosity (red arrows). Dissolution of early cement is interpreted to have recreated intergranular porosity (yellow arrows). Fracture porosity indicated by black arrow.

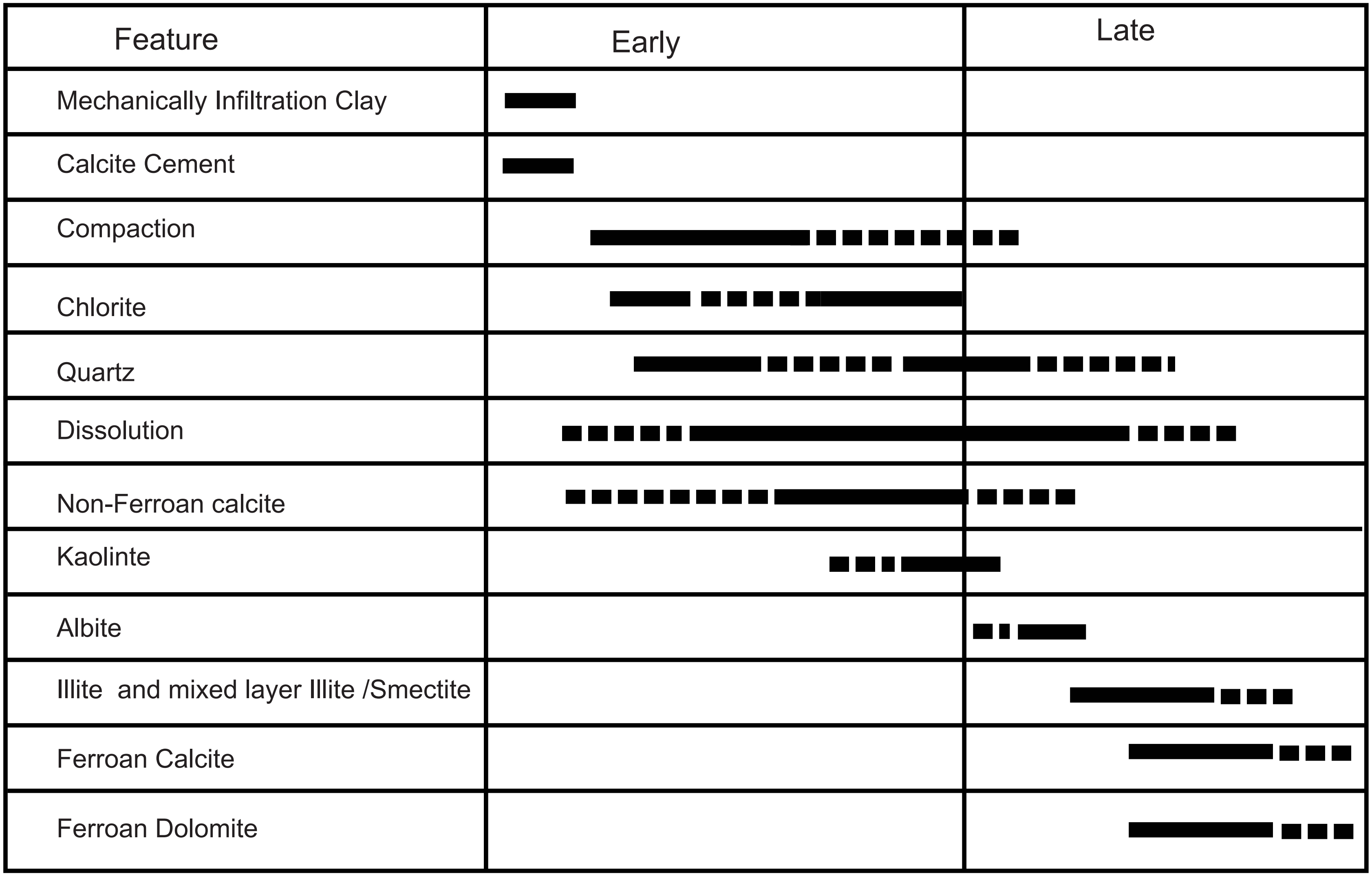

Figure 4.29 - Williams Fork paragenetic sequence. Mechanically infiltrated clays were described in Chapter 3; all other phases and processes are described in Chapter 4. Early and late refer to relative timing; see text for further details. Solid lines indicate a process was common; dashed lines indicate a less common process.

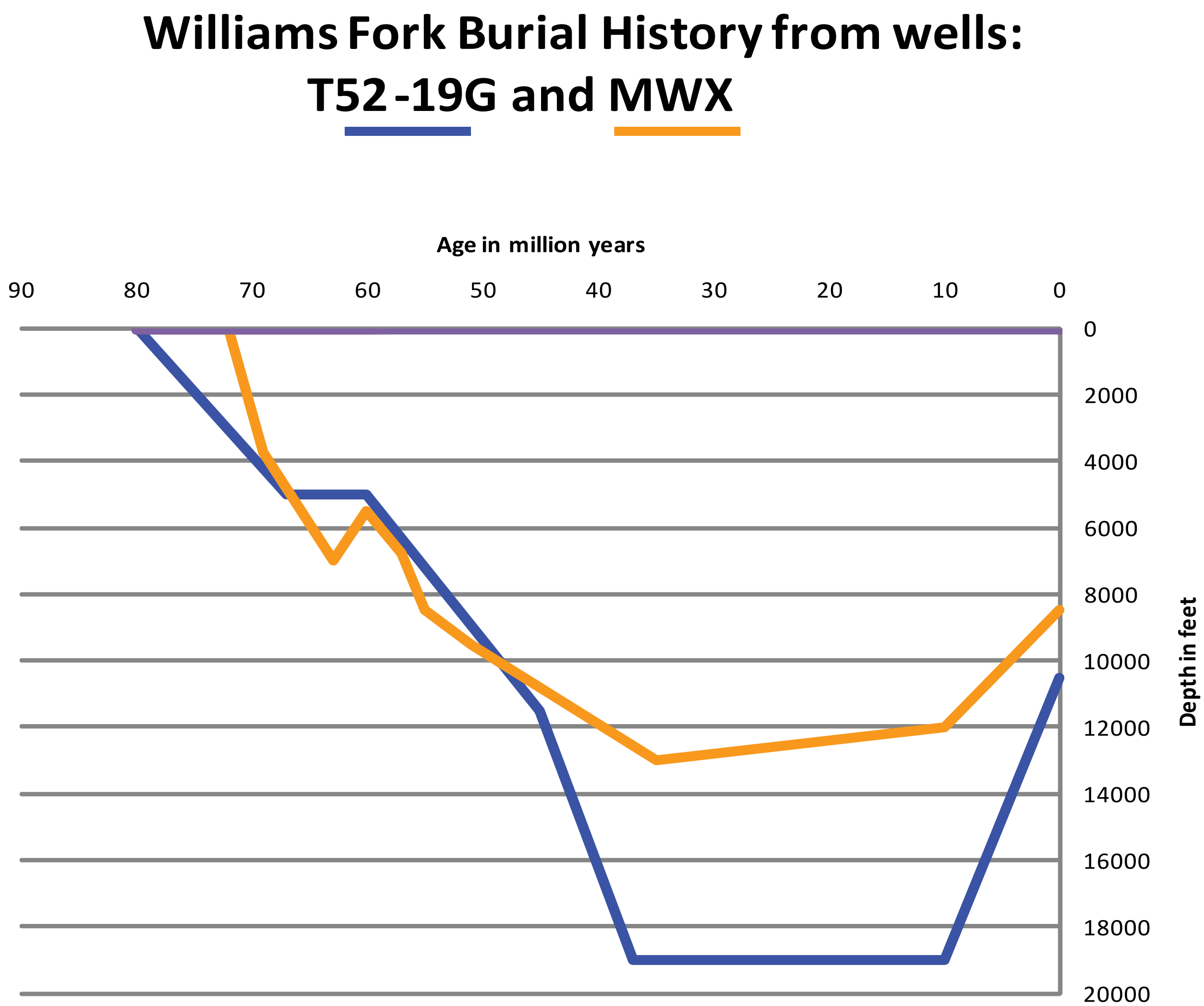

Figure 4.30. Williams Fork burial history from wells in north-central (T52-19G, Piceance Creek Field, Figure 1.6) and south-central (MWX 1, well #4, Figure 1.6) portions of the basin.. In general the two curves show similar histories – initial burial to shallow depths during the late Cretaceous, an increase in burial rates associated with the Laramide orogeny (very late Cretaceous to early Tertiary), and then continued burial through the Tertiary due to loading with continental sediments. Maximum depths vary primarily due to variation in thicknesses of overlying Paleocene and Eocene sediments. Exhumation began about 10 million years ago due to erosion and possibly some tectonic uplift.

cementation (Morad et al., 2000). Assuming a geothermal gradient of ~25°C/km and a near-surface average temperature of 15°C, eo-diagenetic events presumably occurred at burial depths <7000 ft. That depth limit in turn indicates alteration during early burial through the Late Cretaceous and into Early Cenozoic loading associated with the onset of the Laramide Orogeny. Late meso-diagenetic events are interpreted to be associated with higher temperatures (>70 °C) and rapid burial during the Paleogene (Figure 4.30).

The sequential paragenesis is described below in detail. Diagenetic features are presented in the general sequence of their occurrence (Figure 4.29), however, some features formed over long periods of time or formed during both eo- and meso-diagenesis. As such, some mesogenetic features are described out of chronological order.

Infiltrated Clay

One of the earliest eo-diagenetic events was mechanical infiltration of clays. The infiltrated clays only lie on grain surfaces; they never overlie any other authigenic component (Figures 3.19, 3.20). The infiltrated clays are also compacted, indicating that they were emplaced prior to the onset of compaction. Infiltrated clays consisting of clay platelets tangentially arranged around grain surfaces are common in many fluvial deposits (Matlack et al., 1989; Marco et al., 1990; Moraes and De Ros, 1992; Morad et al., 2000; Ketzer et al., 2003b; El Ghali 2006a, 2006b, 2009a). Fluvial sandstones that were originally clay-free can become progressively enriched in clay as a result of the infiltration of muddy surface runoff waters that deposit their fine suspended load in the interstices of sediments (Crone, 1975; Walker, 1976; Moraes and De Ros, 1992; Ketzer et al., 2003b). If infiltrated through the vadose zone, the clays may concentrate in the uppermost phreatic zone (Marco et al., 1990).

In the Williams Fork sandstone, the texture and crystal form (as seen in the polarizing microscope and SEM) show that infiltrated clays are dominated by chlorite and mixed layer illite/smectite (Figure 3.19). These clays make discontinuous grain-coatings that are restricted to grain embayments in fluvial sandstones. The tangential orientation to grain surfaces indicates that the clay-minerals are physically-emplaced, not neoformed (authigenic) clay coats such as fibrous illite or radial chlorite (Wilson and Pittman, 1977; Wilson, 1994; Shammari et al., 2011).

Compaction

Extensive and pervasive mechanical compaction must have occurred fairly early in the burial history of the Williams Fork sandstones, and preceded the onset of cementation otherwise the sandstones would not be so extensively compacted. Very early compaction was most significant for sediments with high mud content. In particular, mudstone intraclasts were squeezed into open pore spaces to form pseudomatrix (Figure 3.3). Mechanical compaction also initiated rearrangement of sandstone grains and led to the formation of long-contacts between grains at the expense of point contacts (Figure 3.4). Eventually, mechanical compaction gave way to pressure solution at grain contacts and produced sutured contacts. Because evidence for pressure solution was observed just at grain contacts and was never observed to affect authigenic clays or the late carbonate cements, it is interpreted to have primarily been a late eogenetic development rather than the product of meso-diagenesis.

Chlorite

One of the earliest eo-diagenetic cements to form was the fibrous chlorite cement that coats grain surfaces (Figure 4.19). This cement if found in the upper half of the Williams Fork Formation and its presence inhibited quartz cementation, which is otherwise the first cement to have formed in most Williams Fork sandstones. Later authigenic chlorite precipitation postdates partial grain dissolution and early quartz and calcite cement formation. This later authigenic chlorite fills intragranular secondary pores (Figure 4.20B) and lines pores where dissolution created voids between host detrital grains and quartz or calcite cement (Figure 4.18). Chlorite cements, however, were never found to post-date diagenetic features interpreted to be exclusively mesogenetic in origin (e.g., dolomite, illite, mixed layer clays, latest calcite replacements), thus all chlorite is interpreted to be eogenetic. Because the distribution of chlorite mimics the distribution of volcanic rock fragments, the latter are considered the source of Fe for the authigenic chlorites.

Quartz

Where early chlorite cement is absent, syntaxial quartz cement is commonly the first diagenetic phase precipitated into an intergranular pore (Figures 3.6, 3.11, 4.3), and its presence resulted in less mechanical compaction in some sandstones. These observations establish the onset of quartz cementation as an early eogenetic event.

Yet syntaxial overgrowths continued forming into the meso-diagenetic stage as evidenced by quartz overgrowths in secondary intergranular pores (Figure 4.6A), around closely packed detrital quartz grains (Figure 4.6B), and in macro and micro fractures.

The silica required for quartz cementation was probably derived from many sources (Giles et al., 2000), which would explain why quartz cementation persisted through eo-diagenesis and into meso-diagenesis. The silica sources probably included (1) Si released by eogenetic dissolution of mafic and feldspar grains, (2) mesogenetic alteration of feldspars to clay minerals that had lower Si/Al ratios than the feldspar, (3) late eogenetic pressure dissolution of quartz grains, and (4) mesogenetic clay minerals transformations like illitization of smectite. The latter is a well-known source of Si for formation of quartz overgrowths (Siever, 1962; Hower et al., 1976; Boles and Franks, 1979).

The observed distribution of quartz overgrowths within the Williams Fork Formation shows no increase in quartz cementation with increasing burial depth (Figure 4.31). Theoretically**,** quartz cementation should increase with increasing burial depth (Bjørlykke and Egeberg, 1993) as increasing temperature with depth normally will accelerate formation of quartz overgrowths (Bjørlykke et al., 1992; Giles et al., 2000; Bjørlykke and Jahren, 2010). The lack of increased quartz cementation with increased burial in the Williams Fork sandstones is interpreted to be the result of the widespread clay matrix, grain coating, and pseudomatrix within the lower Williams Fork Formation. Also, the abundance of early carbonate cement in the lower Williams Fork sandstones inhibited silica overgrowth formation by isolating the grains, reducing the porosity and

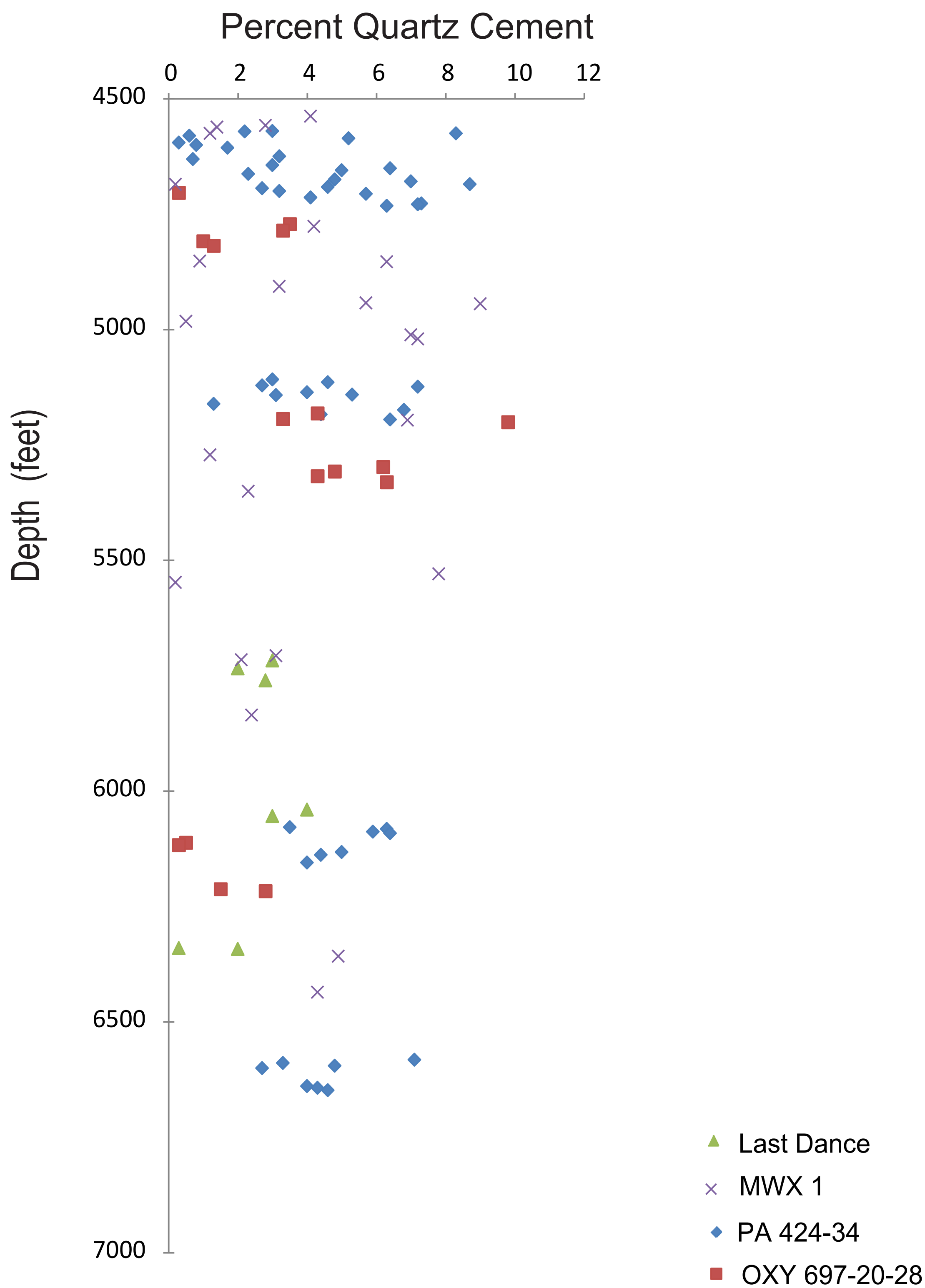

Figure 4.31 - Abundance of quartz cement with depth in the Williams Fork Formation. Percent quartz is relative to total rock volume.

permeability, and thus eliminating fluid mobility and silica influx. The early carbonate cements also inhibited burial compaction, which meant less pressure solution derived silica. A final factor against increasing quartz cement abundance with depth is that late carbonate cement locally replaced silica cement in some sandstones (Figures 4.6B, 4.9B).

Non-ferroan Calcite

The non-ferroan calcite limited the effect of compaction in some sandstones and pores, thus is interpreted to have initiated as an eo-diagenetic phase. It also replaced feldspars and, thus, had to have formed before those feldspars could dissolve during eo-diagenesis. But this calcite primarily overlies (Figures 3.11, 4.6B) and can replace quartz cement (Figure 4.3), thus it is a not an early eo-diagenetic feature. The calcium for the non-ferroan calcite was probably derived from shallow meteoric waters circulating through the sediments and the dissolution of Ca-bearing feldspars and other silicate minerals.

Dissolution of Grains and Cements

Dissolution of feldspar and lithic grains is assumed to have started during early eo-diagenesis. This initial dissolution probably occurred under the influence of fresh-water circulation while overlying Williams Fork fluvial and estuarine sediments were accumulating (e.g. Lonoy et al., 1986).

Dissolution of grains and cements continued throughout eo-diagenesis and into the meso-diagenetic realm as evidenced by dissolution of eogenetic cements such as quartz (Figures 3.5, 3.6) and the formation of secondary pores by dissolution that did not collapse (Figures 3.4A, 3.17, 4.5A, 4.23A). The latter must be post compaction and mesogenetic in origin. The late dissolution features probably formed by circulation of basinal acidic pore fluids through the Williams Fork sandstone (e.g. Morad et al., 2000; Salem et al. 2000).

Kaolinite

Generally, kaolinite post-dated early quartz overgrowth cementation as it occurs in the center of intergranular pores lined by quartz overgrowths. Kaolinite replacement of feldspars was probably concurrent with feldspar dissolution. In base cases, the kaolinite's delicate booklets and platelets (Figures 4.25, 4.26) indicate precipitation after mechanical compaction had ceased, otherwise the crystals would have been squeezed into a pseudomatrix . Because some kaolinite has been illitized, the kaolinite must have preceded illite formation. The kaolinite is thus interpreted to be late eo-diagenetic phenomena with the cations and silica released during feldspar alteration promoting the kaolinite development in both primary and secondary pores.

Albite

Albitization of feldspars in sandstones is typically a burial event that is most common at temperatures above 70°C (e.g., Saigal et al., 1988), with the Na derived from Na-rich basinal brines. By analogy, the albite in the Williams Fork sandstones is interpreted to be a meso-diagenetic feature. Petrographic observations support this interpretation as the albite overgrowths were never observed to underlie eogenetic chlorite, kaolinite, non-ferroan calcite, or quartz cements. Albite, however, is replaced by, thus predates, late ferroan calcite (Figure 4.23B). Albite also predates illite and illite/smectite formation as evidenced by secondary dissolution pores within albitized grains being lined by late authigenic illite and mixed-layer illite/smectite (Figure 4.23B).

Illite and Mixed Layer Illite/Smectite

The development of authigenic illite in both intergranular and secondary porosity was one of the last diagenetic events. The delicate, filamentous authigenic illite postdates quartz and non-ferroan calcite cements, post-dates kaolinite formation (some kaolinite crystals have been illitized), and must post-date compaction as it is not squeezed into pseudomatrix (Figure 4.22). The illitization of chert grains (Figures 3.15, 3.16) and infiltrated smectitic clay is interpreted to have been concurrent with formation of illite cements because the replacive illite also shows no evidence of having been compacted.

Following Morad et al. (2000), illite in the Williams Fork sandstones is interpreted to be a meso-diagenetic product that formed during progressive burial under high temperature (90 to 130°C). Illite formation in sandstone requires a high a_{K+}/a_H^+ ratio in the pore waters (Morad et al., 1994). Morad (1988) reported that the high a_K^+/a_H^+ ratio needed for the illitization process in fluvial sandstones is attributed to the albitization of detrital potassium feldspars, which provided the required K^+ ions to the pore waters. This is interpreted to be the case in Williams Fork sandstones. Late potassium feldspar dissolution also is a potential K^+ source that may have contributed K^+ ions.

Ferroan Calcite and Ferroan Dolomite

Ferroan calcite and dolomite were the last diagenetic events in the Williams Fork sandstones. Both ferroan carbonates overlie and replace all other diagenetic products including quartz (Figures 4.9B, 4.10B, 4.11) and clays (Figures 4.13A, 4.14), and occur in secondary pores (Figures 4.14). These late diagenetic carbonates also occur in microscopic (Figure 4.14A) and macroscopic fractures, fractures that post-date burial compaction and early quartz overgrowths. Collectively all these relationships establish the ferroan carbonates as meso-diagenetic. Their timing relative to each other is not possible to determine as they tend to be mutually exclusive with the ferroan calcite in the middle and upper Williams Fork interval and ferroan dolomite occurring exclusively in the lower Williams Fork Formation (Figure 4.7)

SUMMARY

- Diagenetic processes in the Williams Fork Formation extensively impacted Williams Fork sandstones. Compaction, early and late cementation, dissolution and mineralogical replacements are the volumetrically significant diagenetic processes that characterize the diagenetic evolution of Williams Fork Sandstones. Compaction dominates over all types of cementation in destroying intergranular pore space.
- Early cementation comprises chlorite, quartz, and non-ferroan calcite. Thick chlorite rims, when present, prevented quartz cement. Early quartz and calcite cement stabilized the sandstone framework and limited the effect of compaction in some sandstones. Late cements are dominated by ferroan calcite and dolomite.

- Dissolution extensively affected feldspars, lithic fragments and early cements. Dissolution of grains and cements continued throughout eo-diagenesis and into the meso-diagenetic realm. Replacements, especially by calcite and clay minerals, impacted detrital grains and some early formed cement.

- Timing of diagenetic events are complex but petrographic relationships reveal features formed very early prior to any significant burial (infiltration of clays); phases formed at <70°C during eogenesis (chlorite, early quartz cement, non-ferroan calcite and kaolinite); and authigenic phases formed at higher temperatures in the mesogenetic realm (albite, illite, mixed-layer illite/smectite, ferroan calcite, and dolomite).

- Volumetrically, the eo-diagenetic products are more abundant, which, coupled with the dominance of eo-diagenetic compaction and burial history curves, indicates that the Williams Fork sandstones were highly reactive at fairly shallow (<7,000 ft) burial depths.

CHAPTER FIVE: DISTRIBUTION OF DIAGENESIS IN THE CONTEXT OF SEQUENCE STRATIGRAPHY

INTRODUCTION

In siliciclastic units such as the Williams Fork Formation, diagenetic alterations are controlled by a variety of chemical, physical, and biochemical interactions that have a substantial influence on reservoir quality by modifying primary porosity and governing permeability (e.g., Giles and Marshall, 1986, Bloch et al., 2002; Nadeau, 1998). Linking diagenesis to sequence stratigraphy in siliciclastic sequences is achievable because the controls on sequence stratigraphy components (i.e., relative sea-level and base-level change, and the rate of sediment supply) also affect the type and extent of early diagenetic alterations within sandstones (Taylor et al., 1995; Taylor et al., 2000; Loomis and Crossey, 1996; Dutton and Willis, 1998; Morad et al., 2000; Morad et al., 2010; Ketzer et al., 2002; Ketzer et al., 2003a, 2003b; Al-Ramadan et al., 2005; Ketzer and Morad, 2006; El-Ghali, 2005; El-Ghali et al., 2006a, 2006b, 2006c; El-Gahli, 2008; Mansurbeg et al., 2008; El-ghali et al., 2009a, 2009b; Mansurbeg et al., 2009 and Kordi et al 2011). Changes in accommodation space in fluvial plains are an indirect response to sea-level change, as confirmed by many studies (e.g. Wright and Marriott, 1993; Shanley and McCabe, 1994; Posamentier and Allen, 1999). Blum and Tornqvist (2000) suggested that such changes in depositional base level would influence the types of fluvial systems, frequency of avulsion, and style of vertical and lateral accretion, as well as the architecture of fluvial deposits. The conditions controlling sea-level change and indirectly influencing fluvial base level should also have strong ties to depositional texture and mineralogy of detrital sand, climatic conditions, and patterns of regional ground water flow (Morad et al., 2000). Detrital mineralogy, climate, and ground water flux, in turn, all have a major influence on diagenesis, directly affect eogenesis, and indirectly affect mesogenesis through the products of eogenesis.

This chapter highlights Williams Fork diagenetic alterations as a function of systems tracts, and hence the predictability of diagenetic events within the sequence stratigraphic framework. As presented in Chapter 2, the Williams Fork Formation sandstones in the study area consist of fluvial channel and crevasse splay deposits that formed in lowstand, transgressive, and highstand systems tracts (Patterson et al., 2003). Five composite sequences are recognized within the Williams Fork and Ohio Creek intervals (Figure 1.12), each with its own lowstand, but with transgressive and highstand systems tracts not well differentiated (Patterson et al 2003; Leibovitz, 2010). Patterson et al.'s (2003) sequence stratigraphic framework (Figures 1.9, 1.12) was used to relate Williams Fork diagenetic alteration to individual systems tracts. Other available student theses provide useful insights (e.g. Leibovitz, 2010); however, Patterson et al.'s (2003) work offered the precise depths for sequence boundaries, which helped assign the petrographically and diagenetically studied samples to the appropriate systems tract.

Patterson et al.'s (2003) subdivision of the Williams Fork and Ohio Creek sandstones define the larger-scale alluvial architectural framework of the Piceance Basin. The lowstand deposits are thick, laterally extensive and sandstone prone. In contrast, transgressive and highstand systems tracts contain isolated channel elements within mudstone and siltstone intervals that result in low sand-to-mud ratios (Figures 1.12, 1.13). The lower composite sequences represent alluvial plain deposits during periods of moderate accommodation (Patterson et al., 2003). In contrast, the upper composite sequences were deposited during periods of low accommodation attributed to the onset of the Laramide uplift (Patterson et al., 2003). The final Ohio Creek sequence is characterized by more amalgamated channel and channel-complex elements of lowstand strata.

The five eogenetic and one mesogenetic features described below are the diagenetic products that exhibit spatial variability with respect to systems tracts. All other diagenetic features (mechanical and chemical compaction, grain and cement dissolution, precipitation of non-ferroan and ferroan calcite, kaolinite, albite, dolomite, and most illite and mixed layer illite/smectite) exhibited no relationships to system tracts and are thus not discussed further. Many, but not all, of the features that exhibit no sequence stratigraphic relationships are mesogenetic in origin (Figure 4.29), thus a systems tract control should not necessarily be expected.

INFILTRATED CLAY

The infiltrated clays within the Williams Fork Formation occur in lowstand systems tracts (LST) and highstand systems tracts (HST) sands but rarely in transgressive systems tract (TST) sandstones (Figure 5.1). The occurrence of infiltrated clays in LST and HST sandstones is interpreted to reflect the fact that base level and accommodation space are generally relatively stable (early HST, late LST) or falling (late HST, early LST) during formation of those systems tracts. Sandstone bodies thus persist at the land surface on the flood plain for long periods of time without being covered by floodplain muds. Prolonged exposure allows for clays to infiltrate older

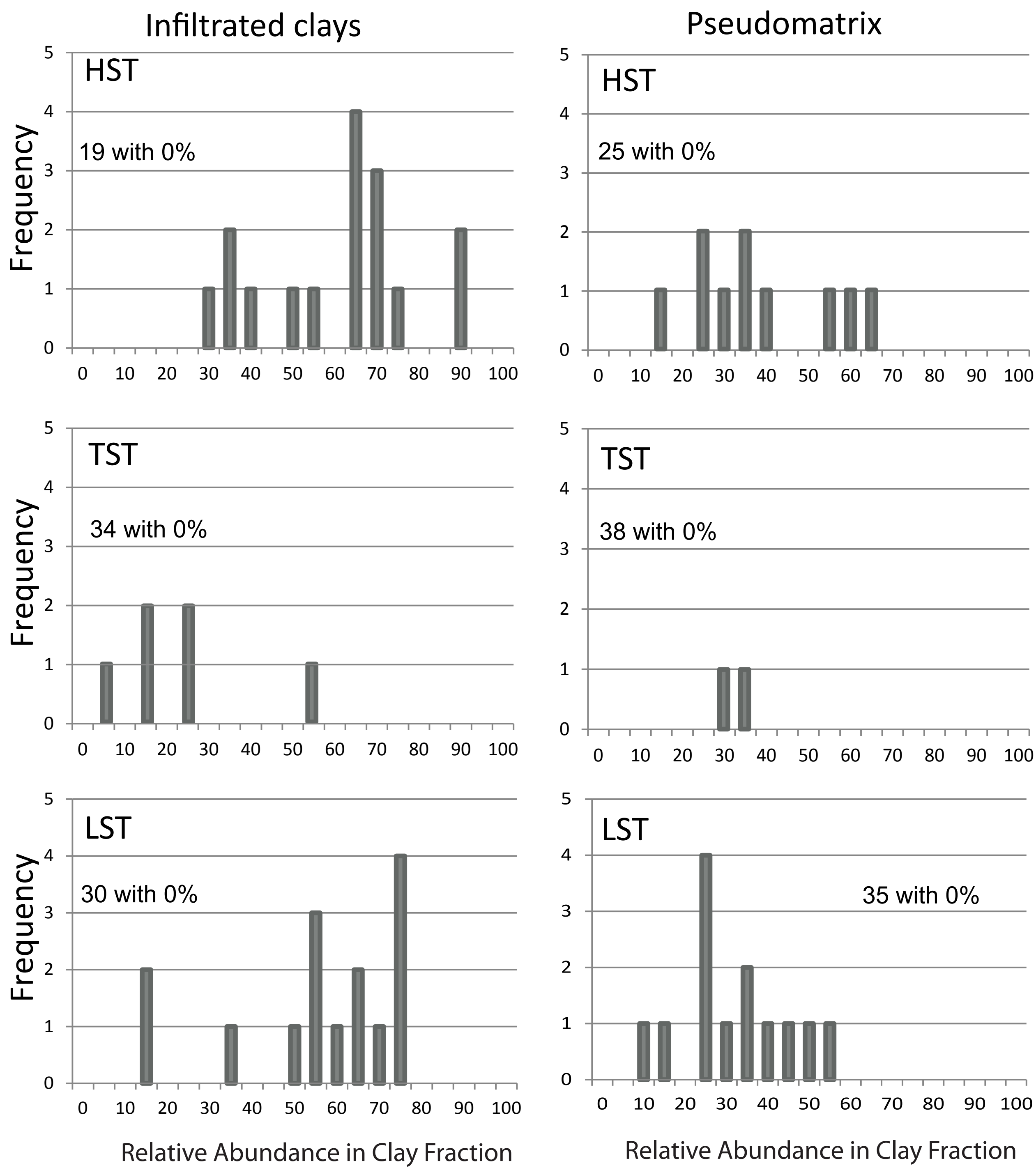

Figure 5.1 - Frequency histograms of infiltrated clay and pseudomatrix as a function of systems tract in the Williams Fork Formation (lowstand = LST, transgressive = TST and highstand = HST).

sandstones when mud-rich flood waters do extend across the floodplain (Ketzer et al., 2003b, El-Ghali et al., 2006a, 2006b, 2009a). Infiltrated clay is thus most common in the LST and HST sands. Lowstand sandstones may also have received more infiltrated clays than sandstones in other systems tracts if they are coarser and have a higher depositional permeability (Matlack et al., 1989, Moraes and De Ros, 1992 and Morad et al., 2010).

In contrast, most channel sandstones in TST deposits probably received no infiltrated clay because the rapid rise in base level and accommodation space of the TST meant relatively high rates of floodplain mud deposition, which in turn meant rapid burial and isolation of sandstones within floodplain mudstones (Ketzer et al., 2003b; El-Ghali et al., 2009a). Quick burial inhibits opportunities for clay infiltration. The lack of an allogenetic influence means the rare occurrence of infiltrated clay in TST deposits (Figure 5.1) represents just autogenetic crevassing and infiltration of clay.

CHLORITE

Authigenic chlorite shows spatial distribution related in part to sequence stratigraphic position. As noted in Chapter 4, chlorite is present in just the upper Williams Fork and upper half of the middle Williams Fork intervals (Figures 4.16 and 4.17). As such it only occurs in and above the TST and HST of the second composite sequence in the Williams Fork Formation (i.e., composite sequences 3, 4, 5 and 6 of Figure 1.12). In these sequences the detrital mud contains Fe-rich clay minerals, and mafic volcanic clasts are present in the sandstones (Chapter 3). All of these detrital sources could have sourced the Fe needed for chlorite. These iron-rich sources are non-existent in the deeper intervals of the Williams Fork formation. As argued in Chapter 3, these stratigraphic variations in the presence of detrital Fe sources is probably a provenance signal, thus the sequence stratigraphic distribution of authigenic chlorite is interpreted to be coincidence rather than causal.

PSEUDOMATRIX

Compaction was pervasive throughout all sandstones and systems tracts, but the formation of pseudomatrix is concentrated in LST and HST sandstones (Figure 5.1) due to the more abundant mud intraclasts within those sediments. Fluvial sands deposited during lateral channel migration and active erosion of the floodplain commonly exhibit abundant mud intraclasts (Morad et al., 2000; El-Ghali et al., 2006a). This happens during deposition of the early LST and late HST when base level fall is associated with decreasing accommodation space (Shanley and McCabe, 1994). Lateral channel migration rather than aggradation occurs due to the decrease in accommodation space, resulting in erosion of floodplain deposits and considerable amounts of mud intraclasts emptying into channel sandstone deposits (Ketzer et al., 2003b). This is interpreted to be the explanation for the relative abundance of pseudomatrix in the HST and LST sandstones, and near absence in the TST sands, of the Williams Fork.

QUARTZ

Sandstones in TST are more likely to have large amounts of quartz cement (7-10% of total rock volume) than sandstones in LST and HST deposits (Figure 5.2). Exactly why this is the case is not entirely clear. In thin section, there is ample

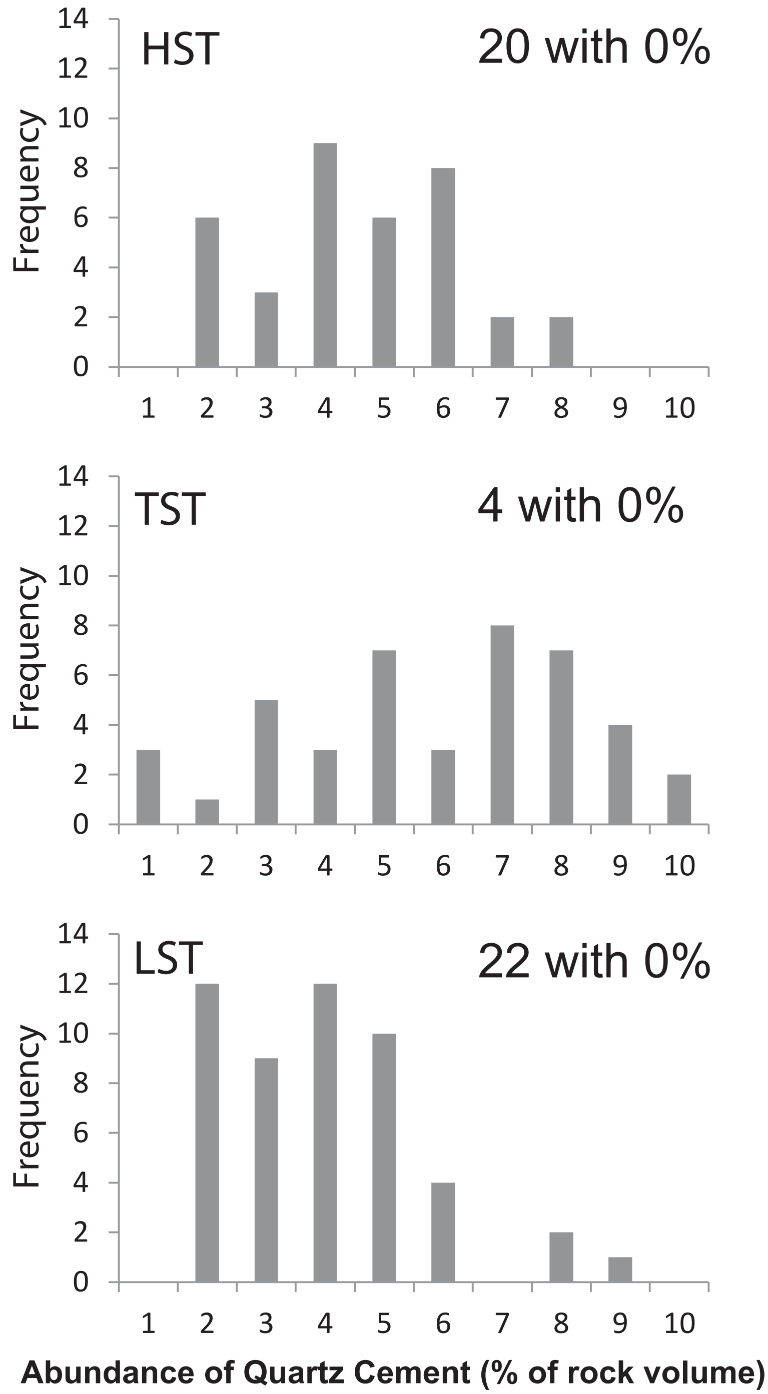

Figure 5.2 - Frequency histograms of quartz cement as a function of systems tract in the Williams Fork Formation (lowstand = LST, transgressive = TST and highstand = HST).

observational evidence that the presence of quartz overgrowths is inversely related to the presence of grain-coating, infiltrated clays and pseudomatrix. That is, those clay features inhibited the development of quartz cements. The paucity of infiltrated clay and pseudomatrix in TST sandstones would thus seem to explain the greater abundance of quartz cements in some TST samples. However, clay contents between 0 and 20% are associated with both high and low amounts of quartz cement in all samples (Figure 5.3) and the TST samples with the largest amounts of quartz cement are just as likely to contain 20% clay as they are to contain <5% clay (Figure 5.3B). Thus total clay content alone cannot explain the presence of more quartz cement in TST sandstones. What other controls may be at play are unknown. Figure 5.3, however, does show that clay content greater than about 25% does explain low quartz cement abundance in all samples, and HST and LST sandstones with >6% quartz cement do have total clay contents generally less than 5%.

REPLACIVE ILLITE

Some authigenic illite is interpreted to have resulted from mesogenetic replacement of smectite associated with infiltrated clay, mud intraclasts, and pseudo-matrix. As such, those authigenic illites show the same distribution as their precursor clays, meaning they are more abundant in LST and HST sandstones relative to TST sandstones. This however is not a causal control by sequence stratigraphic position; rather it is merely an inherited distribution.

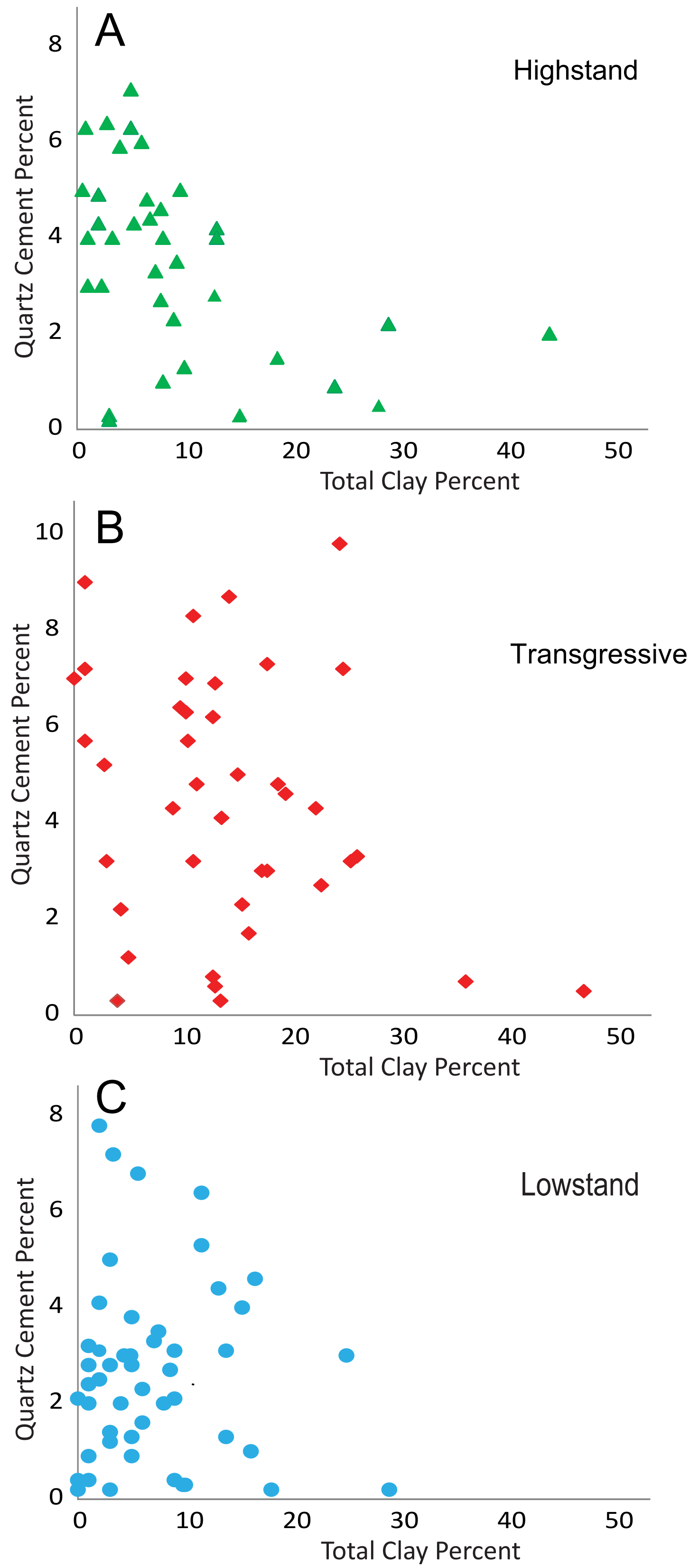

Figure 5.3 – Quartz overgrowth abundance as a function of clay content in (A) highstand, (B) transgressive, and (C) lowstand systems tracts. Data from the Cascade Creek # 697-20-28, Parachute 424-34, Last Dance # 43C-3-792 and MWX1 cores.

DISCUSSION

The eogenetic features in the Williams Fork Formation that do exhibit a systems tract relationship are similar to the types of features described by others as having a sequence stratigraphic control. In particular, this includes infiltration of clays, formation of pseudomatrix and early clay cements, and the mesogenetic illitization of infiltrated clays and pseudomatrix (e.g. Ketzer et al., 2002; Ketzer et al., 2003a, 2003b; Al-Ramadan et al., 2005; Ketzer and Morad, 2006; El-Ghali, 2005; El-Ghali et al., 2006a, 2006b; El-Gahli, 2008; Mansurbeg et al., 2008; El-ghali et al., 2009a, 2009b; Mansurbeg et al., 2009 and Kordi et al 2011). These are features that formed early in the paragenesis, either syndepositionally (infiltrated clays) or most likely while the Williams Fork systems tracts were also forming. These are the type of features most likely to exhibit a sequence stratigraphic control or relationship (Morad et al., 2000; Ketzer et al., 2002; Ketzer et al., 2003b).

Conversely, compaction features and all diagenetic features that post-date the initiation of quartz cementation (e.g., dissolution features, kaolinite, albite, most authigenic illite and smectite, and all carbonates) exhibit no spatial correlation or relation to the Williams Fork sequence stratigraphy. Other researchers have also noted cases where these types of features do not display sequence-stratigraphic controls on their distributions (e.g. El-Ghali et al., 2009a). However, there are also case examples where many of those later features are systematically distributed within a sequence stratigraphic framework (e.g. Ketzer et al., 2003a, El-Ghali et al., 2006a, 2006c; El-Ghali et al., 2009a; Kordi et al., 2011). This illustrates that the controlling functions on diagenesis are complex and not necessarily related to sequence position. Every sandstone has its own unique sedimentologic, stratigraphic, tectonic, burial, and fluid history (Figure 1.2). The greater the time between a diagenetic event and the deposition of a sequence, the greater the likelihood that non-stratigraphic factors determine the spatial distribution the diagenetic feature.

The limited number of diagenetic features that can be related to sequence stratigraphic position in the Williams Fork sandstones might result from the relatively rapid early burial of the formation. Rapid burial and extensive compaction may have controlled the early diagenetic evolution of the sediments more so than changes in pore-water chemistry linked to base level fluctuations and changes in accommodation space.

SUMMARY

Four eogenetic alterations can be placed in a sequence stratigraphic context and the abundance of four of those features can be related to changes in base level and accommodation space. One other feature, illitized infiltrated clays and pseudomatrix also exhibits spatial distributions related to systems tracts, but those relationships are inherited not primary. All other diagenetic features observed in the Williams Fork Formation show no spatial relationships to systems tracts and the Williams Fork's sequence stratigraphic architecture.

The four features that do show sequence stratigraphic controls are: (1) mechanically infiltrated clays, particularly in channel and crevasse splay sandstones in lowstand and highstand systems tracts. (2) Pseudomatrix, which resulted from mechanical compaction of mud intraclasts, occurs mainly in highstand and lowstand systems tracts. (3) Authigenic chlorite formed in the transgressive and highstand systems tracts of the upper half of the Williams Fork Formation because of the abundance of mafic volcanic clasts in that portion of the Formation. (4) Quartz overgrowth abundance is more likely to exceed ~7% in transgressive systems tract sandstones for reasons that are unclear.

CHAPTER SIX: WILLIAMS FORK RESERVOIR QUALITY

INTRODUCTION

The Williams Fork sandstones are an example of a low-permeability tight gas reservoir. The petrophysics and geology of such reservoirs are unique and distinctly different than ordinary reservoir rocks (e.g., Soeder and Randolph, 1987; Spencer, 1989; Soeder and Chowdiah, 1990; Dutton et al., 1995; Byrnes, 1997, Byrnes et al., 2003). Investigating the elements controlling reservoir quality and petrophysical behavior of low-permeability reservoirs is critical to predicting and understanding reservoir performance in low-permeability gas systems (Shanley et al., 2004). In the Williams Fork Formation those key elements are diagenetic and related to occlusion of intergranular pores by compaction, precipitation of authigenic quartz, carbonate, and clay cements, and mesogenetic secondary porosity formation (Aboktef et al 2011).

DATA

Thin-section derived total porosity is quite variable depending on facies (Figure 6.1A, B). Structureless sandstones (Ss) and conglomeratic “mud chip” sandstones (Scg) have the best porosity, averaging 8.1% and 8.4%, respectively. Other sandstones of the fluvial channel association have slightly less porosity (average 5.2% to 6.5%, Figure 6.1B). Specifically, high-angle cross bedded sandstones (Sha), low-angle cross bedded sandstone (Sla), horizontal laminated sandstones (Shl), and ripple cross-laminated sandstones (Sr), have averages of 6.2%, 6.3%, 6.5%, and 5.2%, respectively. In contrast, thin-section porosities are lowest within interbedded siltstones

Distribution of thin section-porosity within facies

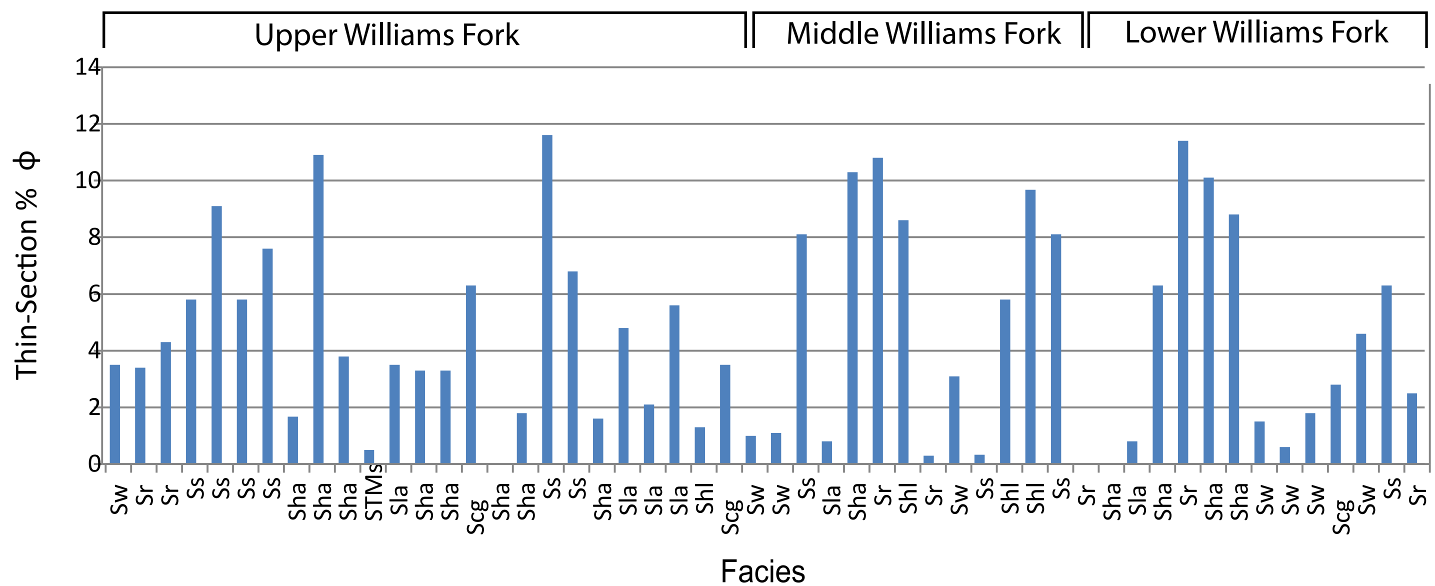

Figure 6.1A - Distribution of thin-section derived porosity as a function of facies within the Williams Fork Formation, Parachute 424-35 core. Data are arranged from shallowest (left) to deepest (right) facies occurrences. Structureless sandstone (Ss) facies and horizontal laminated sandstone (Shl) facies exhibit best porosity value, whereas inter-bedded siltstone and mudstone (STMs) facies and wavy, lenticular, flaser-bedded sandstone (Sw) facies have lowest porosity values.

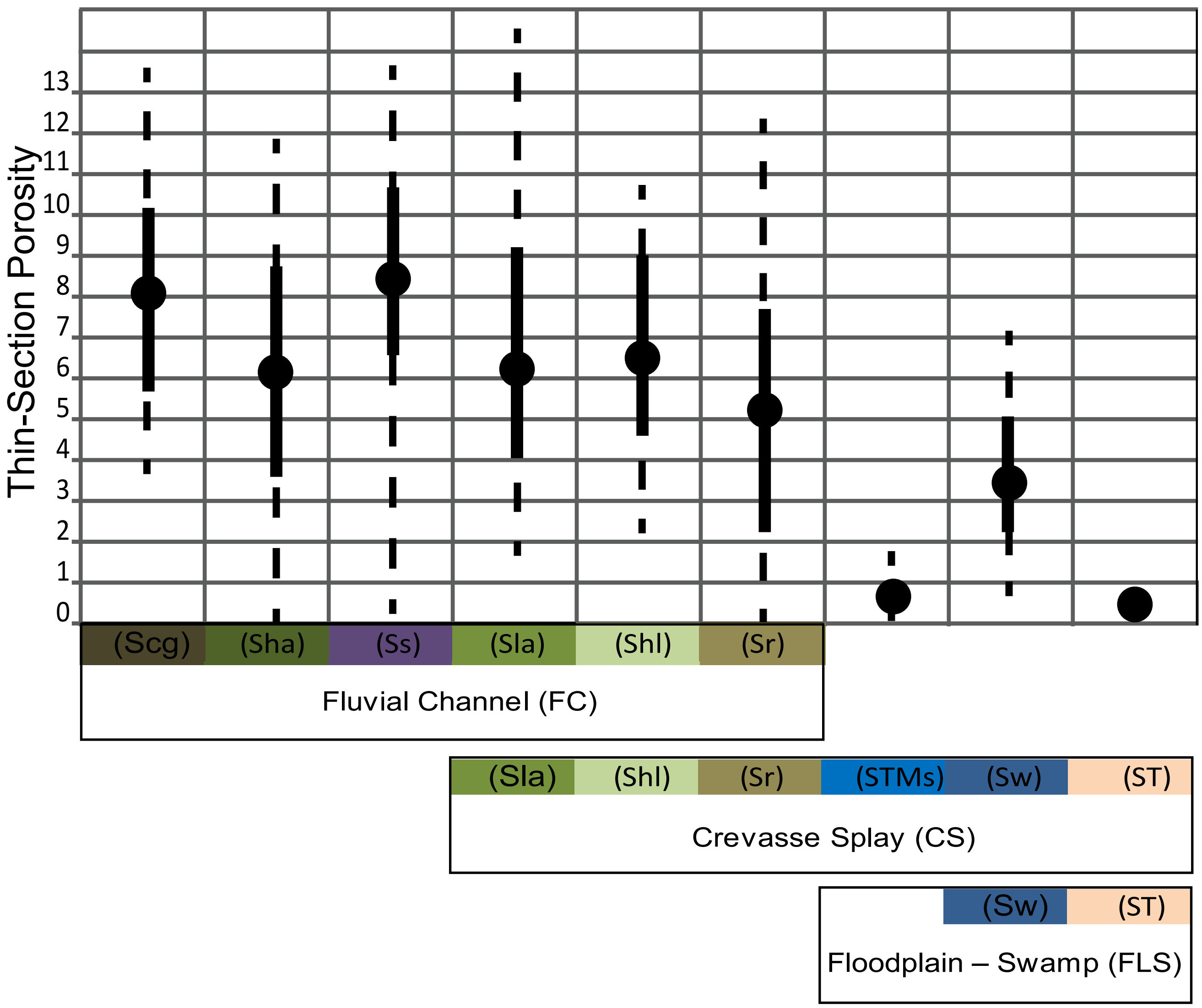

Figure 6.1B - Average (large dot), standard deviation (solid line) and range (dashed line) of porosity as a function of facies in the Williams Fork Formation. Facies are color coded as per Table 2 and grouped by the facies associations discussed in Chapter 2.

and mudstones (STMs) and siltstone (ST) facies, averaging 0.8% and 0.5%, respectively. Lenticular, flaser bedded sandstones (Sw), also have a relatively low average of 3.4%.

Stratigraphically total thin-section porosity does not show depth-related trends (Figure 6.2), which is not surprising given the vertical facies heterogeneity (Figures 2.1, 2.2, and 2.3) throughout the Williams Fork cores. Porosity values vary between wells with MWX1 samples having the highest average thin-section porosity (5.5%, range 0 to 15%) and Last Dance 43C-3-792 thin-section samples having the lowest average thin-section porosity (3.9%, range 0 to 8.4%). BT202, which is from behind the outcrop (Figure 1.6), has dramatically higher thin-section porosity values than the other wells, ranging from 0 to 28.3% and averaging 14.5% (Figure 6.3).

Porosity in the Williams Fork sandstones is dominated by secondary porosity (Figure 6.4) with secondary porosity generally higher than intergranular porosity (Figure 6.5). This is true of all subsurface sandstones except those in the Oxy Cascade Creek 697-20-28 core. For example, in PA 424-34 Parachute core (Figures 6.3, 6.4), intergranular porosity ranges from 0.0 to 6.8% (averaging 1.7%), and partial moldic porosity (intragranular in Figure 6.3) ranges from 0 to 8.3% (averaging 2.5%), and complete moldic porosity ranges from 0.0 to 1.8% (averaging 0.3%). Combined, the secondary moldic pores exceed or equal intergranular porosity in 68% of the Parachute samples (Figure 6.5). Fracture porosity is also more common within the upper and middle Williams Fork intervals in the PA 424-34 core (Figure 6.3). In contrast, Cascade Creek 697-20-28 has intergranular porosity values (0.0 to 10.5%, averaging 5.6%) that

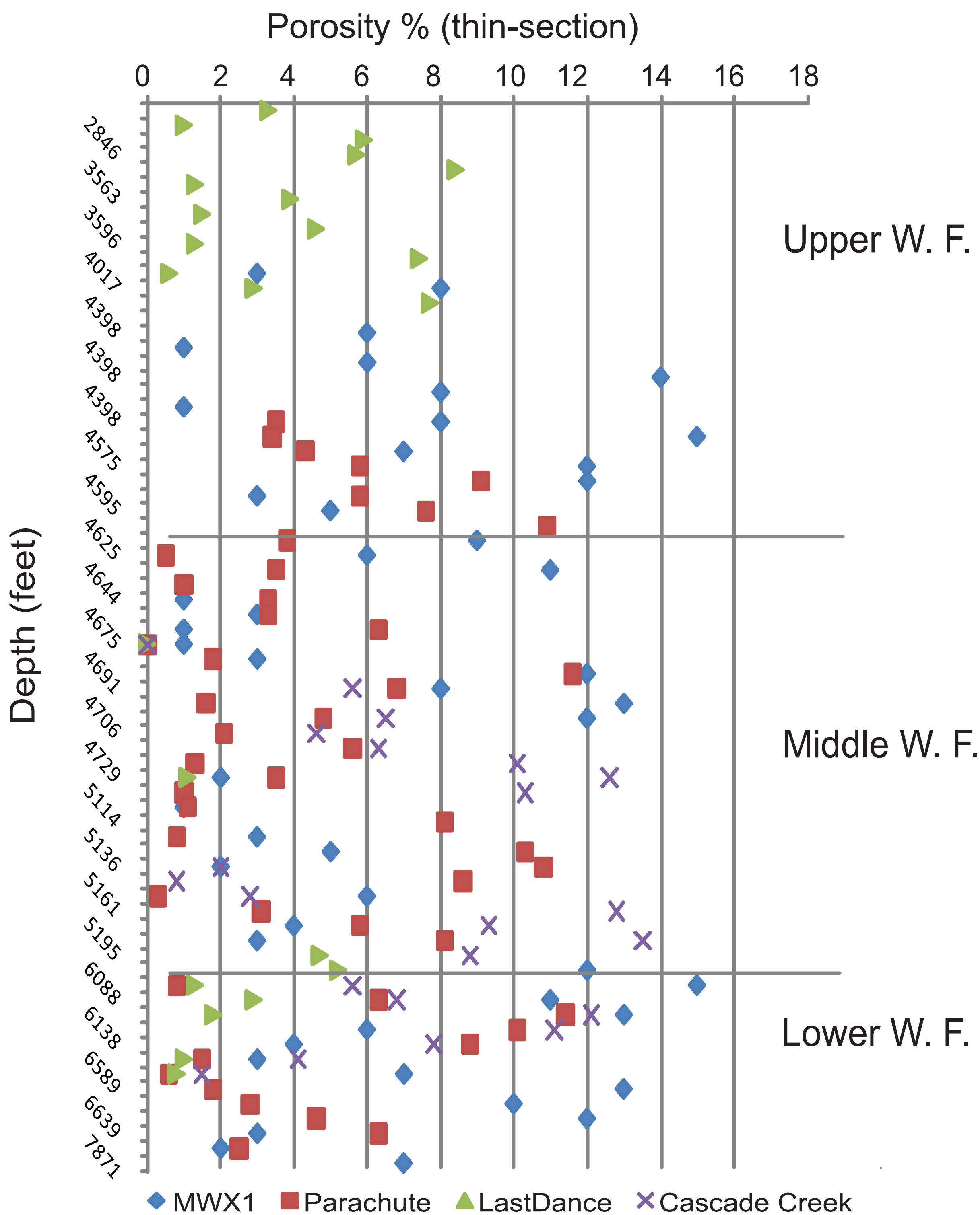

Figure 6.2 -Total thin-section porosity in Williams Fork core samples. Vertical scale depicts sample footages in descending order; it is not a true vertical scale. The MWX1 samples illustrates highest porosity values, whereas the Last Dance samples show the lowest porosity values.

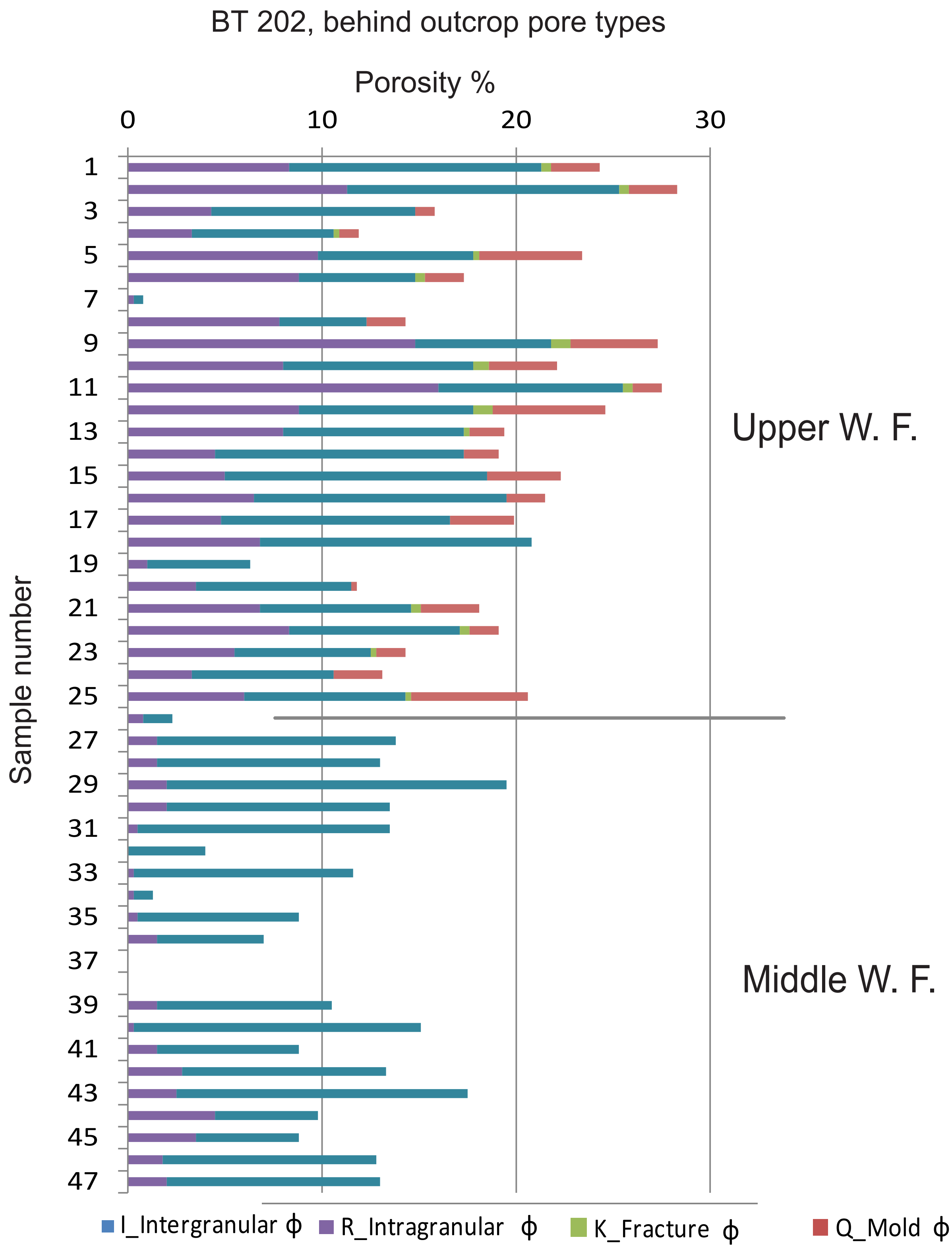

Figure 6.3 - Total thin-section porosity and the relative proportion of different pore types in the BT 202 behind outcrop core. Note that porosity values are higher in the upper Williams Fork interval than the lower interval, and that total porosity is generally greater in this behind outcrop core than in the deeper subsurface cores as exemplified by Figure 6.2. Vertical scale depicts sample footages in descending order; it is not a true vertical scale.

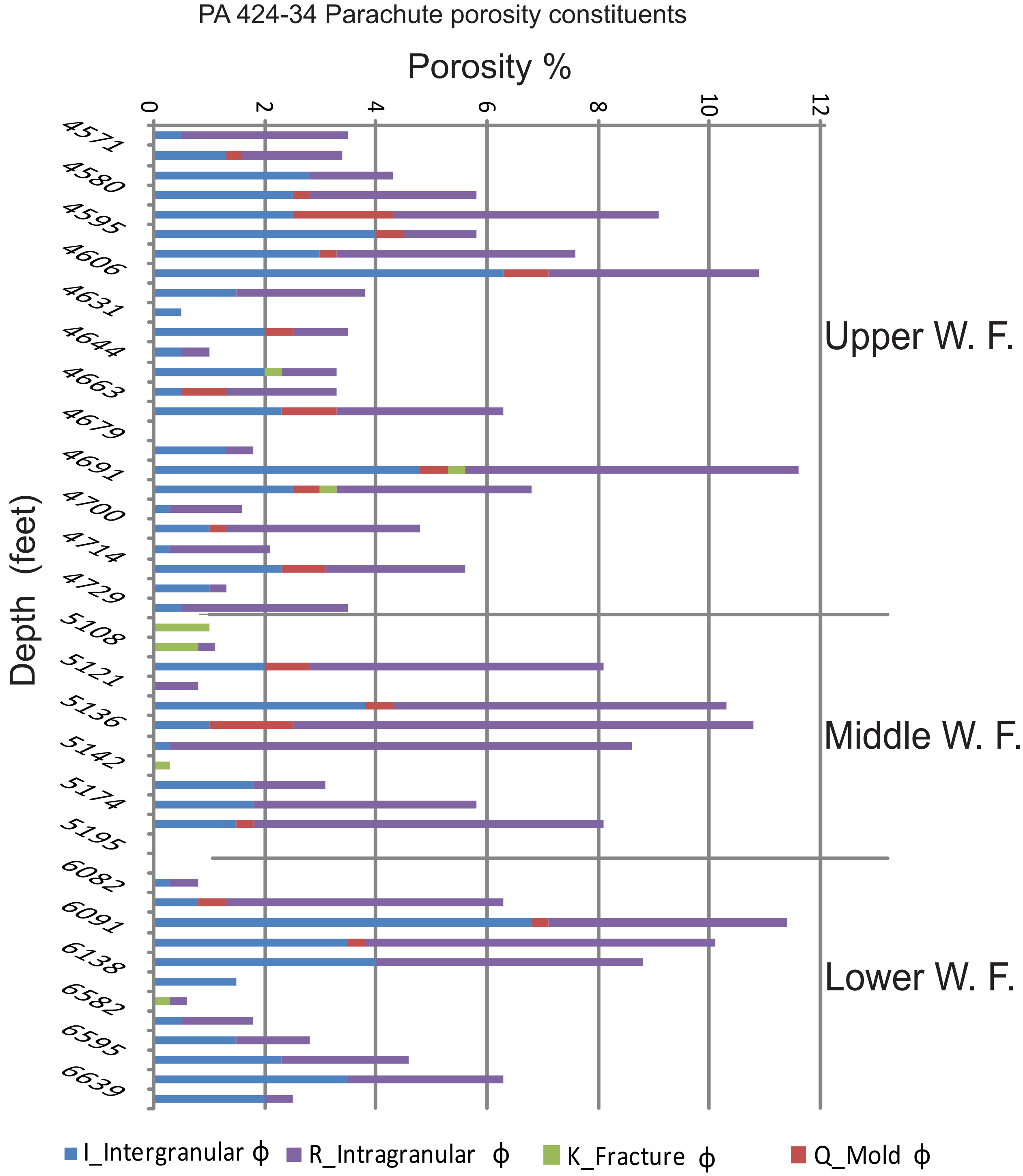

Figure 6.4 - Total thin-section porosity and the relative proportion of different pore types in the PA 424-34 Parachute core. Secondary porosity (intragranular, moldic, and fracture porosity) in most samples is higher than intergranular porosity. Intergranular porosity includes initial primary porosity and intergranular porosity created by the dissolution of cements. Vertical scale depicts sample footages in descending order; it is not a true vertical scale.

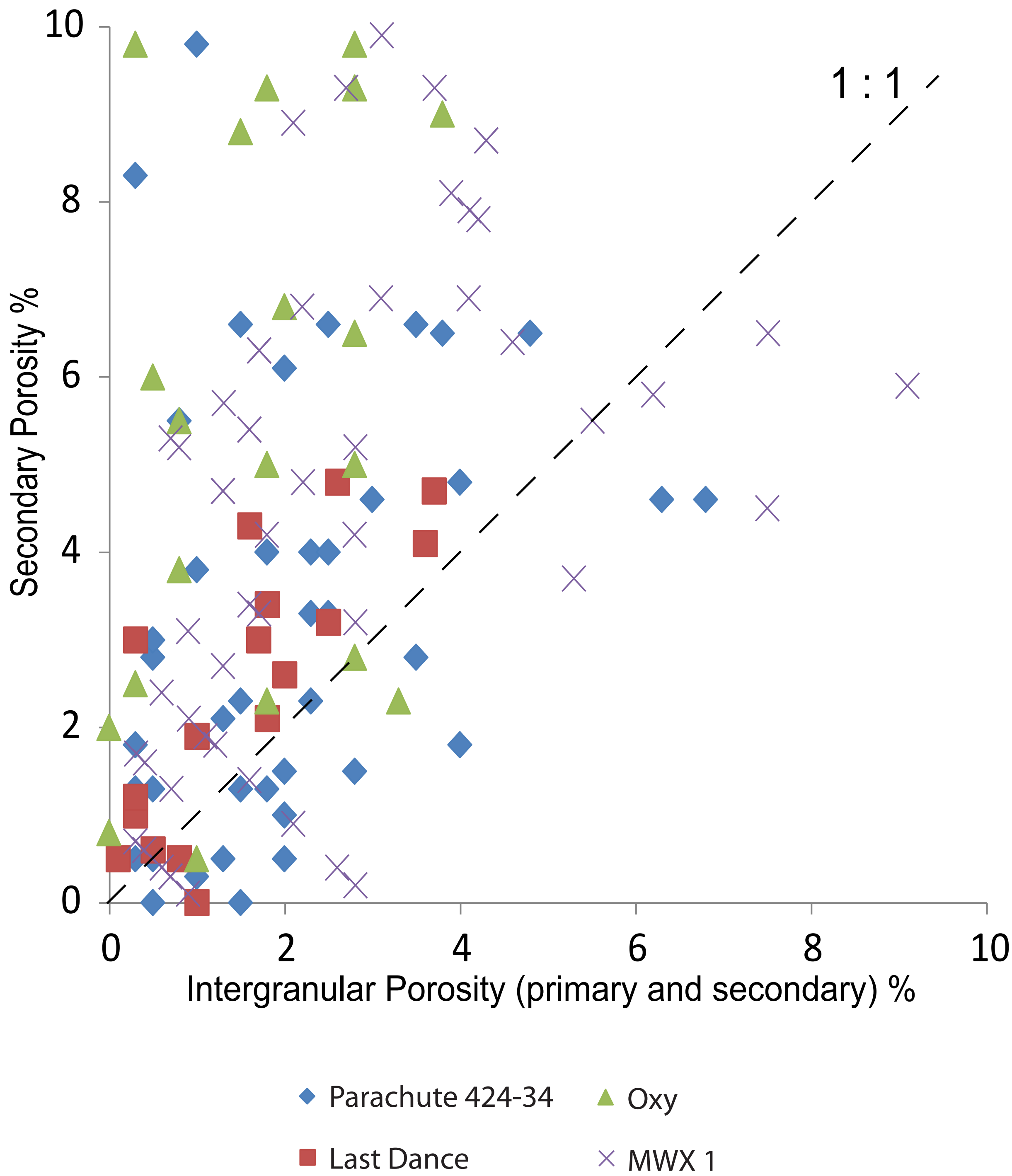

Figure 6.5 - Figure 6.5 - Relative abundance of intergranular porosity (primary and secondary) versus secondary intragranular porosity (partial and complete grain molds) in sandstones. Dashed line is the one-to-one correlation.

are higher than partial moldic (intragranular) porosity (0 to 2.8%, averaging 1.4%) and complete moldic porosity (0 to 3.8%, averaging 1.6%) combined.

Secondary porosity originates from dissolution and occurs mainly as intergranular, intragranular and grain molds (Figures 3.4, 4.23A, 4.28), and as micro and some macro fracture porosity. Most of the pore spaces were formed from dissolution of unstable grains (feldspars, and rock fragments) and early cements (quartz and carbonate). The secondary pores are typically partially filled and/or lined with later authigenic clay that reduces porosity effectiveness (Figure 6.6). Ineffective porosity also exists as microporosity within authigenic clays in intergranular pores (Figures 4.25, 4.26), in clays within replaced feldspars and rock fragments, and within some detrital-clay rich samples. The microporosity associated with intergranular clays forms a portion of total porosity that is hard to count in thin section, but is captured in core-plug porosity. Nonetheless, thin-section porosity generally covaries with core-plug porosity measurements (Figure 6.7).

Permeability values derived from core plug analysis are extremely low in all wells and Williams Fork intervals (Figure 6.8). Values range from less than 0.0001 to 2.1 mD, however more than 70% of permeability values are less than 0.1 mD, and only about 5% of the sandstones have more than 1 mD of permeability (Figure 6.8). Permeability values vary between wells. For example, Last Dance 43C-3-792 core permeability ranges from 0.0 to 1.872 mD, averaging 0.102 mD; Parachute 424-34 core permeability ranges from 0.0002 to 0.608 mD, averaging 0.027 mD; and Occidental 697-20-28 core permeability ranges from 0.005 to 2.1 mD, with an average of 0.197 mD. Stratigraphically, the highest permeabilities tend to occur in upper Williams Fork

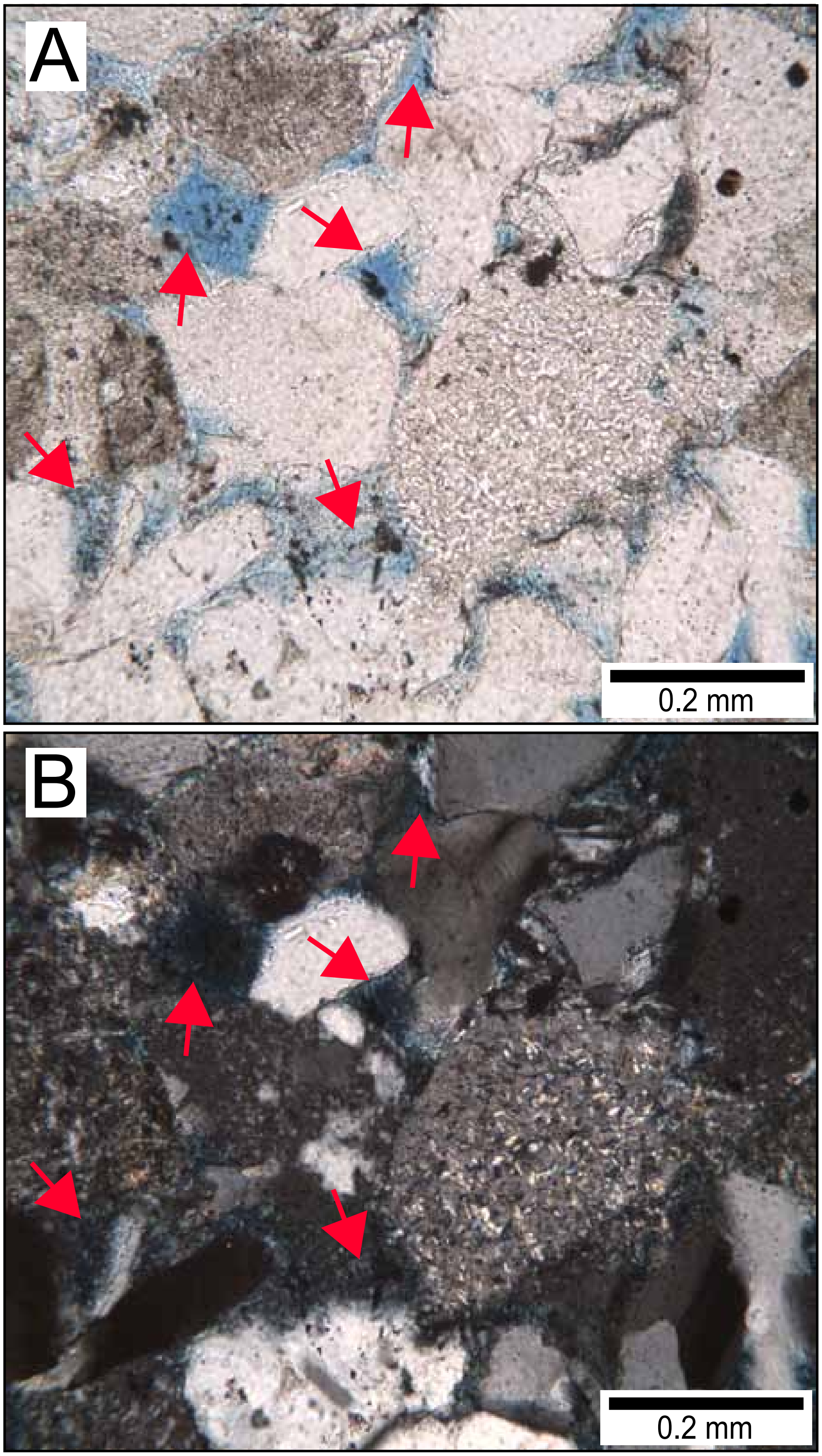

Figure 6.6 - Thin-section photomicrographs Last Dance 4010', (A) plane light and (B) cross nicols, showing secondary pores formed by dissolution that are partially filled with authigenic clay (red arrows) that reduce porosity's effectiveness.

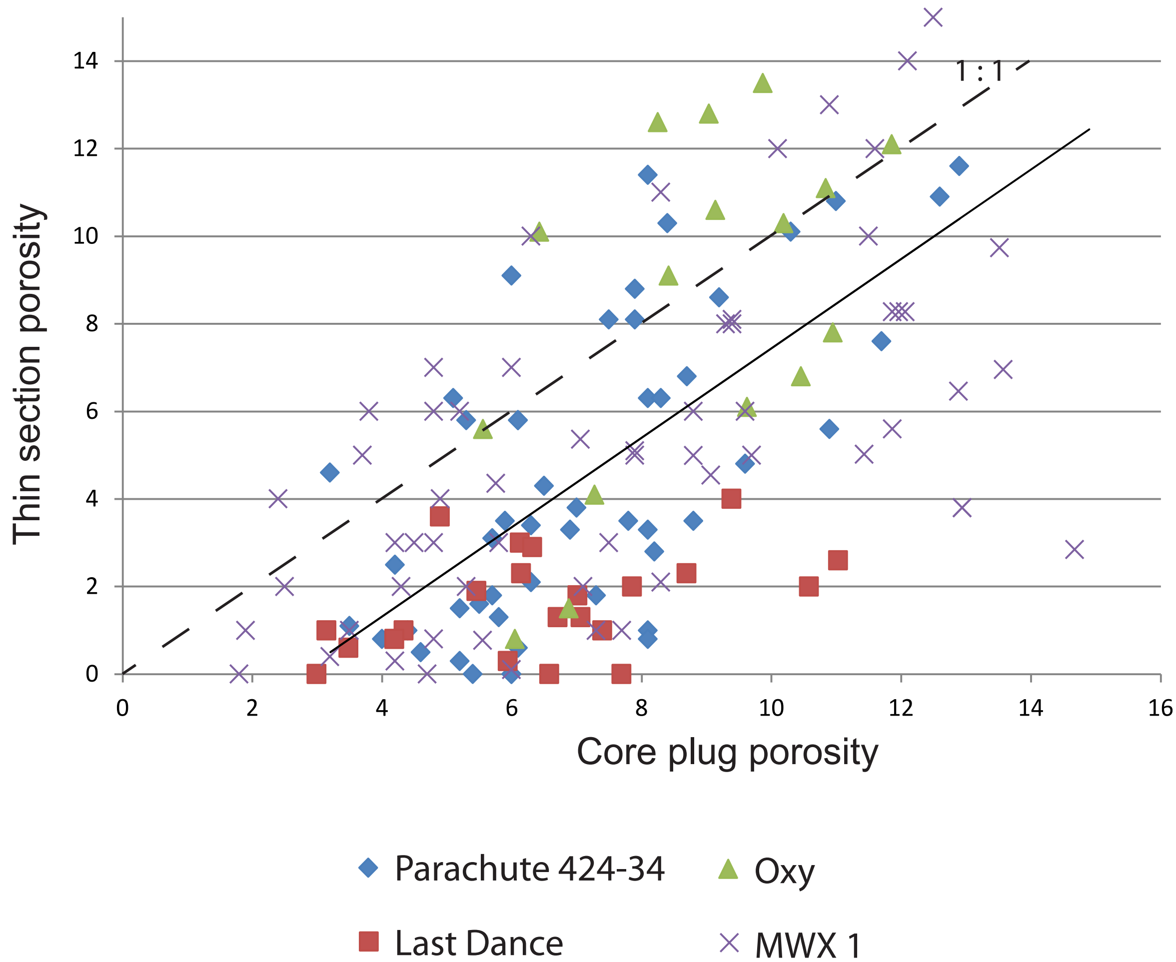

Figure 6.7 - Covariance of thin-section porosity and core-plug porosity. Solid line is the linear regression through the data. Some data points lie proximal to the dashed one-to-one line, indicating that thin-section porosity in those samples has a good correspondence to core-plug porosity. Most samples, however, exhibit more core-plug porosity than thin-section porosity, yet still with a strong correlation between the two.

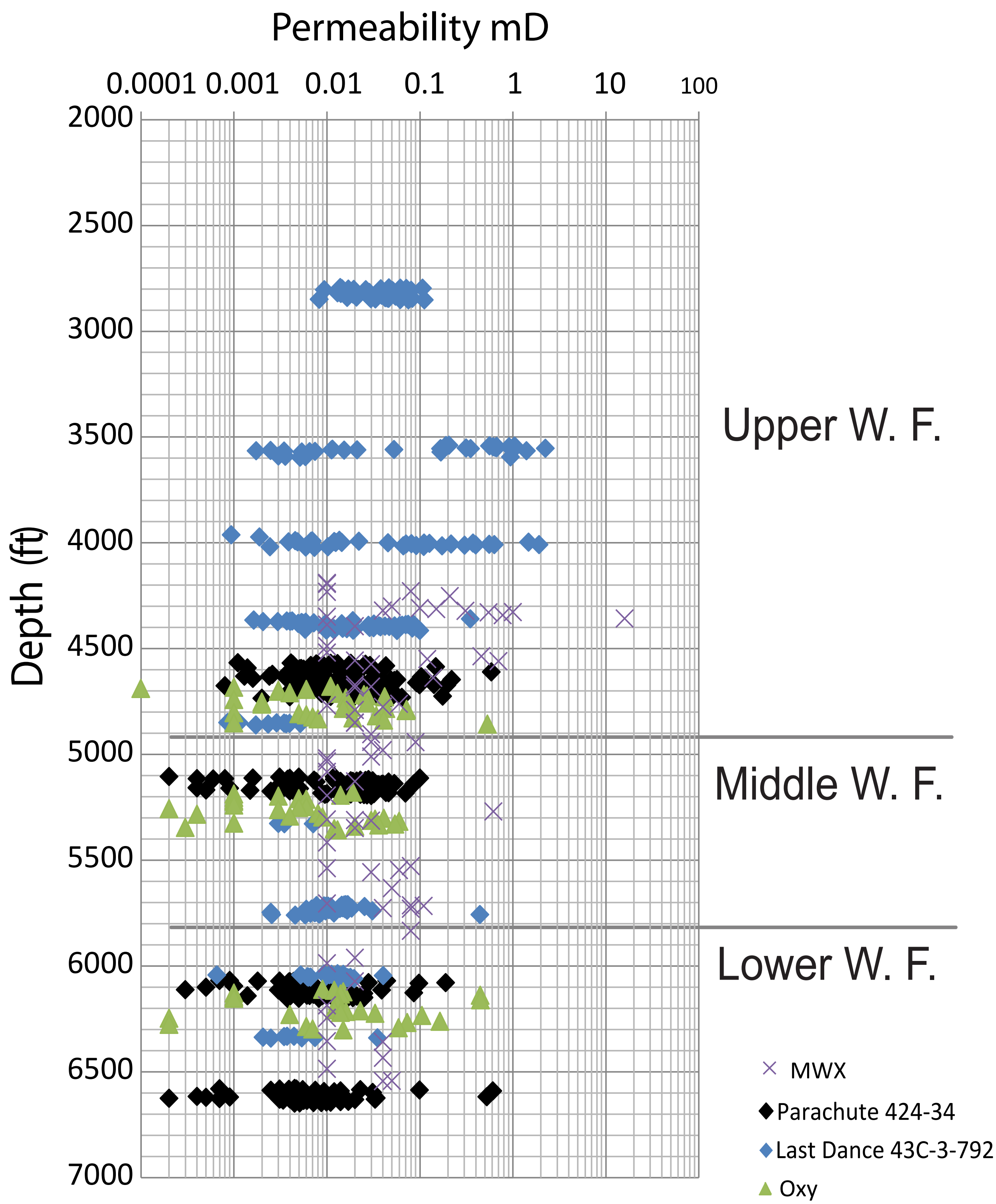

Figure 6.8 - Stratigraphic distribution of permeability. Very low permeability values dominate the section. More than 70% of the permeability readings are less than 0.1 mD, and only about 5% of the values are higher than 1 mD. Best permeability (values > 0.1 md) tend to be in the upper Williams Fork interval.

sandstones (Figure 6.8). For example, in the Last Dance cores, permeability above 4500 ft (uppermost upper Williams Fork section) ranges from less than 0.001 to 1.872 mD and averages 0.157 md whereas, permeability below 4500 feet is generally less than 0.030 mD, averaging 0.011 mD.

Permeability of behind-outcrop Bt 202 sandstones is an exception as those sands have much larger permeability relative to the deep subsurface cores. Permeability behind the outcrop ranges from 0.001 mD to 1996.7mD, and averages 257 mD (Figure 6.9). These high permeability values are attributed to the high sandstone porosity of the behind-outcrop samples that were generated by extensive dissolution of early cement and unstable detrital grains.

In subsurface cores, the best permeability values occur in sandstones with low illite and illite/smectite mixed-layer clay contents (Figure 6.10), as these clays' fibers commonly bridge and occlude pore throats (Figure 4.24). Highly-cemented facies also exhibit low permeability with abundance of carbonate minerals exhibiting an inverse covariance with permeability (Figure 6.11). All cements that fill the intergranular spaces reduce pore throat connections and isolate the late intragranular dissolution porosity, making it disconnected and ineffective.

Discussion

The Williams Fork samples reveal an enormous effect on reservoir quality by the complex diagenetic history, but also that original depositional fabric had an important control on porosity and consequent permeability. The facies that have fabric and textures suggestive of higher porosity and permeability at deposition make better

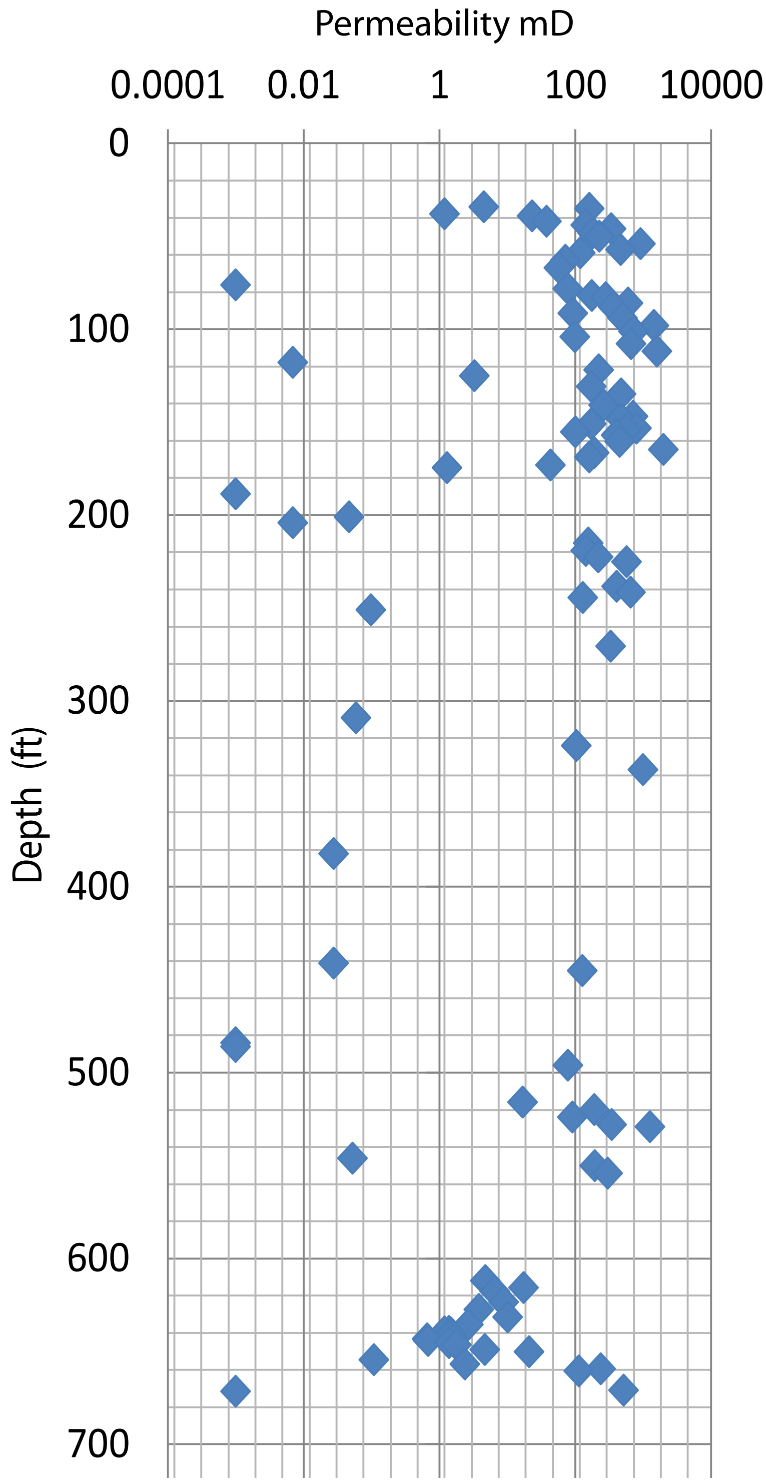

Figure 6.9 - Stratigraphic distribution of permeability within the BT 202 behind-the-outcrop core. In this shallow core, permeability ranges from 1997 mD to 0.001 mD, and averages 257 mD. Over 73% of the measurements are higher than 50 mD.

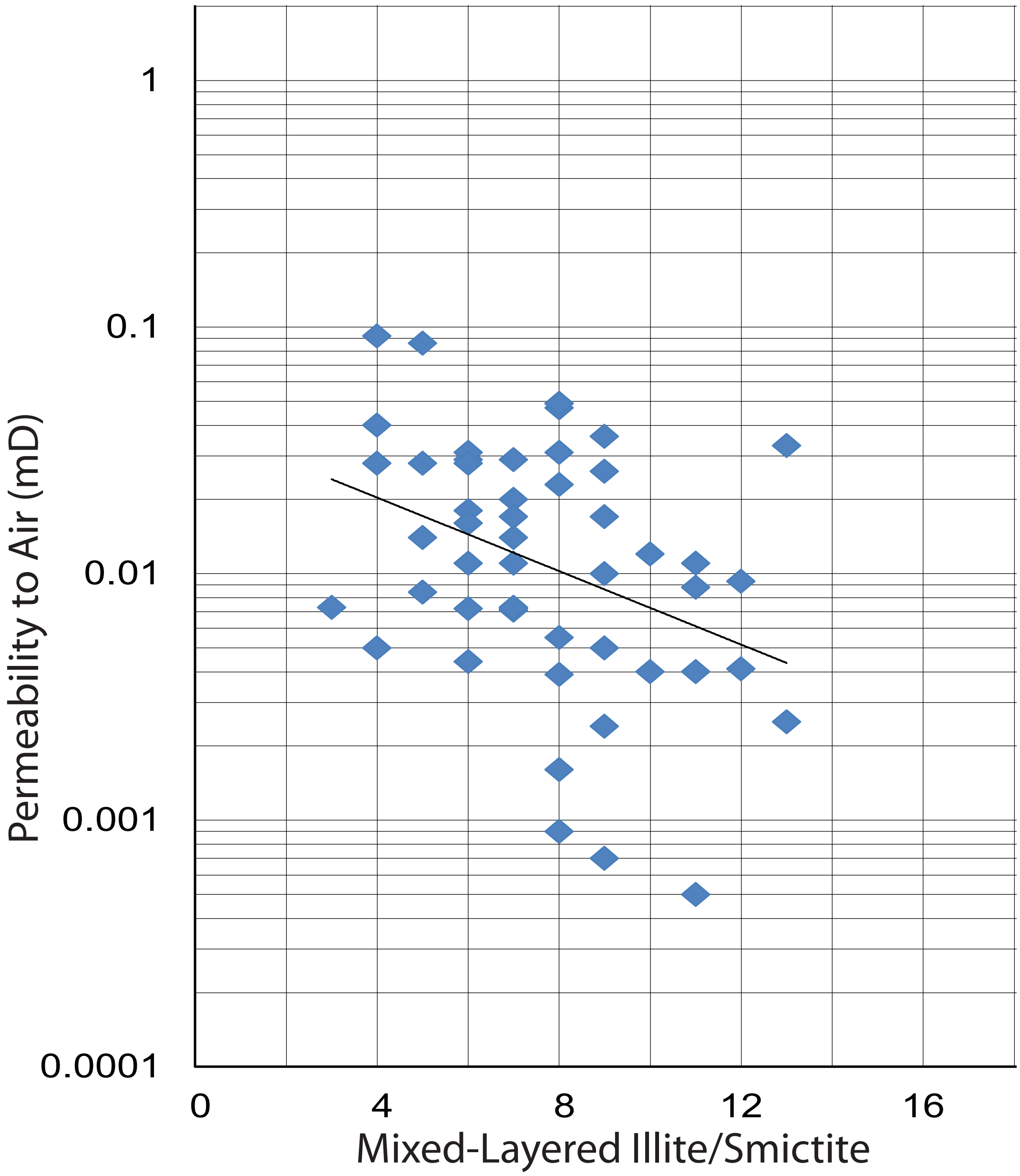

Figure 6.10. Permeability as a function of the abundance of mixed-layer illite/smectite. The moderate covariance of the best-fit trend (solid line) indicates that permeability within sandstones decreases with increasing abundance of illite and illite/smectite mixed-layer clays. Clay abundances (XRD) and permeability values provided by Williams P&E.

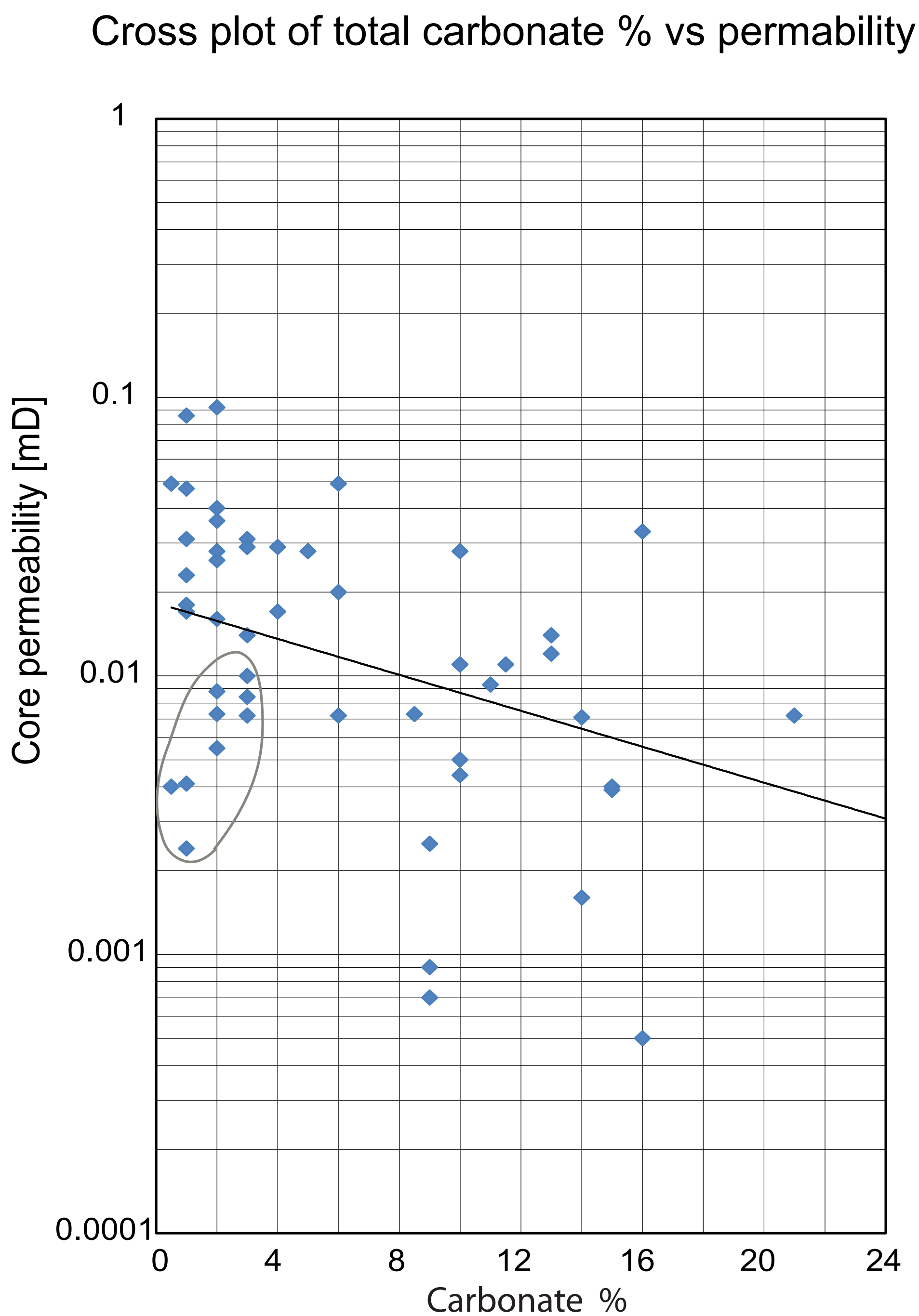

Figure 6.11- Cross plot of permeability verses carbonate content (percent of total mineral volume as deduced) by XRD analysis) in the Parachute 424-34 well. Linear trend line shows permeability decreases with increasing carbonate content (calcite, dolomite) within Williams Fork sandstones. Note that some low carbonate-content samples have permeability less than 0.01 mD (circled) because of high argillaceous content and presence of other cement types. Permeability data provided by Williams P&E.

reservoir targets despite the complex diagenetic history (Figure 6.1). For example, the well-to-moderately sorted, medium-grained, horizontal laminated and structureless sandstone that typically compose the upper portion of channel fills (Chapter 2) show the best reservoir quality, even though they were intensely affected by diagenesis. This suggests that variations in facies-controlled primary porosity impacted the diagenetic events that generated the secondary porosity that dominates the Williams Fork reservoir.

Primary porosity has almost entirely been lost. The paucity of primary porosity is interpreted to result from increased burial compaction and temperature with depth, with temperature accelerating cement precipitation (e.g., Malley et al. 1987). In the absence of any other diagenetic processes, compaction and cementation with progressive burial would have resulted in no reservoirs.

The relative intensity of compaction appears to have affected reservoir quality slightly. The few samples in Figure 6.12 (group 1) with the least compactional porosity loss (COPL) relative to cementational porosity loss (CEPL) have an average core plug porosity and permeability of 5.5% and 0.018 mD, respectively. The samples with intermediate amounts of COPL relative to CEPL (group 2) have a slightly higher average porosity (6.5%) and average permeability (0.020 mD). The samples with the greatest amount of COPL and least amount of CEPL (group 3, Figure 6.12) have the highest average porosity and permeability of 7.0% and 0.186 mD, respectively. These data suggest that there is slightly better reservoir quality when cementation is minimal (CEPL < 10%) even though compaction maybe extreme (> 35% COPL). Although compaction dominates porosity loss, it is the subordinate cementation that generates

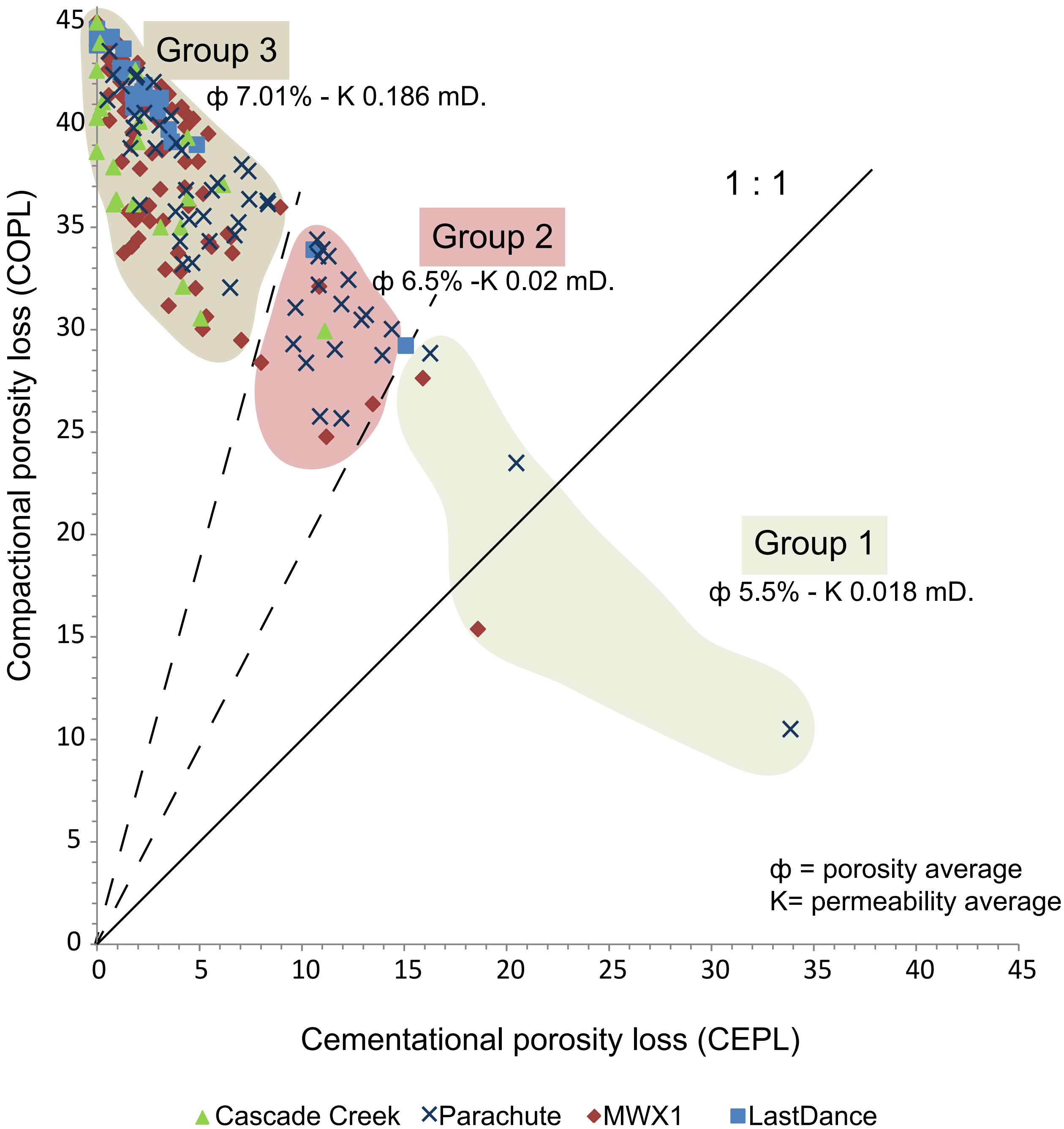

Figure 6.12 - Cross plot of compactional porosity loss versus cementational porosity loss for Williams Fork sandstones core. Diagonal line is line of equal porosity loss by compaction and cementation. The data are arbitrarily separated into three groups based on increasing compactional affects (dashed lines). Porosity and permeability averages are given for the samples in each grouping.

the observed petrophysical variance and has the more deleterious effect on relative reservoir quality.

Two diagenetic pathways promoted formation of reservoir rock. In one pathway, eo-genetic authigenic clay precipitation (mostly chlorite) and early authigenic calcite, where it existed, prevented the formation of quartz overgrowths, minimized (but did not eliminate) compaction effects, protected primary porosity, and preserved some permeability. On the second pathway, compaction and cementation occluded all primary porosity but mesogenetic dissolution of framework grains and carbonate cements created the secondary porosity that dominate the Williams Fork Formation. The selective dissolution of unstable detrital minerals (mainly feldspars, some of volcanic lithics, and some grains that had been replaced by carbonates) formed the intragranular secondary porosity and moldic pores. Dissolution of authigenic cement (commonly carbonates, some quartz) created limited intergranular secondary porosity.

Secondary porosity values show no distinct depth trends (Figure 6.4), which suggests secondary porosity generation is not related to burial depth. Instead it is more likely controlled by the relative abundance of unstable grains and cements that were preferred by dissolution processes within all facies. These secondary pores can enhance permeability when they are connected. However, many of the partial (intragranular) and complete moldic pore spaces are surrounded and isolated by carbonate and/or quartz cements, and may contain authigenic clay. Thus the meso-genetic pathway to reservoir porosity in the Williams Fork produced the classic porous but impermeable “tight” reservoir rock.

Ultimately reservoir quality depends on the relationship between porosity and permeability. Porosity – permeability measurements show good covariance in simple, intergranular porosity networks (Tiab and Donaldson, 2011). Simple pore networks, however, do not exist within the Williams Fork Formation. Williams Fork sandstones demonstrate complex pore-systems that were severely influenced by diagenetic process. Although some sandstone samples show relatively close correlation between porosity and permeability (Figure 6.13), many samples do not follow the covariant trend. In some samples porosity is relatively high but permeability relatively low, reflecting the fact that a reasonable fraction of the total porosity is non-effective porosity. This suggests porosity is either unconnected secondary pores or microporosity related to intergranular clays and micro-dissolution voids. These samples appear on Figure 6.13 with good porosity (up to 10 to 13%) but less than 0.01 mD of permeability. In contrast, a limited number of samples exhibit high permeability with low total porosity, presumably due to good pore connectivity and/or micro fractures. The scatter in Figure 6.13 thus means that predictions of permeability from total porosity values would be unreliable. This is a common predicament when dealing with highly diagenetically altered sandstones (e.g. Kameda et al., 2006).

Permeability is significantly enhanced by natural fractures, which also enhance the overall reservoir quality of the formation. The role of natural fractures in contributing to the improvement of production of natural gas in low-permeability, basin-centered accumulations within the Williams Fork has been reported by others (e.g., Lorenz, and Finley, 1989; Lorenz and Hill, 1994). The low porosity and very low matrix permeability of the Williams Fork sandstones could not account for the delivery of gas from

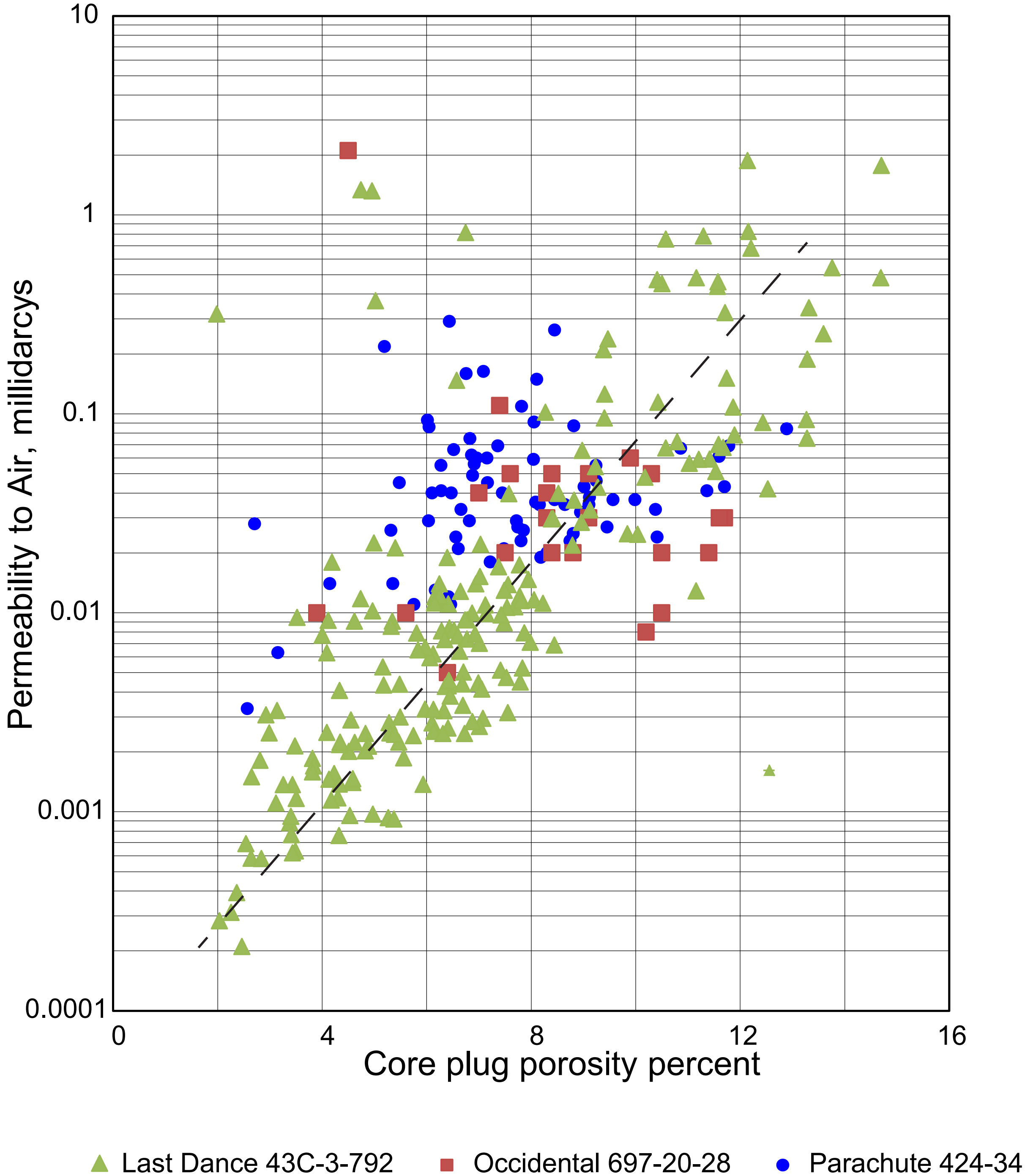

Figure 6.13 - Cross plot of permeability versus porosity in Williams Fork core samples. In general, there is a trend of increasing permeability with increasing porosity (dashed line) but many samples plot off of that trend. Sandstones far to the right of the general trend are interpreted to contain isolated and non-connected secondary pores, clay-related microporosity and/or micro-dissolution porosity, all of which contribute to porosity but not permeability. Samples far to the left of the general trend are interpreted to contain microfractures that contribute to permeability but not to porosity.

underlying source rocks. Similarly the matrix pore systems are not adequate to successfully produce gas from the reservoir without the existence of a natural fracture network. Natural fractures can be seen in core samples and in thin sections (Figure 4.12A, 4.13B). Commonly the fractures are partly or totally cemented by carbonate, quartz and clays. Due to the fact that the core is a limited representation of the reservoir volume, the observed fractures are limited.

Using the classification for low-permeability reservoirs suggested by Soeder and Randolph (1987) and Dutton et al. (1995), the Williams Fork studied samples could be described as a combination of type II and type III low-permeability reservoirs. Type I reservoirs, characterized by sandstone with open intergranular pores and pore throats plugged by authigenic clay minerals, are almost non-existent within the Williams Fork Formation. The very few sandstones with open intergranular pores are limited to behind the outcrop samples and deeper subsurface footages that had extensive dissolution of carbonate cement during late-stage diagenesis but early authigenic chlorite formation that inhibited quartz overgrowths. Cascade Creek 697-20-28 at 4809 ft is one such example where intragranular thin-section porosity is 9.8 percent (Figures 4.4A, 4.6A). But such footages are rare and isolated in any one core.

Type II reservoirs occur in sandstones with highly altered primary pores occluded with authigenic quartz and/or calcite cements. The majority of pores and pore throats are reduced to narrow slots connecting significant secondary pores created by grain dissolution (Dutton et al., 1995). This reservoir type exists widely within the highly altered channel fill and crevasse splay sandstones of the Williams Fork Formation.

Type III reservoir rocks also occur within Williams Fork, and are characterized by micro-porosity in muddy sandstone with intergranular volume largely filled with a detrital clay matrix (e.g., Figure 3.28). This pore structure is common in many rocks with less than 1 µd permeability, and is represented by the sediments deposited in the flood plain and coastal settings that dominant in the lower Williams Fork Formation. It is particularly characteristic of Williams Fork intervals with low sandstone-to mudstone intervals.

SUMMARY

Heterogeneity in reservoir quality is a function of diagenesis, sand body geometry, internal structures, texture, and sandstone provenance (Morad et al, 2010). These in turn determine reservoir fluid characteristics including fluid flow rates, volumes and recovery (Wardlaw and Taylor, 1976; Wardlaw and Cassan, 1979; Weber, 1982). Williams Fork Sandstones represent highly heterogeneous reservoirs that include many non-communicating sandstone facies (Johnson, 1989; Cole and Cumella, 2005; Pranter et al., 2007, 2009), each with different specific and relative porosity characteristics (Figure 6.1). At the micro and macro scales, facies controlled initial porosity and diagenesis yielded two pathways to reservoir quality porosity. Early fluid flux created cements (chlorite, carbonates) that inhibited subsequent quartz cementation, which in turn resulted in preservation of some primary porosity. More typically, all primary porosity was destroyed by compaction and cementation and reservoir porosity is secondary. Facies and provenance determined location of unstable grains that were selectively dissolved by formation waters to create that secondary porosity and its uneven distribution creates heterogeneity at multiple scales.

CHAPTER SEVEN: CONCLUSIONS

Diagenetic processes extensively altered the mineralogy, texture, and fabric of Williams Fork sandstones. The most volumetrically significant diagenetic process was compaction, followed in importance by early and late cementation, dissolution, and replacement by calcite or clay minerals. Early cementation was by chlorite, quartz, and non-ferroan calcite. Dissolution affected feldspars, lithic fragments and cements (quartz and calcite). Late cementation was dominated by ferroan calcite and dolomite. In nearly all sandstones, compaction exceeds cementation in terms of destruction of intergranular pore space.

Timing of diagenetic events are complex but petrographic relationships reveal features formed very early prior to any significant burial (infiltration of clays), eo-diagenetic features formed at <70°C, and late meso-diagenetic features formed at >70°C. Chlorite, early quartz cement, non-ferroan calcite, and kaolinite are the eogenetic authigenic phases. Albite, illite and mixed-layer illite/smectite, and ferroan calcite and dolomite were formed at higher temperatures in the mesogenetic realm. Volumetrically, the eo-diagenetic products are more abundant, which coupled with the dominance of eo-diagenetic compaction, indicates that the Williams Fork sandstones were highly reactive at fairly shallow (<7,000 ft) burial depths.

The main goal of this study was to assess the relationships between the spatial distributions of diagenetic alterations and the sequence stratigraphic framework. Four of the eo-diagenetic features can be linked to specific types of systems tracts. These four are (1) mechanically infiltrated clays, (2) pseudomatrix, (3) authigenic chlorite, and

(4) quartz overgrowths. Mesogenetic illitization of infiltrated clays and pseudomatrix also exhibits spatial distributions related to systems tracts, but those patterns are inherited from the distribution of the precursor clays. All other diagenetic features and processes (all carbonates, compaction, dissolution, and most replacements) exhibit no relationships to system tracts and are not predictable within a sequence stratigraphic framework.

Mechanically infiltrated clays are concentrated in channel and crevasse splay sandstones of lowstand (LST) highstand systems tracts (HST). Concentration of infiltrated clays in these intervals is interpreted to result from exposure of sandstones on the floodplain during periods of base level fall or limited base level rise. During such times, sandstones are covered by repeated flood events that promote the infiltration of clays. Concentration of pseudomatrix (compacted mud clasts) also occurs mainly in channel sandstones of HSTs and LSTs. Concentration of mud intraclasts in these intervals is interpreted to result from lateral channel migration and active erosion of the floodplain when base level fall is associated with decreasing accommodation space. Authigenic chlorite, associates with the HSTs and transgressive systems tracts (TST) of the upper half of the Williams Fork Formation because of the abundance of mafic volcanic clasts in that portion of the formation (a sequence stratigraphic relation due to changes through time in provenance). Quartz overgrowths are more likely to be abundant in TSTs for reasons that are not entirely clear. Excessive amounts of clay content do inhibit quartz cementation, but TST sands with high quartz cement contents are just as likely to have 20% total clay as they are to have <5% clay.

The eogenetic features that do exhibit a systems tract relationship are similar to the types of features described by many prior workers as having a sequence stratigraphic control. These are features that probably formed while the Williams Fork systems tracts were also forming, thus are the type of features most likely to exhibit a sequence stratigraphic control or relationship (Morad et al., 2000; Ketzer et al., 2002; Ketzer et al., 2003b). Conversely, compaction features and all diagenetic features that post-date the initiation of quartz cementation exhibit no spatial correlation or relation to the Williams Fork sequence stratigraphy. This illustrates that the controlling functions on diagenesis are complex and not necessarily related to sequence position. The greater the time between a diagenetic event and the deposition of a sequence/systems tract, the greater the likelihood that non-stratigraphic controlling functions determined the spatial distribution of diagenetic features. In the case of the Williams Fork sandstones, it is speculated that rapid burial and extensive compaction may have controlled the early diagenetic evolution of the sediments more so than base level fluctuations and changes in accommodation space.

The diagenetic analysis of the Williams Fork sandstones also allowed the evaluation of stratigraphic variability in detrital components. The main detrital minerals in the Williams Fork sandstones are quartz, feldspar and lithic (chert, volcanic, and mudstone) fragments. At deposition, the Williams Fork sandstones range from lithic arkose to litharenite. Authigenic components include quartz, clay (illite, mixed layer illite/smectite, chlorite, and kaolinite), carbonates (non-ferroan calcite, ferroan calcite, dolomite and ferroan dolomite), and albite.

Provenance differences are the dominant driver of the major detrital mineralogy differences within Williams Fork stratigraphic horizons. The near absence of potassium feldspar and volcanic rock fragments in the lower Williams Fork interval, and increasing plagioclase content (and hence total feldspar content) upward in the upper half of the Williams Fork Formation are interpreted to result from changes in sediment provenance rather than stratigraphic variability in dissolution and replacement reactions. Compositionally, the lower Williams Fork sands are strictly from sedimentary sources. In contrast, detrital compositions of middle and upper Williams Fork sands indicate the input of detritus from western source terranes (magmatic arcs) and eventually the exhumation and erosion of basement rocks by upper Williams Fork deposition.

The Williams Fork sandstones are an example of a low-permeability tight gas reservoir in which the complex diagenetic history had an enormous impact on reservoir quality. Primary porosity was almost entirely been lost due to burial compaction and cementation with cementation having the more deleterious affect even though compaction destroyed more of the primary porosity. Reservoir rock resulted from the interplay of key diagenetic processes. Eo-genetic authigenic clay precipitation (mostly chlorite) and early authigenic calcite cementation, where they occurred, prevented the formation of quartz overgrowths, minimized (but did not eliminate) compaction effects, and protected some primary porosity. Meso-genetic dissolution of framework grains (feldspars) and carbonate cements created the secondary porosity that dominates the Williams Fork Formation. Permeability values are very low (<0.1 millidarcy) and vary between wells, but can be significantly enhanced by natural fractures.

REFERENCES CITED

Aboktef, A., Pranter, M., and Budd, D., 2011, Sequence-Stratigraphic Controls on Sandstone Diagenesis – An Example from the Williams Fork Formation, Piceance Basin, Colorado, AAPG Search and Discovery Article #90124, http://www.searchanddiscovery.com/abstracts/html/2011/annual/abstracts/Aboktef.html

Al-Ramadan, K., Morad, S., Proust, J. N., and Al-Aasm, I., 2005, Distribution of diagenetic alterations in siliciclastic shoreface deposits within a sequence stratigraphic framework: Evidence from the Upper Jurassic, Boulonnais, NW France, Journal of Sedimentary Research, v. 75, p. 943-959.

Amorosi, A., 1995, Glaucony and sequence stratigraphy; a conceptual framework of distribution in siliciclastic sequences. Journal of Sedimentary Research, v. 65, p. 419-425.

Anjos, S. M. C., de Ros, L.F., and Silva, C. M. A., 2009, Chlorite authigenesis and porosity preservation in the Upper Cretaceous marine sandstones of the Santos Basin, offshore eastern Brazil, *in,* Worden R. H., and Morad, S., eds., Clay Mineral Cements in Sandstones. Special Publication of the International Association of Sedimentologists No. 34, p. 291-316

Berger, A., Gier, S., and Krois, P., 2009, Porosity-preserving chlorite cements in shallow-marine volcaniclastic sandstones; evidence from Cretaceous sandstones of the Sawan gas field, Pakistan. AAPG Bulletin, v. 93, p. 595-615.

Berry, G.W., 1959, Divide Creek field, Garfield and Mesa counties, Colorado, in Symposium on Cretaceous rocks of Colorado and adjacent areas: Rocky Mountain Association of Geologists, p. 89-91,

Bjørlykke, K., and Egeberg, P.K., 1993, Quartz cementation in sedimentary basins. AAPG Bulletin, v. 77, p. 1538-1548.

Bjørlykke, K., and Jahren, J., 2012, Open or closed geochemical systems during diagenesis in sedimentary basins: Constraints on mass transfer during diagenesis and the prediction of porosity in sandstone and carbonate reservoirs. AAPG Bulletin, v. 96, p. 2193-2214.

Bjørlykke, K., Nedkvitne, T., Ramm, M. and Saigal, G. C., 1992, Diagenetic processes in the Brent Group (Middle Jurassic) reservoirs of the North Sea; an overview; Geology of the Brent Group, *in*, Morton, A. C., Haszeldine, R. S., Giles, M. R., and Brown, S., eds., The Petroleum Science and Technology Institute Edinburgh, Uk Geology of the Brent Group. Geological Society Special Publications 61, p. 263-287.

Bloch, S., Lander, R. H., and Bonnell, L., 2002, Anomalously high porosity and permeability in deeply buried sandstone reservoirs; origin and predictability, AAPG Bulletin, v 86, p. 301-328.

Blum, M. D., and Tornqvist, T. E., 2000, Fluvial responses to climate and sea-level change; a review and look forward. Sedimentology, v. 47, p. 2-48.

Boggs, S., Jr., 2009, Petrology of Sedimentary Rocks, Cambridge University Press, New York, NY, United States, 600 p.

Boles, J. R., and Franks, S. G., 1979, Clay diagenesis in Wilcox sandstones of Southwest Texas; implications of smectite diagenesis on sandstone cementation. Journal of Sedimentary Petrology, v. 49, p. 55-70.

Burger, B. J., 2007, A new late Paleocene vertebrate fauna from the Ohio Creek Formation of Western Colorado. The Mountain Geologist, v. 44, p. 141-150.

Byrnes, A. P., 1997, Reservoir characteristics of low-permeability sandstones in the Rocky Mountains; Gas reservoirs in the Rocky Mountains. The Mountain Geologist, v. 34, p. 37-48.

Byrnes, A. P., 2003, Aspects of permeability, capillary pressure, and relative permeability properties and distribution in low-permeability rocks important to evaluation, damage, and stimulation. Proceedings of the Rocky Mountain Association of Geologists—Petroleum Systems and Reservoirs of Southwest Wyoming Symposium, Denver, Colorado, September, 19, 2003.

Carroll, C.J., Robeck, R., Hunt, G., and Koontz W., 2004, Structural implications of underground coal mining in the Mesaverde Group in the Somerset coal field, Delta and Gunnison Counties, Colorado, *in,* Nelson, E.P., and Erslev, E.A., eds., Field trips in the Southern Rocky Mountains, USA. Geological Society of America, Field Guide #5, p. 41-58.

Choquette, P. W., and Pray, L. C., 1970, Geologic nomenclature and classification of porosity in sedimentary carbonates. AAPG Bulletin, v. 54, p. 207-244.

Cole, R., and Cumella, S.P., 2003, Stratigraphic architecture and reservoir characteristics of the Mesaverde Group, southern Piceance Basin, Colorado, *in* Peterson, K.M., Olson, T.M., and Anderson, D.S., eds., Piceance Basin 2003 Guidebook. Rocky Mountain Association of Geologists, p. 385-442.

Cole, R., and Cumella, S., 2005, Sand-body architecture in the lower Williams Fork Formation (Upper Cretaceous), Coal Canyon, Colorado, with comparison to the Piceance Basin subsurface. The Mountain Geologist, v. 42, p. 85-108.

Collins, B. A., *1976*, Coal deposits of the Carbondale, Grand Hogback, and southern Danforth Hills coal fields, eastern Piceance Basin, Colorado: Quarterly of the Colorado School of Mines*, v.* 71*,* 138 p.

Collins, B. A., 1977, Geology of the Coal Basin area, Pitkin County, Colorado, *in* Veal, H.K., ed., Exploration frontiers of the central and southern Rockies. Rocky Mountain Association of Geologists Symposium, p. 363-377.

Collinson, J. D., 1969, The sedimentology of the Grindslow shales and the Kinderscout grit: a deltaic complex in the Namurian of northern England. Journal of Sedimentary Research, v. 39, p. 194-221.

Connolly, J. R., 1965, The occurrence of polycrystallinity and undulatory extinction in quartz in sandstones. Journal of Sedimentary Petrology, v. 35, p. 116-135.

Crone, A. J., 1975, Laboratory and field studies of mechanically infiltrated matrix clay in arid fluvial sediments. PhD dissertation, University of Colorado, Boulder, CO., 162 p.

Cumella, S.P., 2006, Overview of a giant basin-centered gas accumulation, Mesaverde Group, Piceance Basin, Colorado. The Mountain Geologist v. 43, p. 219-224.

Cumella, S. P., and Ostby, D. B., 2003, Geology of the basin-centered gas accumulation, Piceance Basin, Colorado, *in* Peterson, K. M., Olsen, T. M., and Anderson, D. S., eds., Piceance Basin 2003 Guidebook, Rocky Mountain Association of Geologists, p. 171–93.

Cumella, S. P., and J. Scheevel, 2008, The influence of stratigraphy and rock mechanics on Mesaverde gas distribution, Piceance Basin, Colorado, *in* Cumella, S. P., Shanley, K.W., and Camp, W.K., eds., Understanding, exploring, and developing tight-gas sands. AAPG Hedberg Series, no. 3, p. 137-155.

Davis, R. A., 1983, Depositional systems: a genetic approach to sedimentary geology, Englewood Cliffs, N.J., Prentice-Hall, 669 p.

DeCelles, P. G., 2004, Late Jurassic to Eocene evolution of the Cordilleran thrust belt and foreland basin system, western U.S.A. American Journal of Science, v. 304, p. 105-168.

Dickinson, W. R., 1985, Interpreting provenance relations from detrital modes of sandstones, NATO Advanced Study Institutes Series.Series C: Mathematical and Physical Sciences, v. 148, p. 333-361.

Dickinson, W. R., Beard, L. S., Brakenridge, G. R., Erjavec, J. L., Ferguson, R. C., Inman, K. F., Knepp, R. A., Lindberg, F. A., and Ryberg, P. T., 1983, Provenance of North American Phanerozoic sandstones in relation to tectonic setting. Geological Society of America Bulletin, v. 94, p. 222-235.

Dickinson, W. R. and Gehrels, G. E., 2008, Sediment delivery to the cordilleran foreland basin: insights from U-Pb ages of detrital zircons in Upper Jurassic and Cretaceous strata of the Colorado Plateau. American Journal of Science, v. 308, p. 1041-1082.

Dutta, P. K. and Suttner, L. J., 1986, Alluvial sandstone composition and paleoclimate; II, Authigenic mineralogy, Journal of Sedimentary Petrology, v. 56, p. 346-358.

Dutton, S. P. and Willis, B. J., 1998, Comparison of outcrop and subsurface sandstone permeability distribution, Lower Cretaceous Fall River Formation, South Dakota and Wyoming. Journal of Sedimentary Research, v. 68, p. 890-900.

Dutton, S. P., Hamlin, H. S., and Laubach, S. E., 1995, Geologic controls on reservoir properties of low-permeability sandstone, Frontier Formation, Moxa Arch, southwestern Wyoming. Bureau of Economic Geology, University of Texas at Austin, Report of Investigations No. 234, 89 p.

Ehrenberg, S. N., 1993, Preservation of anomalously high porosity in deeply buried sandstones by grain-coating chlorite; examples from the Norwegian continental shelf, AAPG Bulletin, v. 77, p. 1260-1286.

El-ghali, M. A. K., 2005, Depositional environments and sequence stratigraphy of paralic glacial, paraglacial and postglacial upper Ordovician siliciclastic deposits in the Murzuq Basin, SW Libya. Sedimentary Geology, 177, p. 145–173.

El-Ghali, M.A.K., Mansurbeg, H., Morad, S., Al-Aasm, I. and Ajdanlisky, G., 2006a, Distribution of diagenetic alterations in fluvial and paralic deposits within sequence stratigraphic framework: evidence from the Petrohan terrigenous group and the Svidol Formation, lower Triassic, NW Bulgaria. Sedimentary Geology, 190, p. 299–321.

El-Ghali, M.A.K., Mansurbeg, H., Morad, S., Al-Aasm, I. and Ramseyer, K., 2006b, Distribution of diagenetic alterations in glaciogenic sandstones within a depositional facies and sequence stratigraphic framework: evidence from the upper Ordovician of the Murzuq Basin, SW Libya. Sedimentary Geology, v. 190, p. 323–351.

El-Ghali, M.A.K., Tajori, K.G., and Mansurbeg, H., 2006c, The influence of transgression and regression on the spatial and temporal distribution of diagenetic kaolin in the Upper Ordovician glaciogenic sandstones within a sequence stratigraphic framework, Murzuq Basin, SW Libya. Journal of Geochemical Exploration, v. 89, p. 87–91.

El-Ghali, M. A. K., Morad, S., Mansurbeg, H., Caja, M. A., Ajdanlijsky, G., Ogle, N., Al-Aasm, I., and Sirat, M., 2009a, Distribution of diagenetic alterations within depositional facies and sequence stratigraphic framework of fluvial sandstones; evidence from the Petrohan terrigenous group, Lower Triassic, NW Bulgaria. Marine and Petroleum Geology, v. 26, p. 1212-1227.

El-Ghali, M. A. K., Morad, S., Mansurbeg,H., Caja, ., M. A., Sirat, M., and Ogle, N., 2009b, Diagenetic alterations related to marine transgression and regression in fluvial and shallow marine sandstones of the Triassic Buntsandstein and Keuper sequence, the Paris Basin, France. Marine and Petroleum Geology, v. 26, p. 289-309.

Folk, R. L., 1980, Petrology of Sedimentary Rocks, Austin, Texas, Hemphill Publishing Company, 182 P.

Foster, R. M., 2010, Sequence stratigraphy of the Upper Cretaceous middle Williams Fork formation, Piceance Basin, northwestern Colorado: Implications for reservoir sandstones: MS thesis, University of Colorado, Boulder, CO, 263 p.

Fouch, T.D., Lawton, T.F., Nichols, D.J., Cashion, W.B. and Cobban, W.A., 1983, Patterns and timing of synorogenic sedimentation in Upper Cretaceous rocks of central and northeast Utah, *in*, Reynolds, M.W., and Dolly, E.D., eds., Mesozoic Paleogeography of the West-Central United States. SEPM, Rocky Mountain Section, Rocky Mountain Paleogeography Symposium 2, p. 305-328.

German, Q. A., 2006, Analysis of fluvial sandstone-body characteristics and architecture in a high net-to-gross system: Upper Williams Fork Formation, Plateau Creek Canyon, Piceance Basin, Colorado: MS thesis, University of Colorado, Boulder, CO, 175 p.

Giles M. R., Marshall J. D., 1986, Constraints on the development of secondary porosity in the subsurface; re-evaluation of processes. Marine and Petroleum Geology, v. 3, p. 243.

Giles, M. R., Indrelid, S. L., Beynon, G. V., and Amthor, J., 2000, The origin of large-scale quartz cementation; evidence from large data sets and coupled heat-fluid mass transport modeling, *in*, R.H. Worden and Morad, S., eds., Quartz Cementation in Sandstones, Special Publication of the International Association of Sedimentologists No. 29, p. 21-38.

Gretner, P.E., 1981, Geothermics: using temperature in hydrocarbon exploration: American Association of Petroleum Geologists Short Course Note Series #17, 170 p.

Gries, R., 1983, Oil and gas prospecting beneath Precambrian of foreland thrust plates in Rocky Mountains. AAPG Bulletin, v. 67, p. 1-28.

Hancock, N. J. and Taylor, A. M., 1978, Clay mineral diagenesis and oil migration in the Middle Jurassic Brent Sand Formation: sandstone diagenesis. Journal of the Geological Society of London, v. 135, p. 69-72.

Harper, E. S., 2011, Fluvial architecture of the lower Williams Fork Formation (middle Mesaverde Group), Douglas Creek Arch, Colorado: MS thesis, University of Colorado, Boulder, CO, 211 p.

Hettinger, R.D. and Kirschbaum, M.A., 2002, Stratigraphy of the Upper Cretaceous Mancos Shale (upper part) and Mesaverde Group in the southern part of the Uinta and Piceance Basins, Utah and Colorado. United State Geological Survey Geologic Investigation Series I-2674, p.21.

Hettinger, R. D., and Kirschbaum, M. A., 2003, Stratigraphy of the Upper Cretaceous Mancos Shale, upper part, and Mesaverde Group in the southern part of the Uinta and Piceance Basins, Utah and Colorado Petroleum Systems and Geologic Assessment of Oil and Gas in the Uinta-Piceance Province, Utah and Colorado. USGS Digital Data Series v. 69-B chapter 12, 25 p.

Hewlett, A. C., 2010, Fluvial architecture and static connectivity of the Williams Fork Formation, Central Mamm Creek Field, Piceance Basin, Colorado: MS thesis, University of Colorado, Boulder, CO, 228 p.

Hoak, T. E., and Klawitter, A. L., 1997, Prediction of fractured reservoir production trends and compartmentalization using an integrated analysis of basement structures in the Piceance Basin, western Colorado, *in* T. E. Hoak, A. L. Klawitter, and P. K. Blomquist, eds., Fractured reservoirs, characterization and modeling: Denver, Colorado, Rocky Mountain Association of Geologists, p. 67–102

Holmes, W. H., 1877, Report on the San Juan district, Colorado, *in* Hayden, F. V., Ninth annual report of the United States Geological and Geographical Survey of the Territories embracing Colorado and parts of adjacent territories, being a report of progress of the exploration for the year 1875, p. 237-276.

Hower, J., Eslinger, E., Hower, M.E., and Perry, E. A. 1976, Mechanism of burial metamorphism of argillaceous sediment; 1, Mineralogical and chemical evidence, Geological Society of America Bulletin, vol. 87, no. 5, p. 725-737.

Johnson, R. C., 1989, Geologic history and hydrocarbon potential of Late Cretaceous-age, low-permeability reservoirs, Piceance Basin, western Colorado. U.S. Geological Survey, Bulletin, v. 1787-E, 51 p.

Johnson, R.C., and Flores, R.M., 2003, History of the Piceance Basin from Latest Cretaceous Through Early Eocene and the Characterization of Lower Tertiary Sandstone Reservoirs, *in* Peterson, K.M., Olson, T.M., and Anderson, D.S., ed., Piceance Basin 2003 Guidebook, Rocky Mountain Association of Geologists, p. 21-61.

Johnson, R. C., and S. B. Roberts, 2003, The Mesaverde total petroleum system, Uinta-Piceance Province, Utah and Colorado; Petroleum systems and geologic assessment of oil and gas in the Uinta-Piceance Province, Utah and Colorado. US Geological Survey Digital Data Series DDS-69-B, 63 p.

Kameda, A., Dvorkin, J., Keehm, Y., Nur, A., and Bosl, W., 2006, Permeability-porosity transforms from small sandstone fragments. Geophysics, v. 71, p. N11-N19.

Keller, W. D., 1970, Environmental aspects of clay minerals, Journal of Sedimentary Petrology, v 40, p. 788-813.

Ketzer, J. M. and Morad, S., 2006, Predictive distribution of shallow marine, low-porosity (pseudomatrix-rich) sandstones in a sequence stratigraphic framework—example from the Ferron sandstone, Upper Cretaceous, USA. Marine and Petroleum Geology, v. 23, p. 29-36.

Ketzer, J. M., Morad, S., Evans, R., and Al-Aasm, I.S., 2002, Distribution of Diagenetic Alterations in Fluvial, Deltaic, and Shallow Marine Sandstones Within a Sequence Stratigraphic Framework: Evidence from the Mullaghmore Formation (Carboniferous), NW Ireland. Journal of Sedimentary Research, v. 72, p. 760-774.

Ketzer, J. M., Holz, M., Morad, S., and Al-Aasm, I. S., 2003a, Sequence stratigraphic distribution of diagenetic alterations in coal-bearing, paralic sandstones: evidence from the Rio Bonito Formation (early Permian), southern Brazil. Sedimentology, vol. 50, p. 855-877.

Ketzer, J.M., Morad , S., and Amorosi, A., 2003b, Predictive clay cementation in a sequence stratigraphy framework, *in* Worden, R.H., and Morad, S., eds., Clay Mineral Cements in Sandstones, International Association of Sedimentologists, Special Publication 34, p. 42-59.

Kirschbaum, M. A., and Hettinger, R. D., 2004, National assessment of oil and gas project: Facies analysis and sequence-stratigraphic framework of upper Campanian strata (Nelsen and Mount Garfield formations, Bluecastle Tongue of the Castlegate Sandstone, and Mancos Shale), eastern Book Cliffs. Colorado and Utah: US Geological Survey Digital Data Series DDS-69-G, version, 1, 40 p.

Kordi, M., Turner, B., and Salem, A. M. K., 2011, Linking diagenesis to sequence stratigraphy in fluvial and shallow marine sandstones: Evidence from the Cambrian–Ordovician lower sandstone unit in southwestern Sinai, Egypt. Marine and Petroleum Geology, vol. 28, p. 1554-1571.

Kogure, T. and J. F. Banfield, 1998, Direct identification of the six polytypes of chlorite characterized by semi-random stacking. American Mineralogist, v. 83, p. 925-930.

Kuuskraa, V. A., 2007, A Decade of Progress in Unconventional Gas, Advanced Resources International, Arlington, Va., July 6, 2007.

Laubach, S. E., Robert, L., Christopher, W. E. Ozkan, A., 2006, Fracture opening, burial diagenesis, and fracture sealing as linked processes controlling permeability in Upper Cretaceous Mesaverde Group sandstones, Piceance Basin, Colorado. Geological Society of America *Abstracts with Programs*, Vol. 38, No. 7, p. 26

Law, B. E., 2002, Basin-Centered Gas Systems, AAPG Bulletin, v. 86, p. 1891-1919.

Leibovitz, M. B., 2010, Sequence stratigraphy of the upper cretaceous upper Williams Fork Formation, Piceance Basin, northwest Colorado, and its contribution to the basin-centered gas accumulation: MS thesis, University of Colorado, Boulder, CO, 169 p.

Liu L. Y., Qu, Z. H., and Sun, W., 1998, Properties of clay mineral of clastic rock in Shanshan Oil Field, Xinjiang, Journal of Northwest University (Natural Science Edition), v. 131, p. 443-446.

Longstaffe, F. J., 1989, Stable isotopes as tracers in clastic diagenesis, *in* Hutcheon, I.E., eds., Burial Diagenesis, Mineralogical Association of Canada Short Course v. 15, p. 201-278.

Lonoy, A., Akselsen, J., and Ronning, K., 1986, Diagenesis of a deeply buried sandstone reservoir; Hild Field, northern North Sea. Clay Minerals, v. 21, p. 497-511.

Loomis, J.L., and Crossey, L.J., 1996, Diagenesis in a cyclic, regressive siliciclastic sequence: the Point Lookout Sandstone, San Juan Basin, Colorado, *in,* Crossey, L.J., Loucks, R.G., and Totten, M.W., ed., Siliciclastic Diagenesis and Fluid Flow: Concepts and Applications, SEPM Special Publication 55, p. 23-36.

Lorenz, J. C., 1983, Reservoir sedimentology of Mesaverde rocks at the Multiwall Experiment site and east central Piceance Creek Basin. Sandia National Laboratories, SAND87-0040, UC-92a, p. 38.

Lorenz, J. C., 1987, Reservoir sedimentology of Mesaverde rocks at the multiwell experiment site and East Central Piceance Creek Basin. Sandia National Laboratories, SAND87-0040, UC-92a, p. 38.

Lorenz, J. C., 1988, Geology, Chap. 3 in Multiwell Experiment final report—II, The paludal interval of the Mesaverde Formation. Sandia National Laboratories, Report SAND88-1008, UC-92, p. 501.

Lorenz, J. C., 1989, Reservoir sedimentology of rocks of the Mesaverde Group, Multiwell Experiment site and east-central Piceance Basin, Northwest Colorado; Geology of tight gas reservoirs in the Pinedale Anticline area, Wyoming, and at the Multiwell Experiment site, Colorado. U.S. Geological Survey Bulletin, vol. B 1886, p. K1-K24.

Lorenz, J. C., 1990, Geology, Chap. 3 in Multiwell Experiment final report part IV, The fluvial interval of the Mesaverde Formation. Sandia National Laboratories, Report SAND89-2612/A, UC-132, p. 448.

Lorenz, J. C. and Finley, S. J., 1989, Differences in fracture characteristics and related production; Mesaverde Formation, northwestern Colorado, SPE Formation Evaluation, v. 4, p. 11-16.

Lorenz, J. C., and Hill, R.E., 1994, Subsurface fracture spacing: comparison of inferences from slant/horizontal core and vertical core in Mesaverde reservoirs. SPE Formation Evaluation v.9, p. 66-72.

Lorenz, J. C., Heinz, D. M., Clark, J. A., and Searls, C. A., 1985, Determination of widths of meander-belt sandstone reservoirs from vertical downhole data, Mesaverde Group, Piceance Creek Basin, Colorado. AAPG Bulletin, v. 69, p. 710–721.

Lundegard, P. D., 1989, Temporal reconstruction of sandstone diagenetic histories, *in* Hutcheon, I.E., eds., Burial Diagenesis. Mineralogical Association of Canada Short Course v. 15, p. 161-200.

Lundegard, P. D., 1992, Sandstone porosity loss; a "big picture" view of the importance of compaction, Journal of Sedimentary Petrology, v. 62, p. 250-260.

Malley, P., Jourdan, A., and Weber, F., 1986, Etudes des inclusions fluides dans les nourrissages siliceux des gres reservoir de Mer du Nord: une nouvelle lecture possible de l'histoire diagenetique du Brent de la region d'Alwyn. Academie des Sciences (Paris), Comptes Rendus, Serie II, v. 302, p. 653-658.

Mansurbeg, H., Morad, S. Salem, A., Marfil, R., El-ghali, M. A. K., Nystuen, J. P., Caja, M. A., Amorosi, A., Garcia, D. and La Iglesia, A., 2008, Diagenesis and reservoir quality evolution of Palaeocene deep-water, marine sandstones, the Shetland-Faroes Basin, British continental shelf. Marine and Petroleum Geology, v. 25, p. 514-543.

Mansurbeg, H., Caja, M. A., Marfil, R., Morad, S., Remacha, E., Garcia, D., Martín-Crespo, T., El-Ghali, M. A. K., and Nystuen, J. P., 2009, Diagenetic evolution and porosity destruction of turbiditic hybrid arenites and siliciclastic sandstones of foreland basins: Evidence from the Eocene Hecho Group, Pyrenees, Spain. Journal of Sedimentary Research, v. 79, p. 711-735.

Marco, A., Moraes, S., and de Ros, L. F., 1990, Infiltrated clays in fluvial Jurassic sandstones of Reconcavo Basin, northeastern Brazil. Journal of Sedimentary Petrology, v. 60, p. 809-819.

Matlack, K. S., Houseknecht, D. W., and Applin, K. R., 1989, Emplacement of clay into sand by infiltration. Journal of Sedimentary Research, v. 59, p. 77-87.

McKay, J. L., Longstaffe, F. J., and Plint, A. G, 1995, Early diagenesis and its relationship to depositional environment and relative sea-level fluctuations (Upper Cretaceous Marshybank Formation, Alberta and British Columbia). Sedimentology, v. 42, p. 161-190.

Moore, D. M. and Reynolds, R. C., Jr., 1997, X-ray diffraction and the identification and analysis of clay minerals. Oxford University Press, Oxford, United Kingdom, 322 p.

Morad, S., 1988, Albitized microcline grains of post-depositional and probable detrital origins in Brottum Formation sandstones (upper Proterozoic), Sparagmite region of Southern Norway. Geological Magazine, v. 125, p. 229–239.

Morad, S., Ben Ismail, H., De Ros, L.F., Al-Aasm, I.S., and Serrhini, N.E., 1994, Diagenesis and formation water chemistry of Triassic reservoir sandstones from southern Tunisia. Sedimentology, vol. 41, p. 1253–1272.

Morad, S., Ketzer, J. M., and De Ros, L. F., 2000, Spatial and temporal distribution of diagenetic alterations in siliciclastic rocks: implications for mass transfer in sedimentary basins. Sedimentology, v. 47, p. 95-120.

Morad, S., Al-Ramadan, K., Ketzer, J. M., and de Ros, L. F., 2010, The impact of diagenesis on the heterogeneity of sandstone reservoirs; a review of the role of depositional facies and sequence stratigraphy; Advances in sandstone reservoir quality prediction. AAPG Bulletin, v. 94, p. 1267-1309.

Moraes, M. A., and De Ros, L. F., 1992, Depositional, infiltrated and authigenic clays in fluvial sandstones of the Jurassic Sergi Formation, Recôncavo Basin, northeastern Brazil. *in,* D. W. Houseknecht and E.D. Pittman, eds., Origin, Diagenesis, and Petrophysics of Clay Minerals in Sandstones. SEPM Special Publication 47, p. 197-208.

Moss, S. J. and Tucker, M. E., 1996, Dolomitization associated with transgressive surfaces; a Mid-Cretaceous example. Sedimentary Geology, v. 107, p. 11-20.

Nadeau, P. H., 1998, An experimental study of the effects of diagenetic clay minerals on reservoir sands. Clays and Clay Minerals, v. 46, p. 18-26.

Odin, G. S., 1990, Clay mineral formation at the continent-ocean boundary; the verdine facies, Clay Minerals, v. 25, p. 477-483.

Ozkan, A., 2010, Structural diagenetic attributes of Williams Fork sandstones with implications for petrophysical interpretation and fracture prediction, Piceance Basin, Colorado, PhD thesis, University of Texas at Austin, Austin, Texas.

Ozkan, A., Cumella, S.P., Milliken, K.L., and Laubach, S.E., 2011, Prediction of lithofacies and reservoir quality using well logs, Late Cretaceous Williams Fork Formation, Mamm Creek field, Piceance Basin, Colorado. AAPG Bulletin, v. 95, p. 1699-1723.

Patterson, P. E., Kronmueller, K., and Davies, T. D., 2003, Sequence stratigraphy of the Mesaverde Group and Ohio Creek conglomerate, northern Piceance Basin, Colorado, *in* K. M. Peterson, T. M. Olson, and D. S. Anderson, eds., Piceance Basin 2003 Guidebook: Denver, Colorado, Rocky Mountain Association of Geologists, p. 115–129.

Payne, D. F., K. Tuncay, A. Park, J. B. Comer, and P. Ortoleva, 2000, A Reaction-transport-mechanical approach to modeling the interrelationships among gas generation, over pressuring, and fracturing: Implications for the Upper Cretaceous natural gas reservoirs of the Piceance Basin, Colorado. AAPG Bulletin, v. 84, p. 545-565.

Peng, J., Liu, L., Wang, Y., Liu, J., 2009, Origin and controlling factors of chlorite coatings—an example from the reservoir of T3x Group of the Baojie area, Sichuan Basin, China, Petroleum Science, v. 6p. 376-382.

Pe-Piper, G. and Weir-Murphy, S., 2008, Early diagenesis of inner-shelf phosphorite and iron-silicate minerals, Lower Cretaceous of the Orpheus

Graben, southeastern Canada: implications for the origin of chlorite rims. AAPG Bulletin, v. 92, p. 1153-1168.

Pettijohn, F. J., Potter, P. E., and Siever, R., 1987, Sand and Sandstone. Springer-Verlag, New York, NY, United States, 553 p.

Pitman, J. K., Spencer, C. W., and Pollastro, R. M., 1989, Petrography, mineralogy, and reservoir characteristics of the Upper Cretaceous Mesaverde Group in the east-central Piceance Basin, Colorado, U.S. Geological Survey Bulletin, vol. B 1787-G, p. G1-G31.

Pittman, E. D., Larese, R. E., and Heald, M. T., 1992, Clay coats; occurrence and relevance to preservation of porosity in sandstones; Origin, diagenesis, and petrophysics of clay minerals in sandstones, *in,* D. W. Houseknecht and E.D. Pittman, eds., Origin, Diagenesis, and Petrophysics of Clay Minerals in Sandstones. SEPM Special Publication 47, p. 241-255.

Posamentier, H. W., and Allen, G.P., 1999. Siliciclastic Sequence Stratigraphy - Concepts and Applications. SEPM Concepts in Sedimentology and Paleontology Series, no. 7, SEPM (Society for Sedimentary Geology), Tulsa, OK, 210 p.

Pranter, M. J. and Sommer, N. K., 2011, Static connectivity of fluvial sandstones in a lower coastal-plain setting: An example from the Upper Cretaceous lower Williams Fork Formation, Piceance Basin, Colorado. AAPG Bulletin, v. 95, p. 899-923.

Pranter, M. J., Ellison, A. I., Cole, R. D., and Patterson, P. E., 2007, Analysis and modeling of intermediate-scale reservoir heterogeneity based on a fluvial point-bar outcrop analog, Williams Fork Formation, Piceance Basin, Colorado. AAPG Bulletin, v. 91, p. 1025-1051.

Pranter, M.J., Vargas, M.F., and Davis, T.L., 2008, Characterization and 3-D reservoir modeling of fluvial sandstones of the Williams Fork Formation, Rulison field, Piceance Basin, Colorado, U.S.A: Journal of Geophysics and Engineering, v. 5, p. 158-172.

Pranter, M. J., Cole, R. D., Panjaitan, H., and Sommer, N. K., 2009, Sandstone-body dimensions in a lower coastal-plain depositional setting: Lower Williams Fork Formation, Coal Canyon, Piceance Basin, Colorado. AAPG Bulletin, v. 93, p. 1379-1401.

Read, J. F. and A. D. Horbury, 1993, Eustatic and tectonic controls on porosity evolution beneath sequence-bounding unconformities and parasequence disconformities on carbonate platforms, *in* Horbury, A.D., and Robinson, A.G., eds., Diagenesis and Basin Development: AAPG Studies in Geology #36, p. 155-197.

Ryer, T.A., and McPhillips, M., 1983, Early Late Cretaceous Paleogeography of East-Central Utah, *in*, Reynolds, M.W., and Dolly, E.D., eds., Mesozoic Paleogeography of the West-Central United States. SEPM, Rocky Mountain Section, Rocky Mountain Paleogeography Symposium 2, p. 253-272

Saigal, G. C., Morad. S., Bjørlykke, K., Egeberg, P.K., and Aagaard, 1988, Diagenetic albitization of detrital K-feldspars in Jurassic, Lower Cretaceous and Tertiary elastic reservoir rocks from offshore Norway. I. Textures and origin. Journal of Sedimentary Petrology, v. 58, p. 1003-1013.

Salem, A. M., Morad, S., Mato, L. F., and Al-Aasm, I. S., 2000, Diagenesis and reservoir-quality evolution of fluvial sandstones during progressive burial and uplift: evidence from the Upper Jurassic Boipeba Member, Recôncavo Basin, Northeastern Brazil. AAPG Bulletin, v. 84, p. 1015-1040.

Schmidt, V. and McDonald, D.A, 1979, The role of secondary porosity in the course of sandstone diagenesis, *in,* Scholl P. A. and Schluger P. R, eds., Aspects of Diagenesis, SEPM Special Publication 29, p. 175–207.

Seemann, U., 1979, Diagenetically formed interstitial clay minerals as a factor in Rotliegend Sandstone reservoir quality in the North Sea. Journal of Petroleum Geology, v. 1, p. 55-62.

Shaak, R. V., 2010, Stratigraphic architecture of shallow-marine to coastal- plain parasequences: Lower Williams Fork Formation, southeastern Piceance Basin, Colorado. MS thesis, University of Colorado, Boulder, CO, 176 p.

Shammari, S., Franks, S., and Soliman, O.M., 2011, Depositional and facies controls on infiltrated/inherited clay coatings: Unayzah sandstones, Saudi Arabia. GeoArabia, v. 16, p. 211.

Shanley, K. W. and McCabe, P. J., 1994, Perspectives on the sequence stratigraphy of continental strata. AAPG Bulletin, v. 78, p. 544-568.

Shanley, K. W., Cluff, R. M., and Robinson, J. W., 2004, Factors controlling prolific gas production from low-permeability sandstone reservoirs: Implications for resource assessment, prospect development, and risk analysis. AAPG Bulletin, v. 88, p. 1083-1121.

Siever, R., 1962, Silica solubility, O degrees -200 degrees C and the diagenesis of siliceous sediments, Journal of Geology, v. 70, p. 127-150.

Soeder, D. J. and P. Chowdiah, 1990, Pore geometry in high- and low-permeability sandstones, Travis Peak Formation, East Texas. SPE Formation Evaluation, v. 5, p. 421-430.

Soeder, D. J. and Randolph, P. L., 1987, Porosity, permeability, and pore structure of the tight Mesaverde Sandstone, Piceance Basin, Colorado. SPE Formation Evaluation, v. 2, p. 129-136.

Sommer, F., 1978, Diagenesis of Jurassic sandstones in the Viking Graben; Sandstone diagenesis, Journal of the Geological Society of London, vol. 135, p. 63-67.

Spencer, C. W., 1989, Review of characteristics of low-permeability gas reservoirs in Western United States, AAPG Bulletin, v. 73, p. 613-629.

Spoetl, C., Houseknecht, D. W., and Longstaffe, F. J., 1994, Authigenic chlorites in sandstones as indicators of high-temperature diagenesis, Arkoma foreland basin, USA. Journal of Sedimentary Research, v. 64, p. 553-566.

Stonecipher, S. A., 2000, Applied Sandstone Diagenesis - Practical Petrographic Solutions for a Variety of Common Exploration, Development and Production Problems. SEPM, Short Course Notes No. 50, 143 p.

Stonecipher, S.A., Winn, Jr., R.D. and Bishop, M.G., 1984, Diagenesis of the Frontier Formation, Moxa Arch: a function of sandstone geometry, texture and composition, and fluid flux, *in* D.A. McDonald and R.C. Surdam, eds., Clastic Diagenesis: AAPG Memoir 37, 289-316.

Taylor, K. G., Gawthorpe, R. L., and Van Wagoner, J. C., 1995, Stratigraphic control on laterally persistent cementation, Book Cliffs, Utah. Journal of the Geological Society of London, v. 152, p. 225-228.

Taylor, K.G., Gawthorpe, R.L., Curtis, C.D., Marshall, J.D., and Awwiller, D.N., 2000, Carbonate cementation in a sequence-stratigraphic framework: Upper Cretaceous sandstones, Book Cliffs, Utah-Colorado. Journal of Sedimentary Research, v. 70, p. 360 - 372.

Taylor, T. R., Giles, M. R., Hathon, L. A., Diggs, T. N., Braunsdorf, N. R., Birbiglia, G. V., Kittridge, M. G., Macaulay, C. I., and Espejo, I. S., 2010, Sandstone diagenesis and reservoir quality prediction; models, myths, and reality. AAPG Bulletin, v. 94, p. 1093-1132.

Tiab, D., and Donaldson, E.C., 2011, Petrophysics: Theory and Practice of Measuring Reservoir Rock and Fluid Transport Properties. Gulf Professional Publishing, 955 p.

Tucker, M. E., 1993, Carbonate sequence stratigraphy, diagenesis, and porosity prediction. AAPG Bulletin, v. 77, p. 1670.

Tucker, M., 1988, Techniques in sedimentology, Oxford [Oxfordshire] ; Boston :, Blackwell Scientific Publications.

Tyler, R. and McMurry, R. G., 1995, Genetic stratigraphy, coal occurrence, and regional cross section of the Williams Fork Formation, Mesaverde Group, Piceance Basin, northwestern Colorado. Colorado Geological Survey, Open File Report 95-2, 42 p., 42 p.

Verbeek, E.R., and Grout, M.A., 1984, Fracture studies in Cretaceous and Paleocene strata in and around the Piceance basin, Colorado; preliminary results and their bearing on a fracture-controlled natural-gas reservoir at the MWX site. U.S. Geological Survey Open-File, vol. Report 84-156.

Walker, R.G., 1992, Facies, facies models and modern stratigraphic concepts, *in*, Walker, R.G., and James, N.P., eds., Facies Models Response to Sea Level Change. Geological Association of Canada, p, 1-14.

Walker, T. R., 1976, Diagenetic origin of continental red beds, *in* Falke, H., ed., The Continental Permian in Central, West and South Europe: proceedings of the NATO Advanced Study Institute held at the Johannes Gutenberg University, Mainz, FRG, 23 September-4 October, 1975, D. Reidel Publishing Co., Dordrecht, Holland, p. 240-282.

Wardlaw, N. C. and Cassan, J. P., 1979, Oil recovery efficiency and the rock-pore properties of some sandstone reservoirs. Bulletin of Canadian Petroleum Geology, v. 27, p. 117-138.

Wardlaw, N. C. and Taylor, R. P., 1976, Mercury capillary pressure curves and the interpretation of pore structure and capillary behavior in reservoir rocks. Bulletin of Canadian Petroleum Geology, v. 24, p. 225-262.

Weber, K. J., 1982, Influence of common sedimentary structures on fluid flow in reservoir models, Journal of Petroleum Technology, v. 34, p. 665-672.

Wilson, M. D., 1994, Non-compositional controls on diagenetic processes , *in* M. D. Wilson, A. P. Byrnes, S. Bloch, P. T. Stanton, J. R. Wood, and J. H. McGowen, eds., Reservoir Quality Assessment and Prediction in Clastic Rocks. SEPM Short Course Notes 30, p. 161–182.

Wilson, M. D. and Pittman, E. D., 1977, Authigenic clays in sandstones; recognition and influence on reservoir properties and paleoenvironmental analysis. Journal of Sedimentary Petrology, v. 47, p. 3-31.

Worden, R. H. and Burley, S. D., 2009, Sandstone Diagenesis: The Evolution of Sand to Stone, *in* S. D. Burley and R. H. Worden, eds., Sandstone Diagenesis: Recent and Ancient, Blackwell Publishing Ltd., Oxford, UK, p. 1-44.

Wright, V. P. and Marriott, S. B., 1993, The sequence stratigraphy of fluvial depositional systems: the role of floodplain sediment storage. Sedimentary Geology, v. 86, p. 203-210.

Yurewicz, D. A., Bohacs, K. M., Yeakel, J. D., and Kronmueller, K., 2003, Source rock analysis and hydrocarbon generation, Mesaverde Group and Mancos Shale, northern Piceance Basin, Colorado, *in* Peterson, K. M., Olson, T. M., and Anderson, D. S., eds., Piceance Basin 2003 Guidebook: Rocky Mountain Association of Geologists, p. 130-153.

Yurewicz, D.A., Bohacs, K.M., Kendall, J., Klimentidis, R.E., Kronmueller, K., Meurer, M.E., Ryan, T.C., and Yeakel, J.D., 2008, Controls on gas and water distribution, Mesaverde basin-centered gas play, Piceance Basin, Colorado, *in* S.P. Cumella, K.W. Shanley, and W.K. Camp, eds., Understanding, exploring, and developing tight-gas sands. AAPG Hedberg Series, no. 3, p. 105 – 136.

Zuffa, G. G., Cibin, U., and Di Giulio, A., 1995, Arenite petrography in sequence stratigraphy. Journal of Geology, v. 103, p. 451-459.

Appendix A – Thin Section Point Count Data

Four hundreds point per thin section were counted and the resultant data compiled into the tables presented in this appendix. Point count categories included grain type (e.g., quartz, feldspar, chert, volcanic rock fragment, carbonate rock fragment, etc.), detrital clay, authigenic clay, pore type (e.g., intergranular, intragranular, moldic, microfracture), cement types (e.g., quartz, calcite), and replacement phases (carbonates, feldspars). Data are presented by footage within each well.

Most of the thin sections were donated by various companies and only half the slides were at best stained for feldspars and carbonates. Cover slips on those slides were permanent and could not be removed, thus restaining those sections was not possible. In such cases, only the stained half of the slide was point counted.

Well	Depth (ft.)	Systems Tract	Williams Fork Interval	Core-plug porosity (%)	Core permeability (mD)	Total Point Count Percentage (based on values in blue columns)	Quartz, monocrystalline (%)	Quartz, polycrystalline (%)	Total Quartz (%)	K-Feldspar (%)	Plagioclase (%)	Total Feldspar (%)	Total lithic (%)	Argillaceous lithic (%)	Non-Argillaceous Sedimentary Lithics (%)	Total Sedimentary Lithics (Argillaceous + Non-argillaceous) (%)	Volcanic Rock Fragment (%)	Metamorphic Rock Fragment (%)
PA 424-34	4570	TST	upper	5.9	0.011	100.6	46.3	1.5	47.8	6.8	5.8	12.6	11.7	0.2	10.3	10.5	1.2	
PA 424-34	4571	TST	upper	6.3	0.036	100.1	50.8	1.8	52.6	6.8	8.3	15.1	5.9	0.4	5.5	5.9	0	
PA 424-34	4575	TST	upper	6.5	0.051	100.2	44.5	1.5	46	10	9	19	10.5	0.5	8	8.5	2	
PA 424-34	4580	TST	upper	5.3	0.021	100.4	46.8	1.3	48.1	8.8	7	15.8	13.1	4.3	7.4	11.7	1.4	
PA 424-34	4586	TST	upper	6	0.054	100.7	52.5	2.5	55		13.8	13.8	6.3	0.3	5	5.3	1	
PA 424-34	4595	TST	upper	6.1	0.023	100.7	35	0.5	35.5	10.5	7.8	18.3	22.8	13.5	7.3	20.8	2	
PA 424-34	4600	TST	upper	11.7	0.03	100.3	25.8	1	26.8	7.5	14.5	22	18.1	2.8	11	13.8	4	0.3
PA 424-34	4606	TST	upper	12.6	0.059	100.4	21	1.3	22.3	8.3	20	28.3	16.8	4	9.2	13.2	3.6	
PA 424-34	4625	TST	upper	7	0.02	100.6	32.5	0.3	32.8	6.8	25	31.8	10.8	2.3	6.5	8.8	2	
PA 424-34	4631	TST	upper	4.6	0.011	100.4	26.1		26.1	7.3	4.5	11.8	10.3	2	5.3	7.3	3	
PA 424-34	4644	TST	upper	7.8	0.018	100.1	31.5	1	32.5	8.3	16	24.3	11.6	4.3	5.8	10.1	1.5	
PA 424-34	4651	TST	upper	8.1	0.086	100.6	40.5	4	44.5	8.3	4.3	12.6	15.8	0.8	12	12.8	2.2	0.8
PA 424-34	4655	TST	upper	6.9	0.056	100.1	41	2.8	43.8	5.8	8.5	14.3	11.3	0.8	7.5	8.3	3	
PA 424-34	4663	TST	upper	8.1	0.149	100.3	40.3	1.8	42.1	5.3	12	17.3	12.8	1.3	7.5	8.8	4	
PA 424-34	4675	TST	upper	8.1	0.059	100.3	31	0.5	31.5	5.3	10	15.3	19.8	1	15.5	16.5	2.5	0.8
PA 424-34	4679	TST	upper	5.4	0.014	100.0	40	0.3	40.3	5.8	2.8	8.6	16.5	0.5	13	13.5	3	
PA 424-34	4685	TST	upper	7.3	0.018	100.0	35.8	0.3	36.1	4.3	7.8	12.1	25.8	0.3	22.8	23.1	2.7	
PA 424-34	4691	TST	upper	12.9	0.084	100.4	26.8	2.8	29.6	8.8	10.8	19.6	12.8	0.5	11.3	11.8	1	
PA 424-34	4694	TST	upper	8.7	0.035	100.5	29.3	2.3	31.6	8.3	10.5	18.8	13.4	1.1	10.5	11.6	1.8	
PA 424-34	4700	TST	upper	5.5	0.045	100.0	28.5	1	29.5	6.3	11	17.3	22.6	0.8	19.1	19.9	2.2	0.5
PA 424-34	4706	TST	upper	9.6	0.037	100.0	42.8	2	44.8	6.8	10	16.8	11.5	0.2	10.3	10.5	1	
PA 424-34	4714	TST	upper	6.3	0.041	100.7	27.3	1.5	28.8	12.3	7.8	20.1	19.7	0.4	16.3	16.7	3	
PA 424-34	4727	TST	upper	10.9	0.067	100.3	29.3	3	32.3	8.5	9.8	18.3	17	0.5	14.4	14.9	2.1	
PA 424-34	4729	TST	upper	5.8	0.011	100.7	29.8		29.8	6	5.5	11.5	25.5		22.2	22.2	3.3	
PA 424-34	4732	TST	upper	8.8	0.087	100.2	33	2.3	35.3	10.3	14	24.3	19.8		17.8	17.8	2	
PA 424-34	5108	LST	middle	4.4	0.027	100.2	25.5		25.5		0.8	0.8	15		15	15		
PA 424-34	5114	LST	middle	3.5	0.0054	100.0	40.3	0.8	41.1		1.3	1.3	14.3	0.5	11	11.5	2.8	
PA 424-34	5121	LST	middle	7.5	0.053	100.1	43	1.5	44.5		10.8	10.8	14.5	1.5	12	13.5	1	
PA 424-34	5124	LST	middle	4	0.018	100.5	33.3		33.3	1.5	7	8.5	14.8		12.1	12.1	2.7	
PA 424-34	5136	LST	middle	8.4	0.053	100.4	40.8	2.5	43.3		10.8	10.8	11.8		9.9	9.9	1.9	
PA 424-34	5141	LST	middle	11	0.141	100.4	42.5	4	46.5	0.3	10.5	10.8	14.3		13.7	13.7	0.6	
PA 424-34	5142	LST	middle	9.2	0.072	100.7	36	4.8	40.8	3	8.8	11.8	16.8		15.5	15.5	1.3	
PA 424-34	5161	LST	middle	5.2	0.0034	100.6	40.5		41	1	1.5	2.5	15.3		15.3	15.3	0	
PA 424-34	5174	LST	middle	5.7	0.012	100.8	48.5	0.3	48.8	1.3	5.7	7	16.4		16	16	0.4	
PA 424-34	5184	LST	middle	6.1	0.021	100.0	35.3	2.5	37.8	4	7	11	17.6		15.8	15.8	1.8	
PA 424-34	5195	LST	middle	7.9	0.034	100.1	45	1.3	46.3	2.3	8	10.3	16.5		14.5	14.5	2	
PA 424-34	6078	HST	lower	6	0.011	100.7	41.3		41.3		1	1	16.5		13.5	13.5	3	
PA 424-34	6082	HST	lower	6	0.013	100.8	40	0.3	40.3		2.8	2.8	30.3		29.5	29.5	0.8	
PA 424-34	6088	HST	lower	8.1	0.024	100.0	41.8	0.3	42.1		2.5	2.5	24.3		22.3	22.3	2	
PA 424-34	6091	HST	lower	8.3	0.018	100.2	45.3	0.8	46.1		3.8	3.8	20		19.4	19.4	0	0.6
PA 424-34	6132	HST	lower	8.1	0.017	100.4	35.3		35.3		0.5	0.5	18.3		18	18	0.3	
PA 424-34	6138	HST	lower	10.3	0.036	100.4	36.3	0.3	36.6		7.3	7.3	20	1	16	17	3	
PA 424-34	6155	HST	lower	7.9	0.013	100.0	41.8		41.8		1.8	1.8	9.5		9.5	9.5	0	
PA 424-34	6582	HST	lower	5.2	0.0029	100.1	34.5		34.5		0.3	0.3	18.8		17.1	17.1	1.7	
PA 424-34	6589	HST	lower	6.1	0.0076	100.7	37.5		37.5		1	1	22.5		21.4	21.4	1.1	
PA 424-34	6595	HST	lower	5.7	0.018	100.0	36		36			0	20.8		20	20	0.8	
PA 424-34	6600	HST	lower	8.2	0.018	100.0	32.8		32.8		5.8	5.8	23.5		23.5	23.5	0	
PA 424-34	6639	HST	lower	9.3	0.025	100.2	38		38		6	6	17		16	16	1	
PA 424-34	6643	HST	lower	10.8	0.031	100.2	37.5		37.5		2.3	2.3	17.3	2	14	16	1.3	
PA 424-34	6648	HST	lower	8.4	0.018	100.8	30.5		30.5		3.8	3.8	10.3		10.3	10.3	0	
Cascade Creek	4704		upper	5.56	0.006	100.2	49	1.3	50.3	0.3	0.3	0.6	14.4		13	13	1.4	
Cascade Creek	4752		upper			100.0	21.5		21.5	4.8	0.8	5.6	15		13	13	2	
Cascade Creek	4761		upper			100.1	36.8	2.5	39.3	8	0.8	8.8	23.6		18.3	18.3	5.3	
Cascade Creek	4772		upper			100.0	34.3	1.3	35.6	8.3	2.5	10.8	27.6		19	19	7.8	0.8
Cascade Creek	4786		upper			100.0	38.3	2	40.3	3.8	8.5	12.3	24.4	1.4	14	15.4	9	
Cascade Creek	4809		upper	6.43	0.012	100.2	24.8	1	25.8	7.8	7.8	15.6	25.8	1.3	12	13.3	12.5	
Cascade Creek	4819		upper	8.25	0.044	100.3	36.8	2	38.8	6.3	13	19.3	15.3		13.3	13.3	2	
Cascade Creek	4834		upper	10.19	0.016	100.0	28	0.5	28.5	9.8	10.3	20.1	24.8		23	23	1.2	0.6
Cascade Creek	5182		middle			100.2	41.5	2.3	43.8		3.3	3.3	12.8		4	4	8.8	
Cascade Creek	5194		middle	6.05	0.016	100.4	31.3	1	32.3		3.8	3.8	14.1	1.3	6.3	7.6	6.5	
Cascade Creek	5201		middle			100.0	29		29		3.8	3.8	17	3.5	6.5	10	7	
Cascade Creek	5298		middle	9.04	0.02	100.0	36.8	1.5	38.3		3.8	3.8	16.3	4.3	11.1	15.4	0.9	
Cascade Creek	5308		middle	9.14	0.042	100.1	38.5	3	41.5		6.8	6.8	20.3	2.8	8.8	11.6	8.7	
Cascade Creek	5318		middle	9.87	0.075	100.0	36.8	2	38.8		4.8	4.8	20.1	1.5	11.5	13	6.8	0.3
Cascade Creek	5331		middle	8.42	0.068	100.3	45	1.5	46.5		3	3	22	2	15	17	5	
Cascade Creek	6112		lower	9.63	0.019	100.8	28.3	0.8	29.1		2.8	2.8	18.3	0.3	17.3	17.6	0.7	
Cascade Creek	6117		lower	10.46	0.024	100.7	27.5	3.5	31		4.5	4.5	34.7	4	23	27	7.7	
Cascade Creek	6213		lower	11.66	0.032	100.2	28	1.5	29.5		2	2	19.5	2.5	14.5	17	2.5	
Cascade Creek	6217		lower	10.84	0.019	100.1	20	0.8	20.8		3	3	17.5	7	9.5	16.5	1	
Cascade Creek	6220		lower	10.95	0.02	100.5	28.5	0.8	29.3		3	3	36.5	9.5	21.5	31	5.5	
Cascade Creek	6294		lower	7.28	0.098	100.2	20.5	0.5	21		1.5	1.5	41	9.5	27.5	37	4	
Cascade Creek	63041		lower	6.88	0.031	100.4	30.8	0.8	31.6		5	5	33.1	9.3	21.8	31.1	2	
Last Dance	2813.10	LST	upper	8.6938	.081	100.2	32.5		32.5	6.7	3	9.7	28	2		9	17	0
Last Dance	2835.00	LST	upper	7.3936	.053	100.8	30	0.3	30.3	9	4.8	13.8	37.6	3		28	9	0.6
Last Dance	2846.00	LST	upper	5.4554	.017	100.4	45		45	8	4	12	32	2		23	8	1
Last Dance	2856.00	LST	upper	7.8510	.062	100.3	29.2	0.8	30	7.8	6.3	14.1	28			13.4	14	0.6
Last Dance	3553.30	HST	lower	9.38	0.314	100.3	28		28	18	11	29	32			24	8	0
Last Dance	3563.00	HST	lower	6.71	0.011	100.0	32		32	8	11	19	29	1.9		25	4	0
Last Dance	3568.00	HST	lower	5.93	0.003	100.1	44		44	9	9	18	19.4	2		11	8	0
Last Dance	3573.10	HST	lower	6.58	0.168	100.0	42		42	7	12	19	20			9	11	0
Last Dance	3596.90	HST	lower	4.89	0.005	100.7	31.8		31.8	15	10.3	25.3	23			17	5.2	0.8
Last Dance	3994.00	HST	lower	7.69	0.022	100.5	38		38	5	8	13	33.6			22	11	0.6
Last Dance	4005.90	HST	middle	10.58	0.081	100.0	44.8	1.2	46	4.3	6.3	10.6	32			17	14	1
Last Dance	4017.90	HST	middle	2.99	0.006	100.2	41.6		41.6	4	9.6	13.6	23.5			9	14	0.5
Last Dance	4382.00	LST	middle	4.33	0.005	100.0	54		54	8.6	7	15.6	21			17	2	0
Last Dance	4389.00	TST	middle	11.03	0.071	100.6	46		46	6	10.3	16.3	28			26	2	0
Last Dance	4855.00	LST	lower	3.48	0.005	100.6	41		41	0	1.6	1.6	36			29	7	0
Last Dance	5717.00	LST	lower	6.12	0.008	100.0	58		58	2	4	6	22			21	1	0
Last Dance	5734.20	LST	lower	6.14	0.006	100.0	50.3		50.3		6	6	27			26	1	0
Last Dance	5760.30	LST	lower	6.31	0.006	100.3	43		43	3	6	9	28	3		26	2	0
Last Dance	6040.10	HST	lower	7.06	0.009	100.8	51.1	0.5	51.6	0.6	5	5.6	34			26	7.2	0.8
Last Dance	6054.10	HST	lower	7.01	0.006	100.1	44		44		1	1	37	2.2		16	20	1
Last Dance	6339.60	HST	lower	3.14	0.007	100.0	38		38		1.8	1.8	23			21	2	0
Last Dance	6342.00	HST	lower	4.19	0.035	100.8	42.2	1.8	44		2	2	32			30	2	0
MWX-1	4191.9	HST	upper	3.2	0.01	100.4	48		48	0	9	9	14	0.3	8	8.3	3	
MWX-1	4193.4	HST	upper	2.5	0.01	100.2	61.8	1.2	63	1	4	5	10	4	5	9	1	
MWX-1	4195.6	HST	upper	1.7	0.01	100.4	46.1	0.9	47	0	1	1	9	2	7	9		
MWX-1	4231.3	LST	upper	4.7	0.08	100.6	50		50	1	5	6	27	8	13	21	6	
MWX-1	4234.3	LST	upper	2.5	0.01	100.0	41		41	0	3	3	18	3	12	15	3	
MWX-1	4253.8	LST	upper	5.6	0.21	100.4	56		56	0	0.01	0.01	20	3	15.1	18.1	1.9	
MWX-1	4303.9	LST	upper	2.8	0.05	100.6	46		46	4	2	6	27	8	13	21	6	
MWX-1	4311.2	LST	upper	7	0.1	100.6	41		41	2	4	6	26	3	14	17	8	1
MWX-1	4314.2	LST	upper	6	0.15	100.1	55	1	56	2	5	7	16	2	13	15	1	
MWX-1	4322.2	LST	upper	3	0.04	100.4	42		42	3	2	5	22	8	12	20	2	
MWX-1	4324.2	LST	upper	6.7	0.31	100.5	57		57	3	4	7	20	4	15	19	1	
MWX-1	4328.1	LST	upper		0	100.3	45		45	5	4	9	20	7.3	8	15.3	4	0.7
MWX-1	4329	LST	upper	7.5	1	100.4	49		49	2	0.01	2.01	28	7	19	26	2	
MWX-1	4331.2	LST	upper	9.5	0.55	100.7	48		48	3	3	6	20	5	10	15	5	
MWX-1	4344	LST	upper	7.8	0.78	100.7	42		42.0	0	4	4	22	0	22	22	0	
MWX-1	4351.3	LST	upper	1.5	0.01	100.6	27		27	3	3	6	29	6	22.6	28.6	0.4	
MWX-1	4359.5	LST	upper	5.3	16	100.1	54.8	1.2	56	2	4	6	20	3	14	17	3	
MWX-1	4389.2	LST	upper	3.4	0.01	100.0	34		34	0	6	6	24	6	14	20	2	2
MWX-1	4396.2	LST	upper	4	0.02	100.4	39		39	1	6	7	22	1	19.1	20.1	1.9	
MWX-1	4490.4	LST	upper	4.8	0.01	100.3	39		39	3	6	9	15	1	11	12	3	
MWX-1	4520.2	LST	upper	4.1	0.01	100.0	44		44	5	7	12	12	3	8.1	11.1	0.9	
MWX-1	4537.8	LST	upper	5.6	0.46	100.9	44		44	2	2	4	25	1	23	24	1	
MWX-1	4550.5	LST	upper	6.2	0.12	100.0	51.8	1.2	53	4	4	8	21	6	11	17	4	
MWX-1	4557.8	LST	upper	7	0.02	100.7	48		48	4	5	9	25	0.8	21	21.8	2	1.2
MWX-1	4561.8	LST	upper	6.7	0.7	100.8	49		49	4	6	10	25	3	18	21	4	
MWX-1	4575.2	LST	upper	7	0.03	100.2	58		58	4	7	11	14	1	13	14	0	
MWX-1	4639.6	HST	upper	4.5	0.14	100.0	59		59	9	6	15	8	1	7	8		
MWX-1	4673.2	HST	upper	4.6	0.02	100.0	49		49	2	4	6	22	1	16	17	3	
MWX-1	4682.2	HST	upper	5.1	0.03	100.0	50		50	1	17	18	22	1	21	22	2	
MWX-1	4685.5	HST	upper	4	0.02	100.0	35		35	4	14	18	26	2.09	20.9	22.99	3.01	
MWX-1	4763.5	HST	upper	5.8	0.06	100.3	46		46	7	9	16	24	0	24	24		
MWX-1	4770.5	HST	upper	4.4	0.01	100.0	41		41	3	12	15	18	1	16	17	1	
MWX-1	4776.8	HST	upper	7	0.04	100.5	40		40	5	16	21	24	4	16	20	4	
MWX-1	4791.8	HST	upper	5.8	0.02	100.8	44		44	5	9	14	26	2	24	26		
MWX-1	4851.8	HST	upper	5.3	0.02	100.7	50		50	1.7	11	12.7	16	2	12	14	2	
MWX-1	4853.1	HST	upper	5.1	0.02	100.4	45		45	3	9	12	16	0.9	13.6	14.5	1.4	0.1
MWX-1	4906.5	HST	upper	7.5	0.03	100.3	59		59	2	6	8	7	0	7	7		
MWX-1	4942.4	HST	upper	6.8	0.03	100.8	50		50	3	10	13	16	3	8	11	5	
MWX-1	4944.3	HST	upper	8.4	0.09	100.1	48.3	0.7	49	1	8	9	17	5	10	15	2	
MWX-1	4962.2	HST	middle	4	0.04	100.5	21		21	9	11	20	7	0	7	7		
MWX-1	5011.8	HST	middle	3.4	0.03	100.3	39		39	28	11	39	12	8	2	10	2	
MWX-1	5020.4	HST	middle	2	0.01	100.8	21		21	10	15	25	7	0	7	7		
MWX-1	5035.8	HST	middle	2.5	0.01	100.9	27		27	6	8	14	19	10	9	19		
MWX-1	5084.8	HST	middle	6.8	0.01	100.2	35		35	13	16	29	20	1	21	22		
MWX-1	5129.5	HST	middle	7.9	0.02	100.7	37		37	11	17	28	20	1	19	20	3	
MWX-1	5196.4	HST	middle	2.4	0.01	100.6	33		33	2	11	13	22	0	21	21	1	
MWX-1	5271.6	HST	middle	3.6	0.62	100.5	43		43	3	5	8	21	0	18	18	2	1
MWX-1	5305.5	HST	middle	2.5	0	100.0	31		31	4	10	14	8	2	2	4	4	
MWX-1	5308.8	HST	middle	4.6	0.01	100.3	46		46	3	12	15	15	0	12	12	3	
MWX-1	5312.5	HST	middle	5	0.02	100.1	49		49	5	9	14	17	5.6	7	12.6	4	0.4
MWX-1	5315.5	HST	middle	4.1	0.03	100.4	51		51	4	7	11	19	8	8	16	3	
MWX-1	5350.5	HST	middle	5.8	0.02	100.3	42		42	3	14	17	20	1	19	20		
MWX-1	5380.4	HST	middle	1.6	0	100.0	42		42	9	9	18	12	0	10	10	2	
MWX-1	5416.2	HST	middle	4.2	0.01	100.4	48		48	11	13	24	11		10	11		
MWX-1	5529.5	HST	middle	5.2	0.08	100.5	55	1	56	2	6	8	9	2.3	1	3.3	5	0.7
MWX-1	5540.5	HST	middle	3.1	0.01	100.0	42		42	5	11	16	7	2	4	6	1	
MWX-1	5547.9	HST	middle	5.7	0.06	100.8	52.1	0.9	53	5	10	15	10	0	7	7	3	
MWX-1	5559.2	HST	middle	7.3	0.03	100.0	51		51	3	4	7	10	1	8	9	1	
MWX-1	5633.5	HST	middle	5.5	0.05	100.0	53		53	3	9	12	6	1	6	6		
MWX-1	5706.5	HST	middle	5.9	0.01	100.4	48		48	1	6	7	7	1	4	5	2	
MWX-1	5715.5	HST	middle	7.2	0.08	100.1	52		52	1	9	10	10	2	7.2	9.2	0.8	
MWX-1	5717.5	HST	middle	9.4	0.11	100.2	56		56	2	6	8	16	7	9	16		
MWX-1	5728.5	HST	middle	8.1	0.04	100.2	45		45	1	10	11	7	4	3	7	0	
MWX-1	5731.5	HST	middle	7.5	0.05	100.2	55		55	0	6	6	9	6	2	8	1	
MWX-1	5810.5	HST	middle	7	0.08	100.0	34		34	0	6	6	14	9	5	14	0	
MWX-1	5814.5	HST	middle	2.7	0	100.2	49		49	0	9	9	14	7	6.3	13.3	0.7	
MWX-1	5835.5	HST	lower	6.6	0.08	100.6	46		46	0	7	7	18	9	9	18	0	
MWX-1	5874.5	HST	lower	3.2	0	100.0	44		44	2	5	7	22	5	16.8	21.8	0.2	
MWX-1	5963.4	HST	lower	5.3	0.02	100.0	43		43	4	3	7	25	8.4	15	23.4	1	0.6
MWX-1	5988.9	HST	lower	4.1	0.01	100.1	45		45	1	4	5	17	1	16	17		
MWX-1	6074.7	HST	lower	8.2	0.02	100.6	56		56	1	7	8	17	8	9	17		
MWX-1	6187.6	HST	lower	1.8	0.01	96.0	40		40	1	4	5	8	6	2	8		
MWX-1	6247.5	HST	lower	4.6	0.02	100.1	51		51	1	6	7	17	12	5	17	0	
MWX-1	6357.6	HST	lower	5.6	0.01	100.3	50		50	1	7	8	11.4	0.4	10	10.4	1	
MWX-1	6360.5	HST	lower	7.6	0.04	100.0	53		53	2	7	9	16.3	5.3	11	16.3	0	
MWX-1	6435.7	HST	lower	4.3	0.02	100.0	43		43	0	6	6	7.1	5.1	2	7.1	0	
MWX-1	6487.5	HST	lower	5.1	0.01	100.0	37		37	1	2	3	12	5	6.7	11.7	0.3	
MWX-1	6544.4	HST	lower	7.3	0.05	100.1	46		46	1	5	6	10	8	2	10	0	
MWX-1	6546.3	HST	lower	8	0.04	100.1	36		36	1	5	6	8	2	6	8	0	
BT 202	54.1			22.2	915.3	100.3	33	4	37		10.5	10.5	6.1	1.8	4.3			
BT 202	57.1			22.2	470.4	100.4	30.3	4.3	34.6		7.3	7.3	7.1	1.3	5.8			
BT 202	66.9			17	57.5	100.3	28.5	0.8	29.3		8.5	8.5	24.3	9.3	15			
BT 202	91.5			19	92.1	100.4	29.8	2	31.8		8	8	19.6	9.3	10.3			
BT 202	94.1			19.2	500.4	100.4	32	3.3	35.3		8.8	8.8	11.3	1.5	9.8			
BT 202	104.1			17.4	99.8	100.1	29.3	1.8	31.1		10.3	10.3	11.3	1.5	9.8			
BT 202	117.9			4.9	0.007	100.2	30.8	0.5	31.3		6.8	6.8	9.5	3	6.5			
BT 202	125.2			12.6	3.3	100.2	28.3	0.8	29.1		13	13	12.3	2	10.3			
BT 202	130.9			20.4	173.9	100.1	26.8	2.8	29.6		7.8	7.8	7.8	0.3	7.5			
BT 202	147.1			22.9	711.8	100.3	34.8		34.8		7	7	8.3	1.3	7			
BT 202	150.95			20.3	174.6	100.3	32.8	0.5	33.3		5	5	11.1	0.8	10.3			
BT 202	154.1			20.9	567.3	100.1	36.5	1.8	38.3		7.3	7.3	7.6	0.8	6.8			
BT 202	155.2			15.8	101.5	100.1	41.3	0.3	41.6		6	6	4.8	0.5	4.3			
BT 202	157.1			20.2	400.3	100.6	37	2	39	9.8	1.3	11.1	11.3	0.3	11			
BT 202	160.5			22.6	454.5	100.8	37.5	2	39.5	8.8	1.3	10.1	5.8	0.5	5.3			
BT 202	166.6			26.4	1996.7	100.8	34	1	35	7.5	1.5	9	4.3		4.3			
BT 202	167.15			23.9	162.2	100.4	29.5	1.3	30.8	8.3	1.3	9.6	9.5	1	8.5			
BT 202	168.8			26.2	163.2	100.0	23.5		23.5	4.5	2.5	7	3.5	0.5	3			
BT 202	173.1			22.9	43.5	100.0	23.5	0.3	23.8	0.8	2.3	3.1	5.6	0.3	5.3			
BT 202	202.1			11.6	0.047	100.4	25.8	1.5	27.3	2.5	3	5.5	6.6	0.3	6.3			
BT 202	207.5			14		100.0	32.3	2.8	35.1	6	3.8	9.8	8.8	0.5	8.3			
BT 202	215.1			22.2	156	100.0	24.5	4	28.5		11.3	11.3	8.5		8.5			
BT 202	219.1			22.5	143.4	100.2	30	2.8	32.8	7.5	2	9.5	8.6	0.3	8.3			
BT 202	222.5			21.9	220.9	100.0	33.5		33.5	6	2.3	8.3	6		6			
BT 202	238.5			22.6	406.7	100.2	29	5.5	34.5	13.8	1.8	15.6	5.8		5.8			
BT 202	241.5			24	661.2	100.2	53	0.5	53.5	23.5		23.5	3.8		3.8			
BT 202	244.5			20.3	130.3	100.3	44	2.5	46.5	4.5		4.5	9.6	1.3	8.3			
BT 202	270.6			23	332.1	100.0	38.8	0.8	39.6	9		9	4.5		4.5			
BT 202	324.2			20.5	104.6	100.0	40.3	1	41.3	9		9	1.5		1.5			
BT 202	337.1			26.6	1005.1	100.0	41.8	1	42.8	3.8		3.8	3.3		3.3			
BT 202	365.2					100.8	39	1.3	40.3	8.3		8.3	8.5		8.5			
BT 202	373.7					100.2	28.5		28.5	5		5	5		5			
BT 202	382.2			8.4	0.028	100.2	36.3	0.8	37.1	6.8		6.8	21.8		21.8			
BT 202	409.65					100.3	33.8	2.3	36.1	6.3		6.3	18.8		18.8			
BT 202	441.2			8.8	0.028	100.3	44.8	0.8	45.6	10.3		10.3	14		14			
BT 202	482.7					100.2	28.5	1	29.5	6.3		6.3	21.5		21.5			
BT 202	484.1			2	0.001	100.3	21.8	2.3	24.1	6		6	19.8		19.8			
BT 202	486.1			3.2	0.001	100.2	28.5	0.8	29.3	6.3		6.3	22.5		22.5			
BT 202	516.1			15.7	17	100.7	39.5	1.3	40.8	10		10	14		14			
BT 202	520.1			20.7	191	100.1	33.5	0.3	33.8	9.8		9.8	13.8		13.8			
BT 202	528.1			23	345.6	100.2	37	2.5	39.5	7.8		7.8	5.8		5.8			
BT 202	530.1			25.2	1259	100.2	40.5	0.5	41	6.5		6.5	5		5			
BT 202	568.5			8.4	0.053	100.2	31.3		31.3	12		12	4.5		4.5			
BT 202	572.6			19.9	105.2	100.4	35	1.3	36.3	10.8		10.8	10.8		10.8			
BT 202	615.8			20.8	17.6	100.4	33.3	0.8	34.1	10.3		10.3	7.8		7.8			
BT 202	639.6			19.2	1.2	100.3	42.3		42.3	6.8		6.8	5.8		5.8			
BT 202	659.5			20.7	240.1	100.2	41.5	1.8	43.3	8.8		8.8	4.5		4.5			

Well	Depth (ft.)	Quartz Overgrowth Cement (%)	Carbonate Cement (%)	Ferroan Calcite (%)	Non-ferroan Calcite (%)	Undifferentiated Calcite (%)	Authigenic Dolomite (%)	Non-ferroan Dolomite (%)	Partial Grain Mold (%)	Interparticle Porosity (%)	Complete Grain Mold (%)	Fracture Porosity (%)	Total Porosity (%)	Carbonaceous Material (%)	Authigenic Clay (%)	Detrital Clay (%)	Total Clay (%)	Pseudomatrix (% of total clay)	Infiltrated Clay (% of total clay)	Muscovite (%)	Biotite (%)	Zircon (%)	Opaque Mineral %
PA 424-34	4570	3	1.9	2.3			0.5		3	0.5			3.5	1	3.6	12.5	16.3						
PA 424-34	4571	2.2	2.3	13.7				1.3	1.8	1.3	0.3		3.4	0.3	1	2.3	3.3						
PA 424-34	4575	8.3	0.7	1.3			0.3	0.5	1.5	2.8			4.3	0.8	2.5	5.5	8					0.5	
PA 424-34	4580	0.6	1.9	1.3			0.5		3	2.5	0.3		5.8	0.3	8	4.5	12.5						0.5
PA 424-34	4586	5.2	4.3	5.7			0.2		4.8	2.5	1.8		9.1		0.5	0.3	0.8						0.3
PA 424-34	4595	0.3	0.2	0.5			2		1.3	4	0.5		5.8	1.5	4	9.5	13.5				0.3		
PA 424-34	4600	7.8	0.3	0.5			3.3	1.3	4.3	3	0.3		7.6	2.8	6.3	6.5	12.8						
PA 424-34	4606	1.7	0.7	1			1.5	0.5	3.8	6.3	0.8		10.9	1.3	9.3	5.8	15.1				0.3		
PA 424-34	4625	3.2	1.7	0.3			1.3	0.3	2.3	1.5			3.8	3	1.5	9.5	11				0.3	0.3	
PA 424-34	4631	0.7								0.5			0.5	12.3		36.1	36.1			0.3	1	0.3	
PA 424-34	4644	3	0.6	1			1.5		1	2	0.5		3.5	4.3	4	13.8	17.8	32	54				
PA 424-34	4651	8.4	4.8	3.3			1.5	0.3	0.5	0.5			1	0.3	3	4.8	7.8			0.3			
PA 424-34	4655	5	2.7	1.3			1.8		1	2		0.3	3.3	1.5	12.8	2.3	15.1						
PA 424-34	4663	2.3		1			1.5		2	0.5	0.8		3	3.5	13.5	3	16.5						
PA 424-34	4675	4.8		2			1		3	2.3	1		6.3	1.8	11	6.8	17.8						
PA 424-34	4679	7	3.3	1.8	8		0.9	1					0	4.3	5.3	3	8.3						
PA 424-34	4685	8.7		2.3			1.5		0.5	1.3			1.8	1.8	5.9	4	9.9						
PA 424-34	4691	4.6	0.8	1.3			0.3	0.3	6	4.8	0.5	0.3	11.6	2	9.5	8	17.5						
PA 424-34	4694	2.7		2.5			0.3	0.5	3.5	2.5	0.5	0.3	6.8	2.8	5.3	15.5	20.8		12	0.3			
PA 424-34	4700	3.2					0.3		1.3	0.3			1.6	1.2	3	20.5	23.5			0.5	0.3		
PA 424-34	4706	5.7		0.3			1.5		3.5	1	0.3		5.7	0.5	12.4	0.5	12.9						
PA 424-34	4714	4.1	4.9	3.1			3.3	0.5	1.8	0.3			2.1	0.5	5.3	8.3	13.6						
PA 424-34	4727	7.3		4.3			1		2.5	2.3	0.8		5.6	0.7	6	7.8	13.8						
PA 424-34	4729	7.2	1.3	0.3			0.5		0.3	1			1.3	4	1.5	17.3	18.8			0.5			
PA 424-34	4732	6.3	0.7	0.4			0.6		3	0.5			3.5	0.2	5.3	3	8.3				0.3		0.5
PA 424-34	5108	3			2		10.8	11.5				1	1	6.3		24	24	63.8		0.3			
PA 424-34	5114	4.6		4	1.3		6	5.3	0.3			0.8	1.1	4.5		16.5	16.5	72					
PA 424-34	5121	2.7		1.5	0.3		3.5	2.8	5.3	2	0.8		8.1	2.8	7.3	1.3	8.6						
PA 424-34	5124	7.2	4.9	12.8	1		4.8	8.8	0.8				0.8	1.3	2.3		2.3						
PA 424-34	5136	4			0.3		1.8	1.8	6	3.8	0.5		10.3	3	9.8	3.5	13.3	42					
PA 424-34	5141	3.3	0.8	0.3			0.8	0.3	8.3	1	1.5		10.8	3	5.5	4	9.5						
PA 424-34	5142	3.1		1.5	0.3		0.5	1	8.3	0.3			8.6	2.5	5.3	8.5	13.8		55				
PA 424-34	5161	1.3		3	1.5		11	6.8				0.3	0.3	3.8	1.3	12.5	13.8	23	68		0.3		
PA 424-34	5174	6.6	0.9	2.9	1.3		5.3	3	1.3	1.8			3.1	0.9	1.8	2.8	4.6						
PA 424-34	5184	4.4		1	0.3		1.5	1.5	4	1.8			5.8	6	6.8	6.3	13.1	51					
PA 424-34	5195	6.4					2.8	0.5	6.3	1.5	0.3		8.1	0.7	6.5	2	8.5						
PA 424-34	6078	3.50			2		15	6.3					0	6.8		8.3	8.3						
PA 424-34	6082	6.3			2.5		7.8	7.5					0	2.5	0.3	0.5	0.8						
PA 424-34	6088	5.90			1.8		10.8	5.3	0.5	0.3			0.8	2.5	4		4						
PA 424-34	6091	3.4	2.2		1.8		3.5	5.8	5	0.8	0.5		6.3	4.5	2.8		2.8						
PA 424-34	6132	5.00			3.3		16.5	4.3	4.3	6.8	0.3		11.4	5.3	0.5		0.5						
PA 424-34	6138	4.4		0.8	1.8		4.3	4	6.3	3.5	0.3		10.1	4.3	6.5	0.3	6.8						
PA 424-34	6155	2.10	5.20		2		20.8	4.5	4.8	4			8.8	2.5	1		1						
PA 424-34	6582	4.1			0.3		12.8	17.3		1.5			1.5	5.5	0.5	4.5	5						
PA 424-34	6589	3.3			1		8.3	13.8	0.3			0.3	0.6	4.8		7.3	7.3	58		0.3	0.3		
PA 424-34	6595	2.8			0.3		12.5	13.8	1.3	0.5			1.8	5.5		6.5	6.5		63				
PA 424-34	6600	2.7	1.2				9	11.3	1.3	1.5			2.8	2.5	5.8	2.6	8.4						
PA 424-34	6639	4	3.6		1.5		8.4	5.3	2.3	2.3			4.6	3.5	6.5	1.5	8					0.3	
PA 424-34	6643	4.3	3.1		2		8.5	8.3	2.8	3.5			6.3	5.3	2.8	2.5	5.3		48				
PA 424-34	6648	4.6	7.9	0.3	1.3		23.5	9.3	0.5	2			2.5	1	5	0.8	5.8						
Cascade Creek	4704	0.3	2.3	3.8	10.8				2.8	2.8			5.6	2	3.3	6.5	9.8				0.3		
Cascade Creek	4752												0	4.3	0.5	52.5	53			0.3	0.3		
Cascade Creek	4761						7			6	0.5		6.5	3.3	9	2.3	11.3			0.3			
Cascade Creek	4772	3.5	0.9	1.4	4.7	3.3			0.3	3.8	0.5		4.6	0.8	4.5	2	6.5				0.3		
Cascade Creek	4786	3.3				2.5				5.5	0.8		6.3	3.5	3.3	3.8	7.1				0.3		
Cascade Creek	4809	1			0.9	0.8	0.3			9.8	0.3		10.1	3.8	3.8	12.3	16.1	22	74				
Cascade Creek	4819	1.3	2.6	2.3		2.8				9.8	2.8		12.6	0.3	5		5						
Cascade Creek	4834		1		1.7	0.5				8.8	1.5		10.3	2.3	9	1.3	10.3	36	53		0.5		
Cascade Creek	5182	7.3	1.8	3.1		4.5				2			2	2.3	18.3	1	19.3		22				
Cascade Creek	5194	3.3	2.4		2.3	13.8				0.8			0.8	1.5	24.3	1.8	26.1		14				
Cascade Creek	5201	9.8				12.5				2.5	0.3		2.8	1	24	0.5	24.5						
Cascade Creek	5298	6.2	2			7				9	3.8		12.8	0.8	12	0.8	12.8						
Cascade Creek	5308	4.8				4.8				6.5	2.8	1.3	10.6	1	9.3	1	10.3		2				
Cascade Creek	5318	7.3	0.9	2.7		3.5				10.5	3		13.5	0.3	7.3	0.8	8.1						
Cascade Creek	5331	6.3				1.8	0.5			6.8	2	0.3	9.1	1.8	9.3		9.3						
Cascade Creek	6112	0.5	3.5	0.9		4.5			2	2.3	1.3	0.5	6.1	7	3.8	24.3	28.1	62	33				
Cascade Creek	6117	0.3	3			1			1.3	5	0.5		6.8	4.3	6.8	8.3	15.1	52	39				
Cascade Creek	6213	1.5		3.3		11.3	1.3			9.3	2.8		12.1	0.8	8.8	9.8	18.6		28	0.3			
Cascade Creek	6217	2.8	4.3	4.2		25.3				9.3	1.8		11.1	0.3	10.5	0.3	10.8						
Cascade Creek	6220		3			9.8			1.5	5	1.3		7.8	3	5.3	2.8	8.1		64				
Cascade Creek	6294					8.5	0.9		1	2.3	0.8		4.1	3	3.3	15.8	19.1		88	0.8	0.3		
Cascade Creek	63041					4	0.3		1	0.5			1.5	1.3		23.3	23.3		72	0.3			
Last Dance	2813.10	5	2.4			6.3			2	0.3			2.3	5.8	9		9						1.2
Last Dance	2835.00	3				7			1				1	1	5.3	1	6.3						0.8
Last Dance	2846.00	2							1.3	0.6			1.9	2	3.7	0.3	4			0.5			1
Last Dance	2856.00	3.8	4			7			1.5	0.5		0.4	2	4.4	5		5	28	72				2
Last Dance	3553.30	3							2.7	1.3			4	2	2.3		2.3						
Last Dance	3563.00	5				4			1	0.3			1.3		4.7	5	9.7	12	86				
Last Dance	3568.00	1							0.3	0			0.3		8	9	17		32			0.4	
Last Dance	3573.10	2.3							0	0			0	1	3.7	6	9.7	22	68	.			6
Last Dance	3596.90	6	2.9			0.8			2.6	1			3.6		4.3		4.3						3
Last Dance	3994.00	1.3	1			1.6							0		7	3	10		62				2
Last Dance	4005.90					0.3			2	0			2		1.5	1.6	3.1				5		1
Last Dance	4017.90		7.2			13.3							0		0.7		0.7						0.3
Last Dance	4382.00	5.3							1				1		2	1	3						0.1
Last Dance	4389.00	3.7				1			2	0.6			2.6		3		3						
Last Dance	4855.00		6.9			9.3			0.6				0.6		1.9	3	4.9	33	52				0.3
Last Dance	5717.00	3				2.1			2	1			3		3.6	1.3	4.9						1
Last Dance	5734.20	2	2.8			0.6			2	0.3			2.3		4	2	6						3
Last Dance	5760.30	2.8	2			1.6	3		1.9	1			2.9		4	1	5	12					3
Last Dance	6040.10	4							1.3				1.3	1	3	0.3	3.3						
Last Dance	6054.10	3				3.3	8		1.8				1.8	1	1		1						
Last Dance	6339.60	0.3	4.9			7	21			1			1		3		3						
Last Dance	6342.00	2	2				14		0.8				0.8		6	4	4						
MWX-1	4191.9	0.2	3.1	1	0.2	4	0.01		0.8	2.2			3		0.9	17	17.9	23	63				
MWX-1	4193.4	0.9	3	1.3	3.3	4	0.01		0.9	5.3	1.8		8		0.7	1	1.7						
MWX-1	4195.6		1		1	27	0.01		0	0.3			0.3		2.1	12	14.1		58				
MWX-1	4231.3	0.4	2	0.8	2	5			1.2	4.2	0.6		6		0.3	1	1.3			0.1			
MWX-1	4234.3				1	28			0.4	0.6			1			8	8						
MWX-1	4253.8	2		3.4	2	5			1.6	7.8	1.6		11			1	1						
MWX-1	4303.9	0.9			1.3	6			1.7	4.3			6		2.4	5	7.4						
MWX-1	4311.2	1.6	3		1	2			3.7	8.2	2.1		14			6	6						
MWX-1	4314.2	2.5	3.9	0.7	2	3			3.3	4.3	0.4	0.1	8.1			0.9	0.9						
MWX-1	4322.2	0.3	4.9		0.01	13			0.3	0.7			1		2.2	10	12.2						
MWX-1	4324.2	1.4			2	2			0.2	7	0.9		8.1			3	3						
MWX-1	4328.1	3.1	1.2		2	3			1.6	11	2.4		15			2	2						
MWX-1	4329	2.8			0.9	5				7			7	2	0.7	3	3.7						
MWX-1	4331.2	0.4	4	2.3	2	6			1.7	9	1.3		12			0.01	0.01						
MWX-1	4344	0.4	4.4		2	15	0.01						0		1.8	9	10.8			0.1			
MWX-1	4351.3	0.2			2	36			0.4				0.4			0.01	0.01						
MWX-1	4359.5	2.1			2	2			3.7	6.3	2		12			0.01	0.01						
MWX-1	4389.2				4	19			0.1	2.9			3			10	10						
MWX-1	4396.2	3.2		4.2	5	14			0.9	3.8	0.3		5			1	1						
MWX-1	4490.4	0.2			1.7	2			0.5	0.3			0.8		3.6	29	32.6	35	49				
MWX-1	4520.2		1		2	2							0			27	27						
MWX-1	4537.8	4.1	2.6		2	3.7			3.9	6.3	1.8		12		1.5	2	3.5						
MWX-1	4550.5				4	3			4.2	3.7	0.8	0.3	9			2	2	6					
MWX-1	4557.8	2.8	2	3.1	2	1.8			2.4	3.6			6			1	1						
MWX-1	4561.8	1.4			0.4	1			0.5	7.4	3.1		11			3	3						
MWX-1	4575.2	1.2			4	3			0.8	4.2			5			3	3				1		
MWX-1	4639.6				5				0.7	8.6	0.7		10			3	3						
MWX-1	4673.2		0.1		1	1			0.7	1.3			2		3.9	8	11.9						
MWX-1	4682.2				1	2			2.3	0.7			3			4	4						
MWX-1	4685.5	0.2		3.8	2	1			0.8	0.2			1			13	13						
MWX-1	4763.5				2	2				1			1		2.3	7	9.3						
MWX-1	4770.5				1	0				1			1			24	24	34	61				
MWX-1	4776.8	4.2			3	2			0.2	1.1			1.3			5	5						
MWX-1	4791.8		1.8		4	3			0.2	1.8			2		2	4	6						
MWX-1	4851.8	0.9			2	1	0.1		4	6.7	1.3		12			6	6						
MWX-1	4853.1	6.3			2	1	0.1		4.1	3.9			8			10	10	37	52				
MWX-1	4906.5	5.2		1	4	0			2.7	9.3			12		1.1	3	4.1						
MWX-1	4942.4	5.7			2	0	0.1		1.8	9.8	0.6	0.8	13			1	1						
MWX-1	4944.3	9			1	2	0.1		1	11			12			1	1						
MWX-1	4962.2	3.5				0							0			45	45		22	1	3		
MWX-1	5011.8	7				0							0				0			1	2.3		
MWX-1	5020.4	7.2				34				0.2			0.2		2.4	1	3.4			1	2		
MWX-1	5035.8		7			25							0			8	8	29		0.01	0.9		
MWX-1	5084.8	6				3			0.3	0			0.3			4	4			1	2		
MWX-1	5129.5				1	2			0.1	2			2.1			4	4			1	2.6		
MWX-1	5196.4	6.9	4.3		1	5							0		2.4	12	14.4				1		
MWX-1	5271.6	4.2	3	2.3	1	7				1			1			5	5				1		4
MWX-1	5305.5		8			15							0			21	21		14	1	2		
MWX-1	5308.8		4		2	5			0.3	2.7			3		2.3	7	9.3				0.01		1
MWX-1	5312.5		2		1	5			1.5	3.2	0.4		5.1			6	6				1		0.01
MWX-1	5315.5		1.7			2.7				2			2			12	12				1		
MWX-1	5350.5	2.3				3				5			5		4	6	10				1		
MWX-1	5380.4					5							0			20	20	22	74		3.8		
MWX-1	5416.2					2	1		2.2	4.8			7		0.4	6	6.4				1		
MWX-1	5529.5	5.8		3.7	1	4	2.5		0.9	5.1			6			2	2				2		
MWX-1	5540.5		8			17	6						0			4	4						
MWX-1	5547.9	0.2	3.6			9	2		2.6	1.4			4			3	3						
MWX-1	5559.2				1	4	3		1.3	8.7			10			3	3						
MWX-1	5633.5				1	5	4		1.1	1.9			3			3	3			1			
MWX-1	5706.5	3.1	3		2	4	0		1.1	13	0.9		15		2.3	9	11.3		12				
MWX-1	5715.5	2.1			1	3	0		2	11			13			9	9	47	35		0.01		
MWX-1	5717.5				2	2	0		3.7	11.3			15			1	1				0.2		
MWX-1	5728.5		8		3	9	3		1.8	9.2			11			3	3				0.2		
MWX-1	5731.5		1.2	2.2	3	6	2		6.8	4.1	1.2	0.9	13		0.2	3	3.2						
MWX-1	5810.5		2		1	19	9		2	4			6			9	9						
MWX-1	5814.5		3		3	11	4		2.8	1.2			4		1.2	2	3.2			0.01			
MWX-1	5835.5	2.4			1	8	3		6.7	7.3			14			1	1			0.2			
MWX-1	5874.5		2.9		1	12	4.3						0			7	7						
MWX-1	5963.4				1	7	7		1	2			3			5	5				1		1
MWX-1	5988.9		0.3		1	1	13			0.1			0.1		2.4	15	17.4			0.3	1		
MWX-1	6074.7				1		9		3.1	3.9			7			2	2						0.01
MWX-1	6187.6		7			1	22		0.5	11.7	0.8		13				0						0.01
MWX-1	6247.5			2.1	1	0	9		0.9	11.1			12			2	2						
MWX-1	6357.6	4.9			3	4	6		2.9	7.9	1.2		12			1	1						
MWX-1	6360.5		1.7		3	4	4		1.8	5.2			7			2	2						
MWX-1	6435.7	4.3			7	8	7		2.8	4.2			7		1.6	9	10.6	33					
MWX-1	6487.5		3		2	3	7						0	1.3	2.7	29	31.7	23	66				
MWX-1	6544.4			4.7	3.2	7	7.2		1.6	1.4			3			13	13						
MWX-1	6546.3		4.1		5	11	12			2			2		2	14	16	26	68				
BT 202	54.1	17.3	2.3			0.5			8.3	13	2.5	0.5	24.3	2.3	16.3								
BT 202	57.1	8				0.3			11.3	14	2.5	0.5	28.3		14.8		14.8						
BT 202	66.9	9.8				4.3			4.3	10.5	1		15.8	0.3	8		8						
BT 202	91.5	12.3				6.5			3.3	7.3	1	0.3	11.9		10.3		10.3						
BT 202	94.1	13.3							9.8	8	5.3	0.3	23.4	0.5	7.8		7.8						
BT 202	104.1	19.8				0.8			8.8	6	2	0.5	17.3		9.5		9.5						
BT 202	117.9					49			0.3	0.5			0.8		0.8		0.8						
BT 202	125.2	19.7				1.8			7.8	4.5	2		14.3	2.8	4.8	1.8	6.6			0.3	0.3		
BT 202	130.9	14				1			14.8	7	4.5	1	27.3	2.8	9.8		9.8						
BT 202	147.1	18.8							8	9.8	3.5	0.8	22.1	1	8.3		8.3						
BT 202	150.95	13.6				0.5			16	9.5	1.5	0.5	27.5	0.3	9		9						
BT 202	154.1	13.7				1			8.8	9	5.8	1	24.6	0.3	7		7			0.3			
BT 202	155.2	18.5				0.5			8	9.3	1.8	0.3	19.4	0.8	8.5		8.5						
BT 202	157.1	14.8							4.5	12.8	1.8		19.1	1.3	4		4						
BT 202	160.5	12.3				3.5			5	13.5	3.8		22.3	0.8	6.5		6.5						
BT 202	166.6	12.6				1.3			6.5	13	2		21.5	0.3	16.8		16.8						
BT 202	167.15	14.5				4.3			4.8	11.8	3.3		19.9	5.8	6		6						
BT 202	168.8	8.6				14.5			6.8	14			20.8	16.5	4.3		4.3				0.3		
BT 202	173.1	5.9				21.5			1	5.3			6.3	12	1.3	20.5	21.8						
BT 202	202.1	7.1				18.5			3.5	8	0.3		11.8	10.8	0.3	12.5	12.8						
BT 202	207.5	11.8				9.3			6.8	7.8	3	0.5	18.1	2	4.3	0.8	5.1						
BT 202	215.1	12.1				3.5			8.3	8.8	1.5	0.5	19.1	3	14		14						
BT 202	219.1	14.6				4.3			5.5	7	1.5	0.3	14.3	0.8	14.8		14.8			0.5			
BT 202	222.5	6.1				12			3.3	7.3	2.5		13.1	1.5	13.5		13.5						
BT 202	238.5	9.8				0.3			6	8.3	6	0.3	20.6	1.8	11.8		11.8						
BT 202	241.5				16.8				0.8	1.5			2.3			0.3	0.3						
BT 202	244.5	3.8			2				1.5	12.3			13.8		19.8		19.8			0.3			
BT 202	270.6	10.3			8.3				1.5	11.5			13		15.3		15.3						
BT 202	324.2	6.1			0.3				2	17.5			19.5		14.8		14.8						
BT 202	337.1	12			10.3				2	11.5			13.5		14	0.3	14.3						
BT 202	365.2	13.3			3.3				0.5	13			13.5		11.8	1.8	13.6						
BT 202	373.7	9.3			40.8					4			4	0.3	7		7			0.3			
BT 202	382.2	7.3			1				0.3	11.3			11.6		14.3		14.3			0.3			
BT 202	409.65	2.5			29.5				0.3	1			1.3		4.5	0.8	5.3			0.5			
BT 202	441.2	13.5			0.8				0.5	8.3			8.8		5.8	1	6.8			0.5			
BT 202	482.7	7.6			17				1.5	5.5			7		7.5	3	10.5			0.3	0.5		
BT 202	484.1	0.3			49.5								0			0.3	0.3			0.3			
BT 202	486.1	0.6			40.5								0			1	1						
BT 202	516.1	12.5			2				1.5	9			10.5		9	1.3	10.3			0.3	0.3		
BT 202	520.1	11.5			4.3				0.3	14.8			15.1		10.5	1	11.5				0.3		
BT 202	528.1	9			10.5				1.5	7.3			8.8		16.5	2.3	18.8						
BT 202	530.1	11.1			4.3				2.8	10.5			13.3		16	3	19						
BT 202	568.5	11.3			6.3				2.5	15			17.5		14.5	2.5	17			0.3			
BT 202	572.6	13.6							4.5	5.3			9.8		15.8	3	18.8			0.3			
BT 202	615.8	12.3			2				3.5	5.3			8.8		18	5.8	23.8			1.3			
BT 202	639.6	10.5			9.3				1.8	11			12.8		9	3.8	12.8						
BT 202	659.5	7.3			1.5				2	11			13		16	5.8	21.8						

Appendix B – Core Descriptions

Sedimentological core descriptions were collected from five cored wells:

- Plateau Creek BT-202,
- Cascade Creek # 697-20-28,
- Puckett/Tosco PA 424-34,
- Last Dance 43C-3-792, and
- Cactus Valley 1 D111.

The Superior MWX 1 core was not described; rather Lorenz's (1987, 1988, 1989, and 1990) description of those cores was utilized.

Core descriptions included lithology, sedimentary structures, grain size, bioturbation, bed thickness, and bed contacts. Lithofacies and facies associations were defined on the basis of that data (see Chapter 2). Keys to the symbols used on the descriptions are included at the end of each core description.

Well Name.............. **Date....................** **Page...1......... Of............**

USGS Number

Conglomeratic Sandstone	Coarse Braned Sandstone	Medium Grained Sandstone	Fine Grained Sandstone	Siltstone	Claystone	Coal	Fractures	Lithology	Core Depth (feet)	High Bioturb	Moderate Bioturb	Low Bioturb	Description and Remarks	Depo. Invironments	Facies
									243						Sla
									245						
															Ms
									250						St
															Sla
									255						Sr
															Sr
									260						
															Sr
									265						Sla
									270						
															Sla
									275						

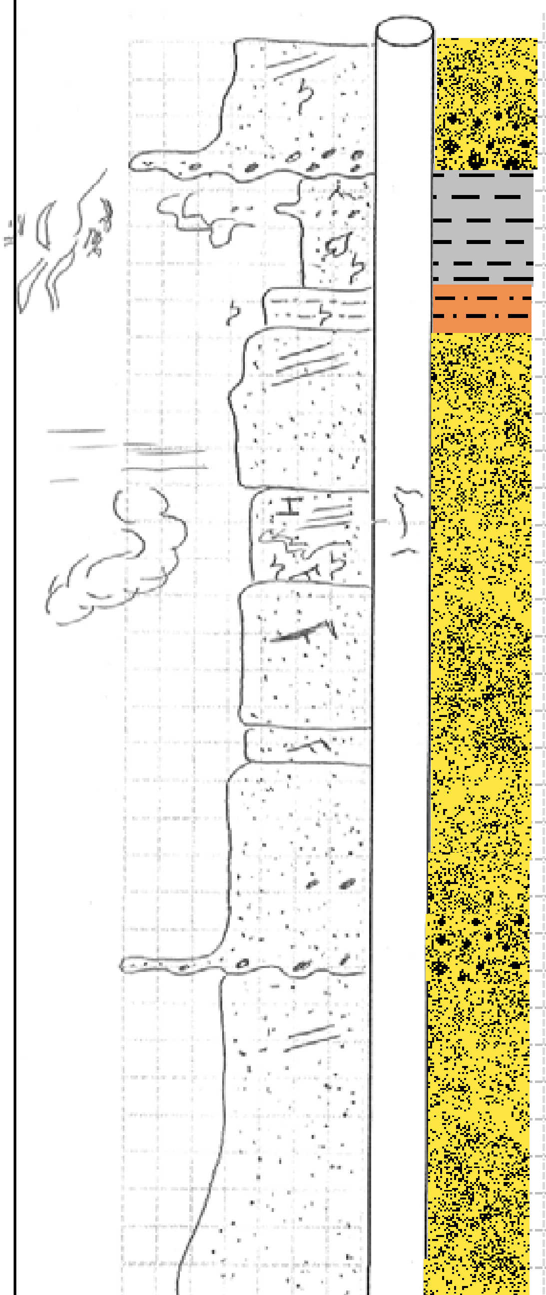

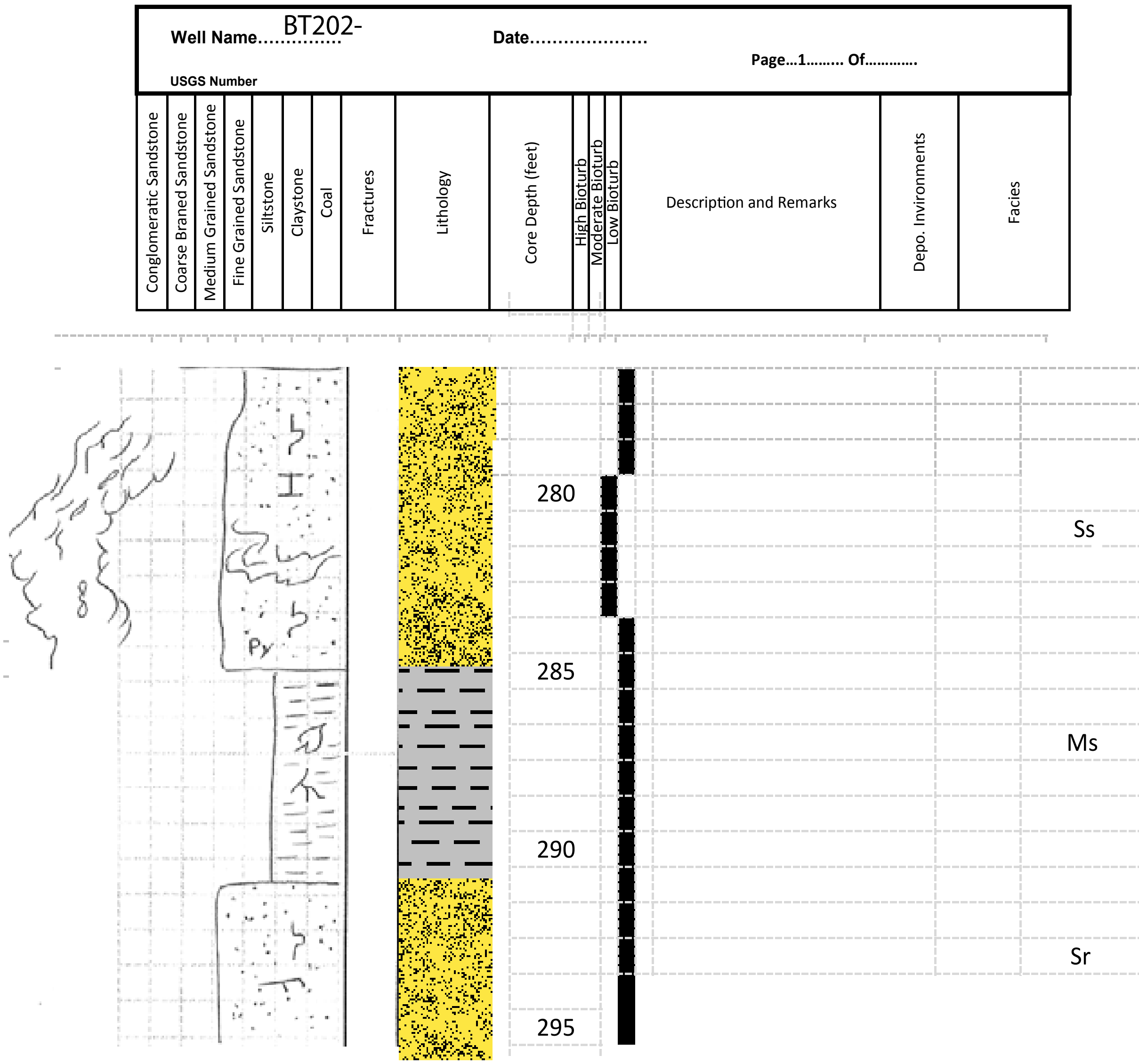
Well Name...............BT202-
Date.....................
Page...1......... Of............
USGS Number
Conglomeratic Sandstone
Coarse Braned Sandstone
Medium Grained Sandstone
Fine Grained Sandstone
Siltstone
Claystone
Coal
Fractures
Lithology
Core Depth (feet)
High Bioturb
Moderate Bioturb
Low Bioturb
Description and Remarks
Depo. Invironments
Facies
Py
280
285
290
295
Ss
Ms
Sr

Well Name.........BT202- **Date**.....................

Page...1......... Of............

USGS Number

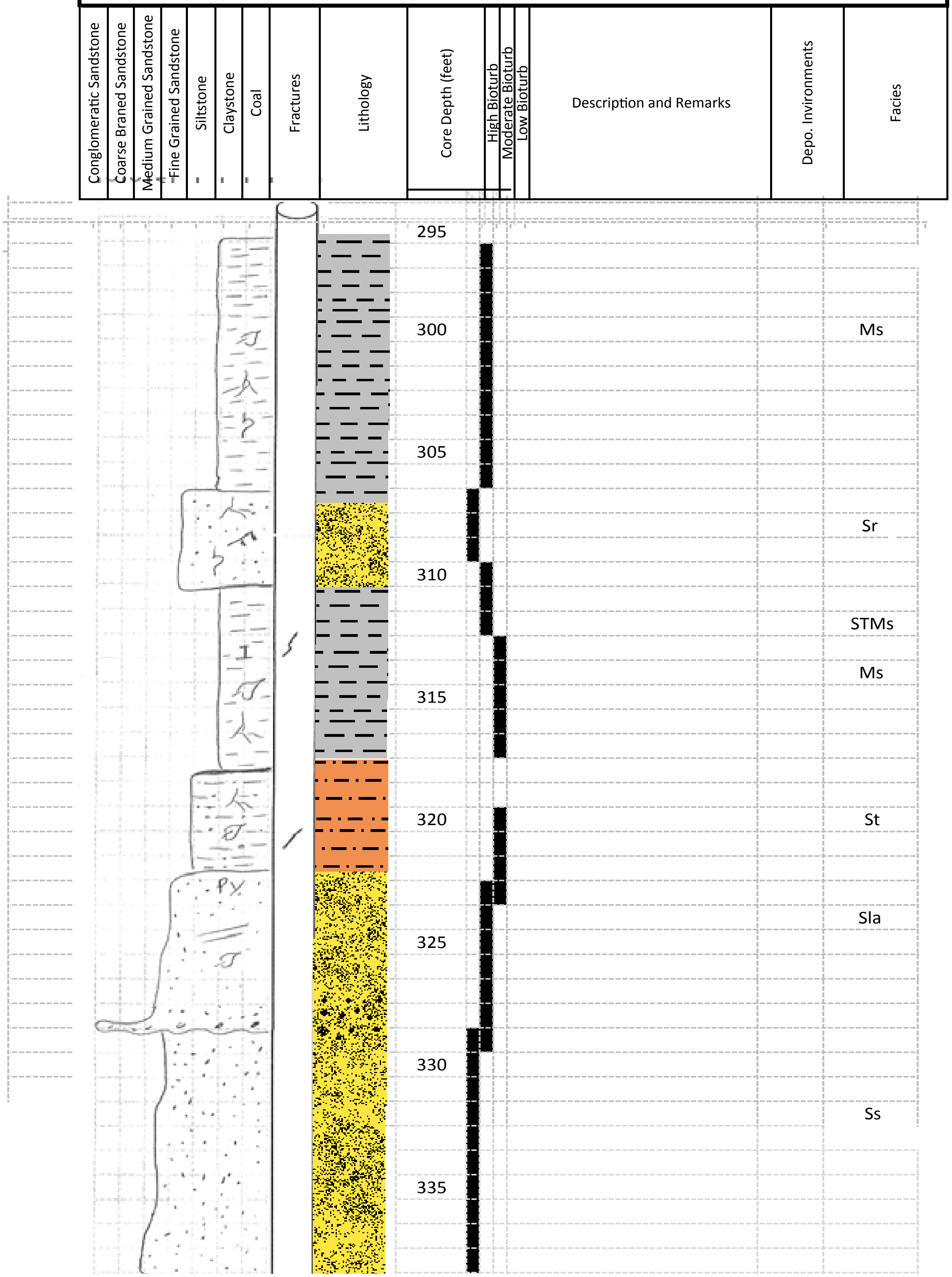

Well Name.............. BT202-   **Date**....................

Page...1......... **Of**............

USGS Number

Conglomeratic Sandstone	Coarse Braned Sandstone	Medium Grained Sandstone	Fine Grained Sandstone	Siltstone	Claystone	Coal	Fractures	Lithology	Core Depth (feet)	High Bioturb	Moderate Bioturb	Low Bioturb	Description and Remarks	Depo. Invironments	Facies

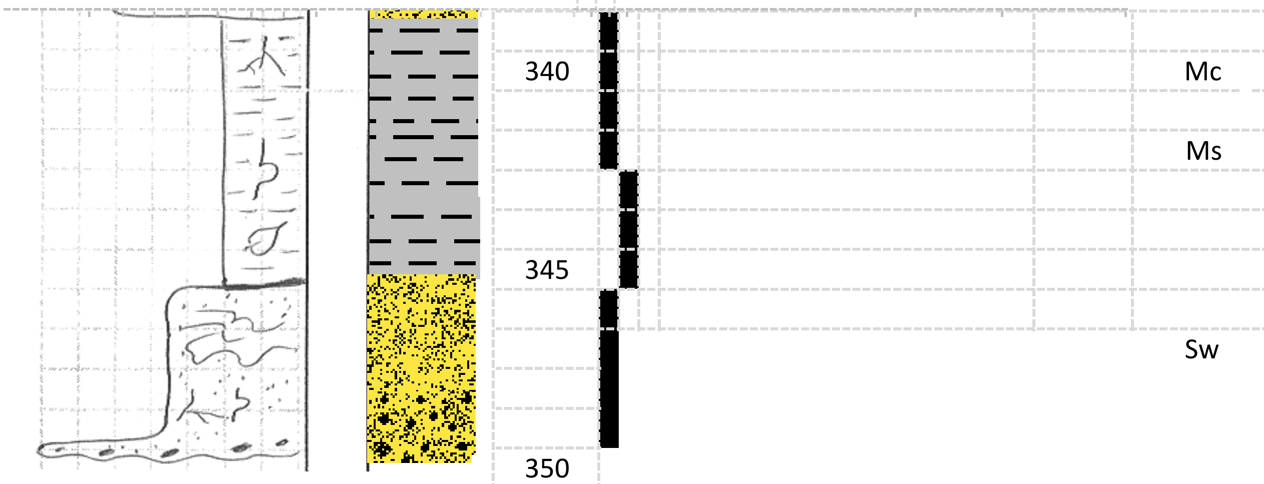

Well Name……BT202… **Date…………………**

Page…3……… Of…10….

USGS Number

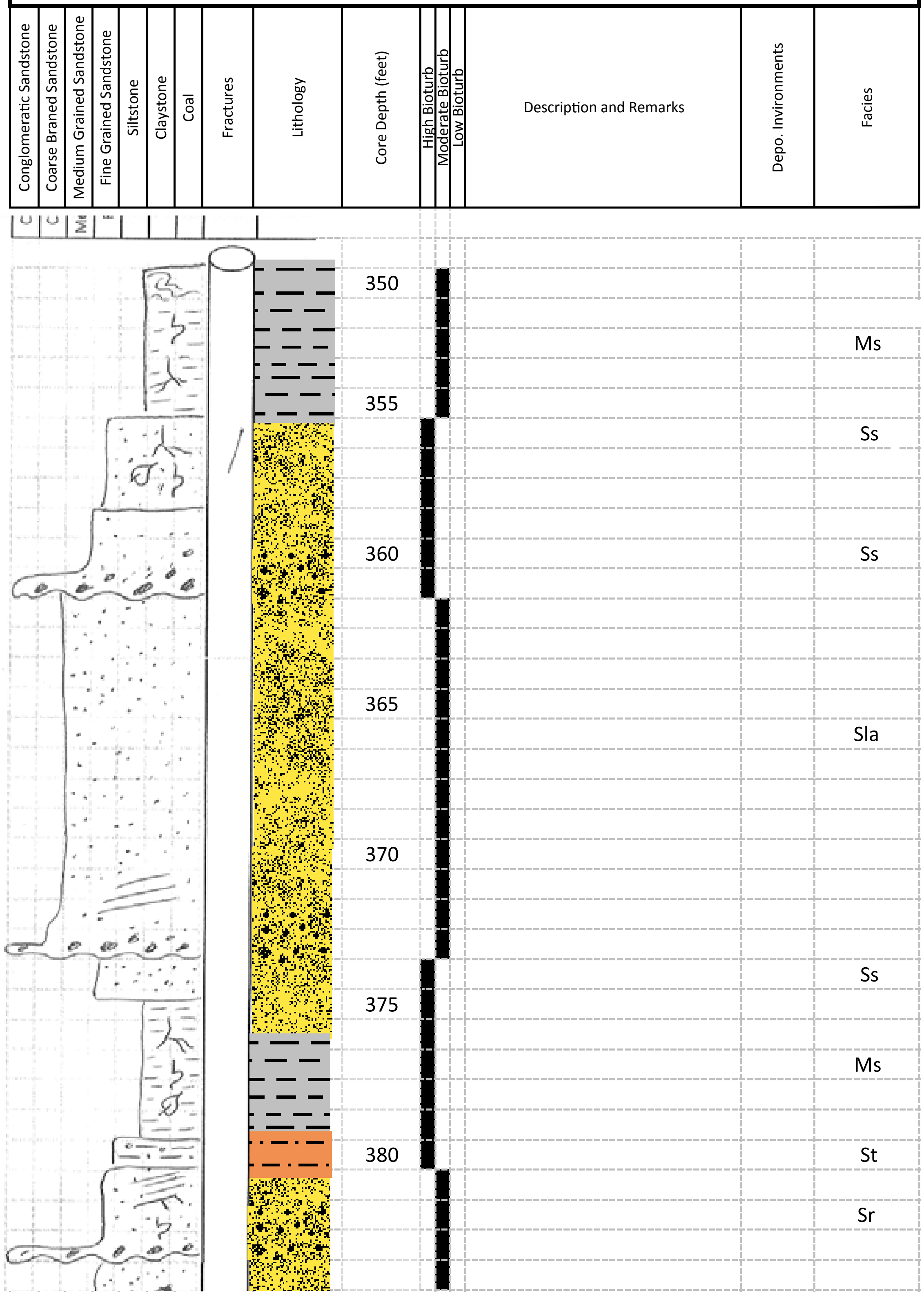

Well Name...............BT202- Date.....................

Page...1......... Of.............

USGS Number

Conglomeratic Sandstone	Coarse Braned Sandstone	Medium Grained Sandstone	Fine Grained Sandstone	Siltstone	Claystone	Coal	Fractures	Lithology	Core Depth (feet)	High Bioturb	Moderate Bioturb	Low Bioturb	Description and Remarks	Depo. Invironments	Facies

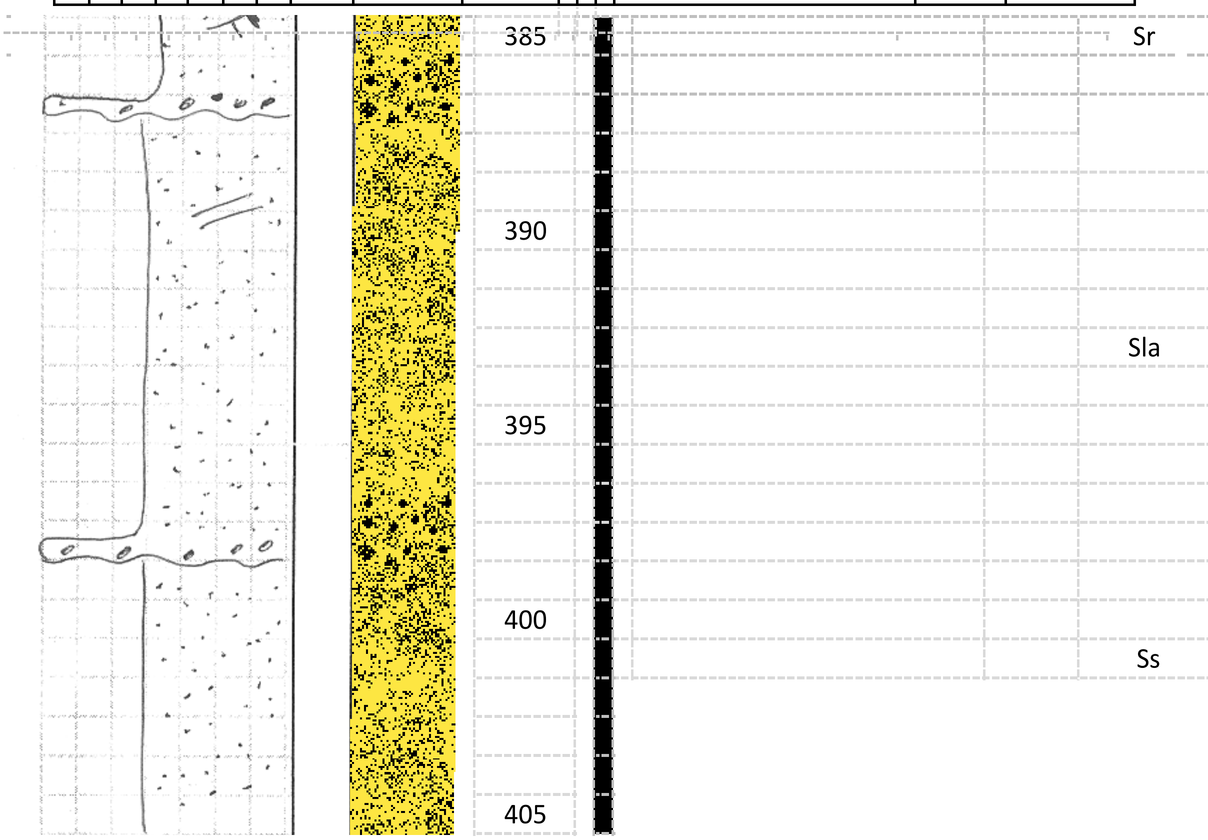

Well Name…BT202… **Date…………………**

Page…4……… Of…10….

USGS Number

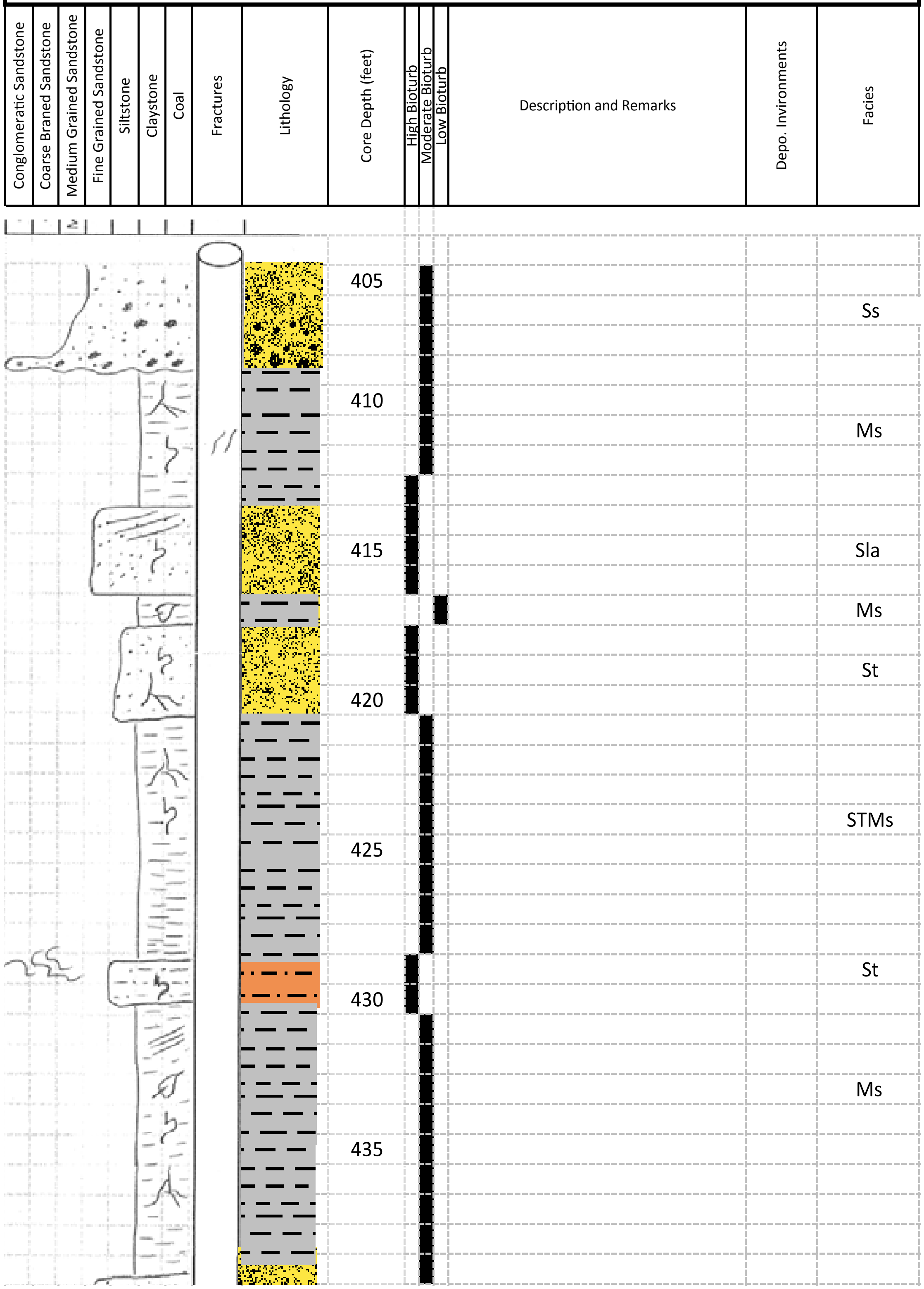

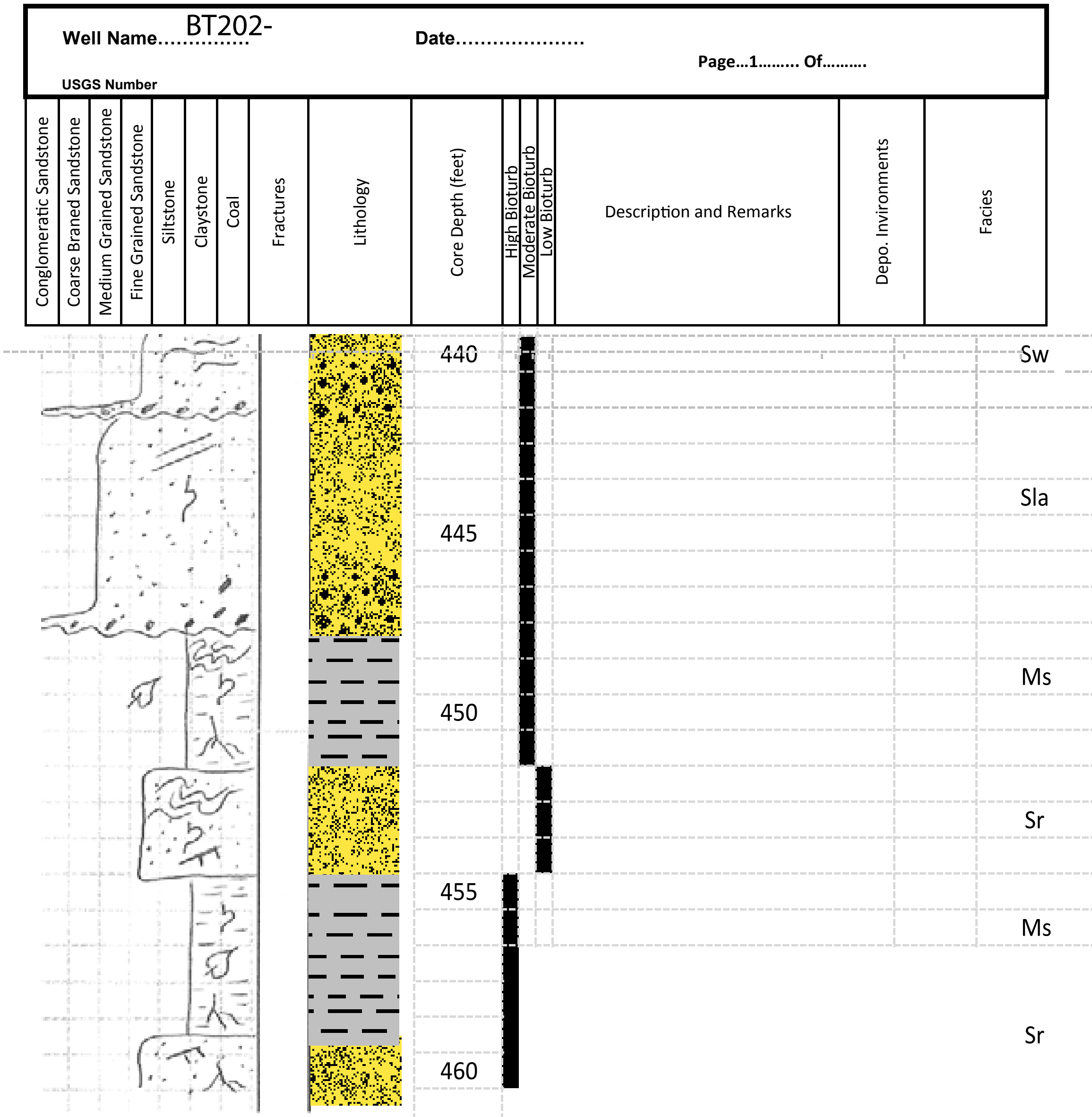

Well Name...............BT202-
Date.....................
Page...1......... Of..........
USGS Number
Conglomeratic Sandstone
Coarse Braned Sandstone
Medium Grained Sandstone
Fine Grained Sandstone
Siltstone
Claystone
Coal
Fractures
Lithology
Core Depth (feet)
High Bioturb
Moderate Bioturb
Low Bioturb
Description and Remarks
Depo. Invironments
Facies
440
445
450
455
460
Sw
Sla
Ms
Sr
Ms
Sr

Well Name…BT202… **Date…………………**

Page…5……… Of……10…….

USGS Number

Conglomeratic Sandstone	Coarse Braned Sandstone	Medium Grained Sandstone	Fine Grained Sandstone	Siltstone	Claystone	Coal	Fractures	Lithology	Core Depth (feet)	High Bioturb	Moderate Bioturb	Low Bioturb	Description and Remarks	Depo. Invironments	Facies

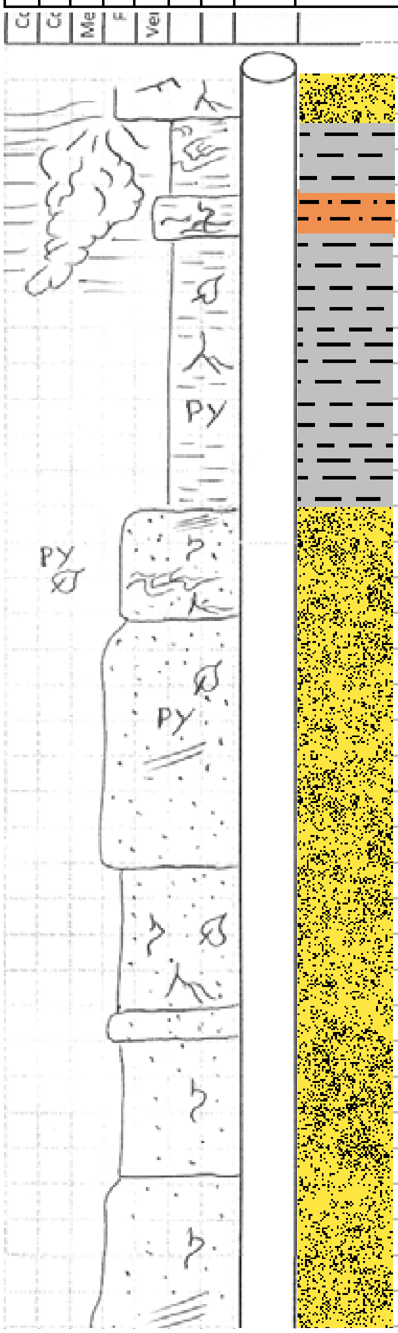

Core Depth (feet)	Facies
460	Sr
	Ms
	St
465	
	Ms
470	
	Sla
475	
	Sla
480	
485	Ss
	Ss
	Ss
490	
	Sla
495	

Well Name......BT202- **Date**.....................

Page...1......... Of.............

USGS Number

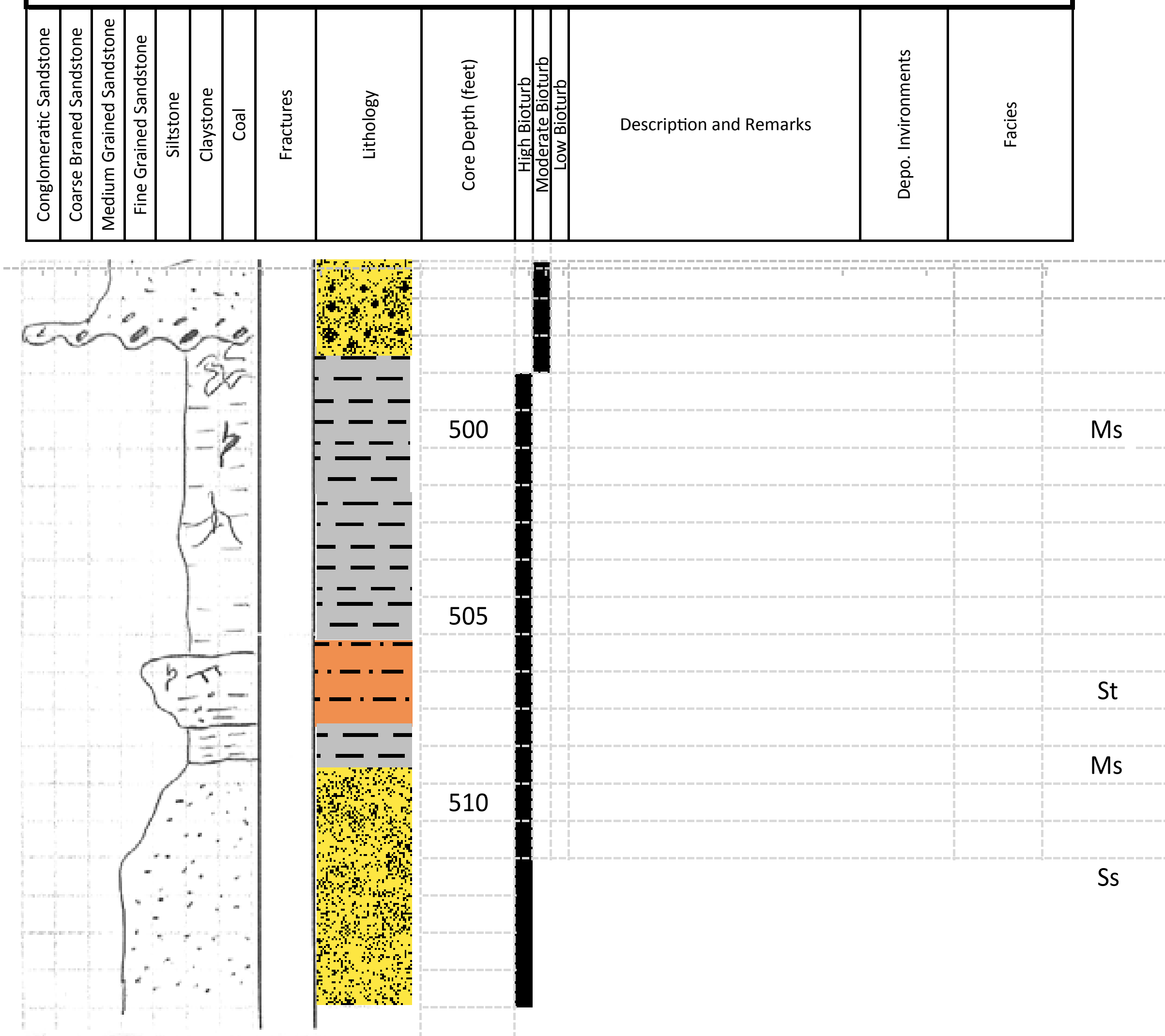

Well Name............... **Date.....................**

Page...1......... Of............

USGS Number

Conglomeratic Sandstone	Coarse Braned Sandstone	Medium Grained Sandstone	Fine Grained Sandstone	Siltstone	Claystone	Coal	Fractures	Lithology	Core Depth (feet)	High Bioturb	Moderate Bioturb	Low Bioturb	Description and Remarks	Depo. Invironments	Facies

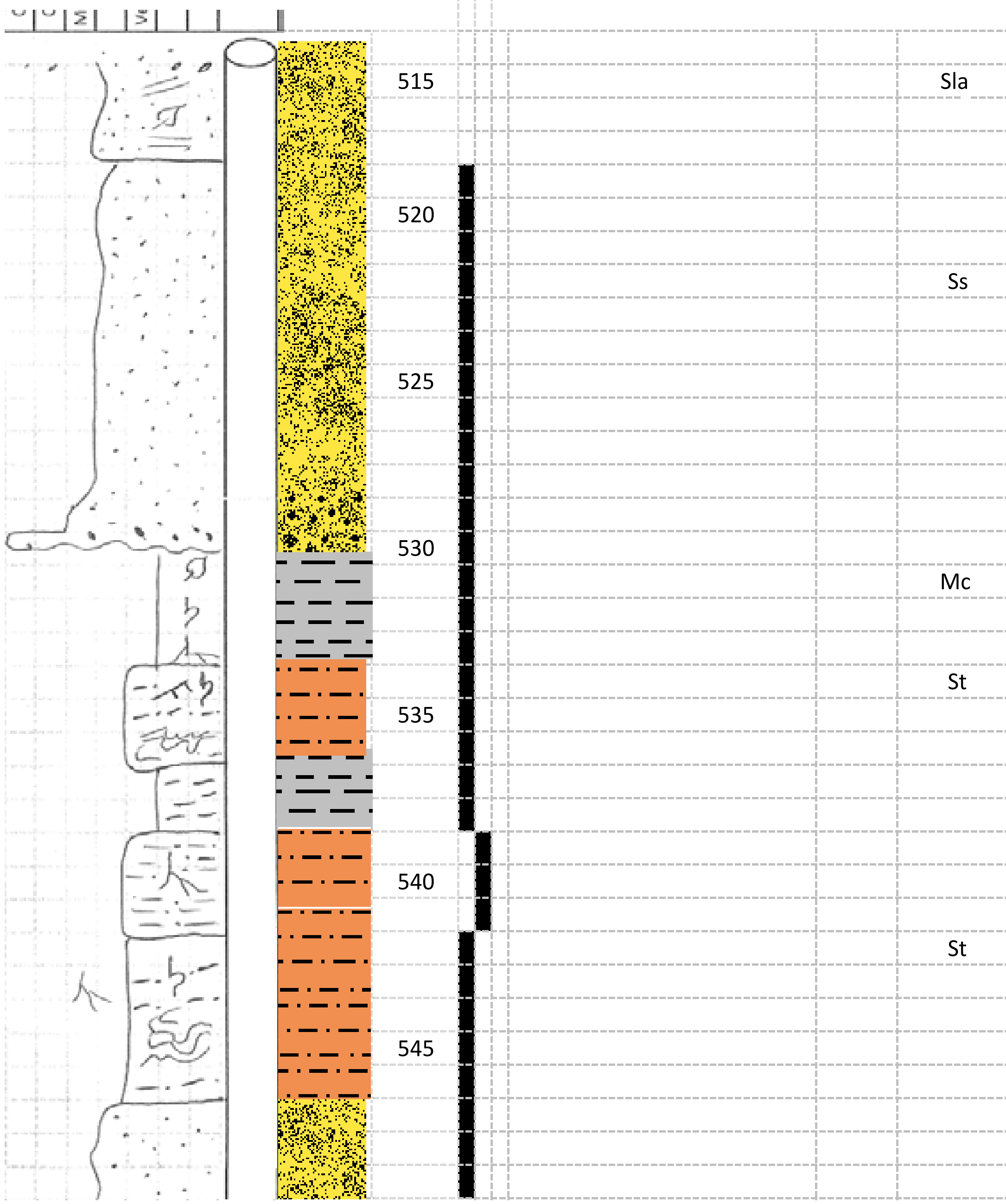

Well Name...............BT202- **Date**.....................

Page...1......... **Of**............

USGS Number

Conglomeratic Sandstone	Coarse Braned Sandstone	Medium Grained Sandstone	Fine Grained Sandstone	Siltstone	Claystone	Coal	Fractures	Lithology	Core Depth (feet)	High Bioturb	Moderate Bioturb	Low Bioturb	Description and Remarks	Depo. Invironments	Facies

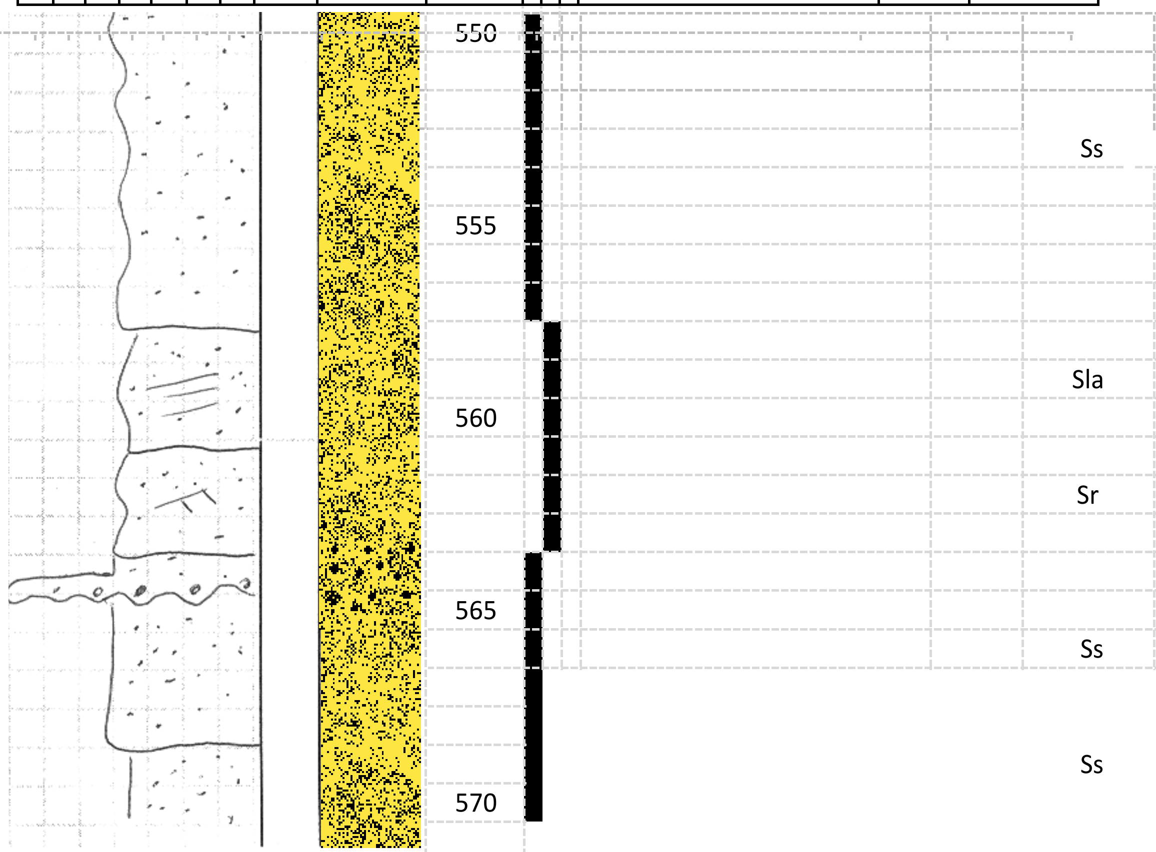

Well Name…BT202… **Date…………………**

Page…7……… Of…10…….

USGS Number

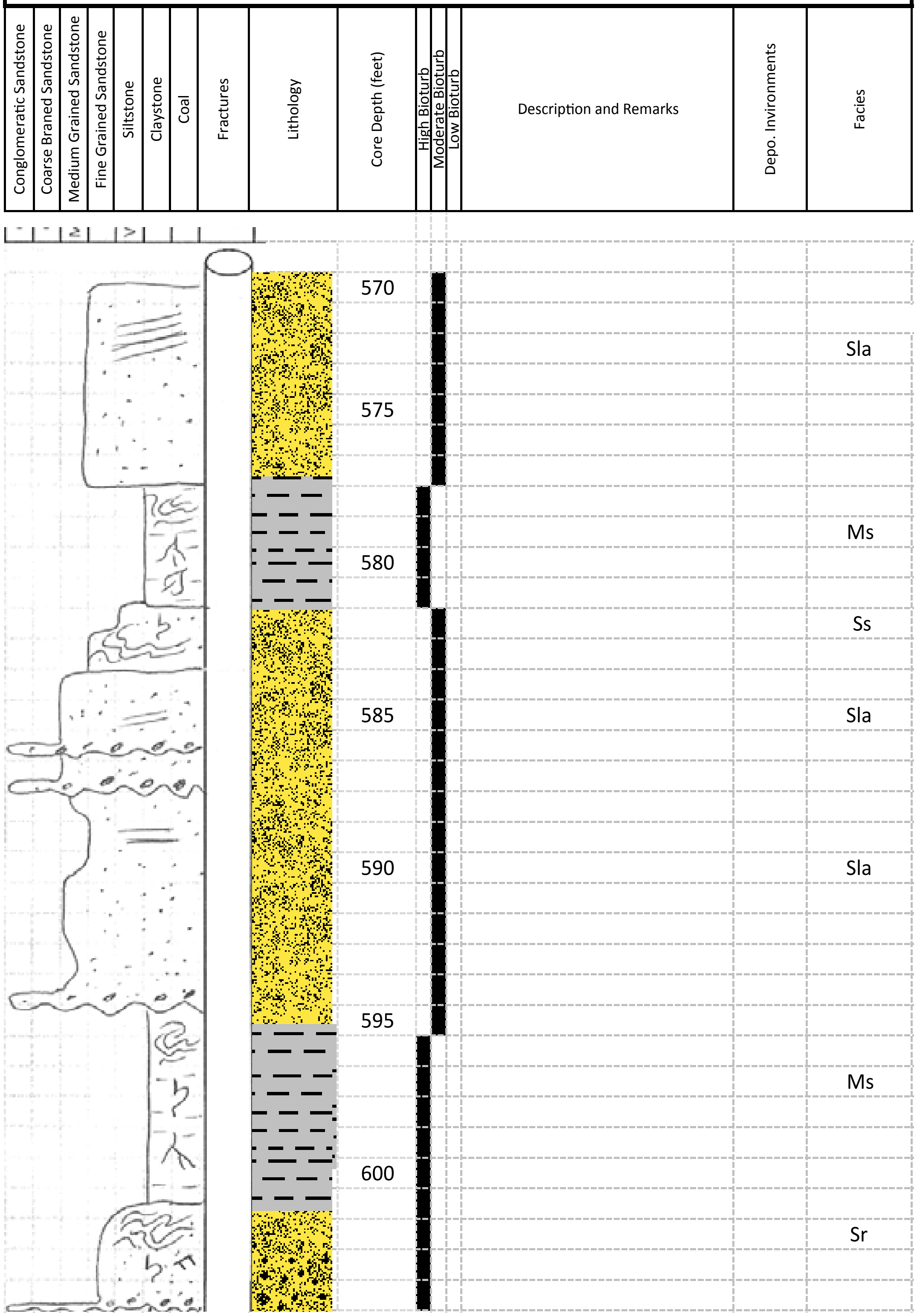

Well Name...............BT202- **Date**.....................

Page...1......... **Of**.............

USGS Number

Conglomeratic Sandstone	Coarse Braned Sandstone	Medium Grained Sandstone	Fine Grained Sandstone	Siltstone	Claystone	Coal	Fractures	Lithology	Core Depth (feet)	High Bioturb	Moderate Bioturb	Low Bioturb	Description and Remarks	Depo. Inviromments	Facies

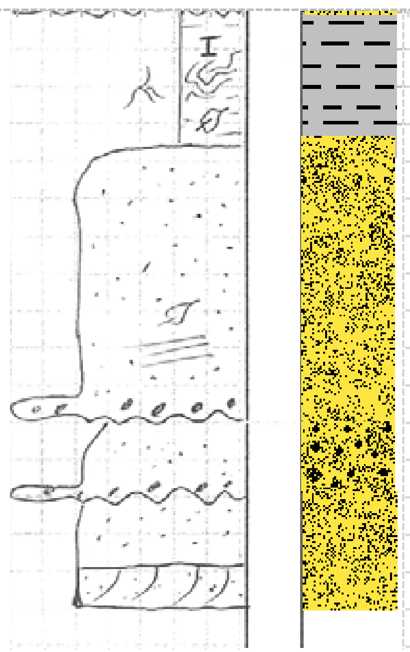

Core Depth (feet)	Facies
605	Ms
610	
	Sla
615	
	Ss
	Ss
620	Sha

Well Name............... **Date.....................**

Page...1......... Of.............

USGS Number

Conglomeratic Sandstone	Coarse Braned Sandstone	Medium Grained Sandstone	Fine Grained Sandstone	Siltstone	Claystone	Coal	Fractures	Lithology	Core Depth (feet)	High Bioturb	Moderate Bioturb	Low Bioturb	Description and Remarks	Depo. Invironments	Facies

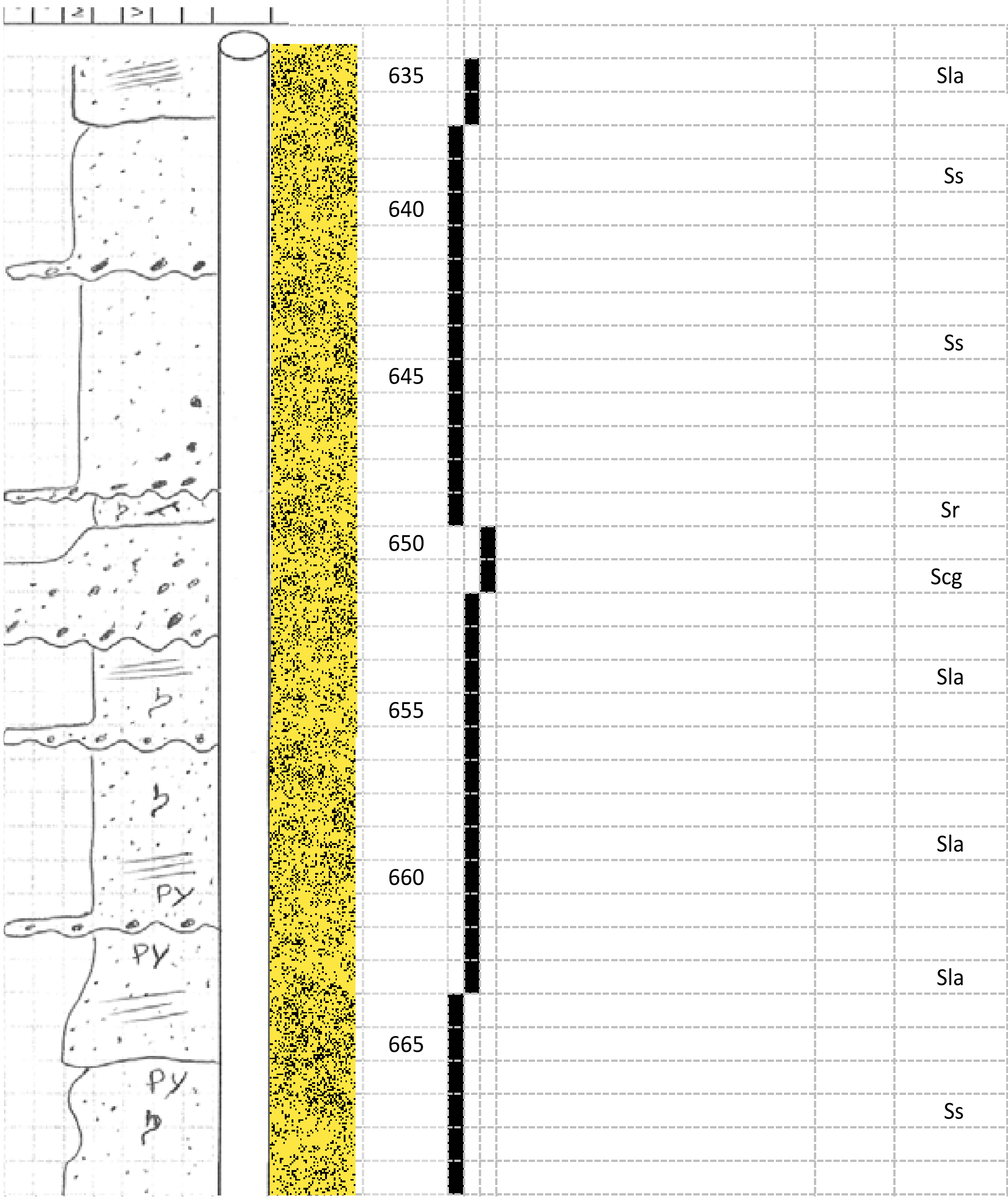

Well Name...BT202-1-10 Date.....................

Page...1......... Of...10...

USGS Number

Conglomeratic Sandstone	Coarse Braned Sandstone	Medium Grained Sandstone	Fine Grained Sandstone	Siltstone	Claystone	Coal	Fractures	Lithology	Core Depth (feet)	High Bioturb	Moderate Bioturb	Low Bioturb	Description and Remarks	Depo. Invironments	Facies

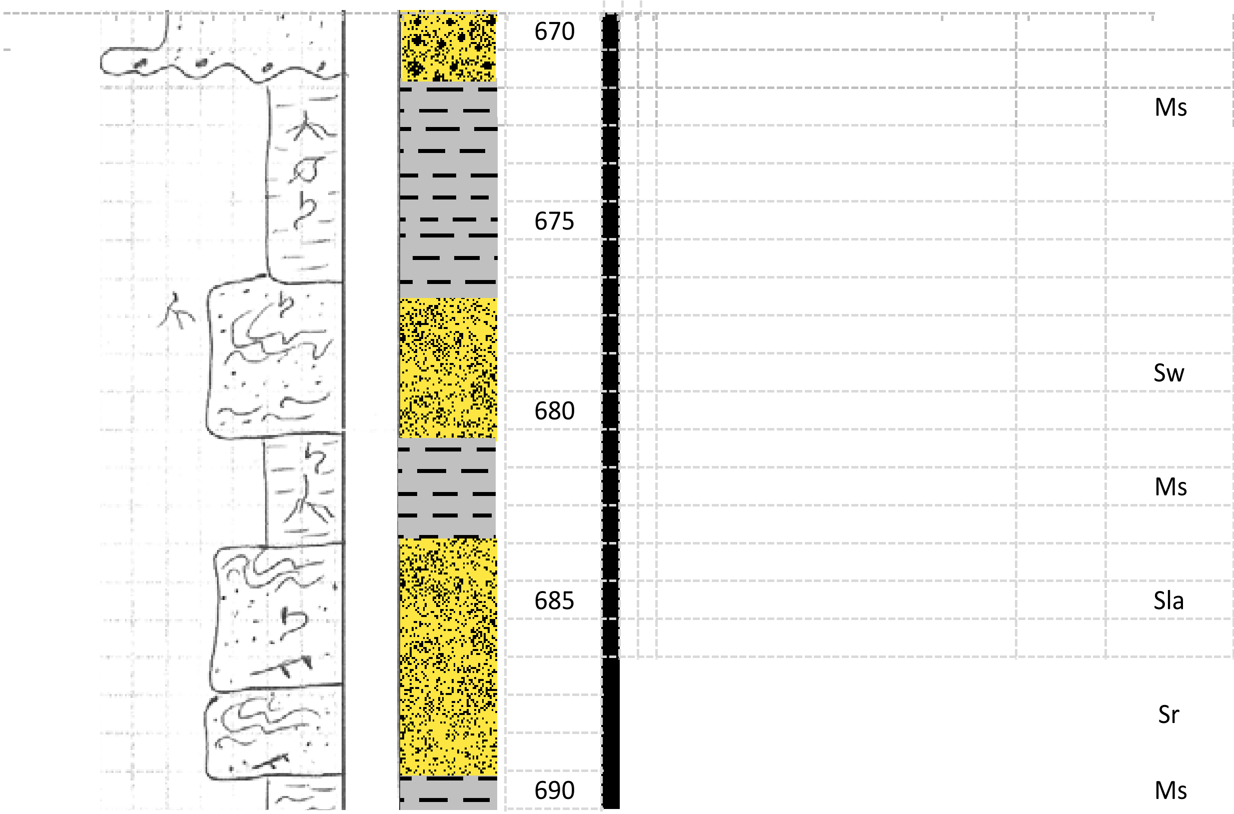

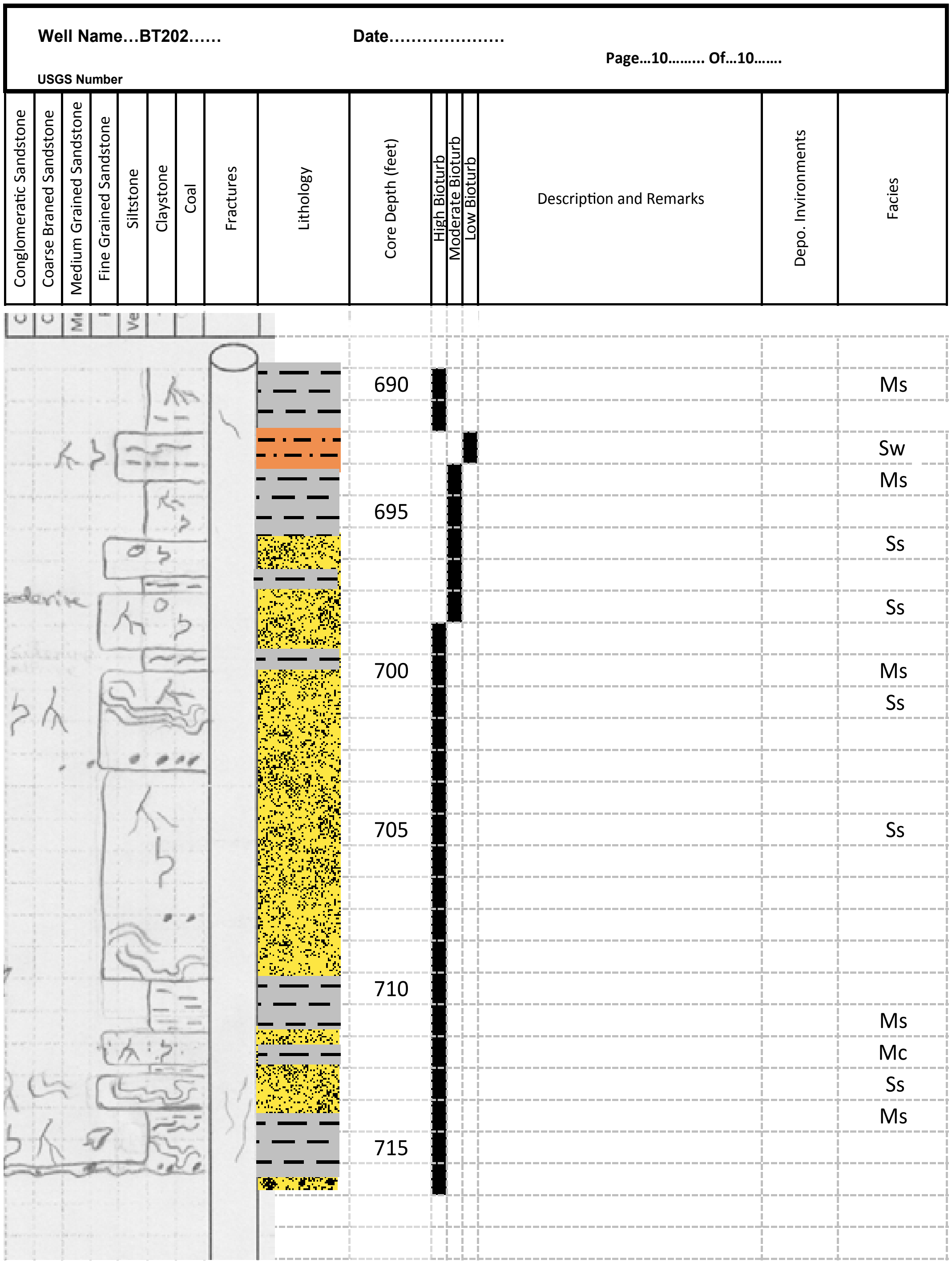

Well Name...BT202......
Date.....................
Page...10......... Of...10.......
USGS Number
Conglomeratic Sandstone
Coarse Braned Sandstone
Medium Grained Sandstone
Fine Grained Sandstone
Siltstone
Claystone
Coal
Fractures
Lithology
Core Depth (feet)
High Bioturb
Moderate Bioturb
Low Bioturb
Description and Remarks
Depo. Invironments
Facies
690
695
700
705
710
715
Ms
Sw
Ms
Ss
Ss
Ms
Ss
Ss
Ms
Mc
Ss
Ms

Grain Size and Sedimentary Structures
Sand
Mud
Coarse
Medium
Fine
V. Fine
Silt
Clay
Coal
Lithology
Depth (feet)
Biotrbation
Lithofacies
Facies Associations
PA 424-34
1 & 2
Facies Associations
FC Fluvial Channel
CS Crevasse Splays
FLS Floodplain – Swamps
Sandstone
Argillaceous Sandstone
Siltstone
Shale / Mudstone
Coal
High-angle cross-bedding
Low-angle cross-bedding
Horizontal lamination
Current-ripple lamination
Carbonaceous - organic material
Root traces
Coal stringers
Burrows
Deformed bedding
Mudstone clasts

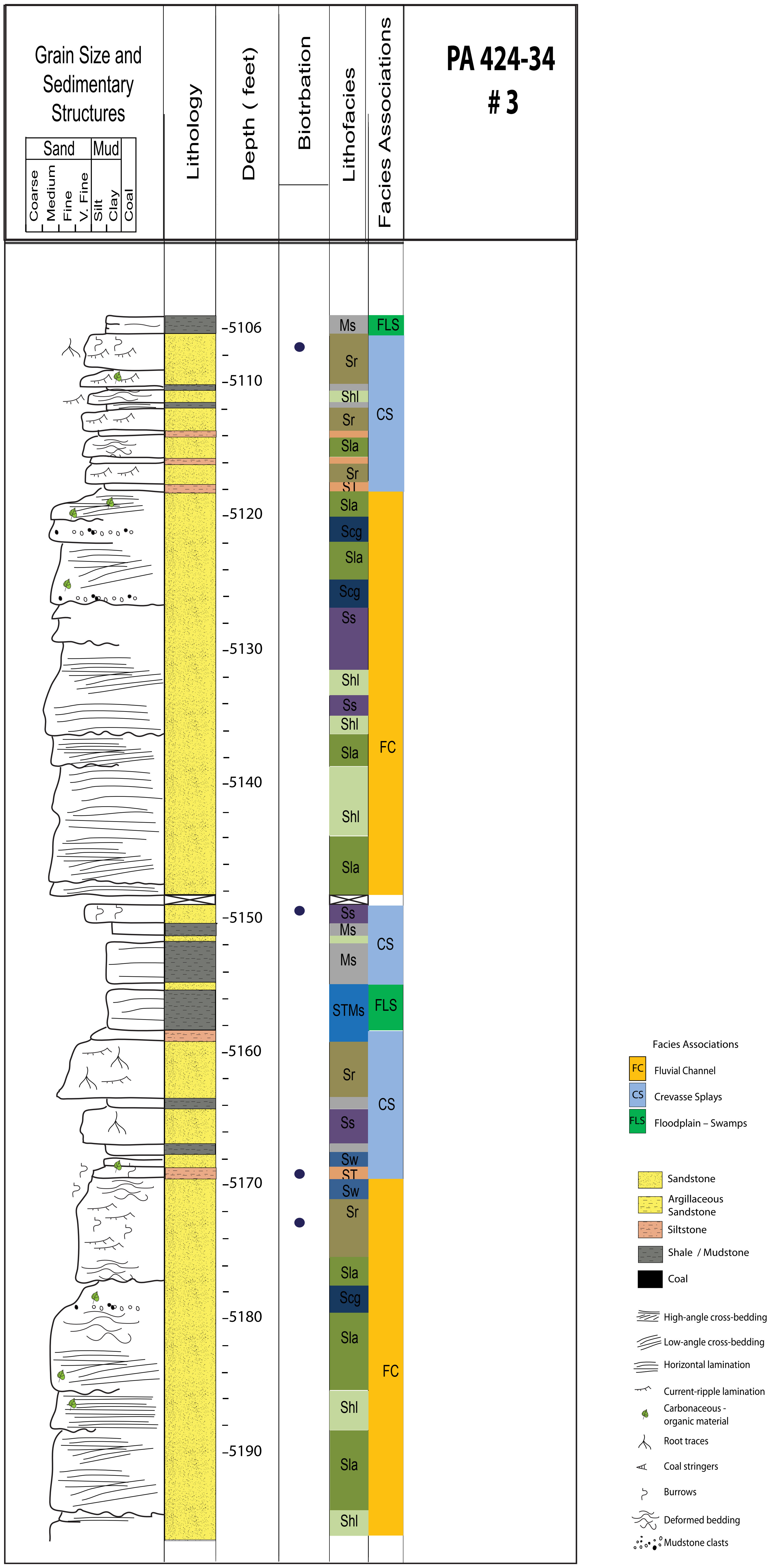

Grain Size and Sedimentary Structures
Sand
Mud
Coarse
Medium
Fine
V. Fine
Silt
Clay
Coal
Lithology
Depth (feet)
Biotrbation
Lithofacies
Facies Associations
PA 424-34
3
-5106
-5110
-5120
-5130
-5140
-5150
-5160
-5170
-5180
-5190
Ms
Sr
Shl
Sr
Sla
Sr
Sl
Sla
Scg
Sla
Scg
Ss
Shl
Ss
Shl
Sla
Shl
Sla
Ss
Ms
Ms
STMs
Sr
Ss
Sw
ST
Sw
Sr
Sla
Scg
Sla
Shl
Sla
Shl
FLS
CS
FC
CS
FLS
CS
FC
Facies Associations
FC
Fluvial Channel
CS
Crevasse Splays
FLS
Floodplain – Swamps
Sandstone
Argillaceous Sandstone
Siltstone
Shale / Mudstone
Coal
High-angle cross-bedding
Low-angle cross-bedding
Horizontal lamination
Current-ripple lamination
Carbonaceous - organic material
Root traces
Coal stringers
Burrows
Deformed bedding
Mudstone clasts

Grain Size and Sedimentary Structures
Sand
Mud
Coarse
Medium
Fine
V. Fine
Silt
Clay
Coal
Lithology
Depth (feet)
Biotrbation
Lithofacies
Facies Associations
PA 424-34
4 & 5
6071
6080
6090
6100
6110
6120
6130
6140
6150
6157
6582
6590
6600
6610
6620
6630
6640
6650
6660
6670
FLS
CS
FC
Facies Associations
FC Fluvial Channel
CS Crevasse Splays
FLS Floodplain – Swamps
Sandstone
Argillaceous Sandstone
Siltstone
Shale / Mudstone
Coal
High-angle cross-bedding
Low-angle cross-bedding
Horizontal lamination
Current-ripple lamination
Carbonaceous - organic material
Root traces
Coal stringers
Burrows
Deformed bedding
Mudstone clasts


Grain Size and Sedimentary Structures
Sand
Mud
Coarse
Medium
Fine
V. Fine
Silt
Clay
Coal
Lithology
Depth (feet)
Biotrbation
Lithofacies
Facies Associations
OXY
697-20-28
1
4680
4690
4780
4710
4720
4730
4740
4750
4760
4770
4780
4790
4800
4810
4820
4830
4840
4850
4860
Facies Associations
FC Fluvial Channel
CS Crevasse Splays
FLS Floodplain – Swamps
Sandstone
Argillaceous Sandstone
Siltstone
Shale / Mudstone
Coal
High-angle cross-bedding
Low-angle cross-bedding
Horizontal lamination
Current-ripple lamination
Carbonaceous - organic material
Root traces
Coal stringers
Burrows
Deformed bedding
Mudstone clasts


OXY
697-20-28
2
Grain Size and Sedimentary Structures
Sand
Mud
Coarse
Medium
Fine
V. Fine
Silt
Clay
Coal
Lithology
Depth (feet)
Biorbation
Lithofacies
Facies Associations
5180
5190
5200
5210
5220
5230
5240
5250
5260
5270
5280
5290
5300
5310
5220
5330
5340
5350
Facies Associations
FC Fluvial Channel
CS Crevasse Splays
FLS Floodplain – Swamps
Sandstone
Argillaceous Sandstone
Siltstone
Shale / Mudstone
Coal
High-angle cross-bedding
Low-angle cross-bedding
Horizontal lamination
Current-ripple lamination
Carbonaceous - organic material
Root traces
Coal stringers
Burrows
Deformed bedding
Mudstone clasts


OXY
697-20-28
3
Grain Size and Sedimentary Structures
Sand
Mud
Coarse
Medium
Fine
V. Fine
Silt
Clay
Coal
Lithology
Depth (feet)
Biotrbation
Lithofacies
Facies Associations
6110
6120
6130
6140
6150
6160
6170
6180
6190
6200
6210
6220
6230
6240
6250
6260
6270
6280
6290
6300
6306
Facies Associations
FC Fluvial Channel
CS Crevasse Splays
FLS Floodplain – Swamps
Sandstone
Argillaceous Sandstone
Siltstone
Shale / Mudstone
Coal
High-angle cross-bedding
Low-angle cross-bedding
Horizontal lamination
Current-ripple lamination
Carbonaceous - organic material
Root traces
Coal stringers
Burrows
Deformed bedding
Mudstone clasts


LastDance
Grain Size and Sedimentary Structures
Sand
Mud
Coarse
Medium
Fine
V. Fine
Silt
Clay
Coal
Lithology
Depth (feet)
Bioturbation
Lithofacies
Facies Associations
Facies Associations
FC Fluvial Channel
CS Crevasse Splays
FLS Floodplain – Swamps
Sandstone
Argillaceous Sandstone
Siltstone
Shale / Mudstone
Coal
High-angle cross-bedding
Low-angle cross-bedding
Horizontal lamination
Current-ripple lamination
Carbonaceous - organic material
Root traces
Coal stringers
Burrows
Deformed bedding
Mudstone clasts

Cactus Valley 1 D111

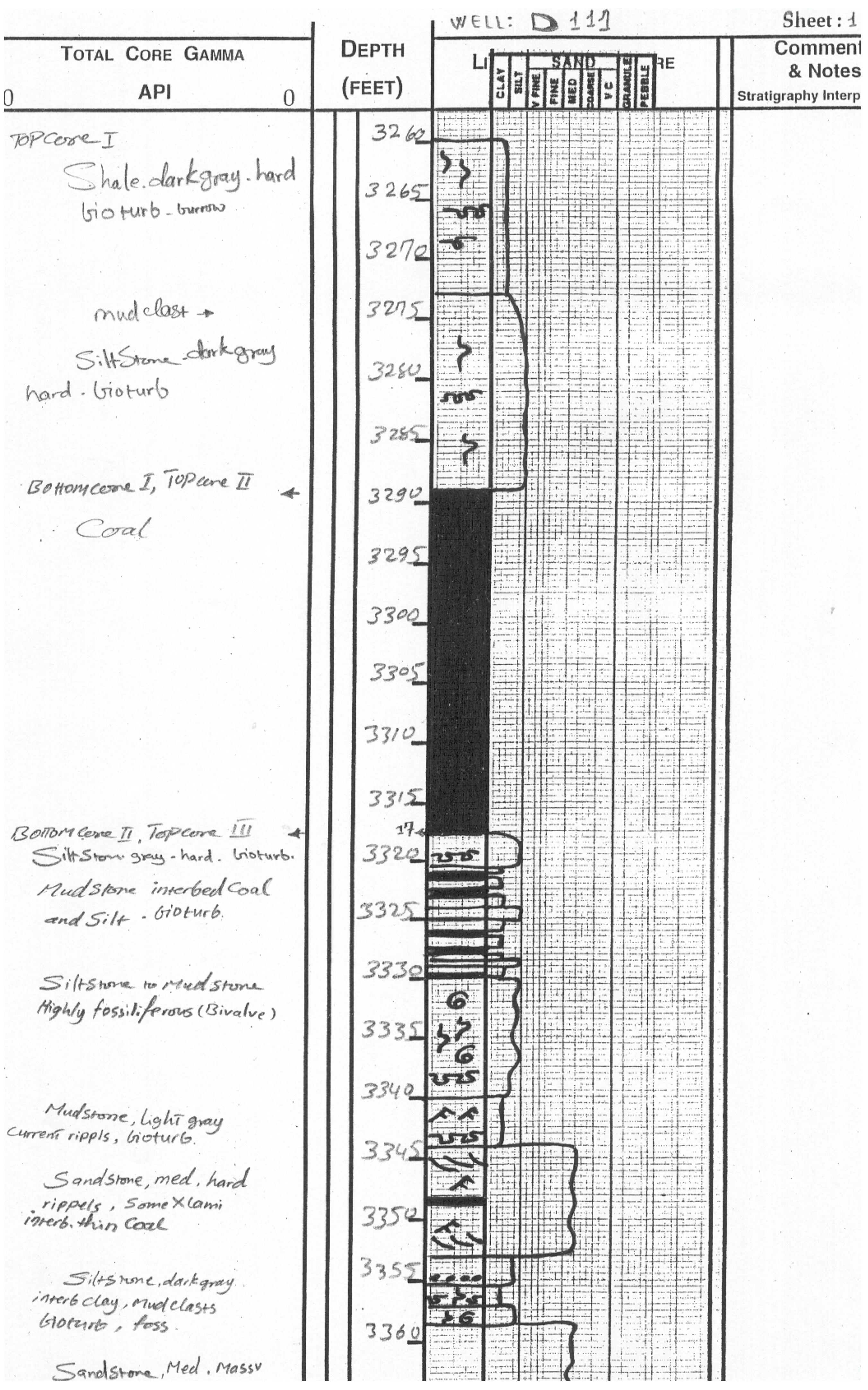

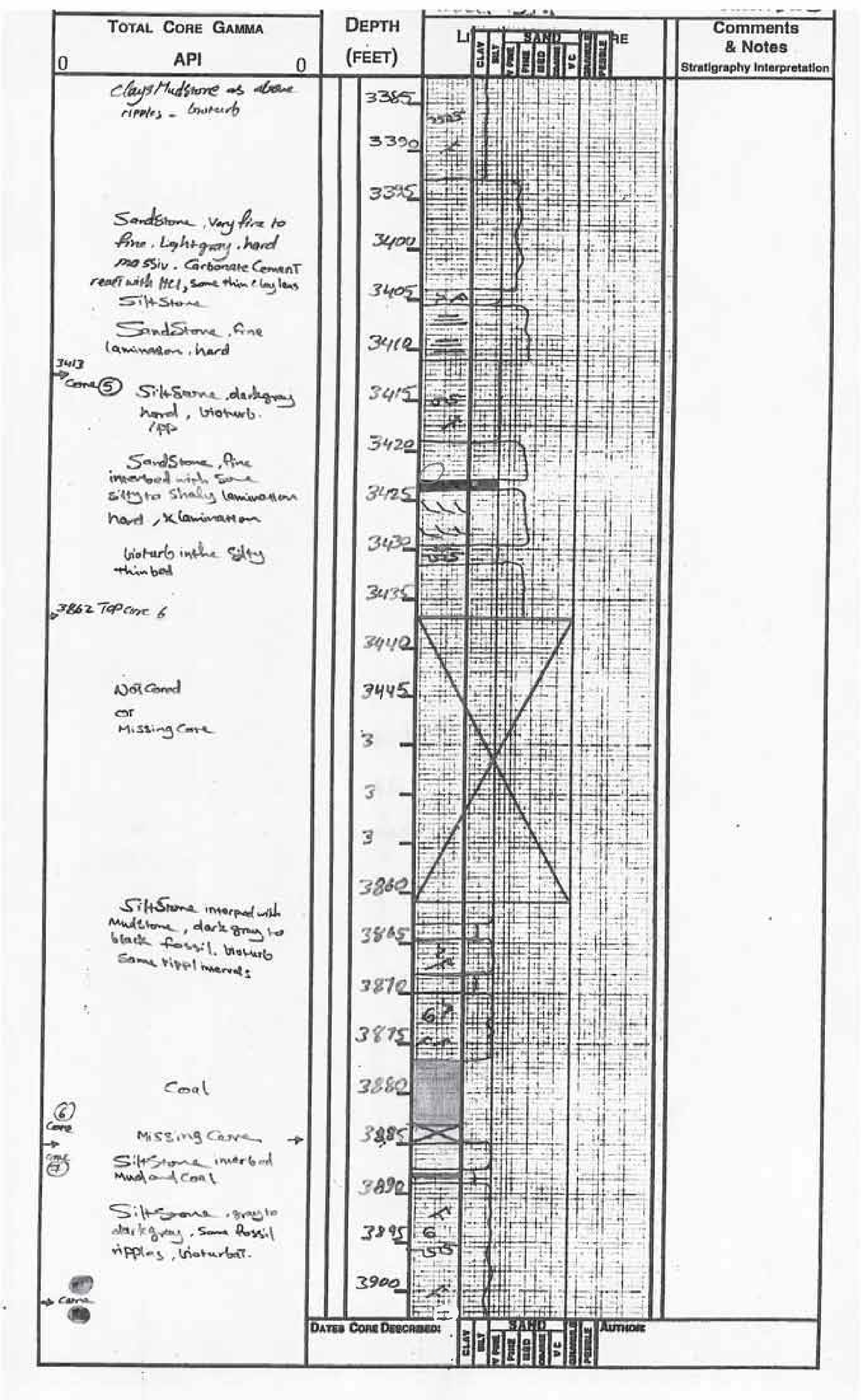

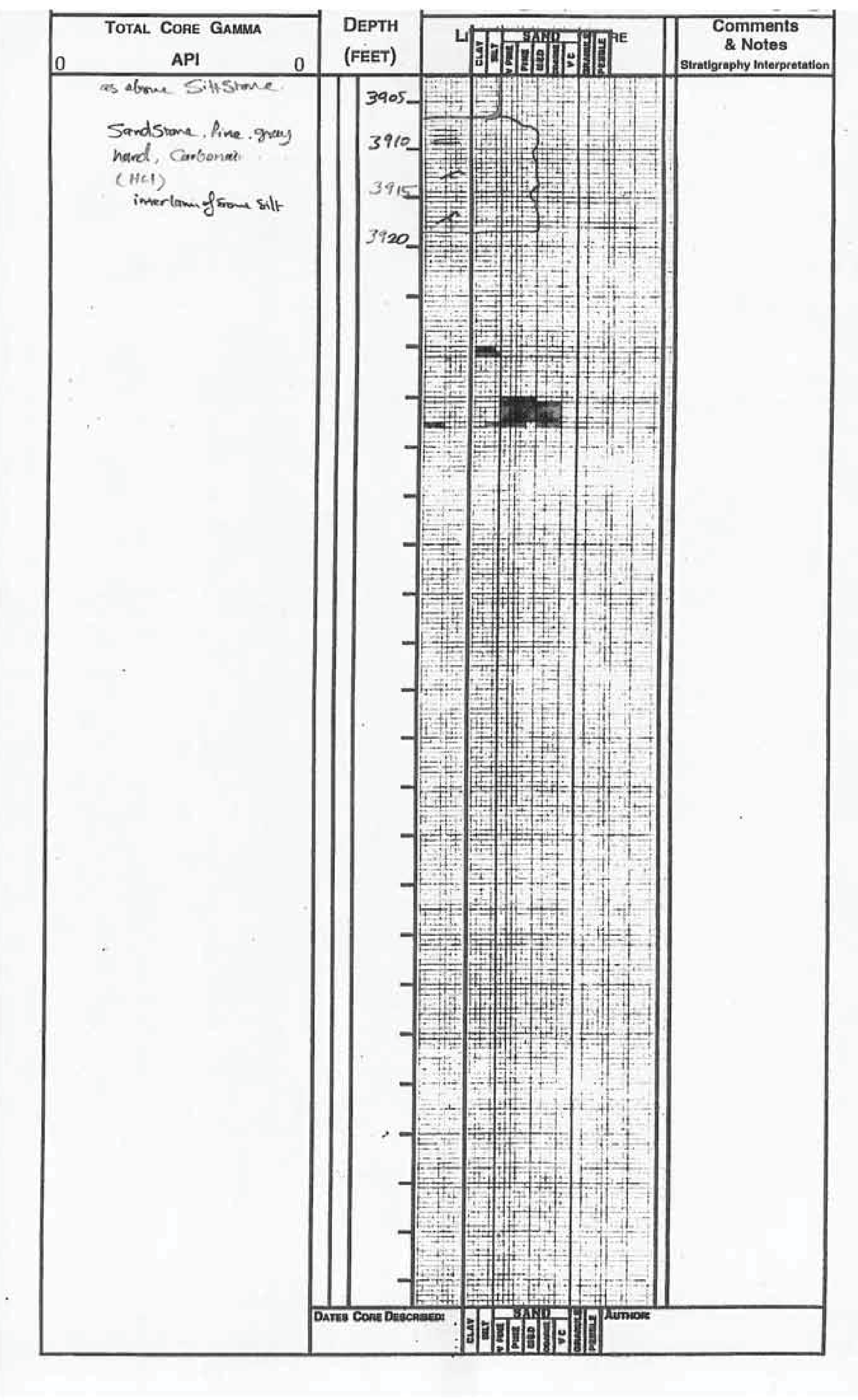

Appendix C – XRD Data

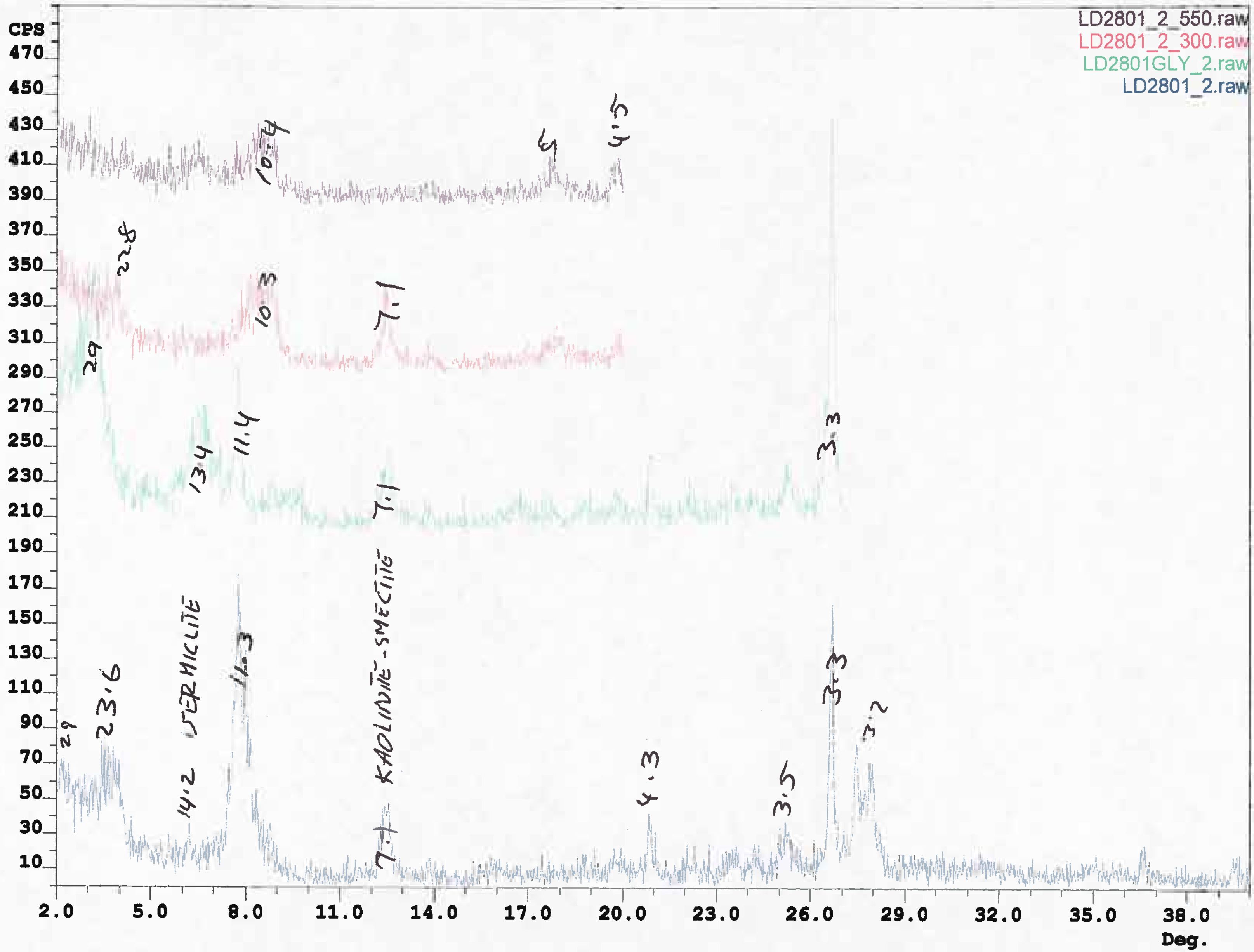
LD2801_2_550.raw
LD2801_2_300.raw
LD2801GLY_2.raw
LD2801_2.raw
CPS
470
450
430
410
390
370
350
330
310
290
270
250
230
210
190
170
150
130
110
90
70
50
30
10
2.0
5.0
8.0
11.0
14.0
17.0
20.0
23.0
26.0
29.0
32.0
35.0
38.0
Deg.
10.4
5
4.5
22.8
10.3
7.1
29
13.4
11.4
7.1
3.3
29
23.6
VERMICLITE
14.2
10.3
KAOLINITE-SMECTITE
7.1
4.3
3.5
3.3
3.2

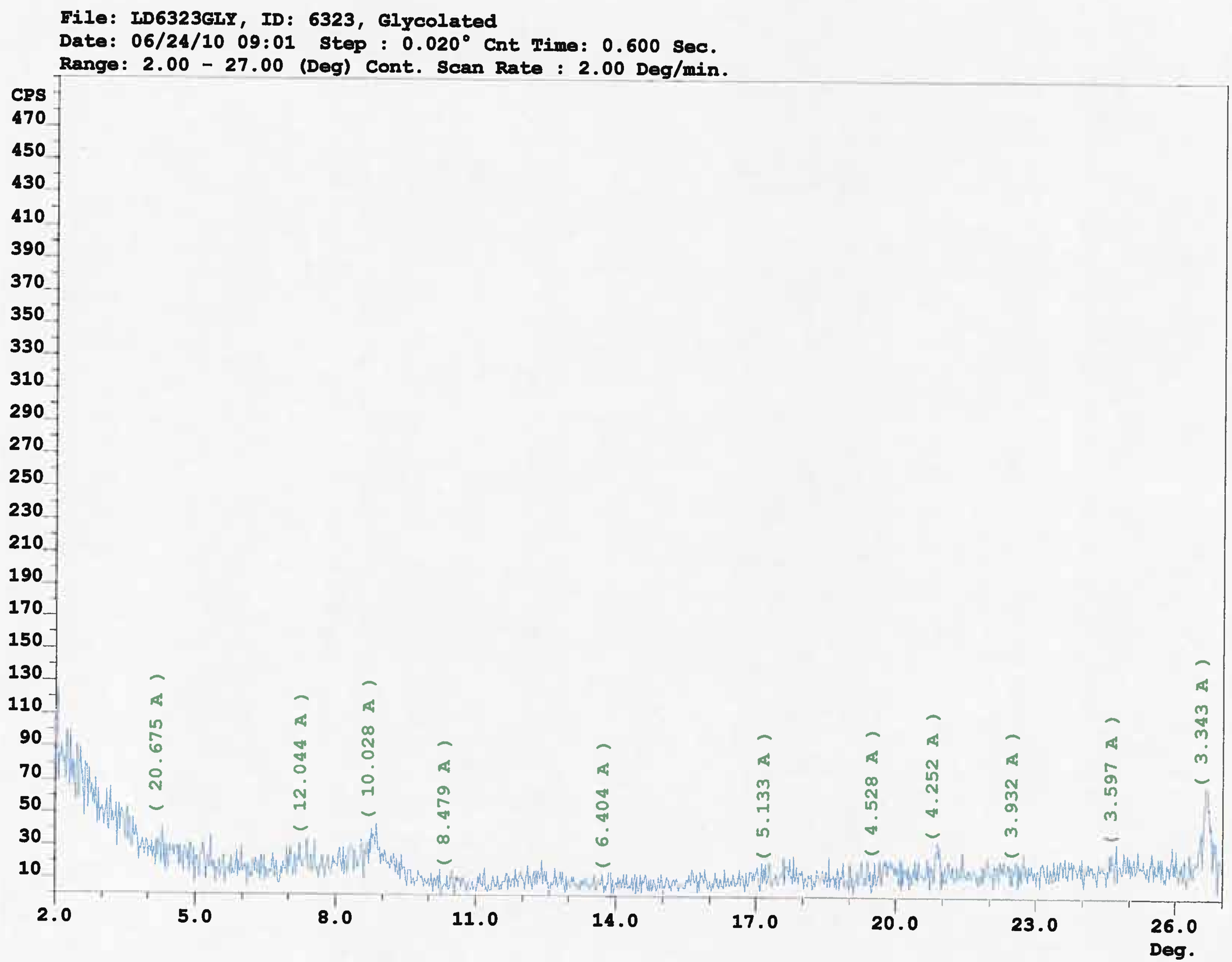
File: LD6323GLY, ID: 6323, Glycolated
Date: 06/24/10 09:01 Step : 0.020° Cnt Time: 0.600 Sec.
Range: 2.00 - 27.00 (Deg) Cont. Scan Rate : 2.00 Deg/min.
CPS
470
450
430
410
390
370
350
330
310
290
270
250
230
210
190
170
150
130
110
90
70
50
30
10
(20.675 A)
(12.044 A)
(10.028 A)
(8.479 A)
(6.404 A)
(5.133 A)
(4.528 A)
(4.252 A)
(3.932 A)
(3.597 A)
(3.343 A)
2.0
5.0
8.0
11.0
14.0
17.0
20.0
23.0
26.0
Deg.

239

File: LD6323GLY, ID: 6323, Glycolated
Date: 06/24/10 09:01 Step : 0.020° Cnt Time: 0.600 Sec.
Range: 2.00 - 27.00 (Deg) Cont. Scan Rate : 2.00 Deg/min.

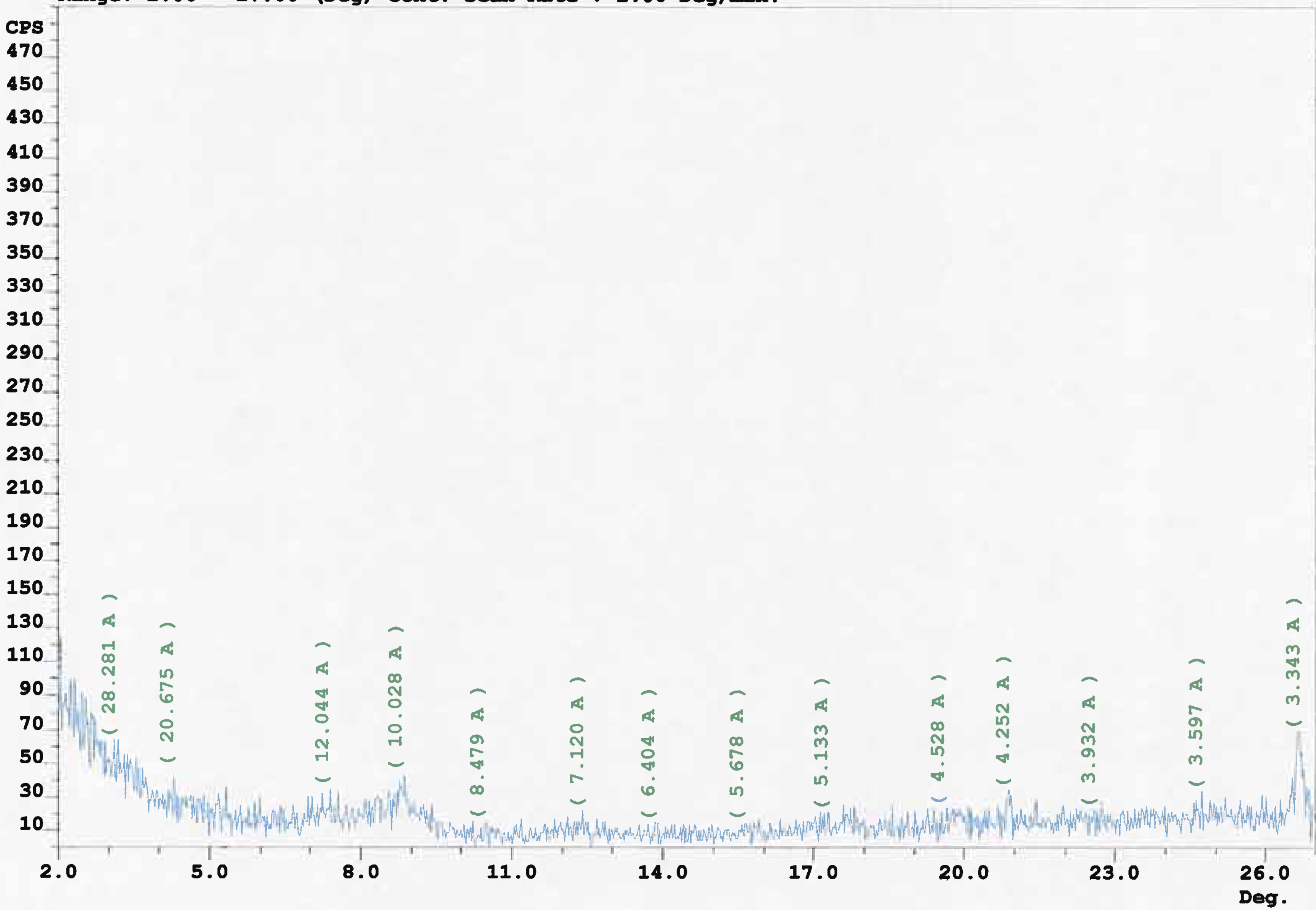

File: LD6323_300, ID: 6323, 300C
Date: 06/24/10 14:32 Step : 0.020° Cnt Time: 0.600 Sec.
Range: 2.00 - 20.00 (Deg) Cont. Scan Rate : 2.00 Deg/min.

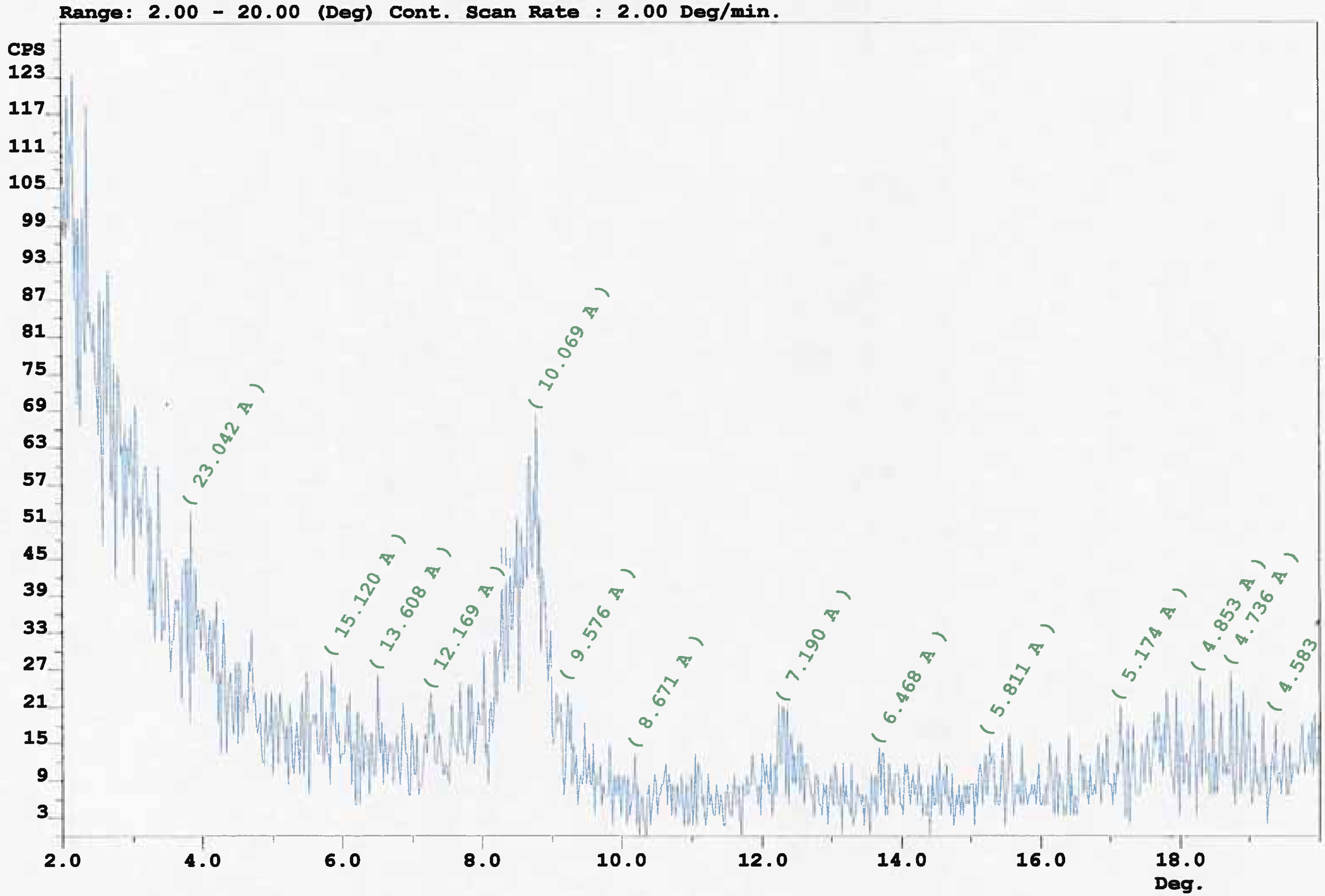

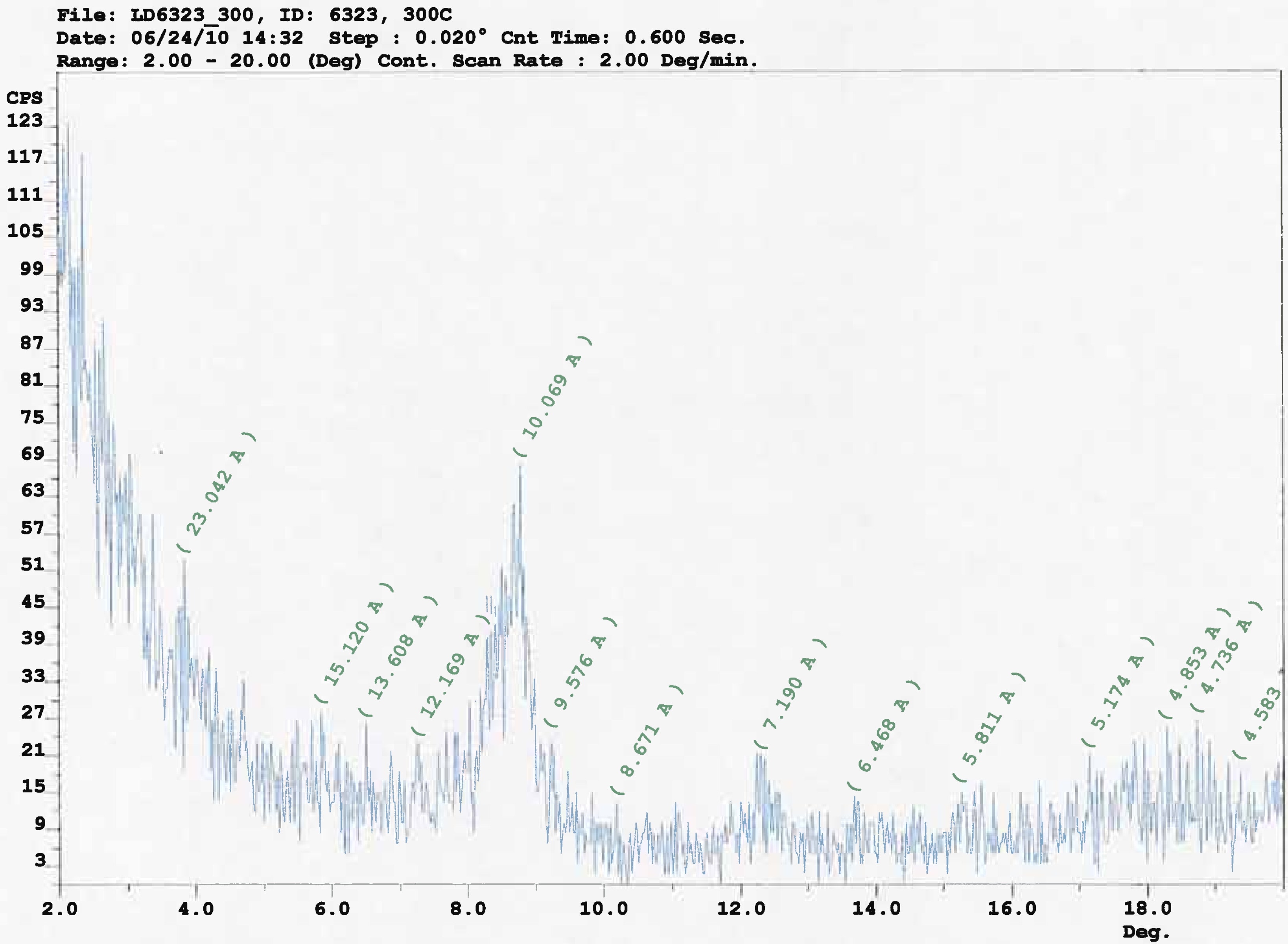

File: LD6323_300, ID: 6323, 300C
Date: 06/24/10 14:32 Step : 0.020° Cnt Time: 0.600 Sec.
Range: 2.00 - 20.00 (Deg) Cont. Scan Rate : 2.00 Deg/min.
CPS
123
117
111
105
99
93
87
81
75
69
63
57
51
45
39
33
27
21
15
9
3
(23.042 A)
(15.120 A)
(13.608 A)
(12.169 A)
(10.069 A)
(9.576 A)
(8.671 A)
(7.190 A)
(6.468 A)
(5.811 A)
(5.174 A)
(4.853 A)
(4.736 A)
(4.583
2.0
4.0
6.0
8.0
10.0
12.0
14.0
16.0
18.0
Deg.

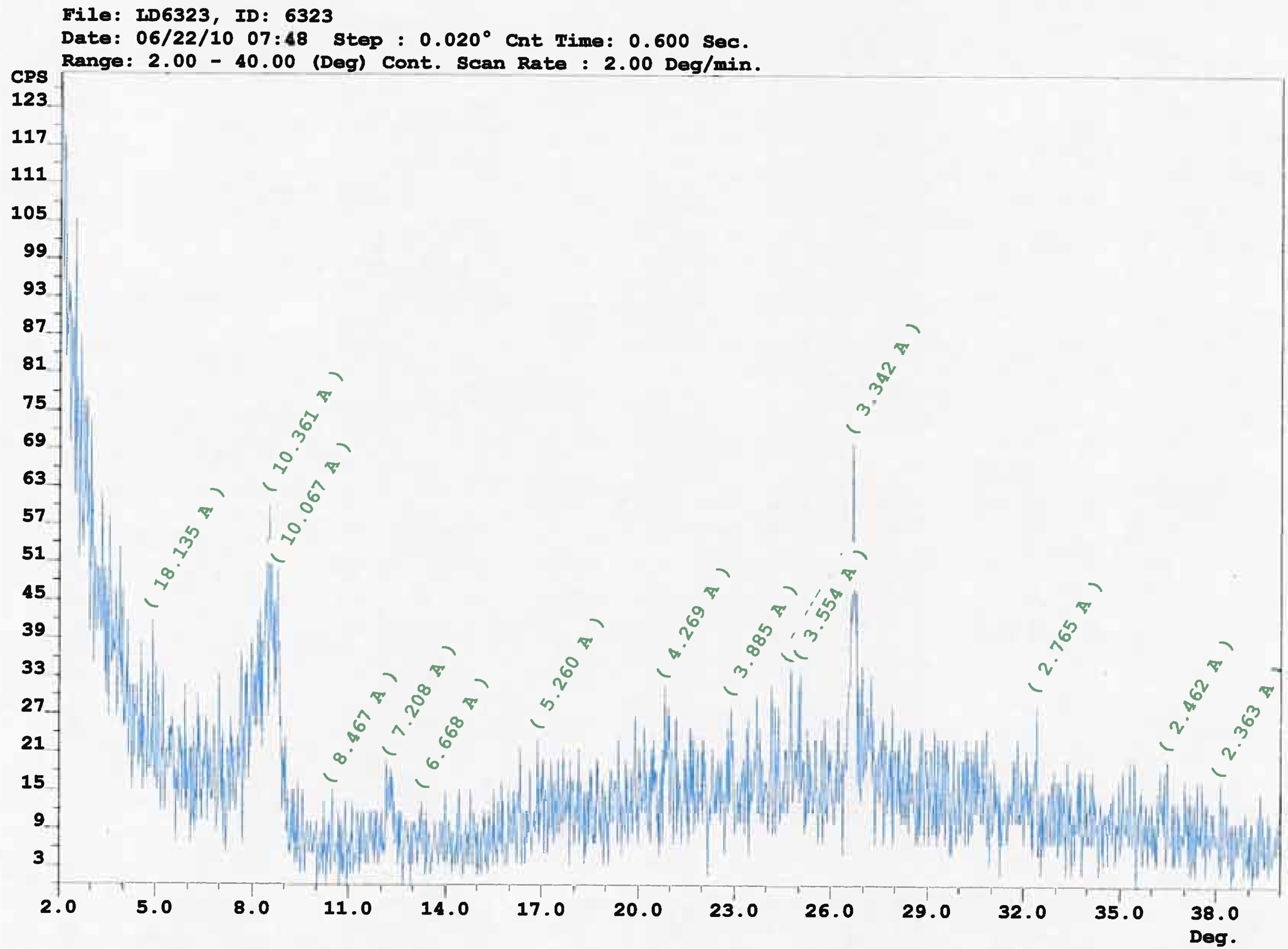
File: LD6323, ID: 6323
Date: 06/22/10 07:48 Step : 0.020° Cnt Time: 0.600 Sec.
Range: 2.00 - 40.00 (Deg) Cont. Scan Rate : 2.00 Deg/min.
CPS
123
117
111
105
99
93
87
81
75
69
63
57
51
45
39
33
27
21
15
9
3
(18.135 A)
(10.361 A)
(10.067 A)
(8.467 A)
(7.208 A)
(6.668 A)
(5.260 A)
(4.269 A)
(3.885 A)
(3.554 A)
(3.342 A)
(2.765 A)
(2.462 A)
(2.363 A
2.0
5.0
8.0
11.0
14.0
17.0
20.0
23.0
26.0
29.0
32.0
35.0
38.0
Deg.

243

File: LD6323, ID: 6323
Date: 06/22/10 07:48 Step : 0.020° Cnt Time: 0.600 Sec.
Range: 2.00 - 40.00 (Deg) Cont. Scan Rate : 2.00 Deg/min.

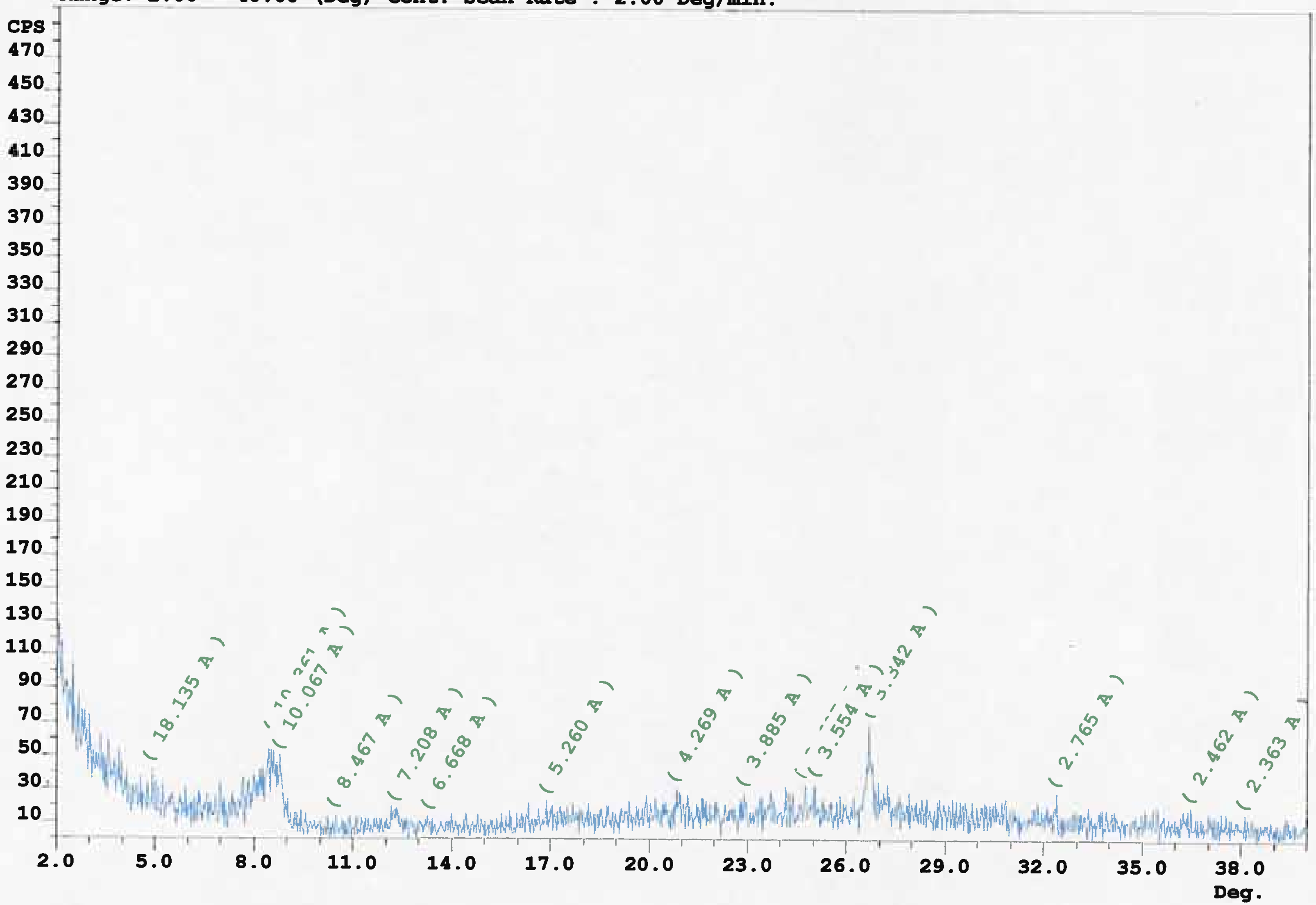

File: LD6315, ID: 6315, Clay Separation
Date: 07/27/10 14:47 Step : 0.020° Cnt Time: 0.600 Sec.
Range: 2.00 - 40.00 (Deg) Cont. Scan Rate : 2.00 Deg/min.

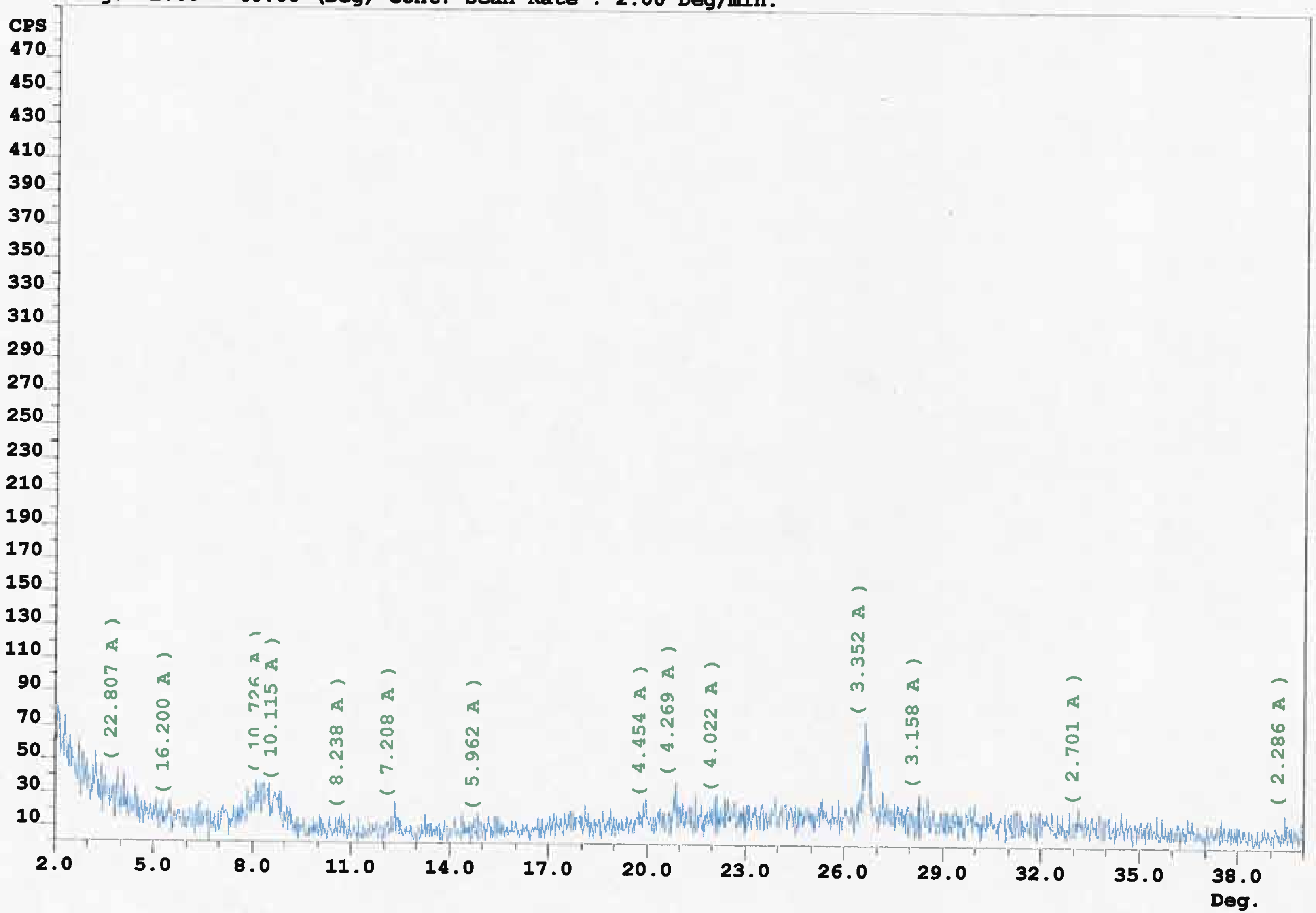

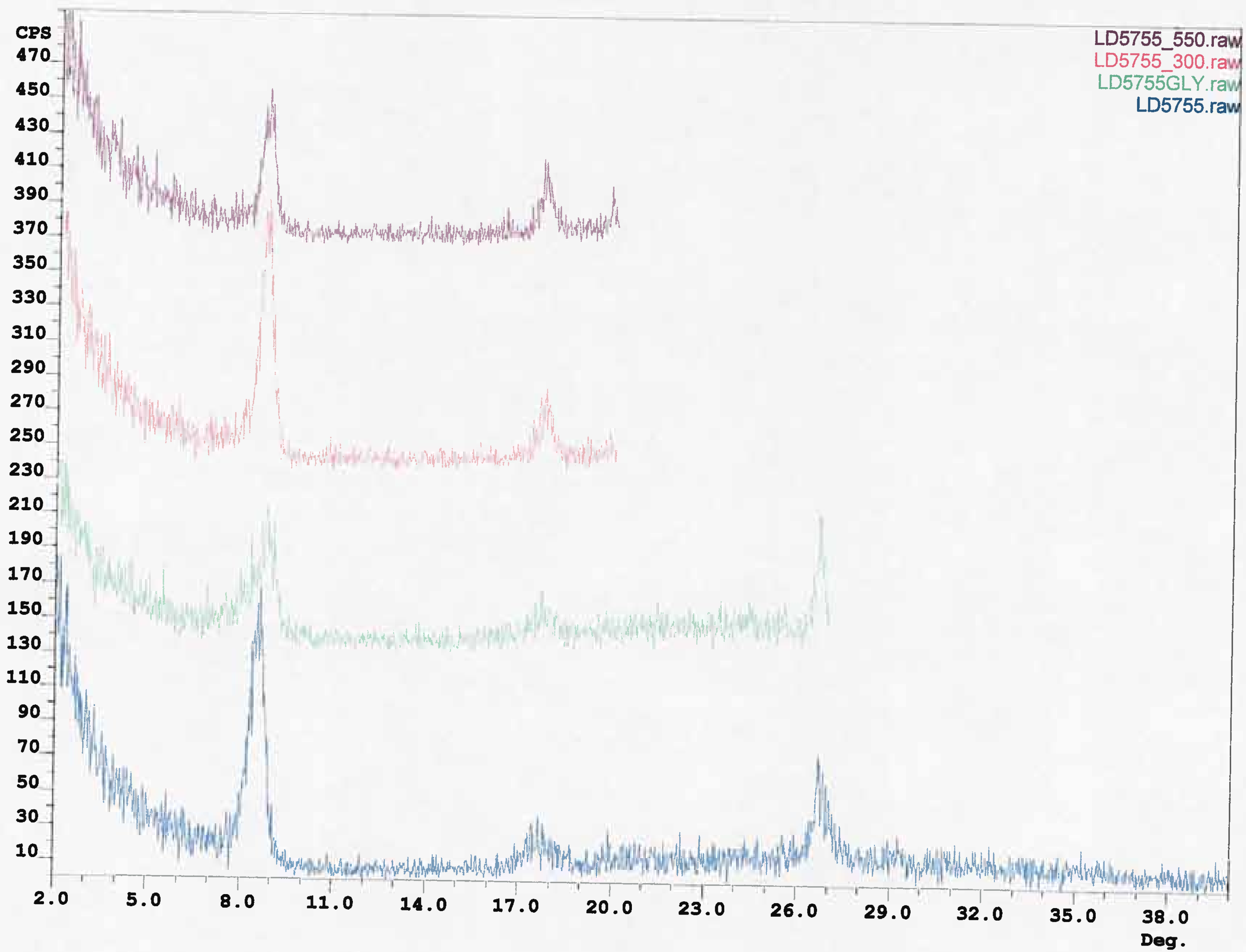
LD5755_550.raw
LD5755_300.raw
LD5755GLY.raw
LD5755.raw
CPS
470
450
430
410
390
370
350
330
310
290
270
250
230
210
190
170
150
130
110
90
70
50
30
10
2.0
5.0
8.0
11.0
14.0
17.0
20.0
23.0
26.0
29.0
32.0
35.0
38.0
Deg.

File: LD2801GLY, ID: 2801, Glycolated
Date: 08/30/10 08:54 Step : 0.020° Cnt Time: 0.600 Sec.
Range: 2.00 - 27.00 (Deg) Cont. Scan Rate : 2.00 Deg/min.

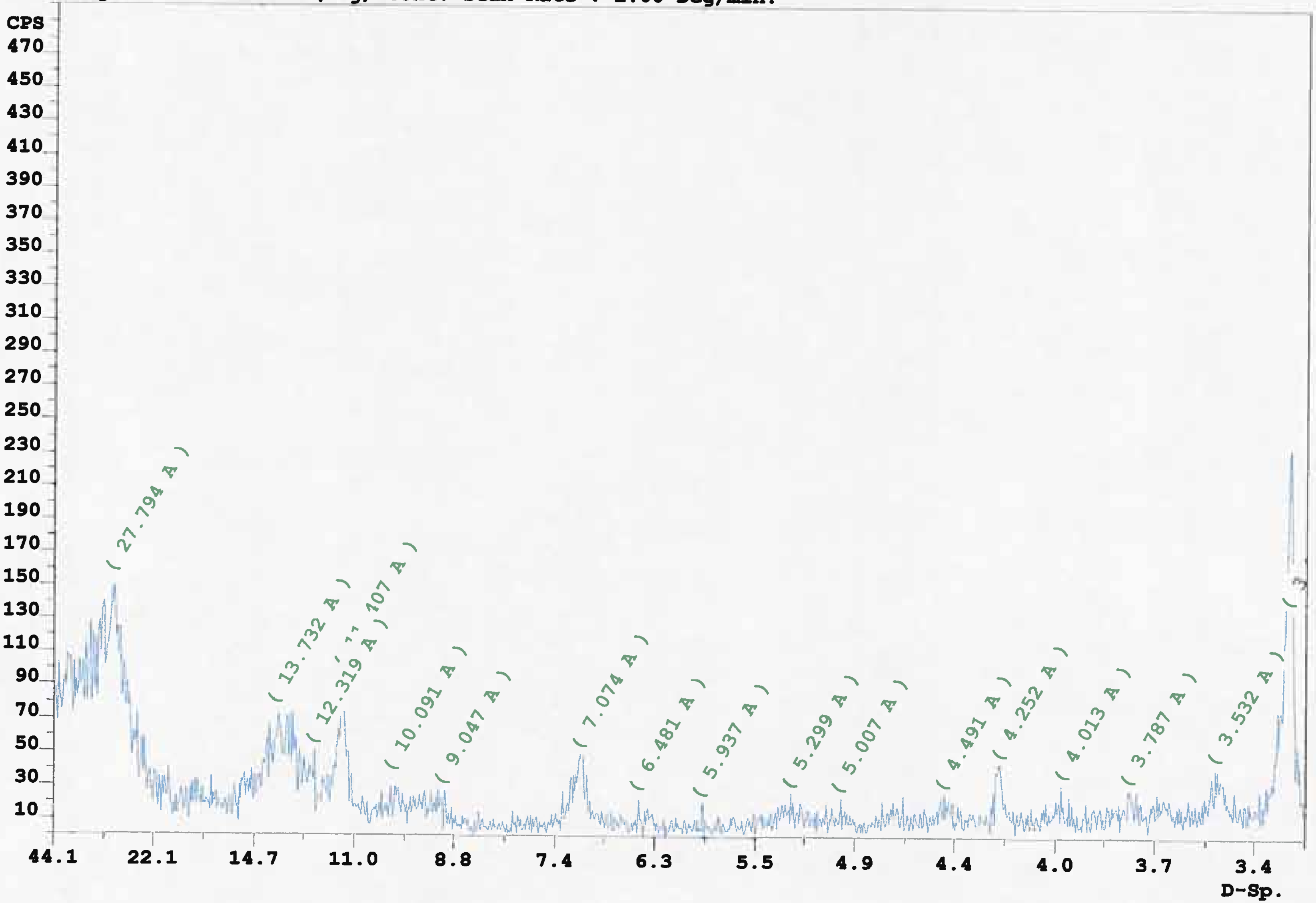

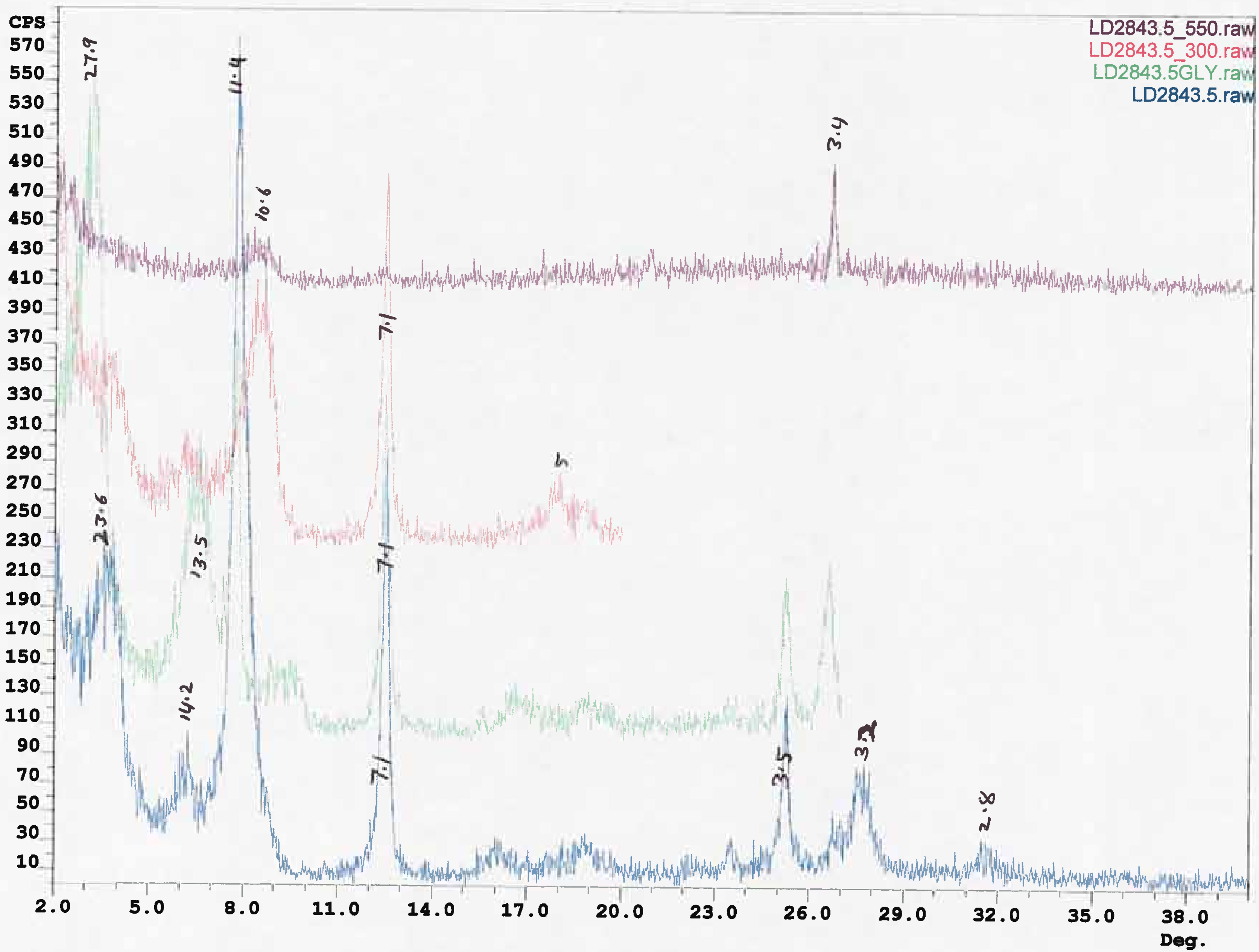
LD2843.5_550.raw
LD2843.5_300.raw
LD2843.5GLY.raw
LD2843.5.raw
CPS
570
550
530
510
490
470
450
430
410
390
370
350
330
310
290
270
250
230
210
190
170
150
130
110
90
70
50
30
10
2.0
5.0
8.0
11.0
14.0
17.0
20.0
23.0
26.0
29.0
32.0
35.0
38.0
Deg.
27.9
11.4
10.6
3.4
7.1
5
23.6
13.5
7.1
14.2
7.1
3.5
3.2
2.8

File: LD2801GLY, ID: 2801, Glycolated
Date: 08/30/10 08:54 Step : 0.020° Cnt Time: 0.600 Sec.
Range: 2.00 - 27.00 (Deg) Cont. Scan Rate : 2.00 Deg/min.

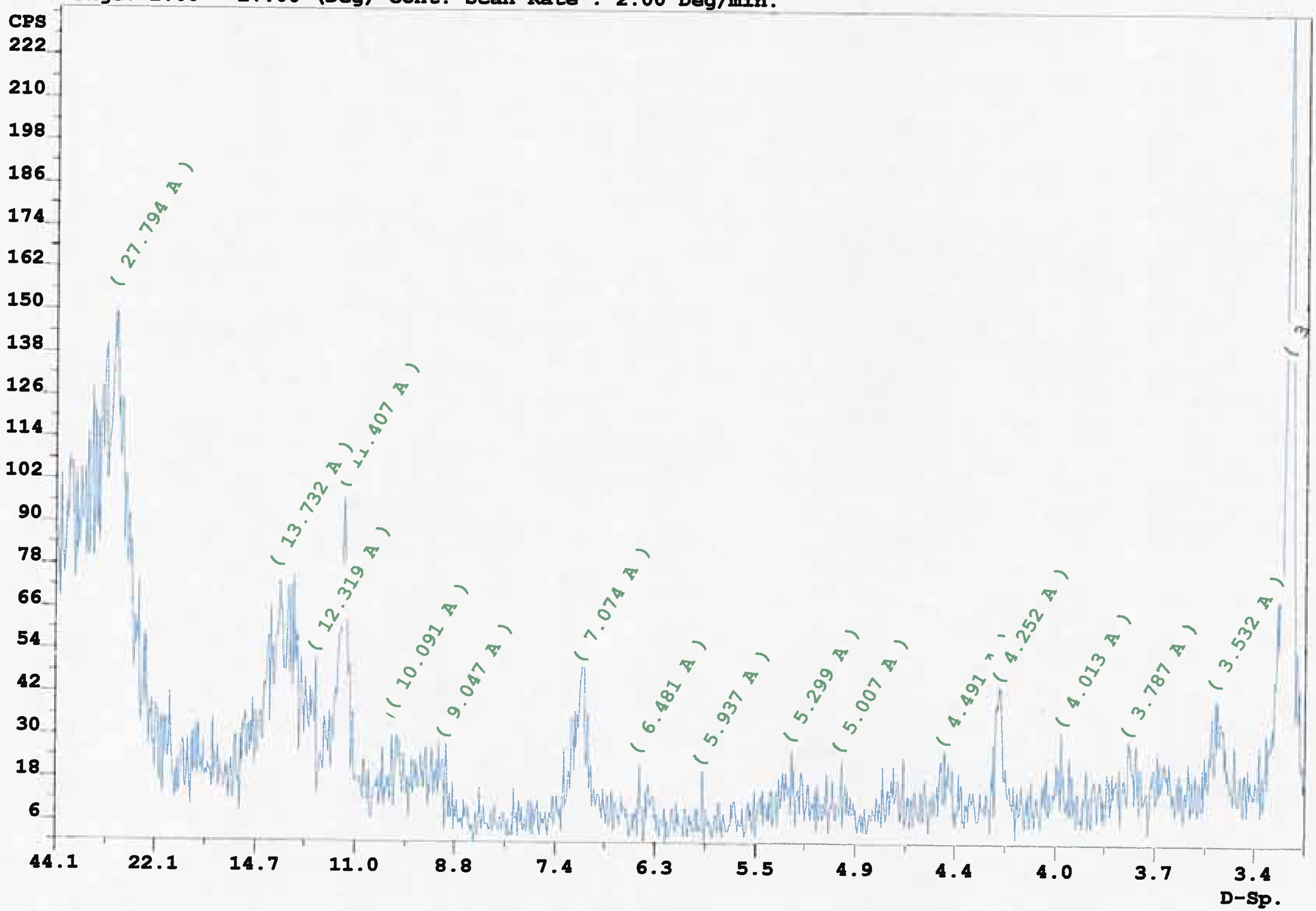

249

File: LD2801GLY, ID: 2801, Glycolated
Date: 08/30/10 08:54 Step : 0.020° Cnt Time: 0.600 Sec.
Range: 2.00 - 27.00 (Deg) Cont. Scan Rate : 2.00 Deg/min.

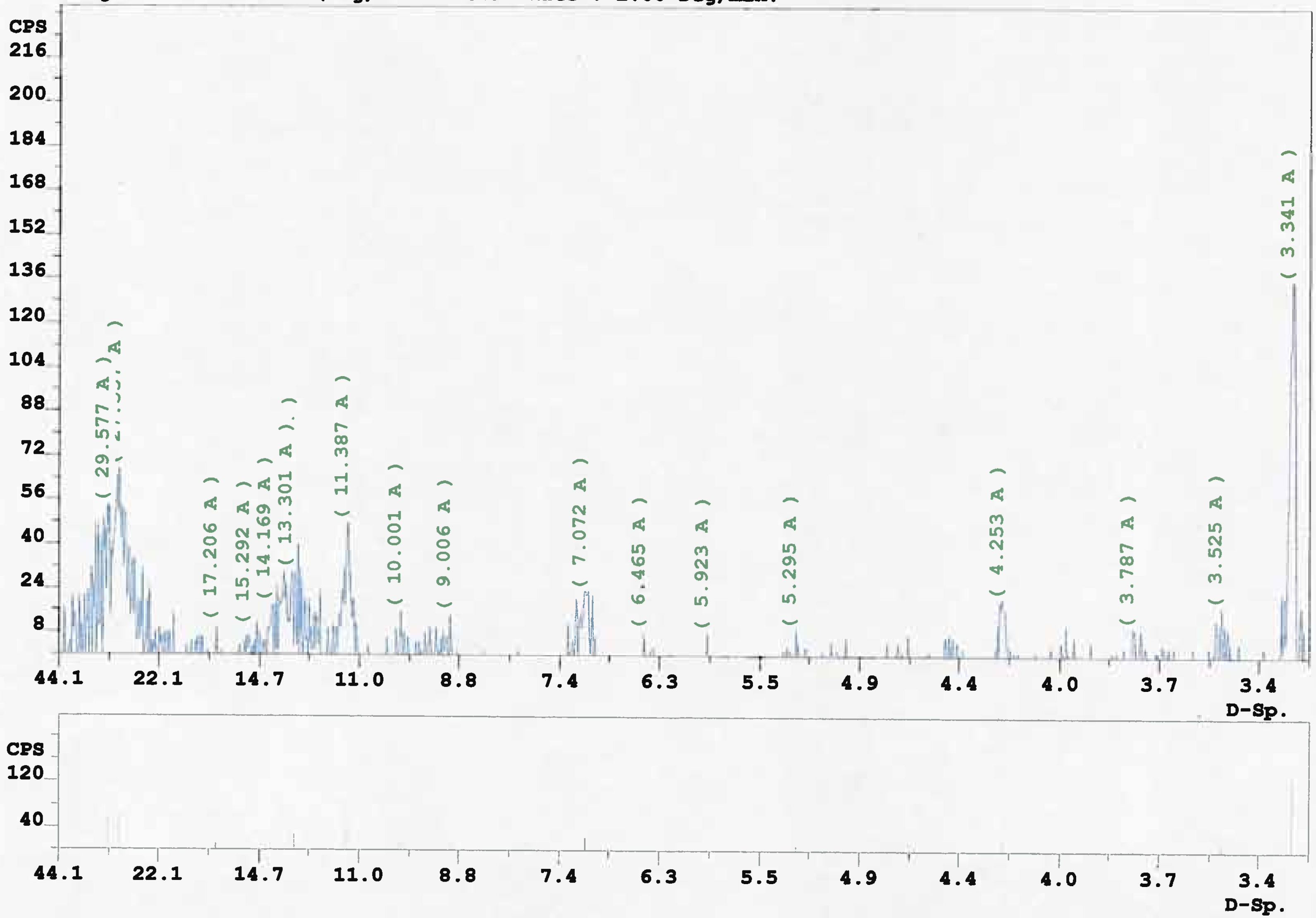

File: LD6323_550, ID: 6323, 550C
Date: 06/25/10 12:32 Step : 0.020° Cnt Time: 0.600 Sec.
Range: 2.00 - 20.00 (Deg) Cont. Scan Rate : 2.00 Deg/min.

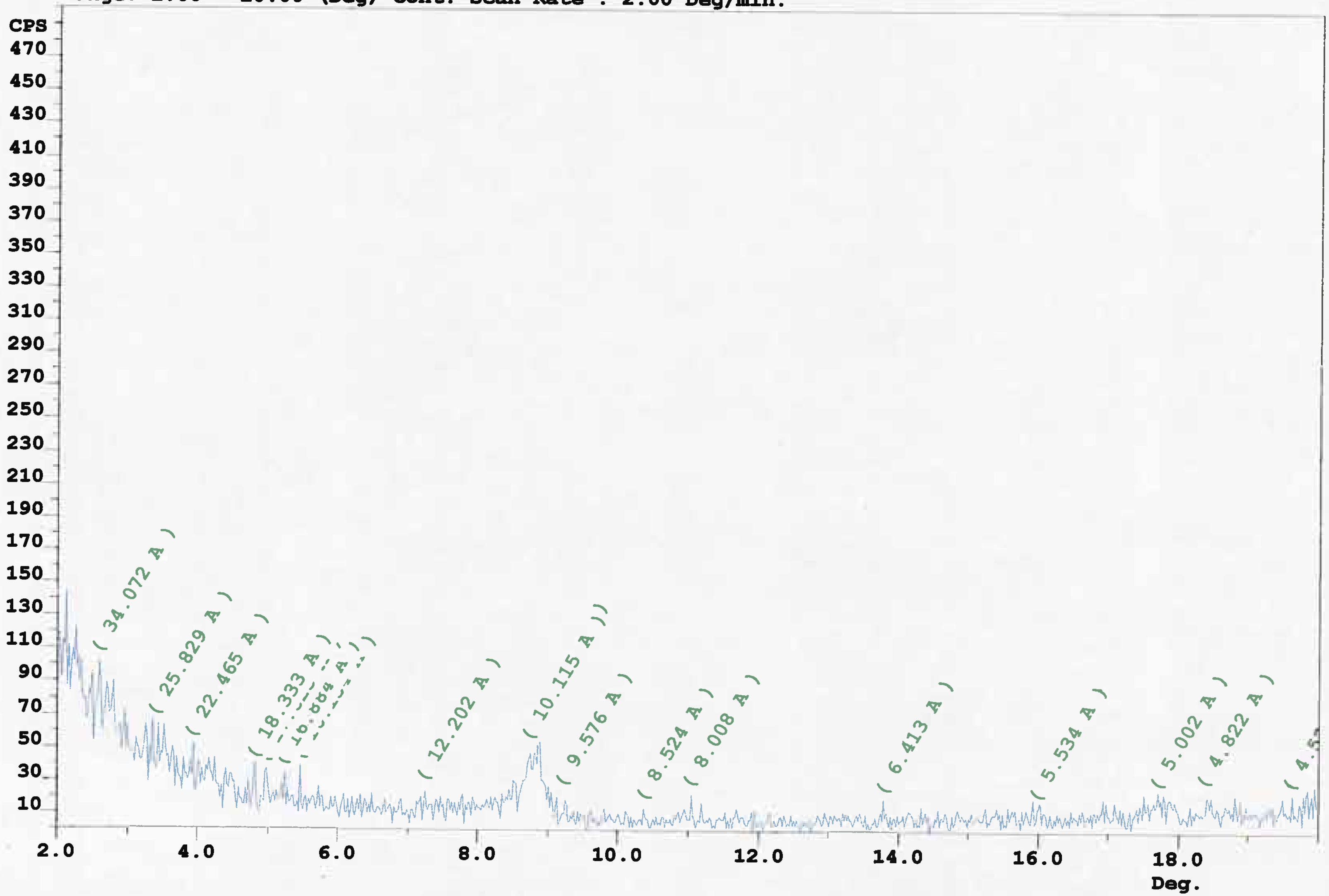

File: LD2801WR, ID: 2801, Whole Rock
Date: 08/27/10 08:44 Step : 0.020° Cnt Time: 0.600 Sec.
Range: 2.00 - 65.00 (Deg) Cont. Scan Rate : 2.00 Deg/min.

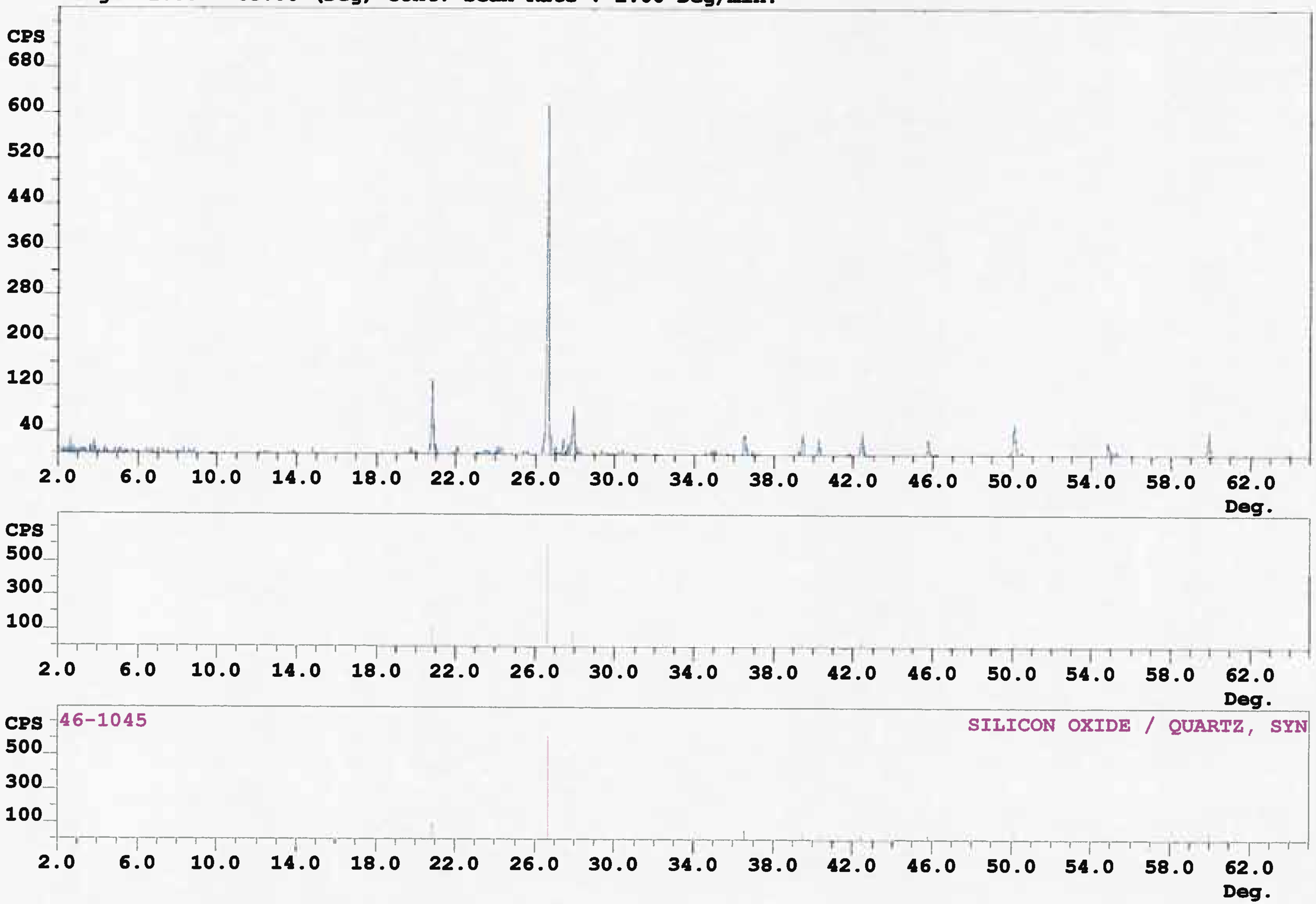

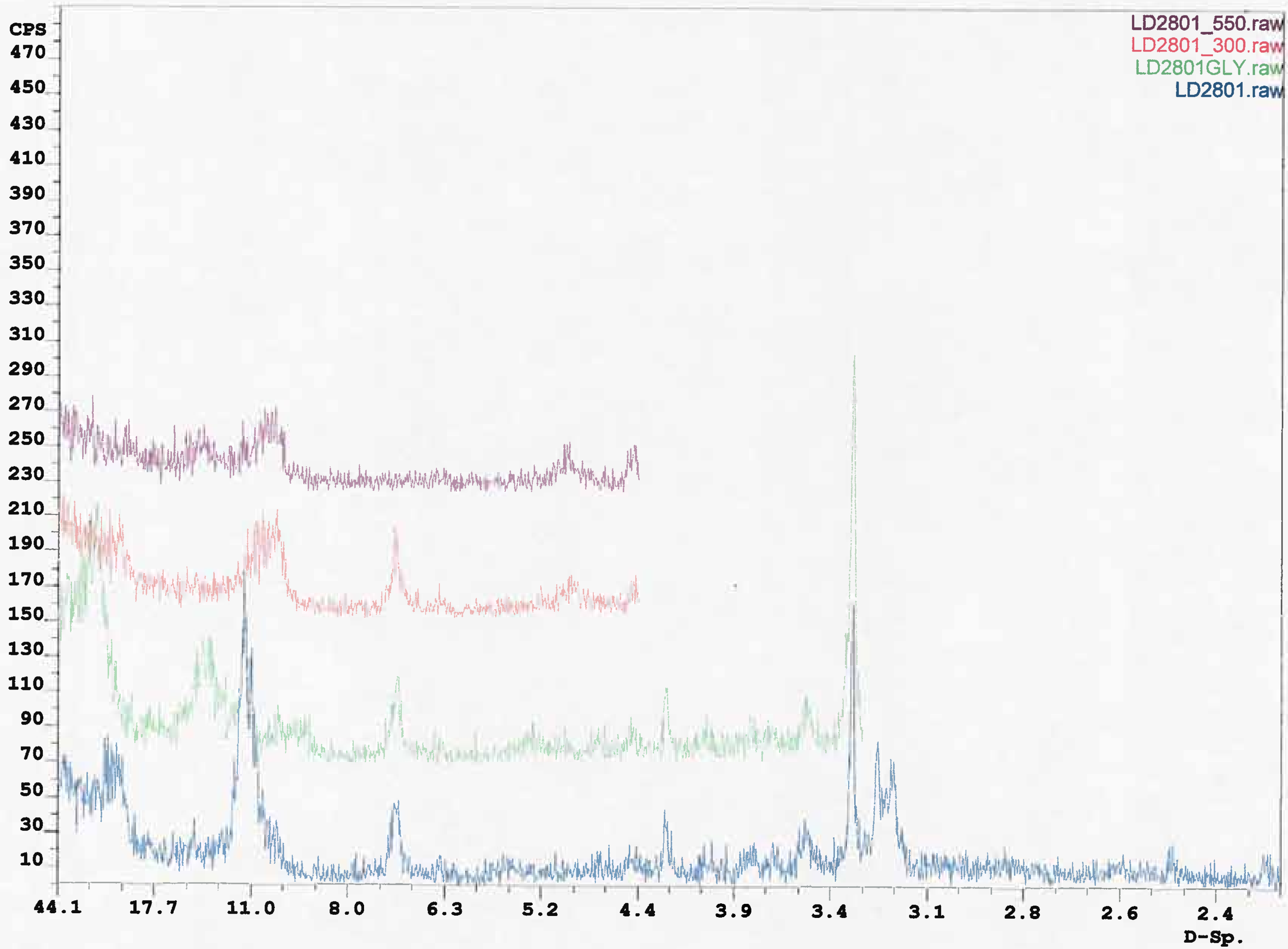
LD2801_550.raw
LD2801_300.raw
LD2801GLY.raw
LD2801.raw
CPS
470
450
430
410
390
370
350
330
310
290
270
250
230
210
190
170
150
130
110
90
70
50
30
10
44.1
17.7
11.0
8.0
6.3
5.2
4.4
3.9
3.4
3.1
2.8
2.6
2.4
D-Sp.

File: LD2801GLY, ID: 2801, Glycolated
Date: 08/30/10 08:54 Step : 0.020° Cnt Time: 0.600 Sec.
Range: 2.00 - 27.00 (Deg) Cont. Scan Rate : 2.00 Deg/min.

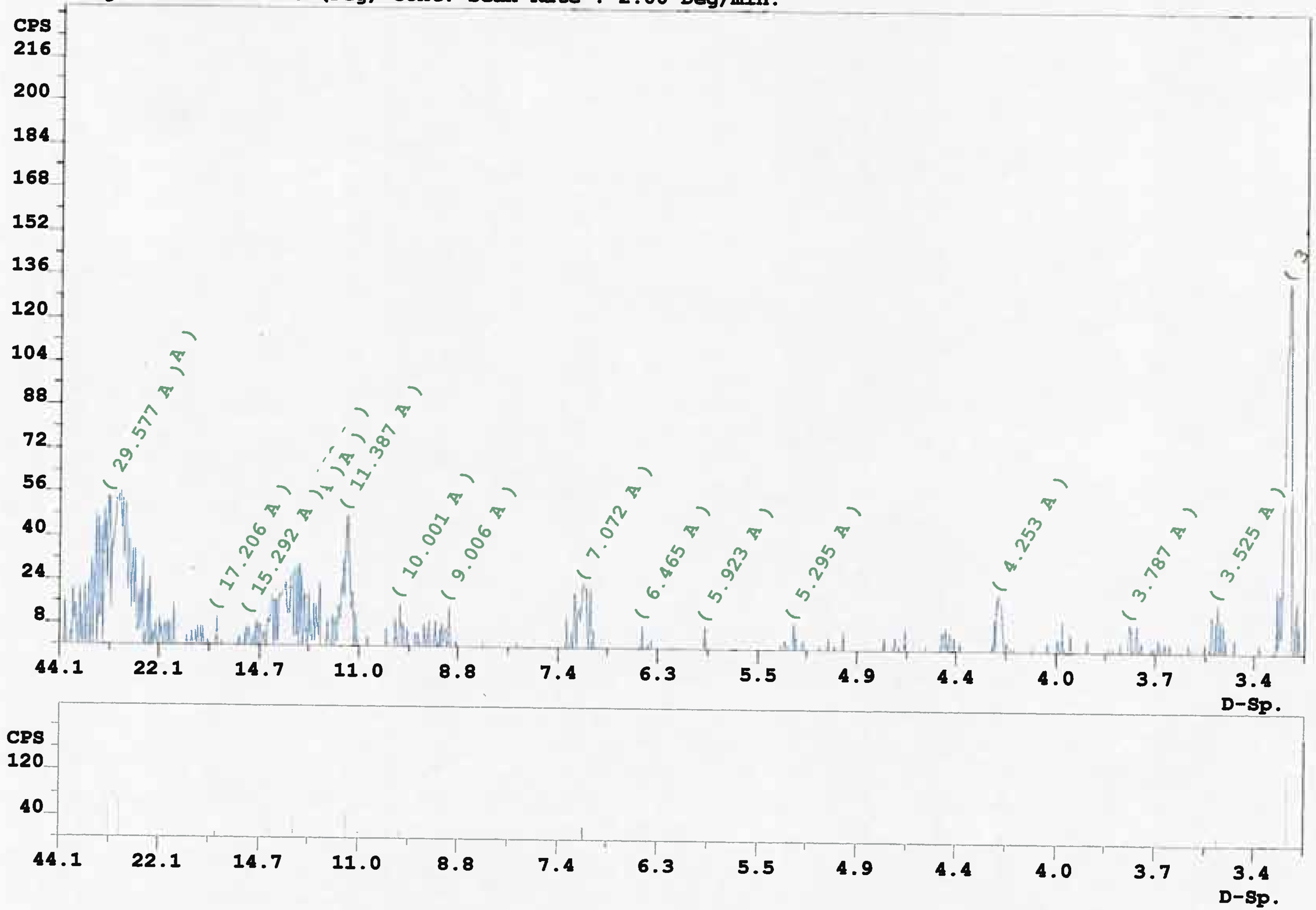

File: LD2801_2, ID: 2801, Clay
Date: 08/23/10 10:23 Step : 0.020° Cnt Time: 0.600 Sec.
Range: 2.00 - 40.00 (Deg) Cont. Scan Rate : 2.00 Deg/min.

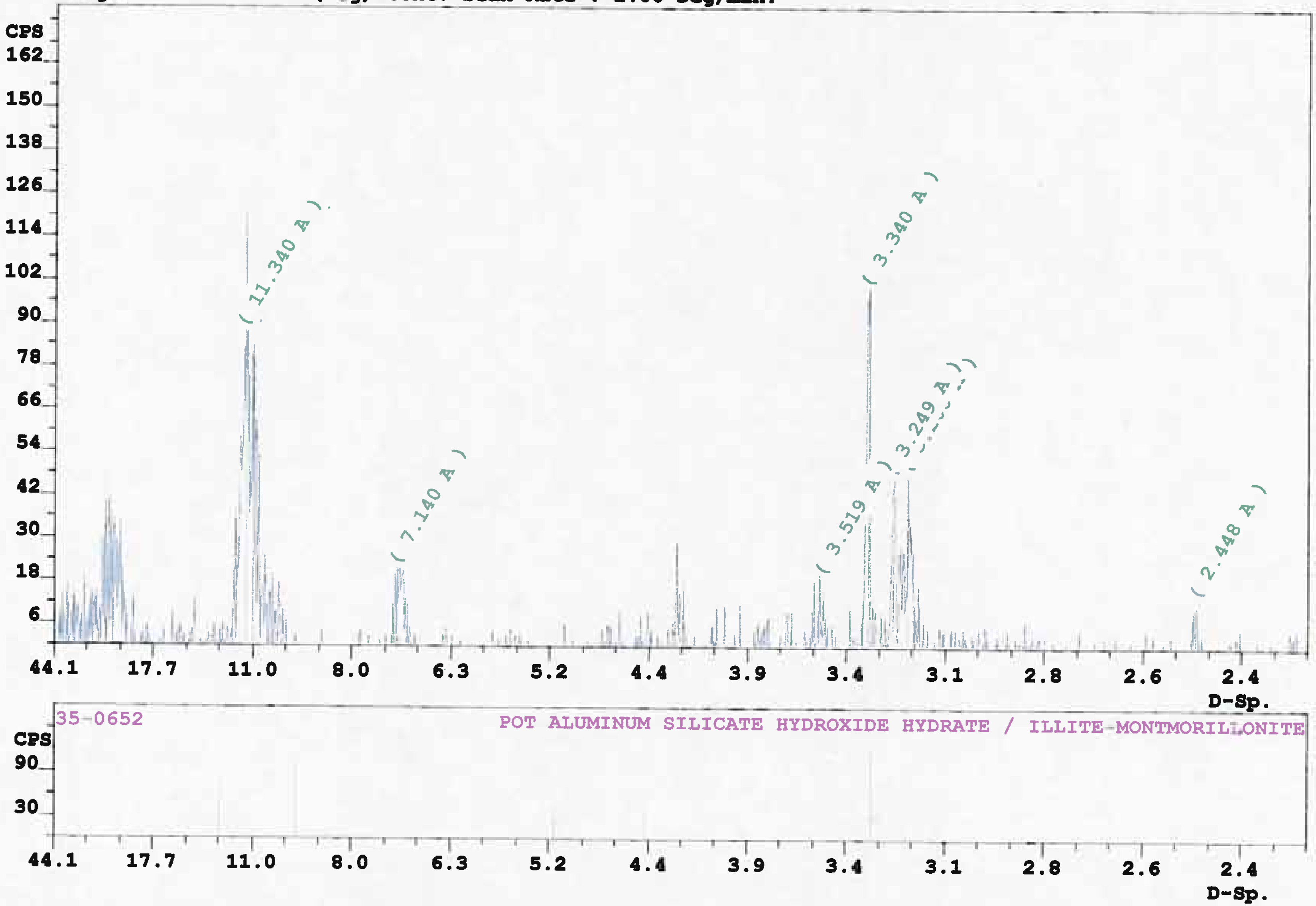

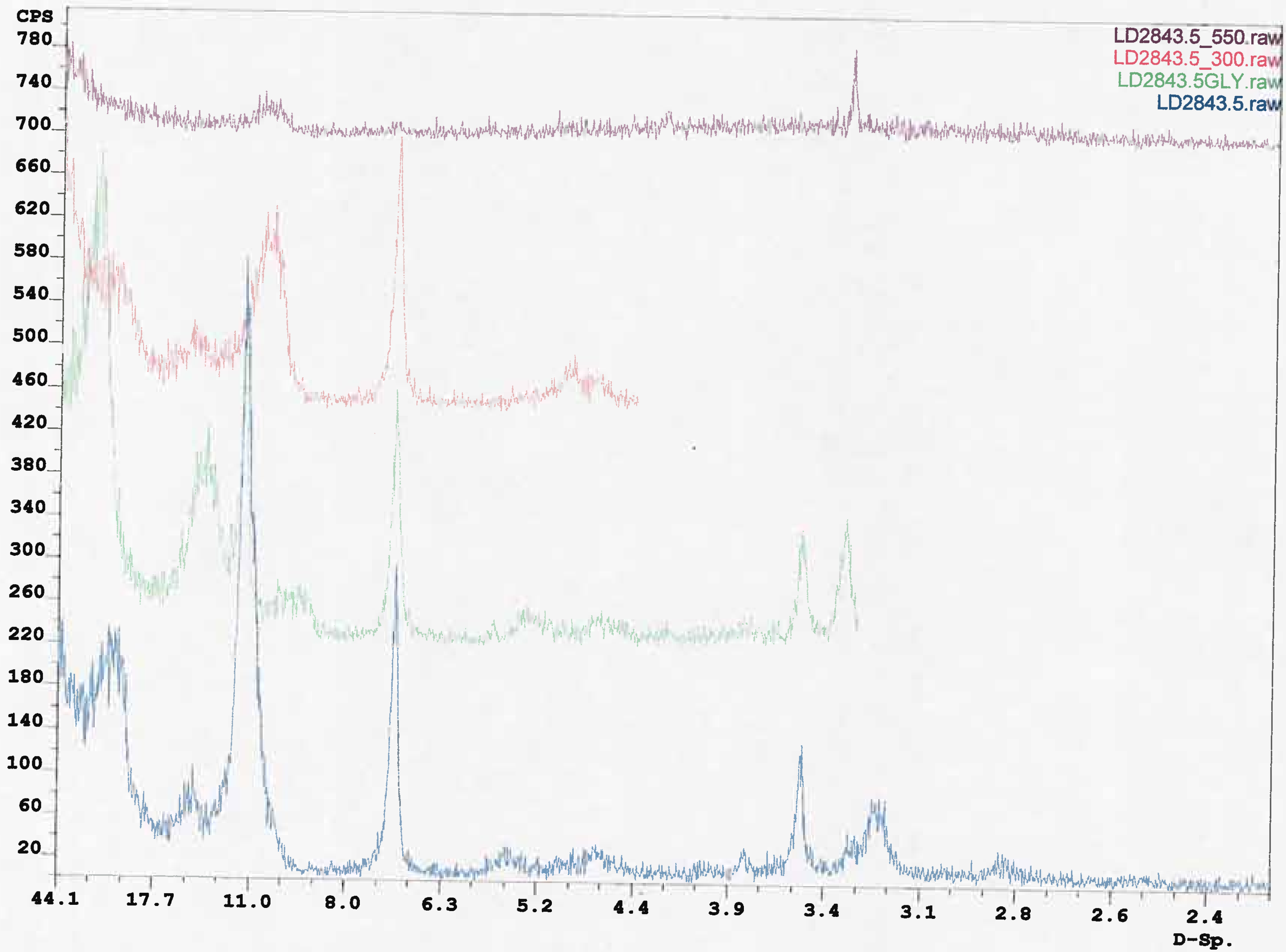

CPS
780
740
700
660
620
580
540
500
460
420
380
340
300
260
220
180
140
100
60
20
LD2843.5_550.raw
LD2843.5_300.raw
LD2843.5GLY.raw
LD2843.5.raw
44.1
17.7
11.0
8.0
6.3
5.2
4.4
3.9
3.4
3.1
2.8
2.6
2.4
D-Sp.

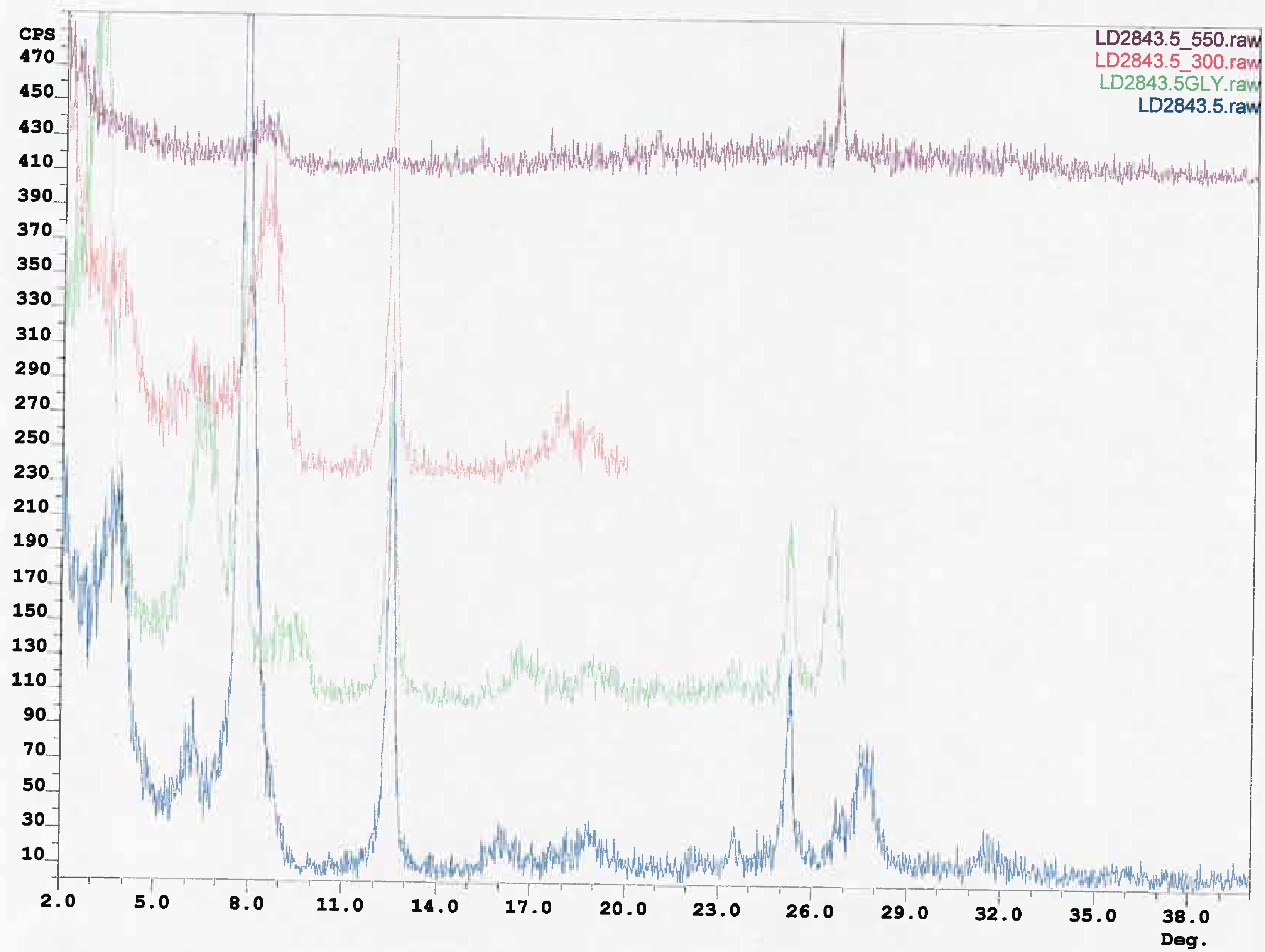
CPS
470
450
430
410
390
370
350
330
310
290
270
250
230
210
190
170
150
130
110
90
70
50
30
10
2.0
5.0
8.0
11.0
14.0
17.0
20.0
23.0
26.0
29.0
32.0
35.0
38.0
Deg.
LD2843.5_550.raw
LD2843.5_300.raw
LD2843.5GLY.raw
LD2843.5.raw

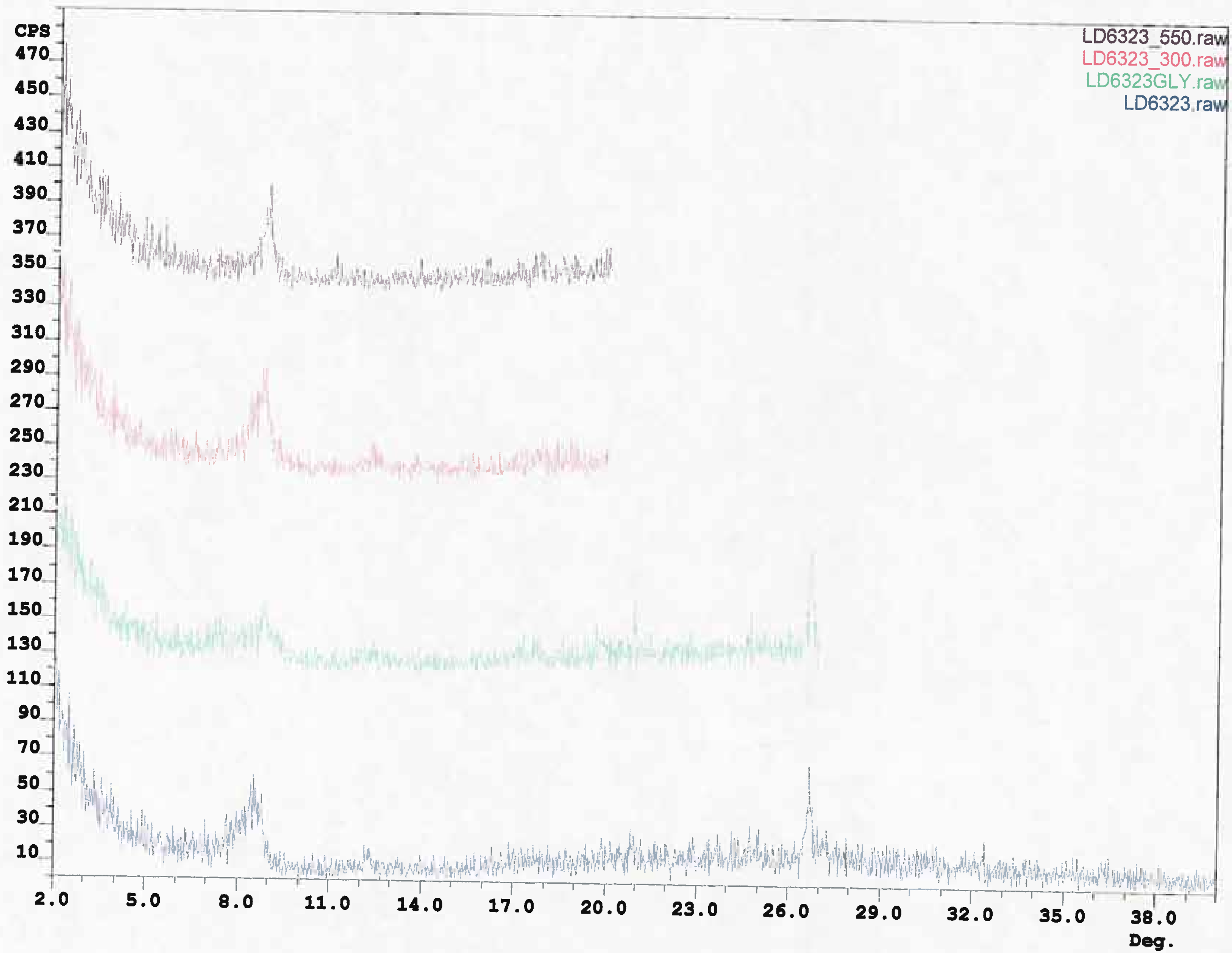
CPS
470
450
430
410
390
370
350
330
310
290
270
250
230
210
190
170
150
130
110
90
70
50
30
10
2.0
5.0
8.0
11.0
14.0
17.0
20.0
23.0
26.0
29.0
32.0
35.0
38.0
Deg.
LD6323_550.raw
LD6323_300.raw
LD6323GLY.raw
LD6323.raw

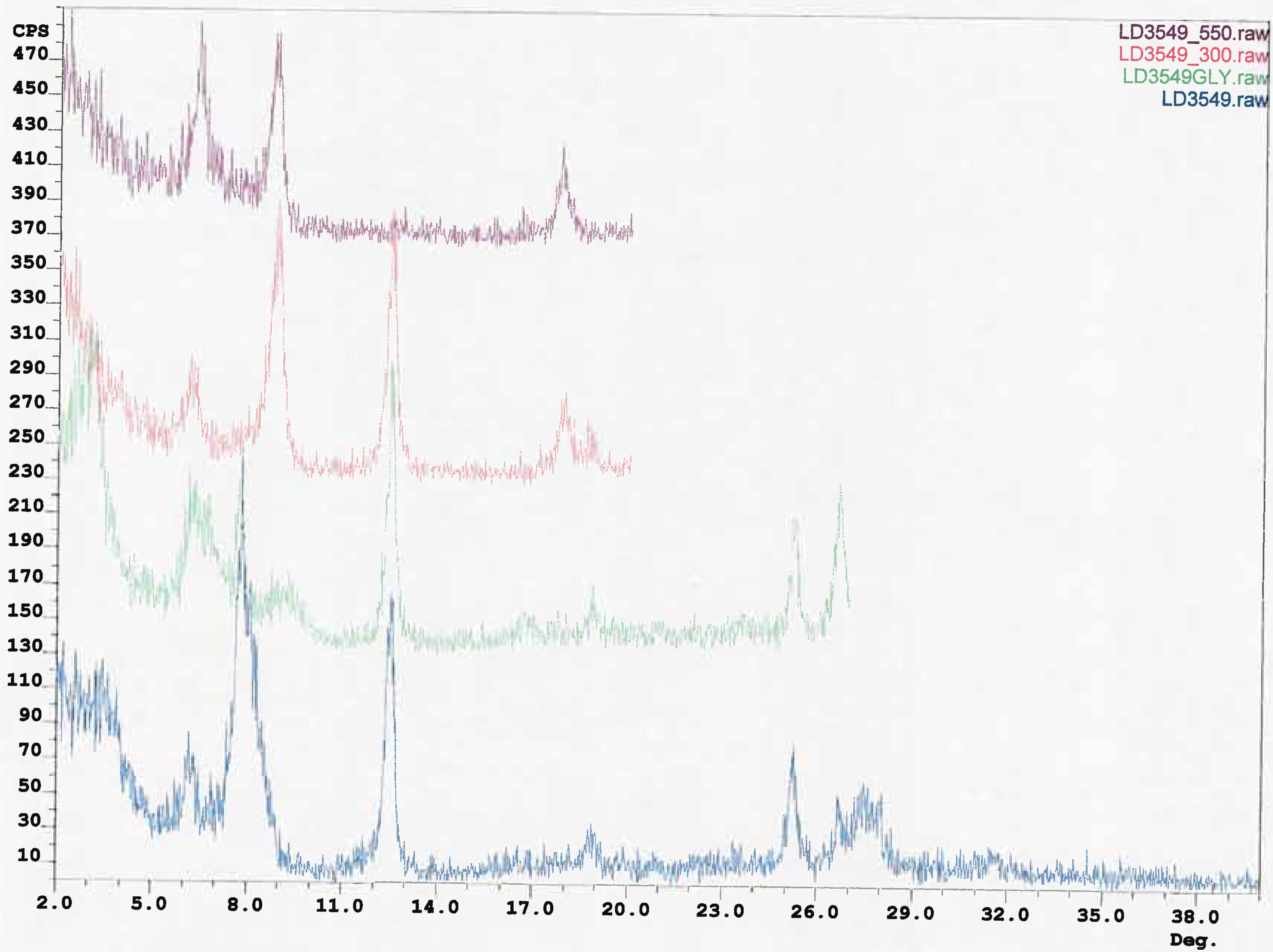
CPS
LD3549_550.raw
LD3549_300.raw
LD3549GLY.raw
LD3549.raw
470
450
430
410
390
370
350
330
310
290
270
250
230
210
190
170
150
130
110
90
70
50
30
10
2.0
5.0
8.0
11.0
14.0
17.0
20.0
23.0
26.0
29.0
32.0
35.0
38.0
Deg.

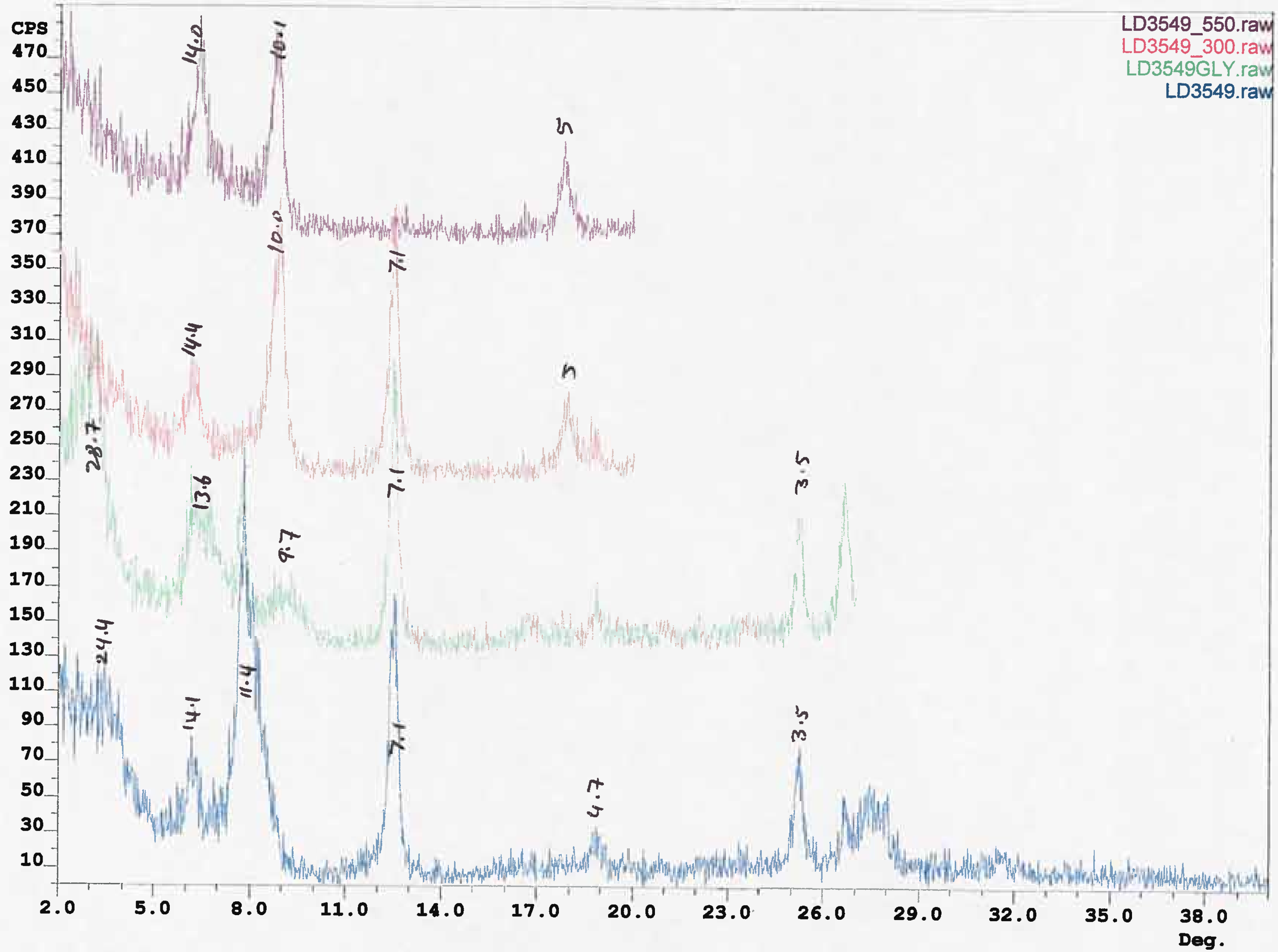
CPS
470
450
430
410
390
370
350
330
310
290
270
250
230
210
190
170
150
130
110
90
70
50
30
10
2.0
5.0
8.0
11.0
14.0
17.0
20.0
23.0
26.0
29.0
32.0
35.0
38.0
Deg.
LD3549_550.raw
LD3549_300.raw
LD3549GLY.raw
LD3549.raw
14.0
10.1
5
10.0
7.1
14.4
5
28.7
13.6
9.7
7.1
3.5
24.4
14.1
11.4
7.1
4.7
3.5

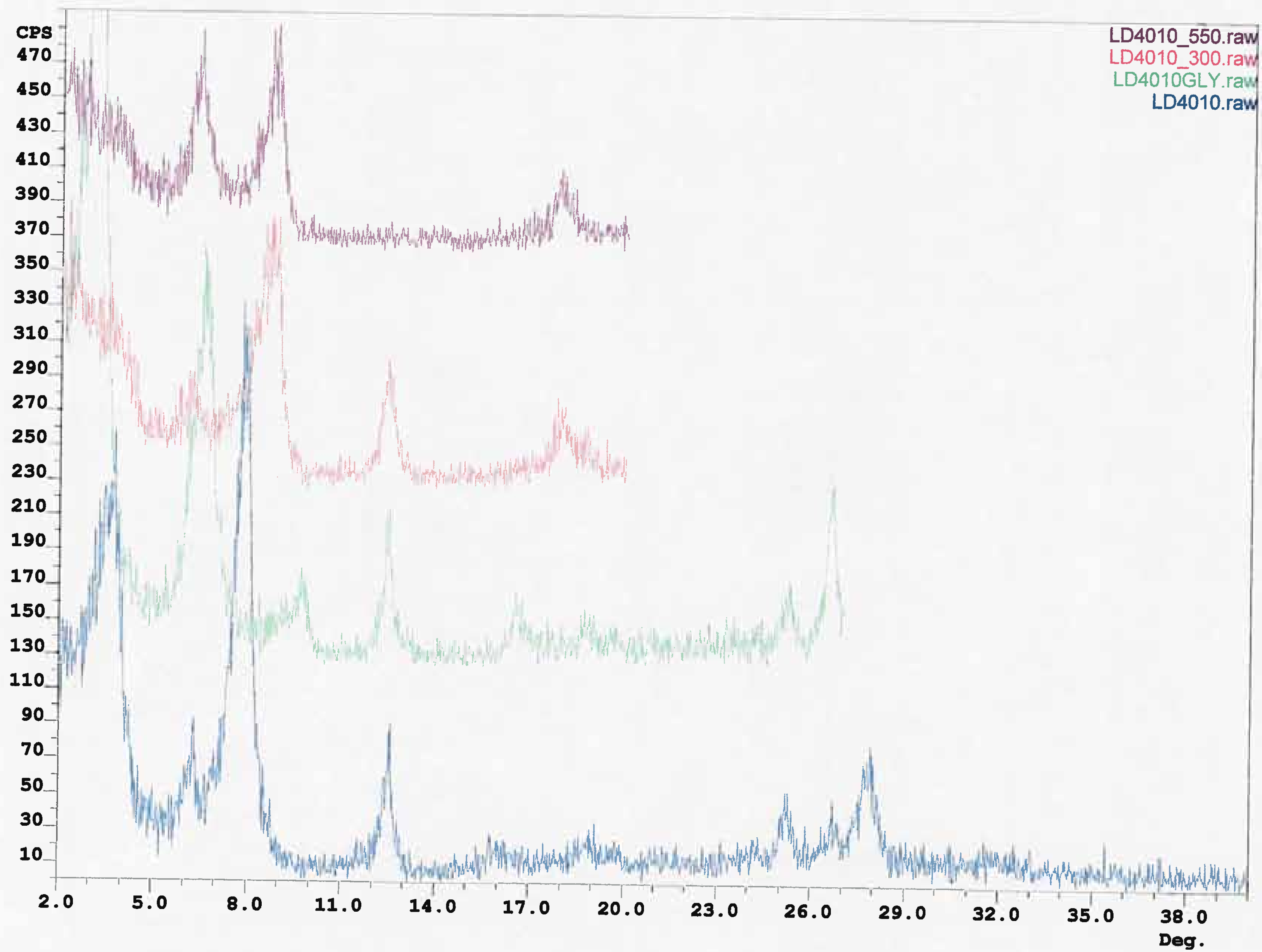
CPS
470
450
430
410
390
370
350
330
310
290
270
250
230
210
190
170
150
130
110
90
70
50
30
10
2.0
5.0
8.0
11.0
14.0
17.0
20.0
23.0
26.0
29.0
32.0
35.0
38.0
Deg.
LD4010_550.raw
LD4010_300.raw
LD4010GLY.raw
LD4010.raw

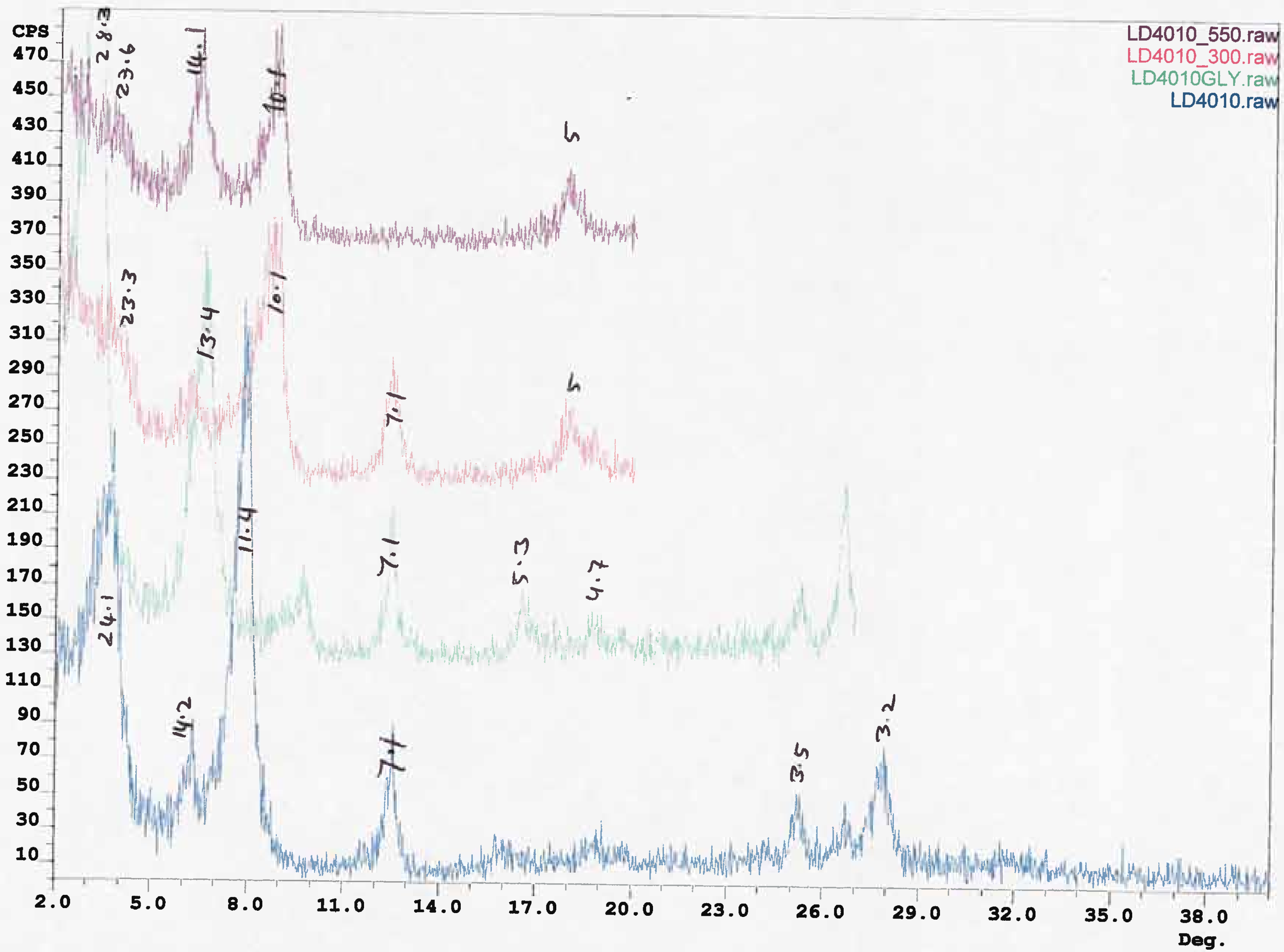
CPS
470
450
430
410
390
370
350
330
310
290
270
250
230
210
190
170
150
130
110
90
70
50
30
10
2.0
5.0
8.0
11.0
14.0
17.0
20.0
23.0
26.0
29.0
32.0
35.0
38.0
Deg.
LD4010_550.raw
LD4010_300.raw
LD4010GLY.raw
LD4010.raw
28.3
23.6
14.1
10.1
5
23.3
13.4
10.1
7.1
5
11.4
7.1
5.3
4.7
24.1
14.2
7.1
3.5
3.2

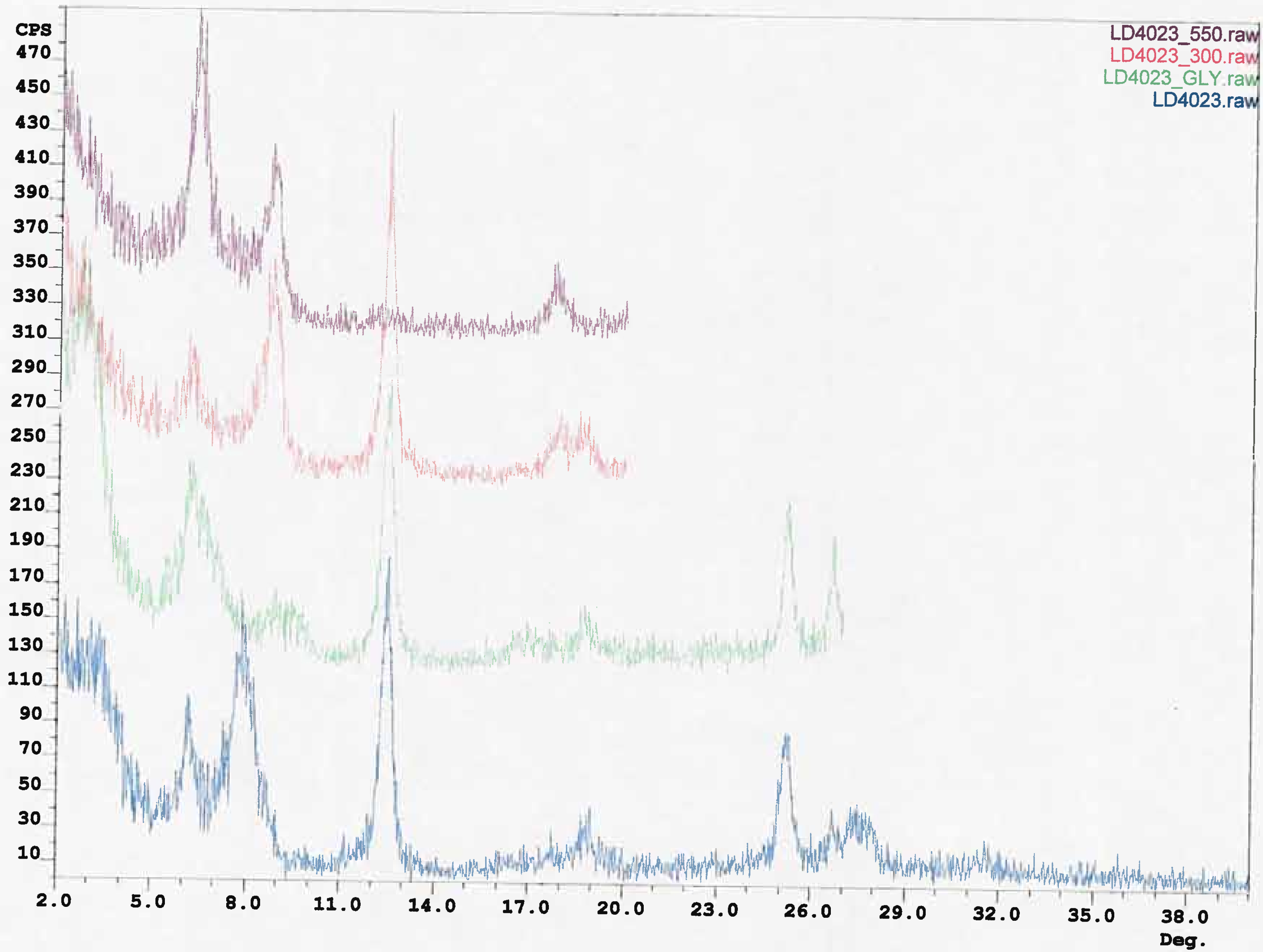
CPS
470
450
430
410
390
370
350
330
310
290
270
250
230
210
190
170
150
130
110
90
70
50
30
10
2.0
5.0
8.0
11.0
14.0
17.0
20.0
23.0
26.0
29.0
32.0
35.0
38.0
Deg.
LD4023_550.raw
LD4023_300.raw
LD4023_GLY.raw
LD4023.raw

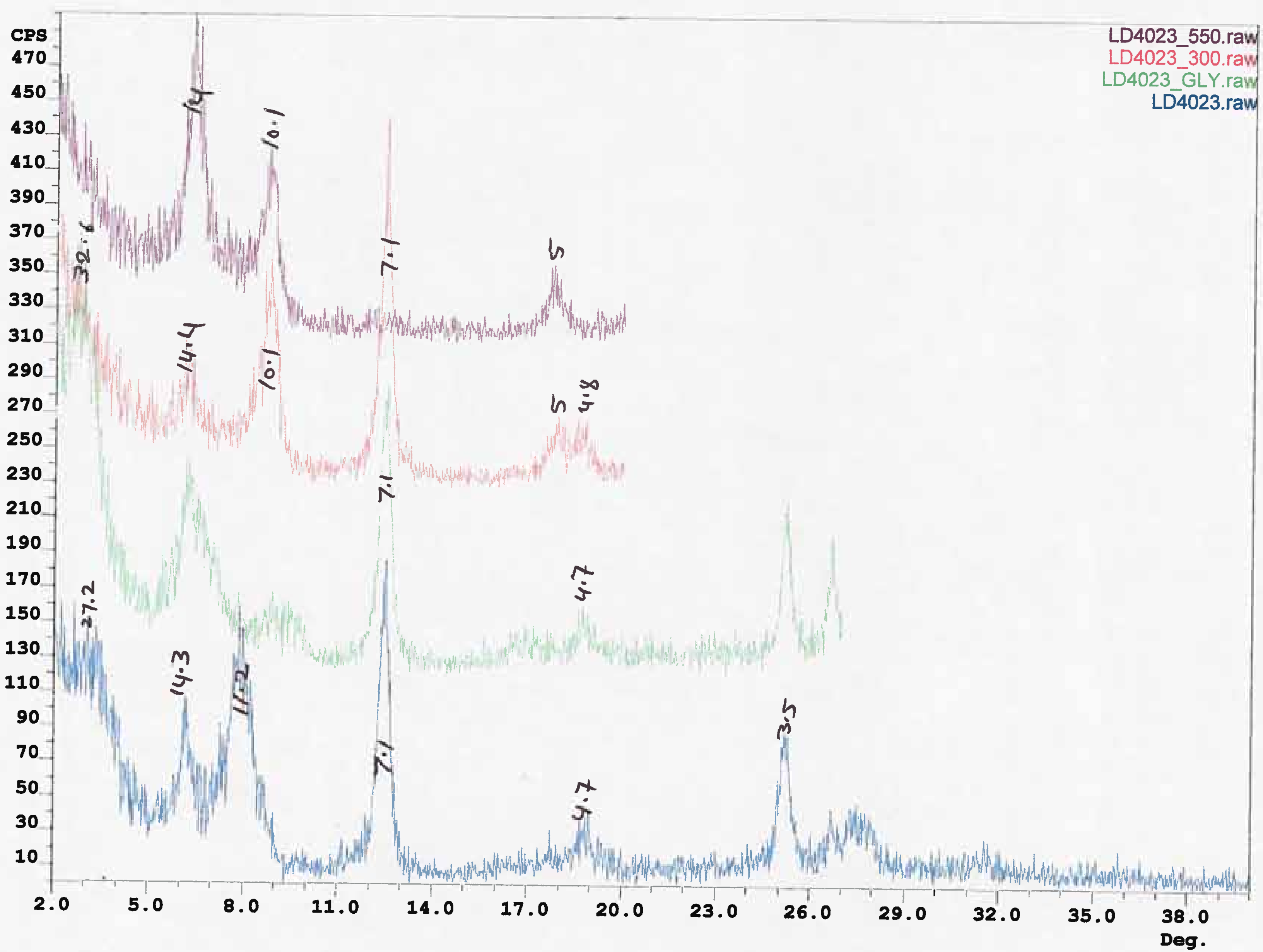
CPS
470
450
430
410
390
370
350
330
310
290
270
250
230
210
190
170
150
130
110
90
70
50
30
10
2.0
5.0
8.0
11.0
14.0
17.0
20.0
23.0
26.0
29.0
32.0
35.0
38.0
Deg.
LD4023_550.raw
LD4023_300.raw
LD4023_GLY.raw
LD4023.raw
14
10.1
7.1
5
32.6
14.4
10.1
5
4.8
7.1
4.7
27.2
14.3
11.2
7.1
4.7
3.5

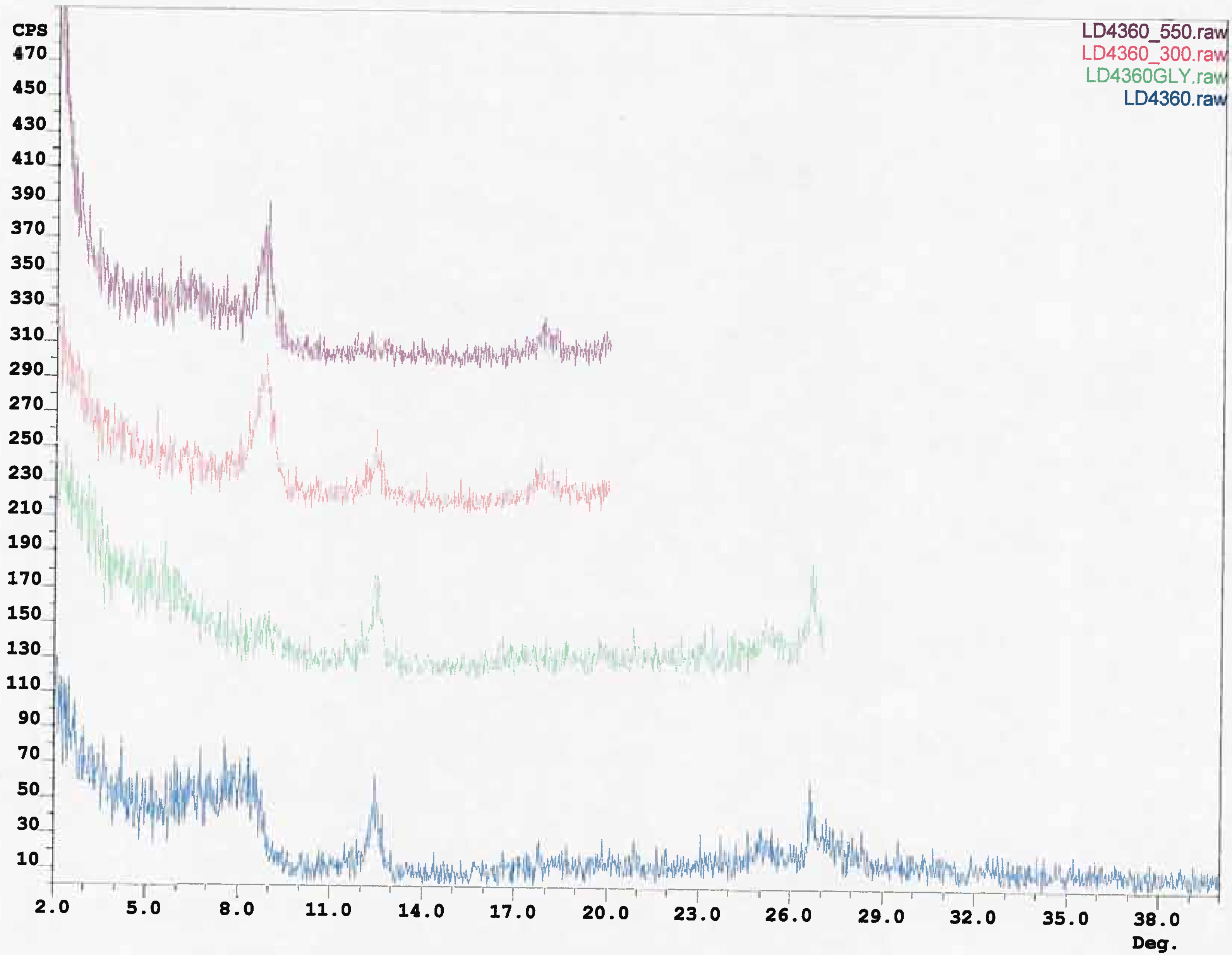
LD4360_550.raw
LD4360_300.raw
LD4360GLY.raw
LD4360.raw
CPS
470
450
430
410
390
370
350
330
310
290
270
250
230
210
190
170
150
130
110
90
70
50
30
10
2.0
5.0
8.0
11.0
14.0
17.0
20.0
23.0
26.0
29.0
32.0
35.0
38.0
Deg.

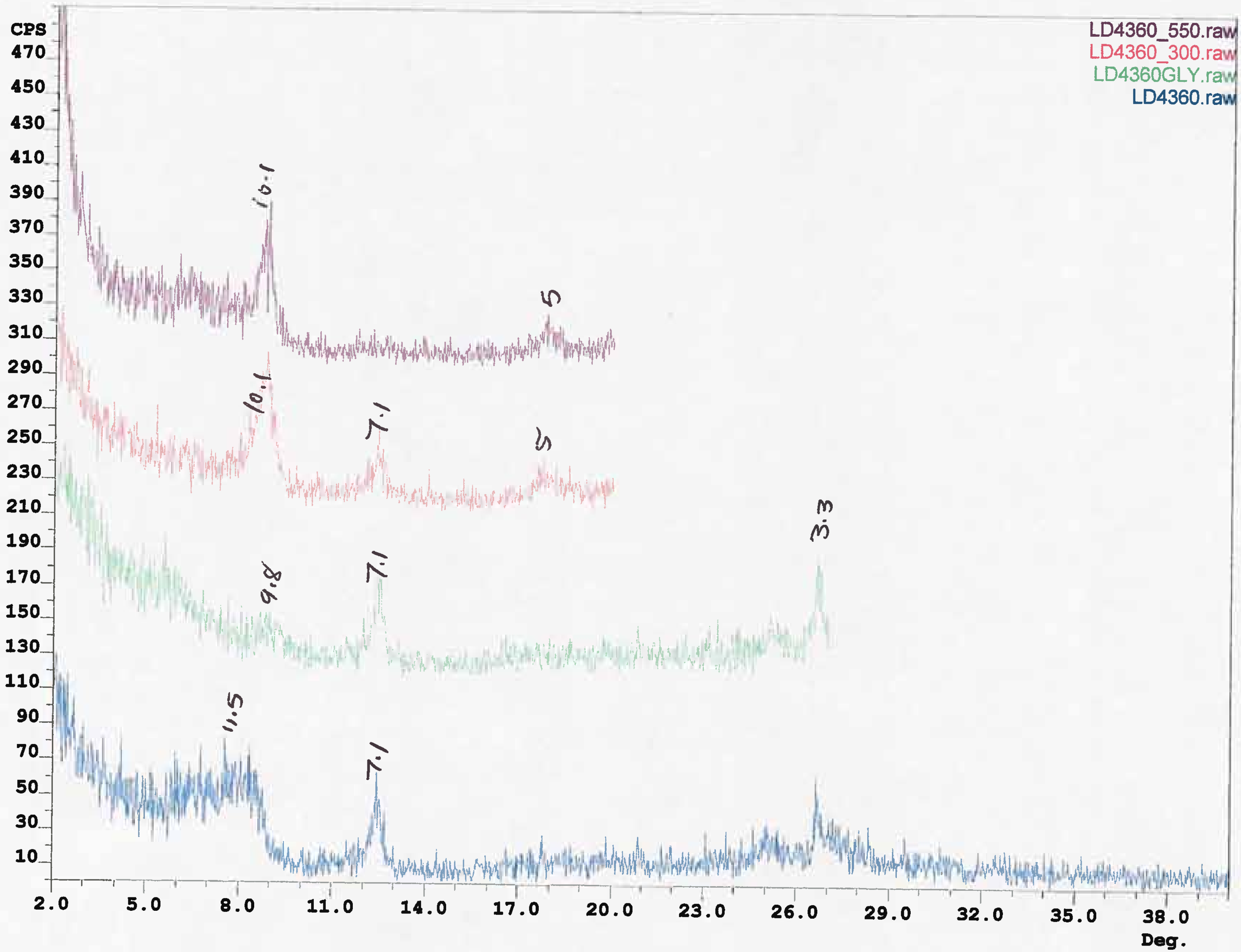
CPS
LD4360_550.raw
LD4360_300.raw
LD4360GLY.raw
LD4360.raw
10.1
5
10.1
7.1
5
3.3
9.8
7.1
11.5
7.1
470
450
430
410
390
370
350
330
310
290
270
250
230
210
190
170
150
130
110
90
70
50
30
10
2.0
5.0
8.0
11.0
14.0
17.0
20.0
23.0
26.0
29.0
32.0
35.0
38.0
Deg.

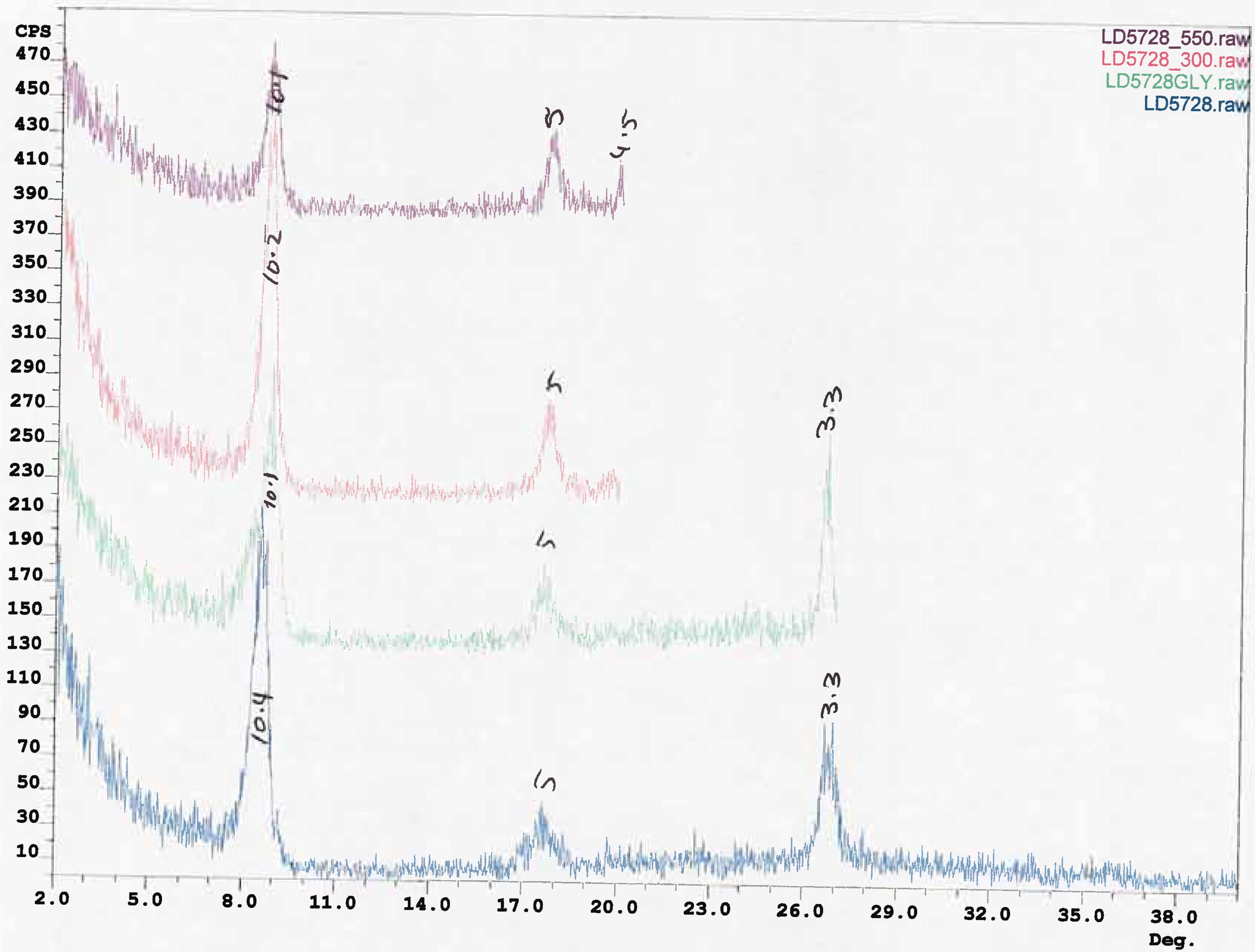
CPS
470
450
430
410
390
370
350
330
310
290
270
250
230
210
190
170
150
130
110
90
70
50
30
10
2.0
5.0
8.0
11.0
14.0
17.0
20.0
23.0
26.0
29.0
32.0
35.0
38.0
Deg.
LD5728_550.raw
LD5728_300.raw
LD5728GLY.raw
LD5728.raw
10.1
5
4.5
10.2
5
3.3
10.1
5
10.4
5
3.3

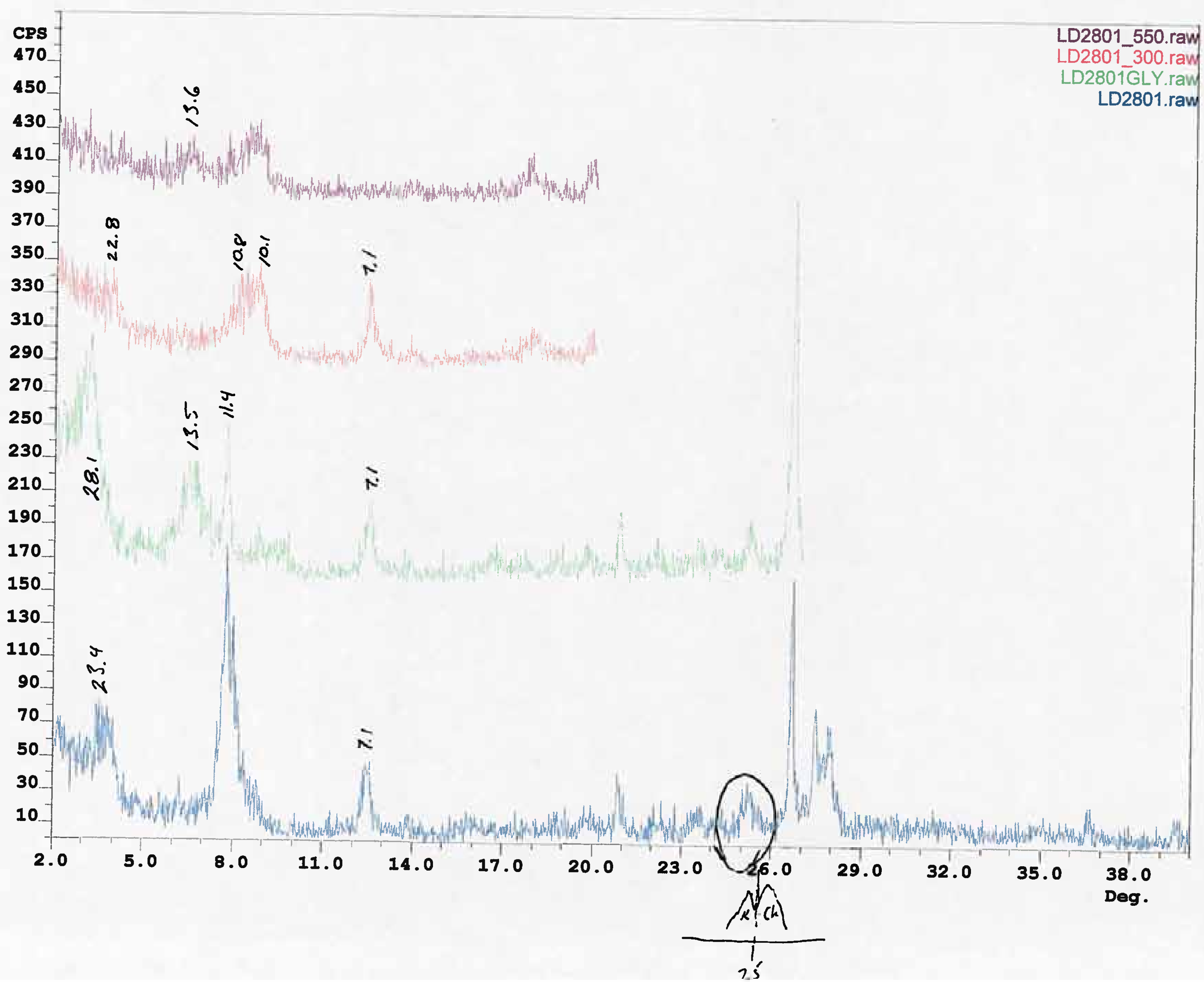
CPS
470
450
430
410
390
370
350
330
310
290
270
250
230
210
190
170
150
130
110
90
70
50
30
10
2.0
5.0
8.0
11.0
14.0
17.0
20.0
23.0
26.0
29.0
32.0
35.0
38.0
Deg.
LD2801_550.raw
LD2801_300.raw
LD2801GLY.raw
LD2801.raw
13.6
22.8
10.8
10.1
7.1
28.1
13.5
11.4
7.1
23.4
7.1
K
Ch
25

268

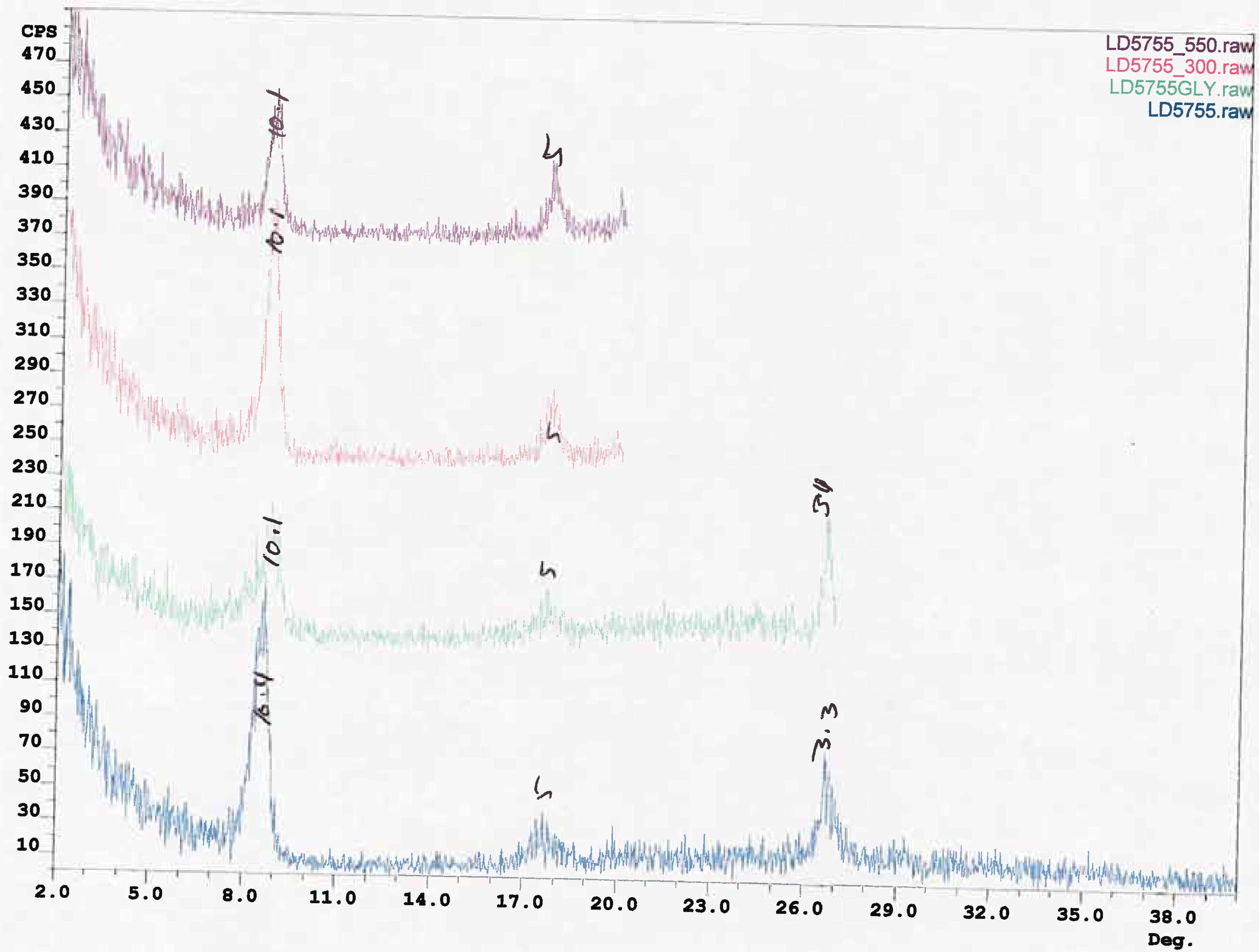
CPS
470
450
430
410
390
370
350
330
310
290
270
250
230
210
190
170
150
130
110
90
70
50
30
10
2.0
5.0
8.0
11.0
14.0
17.0
20.0
23.0
26.0
29.0
32.0
35.0
38.0
Deg.
LD5755_550.raw
LD5755_300.raw
LD5755GLY.raw
LD5755.raw
10.1
10.1
10.1
10.4
5
5
5
5
3.34
3.3

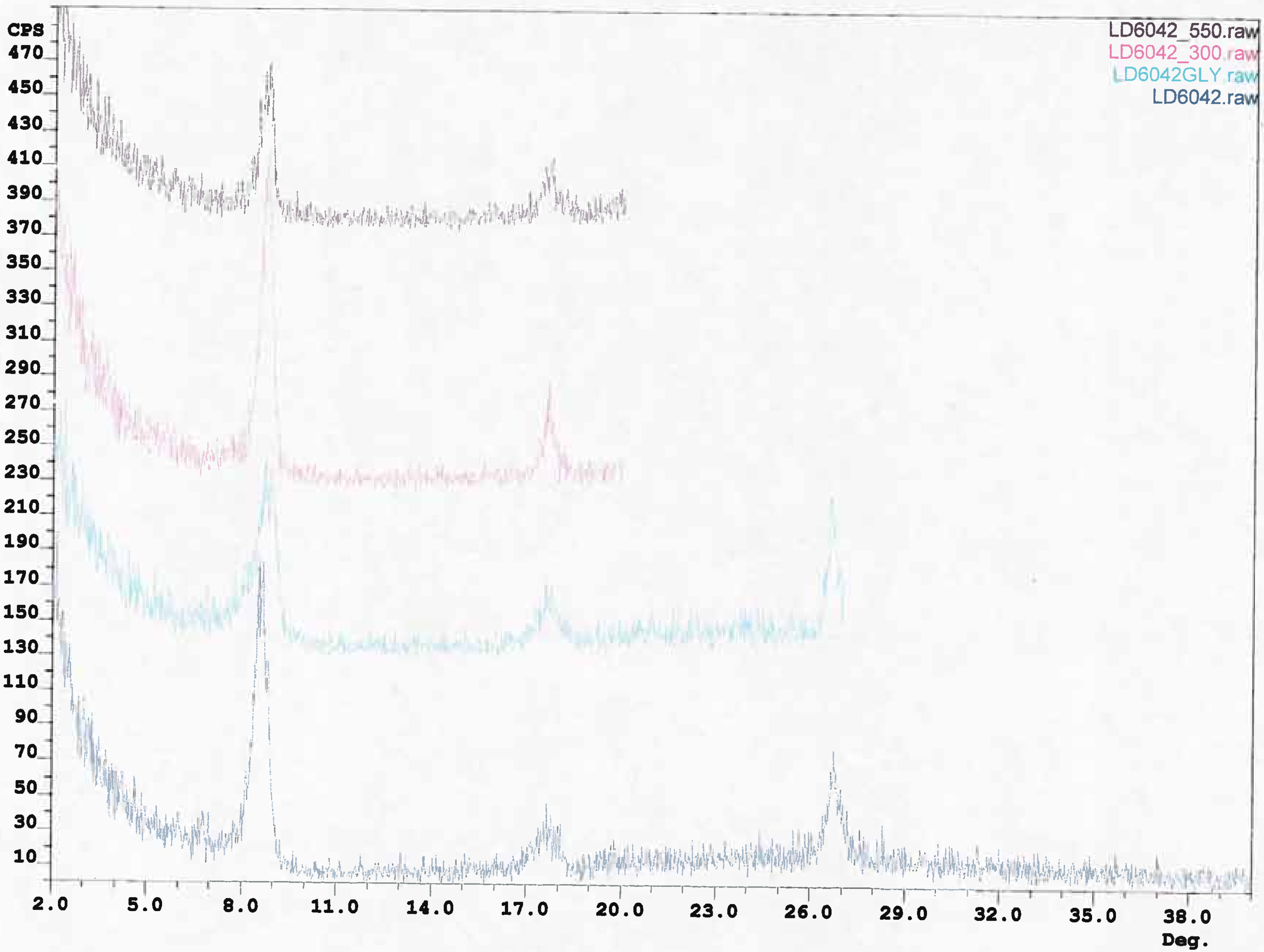
CPS
470
450
430
410
390
370
350
330
310
290
270
250
230
210
190
170
150
130
110
90
70
50
30
10
2.0
5.0
8.0
11.0
14.0
17.0
20.0
23.0
26.0
29.0
32.0
35.0
38.0
Deg.
LD6042_550.raw
LD6042_300.raw
LD6042GLY.raw
LD6042.raw

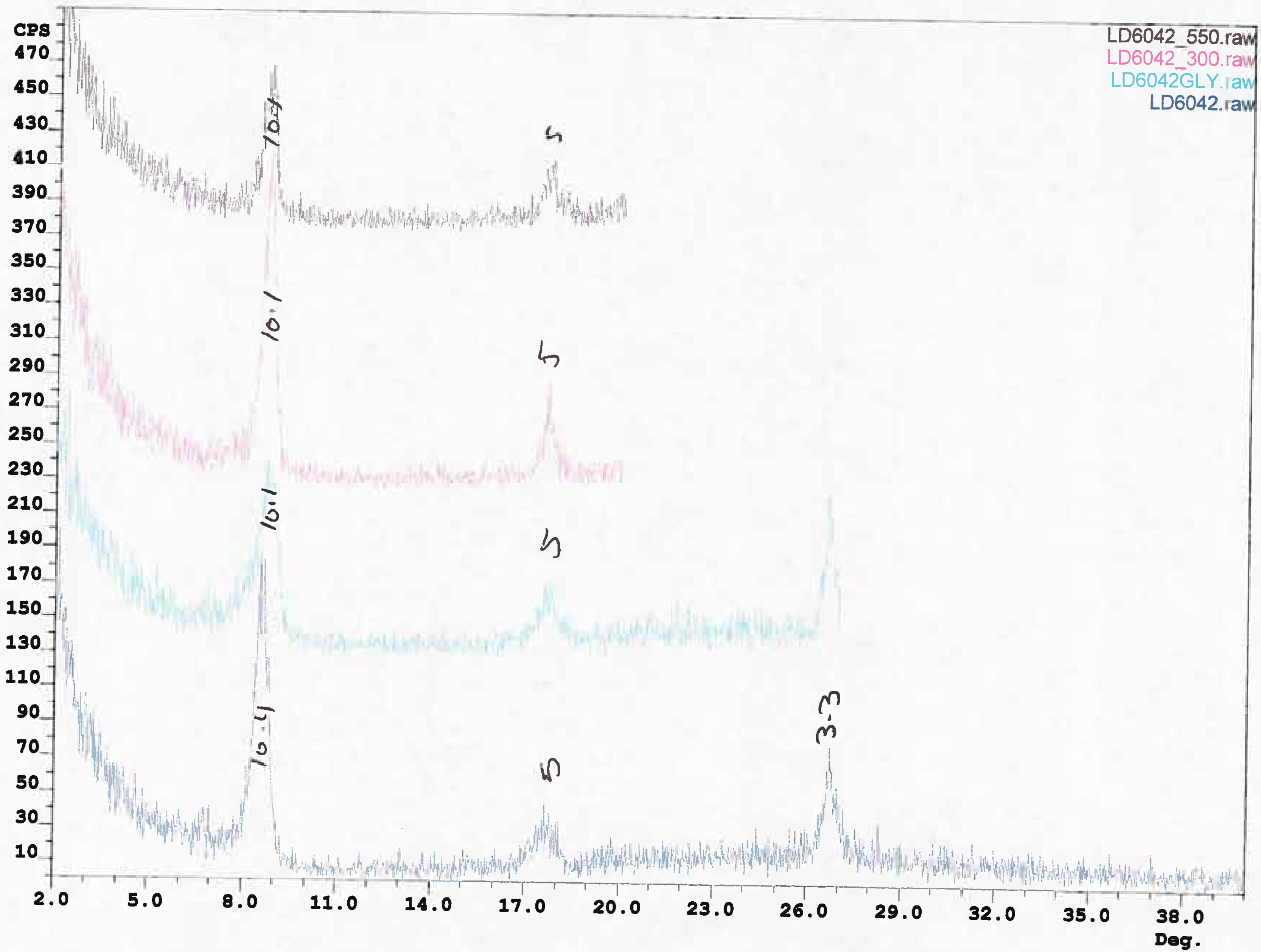
CPS
470
450
430
410
390
370
350
330
310
290
270
250
230
210
190
170
150
130
110
90
70
50
30
10
2.0
5.0
8.0
11.0
14.0
17.0
20.0
23.0
26.0
29.0
32.0
35.0
38.0
Deg.
LD6042_550.raw
LD6042_300.raw
LD6042GLY.raw
LD6042.raw
10.4
5
10.1
5
10.1
5
10.4
5
3.3

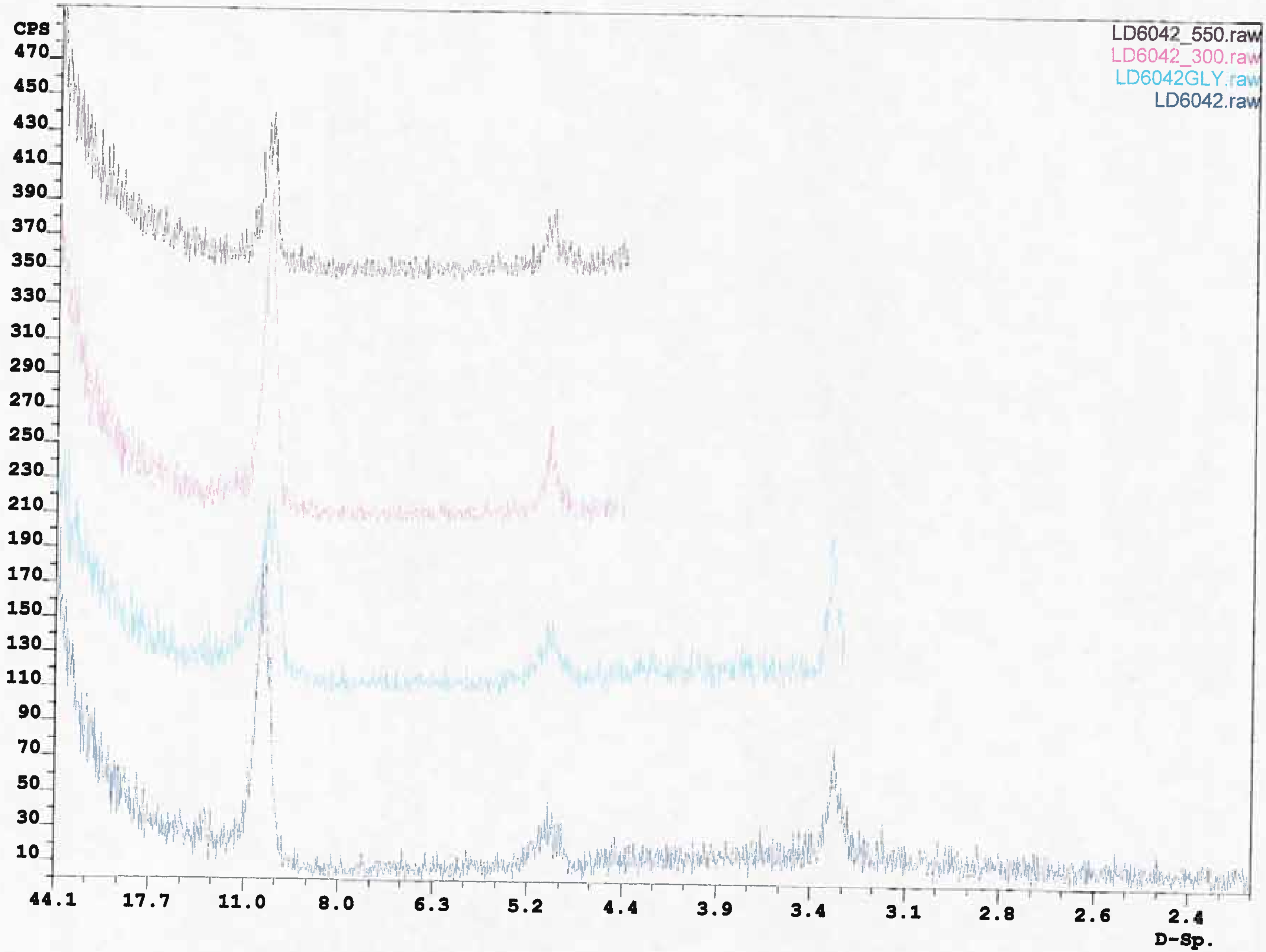
CPS
470
450
430
410
390
370
350
330
310
290
270
250
230
210
190
170
150
130
110
90
70
50
30
10
44.1
17.7
11.0
8.0
6.3
5.2
4.4
3.9
3.4
3.1
2.8
2.6
2.4
D-Sp.
LD6042_550.raw
LD6042_300.raw
LD6042GLY.raw
LD6042.raw

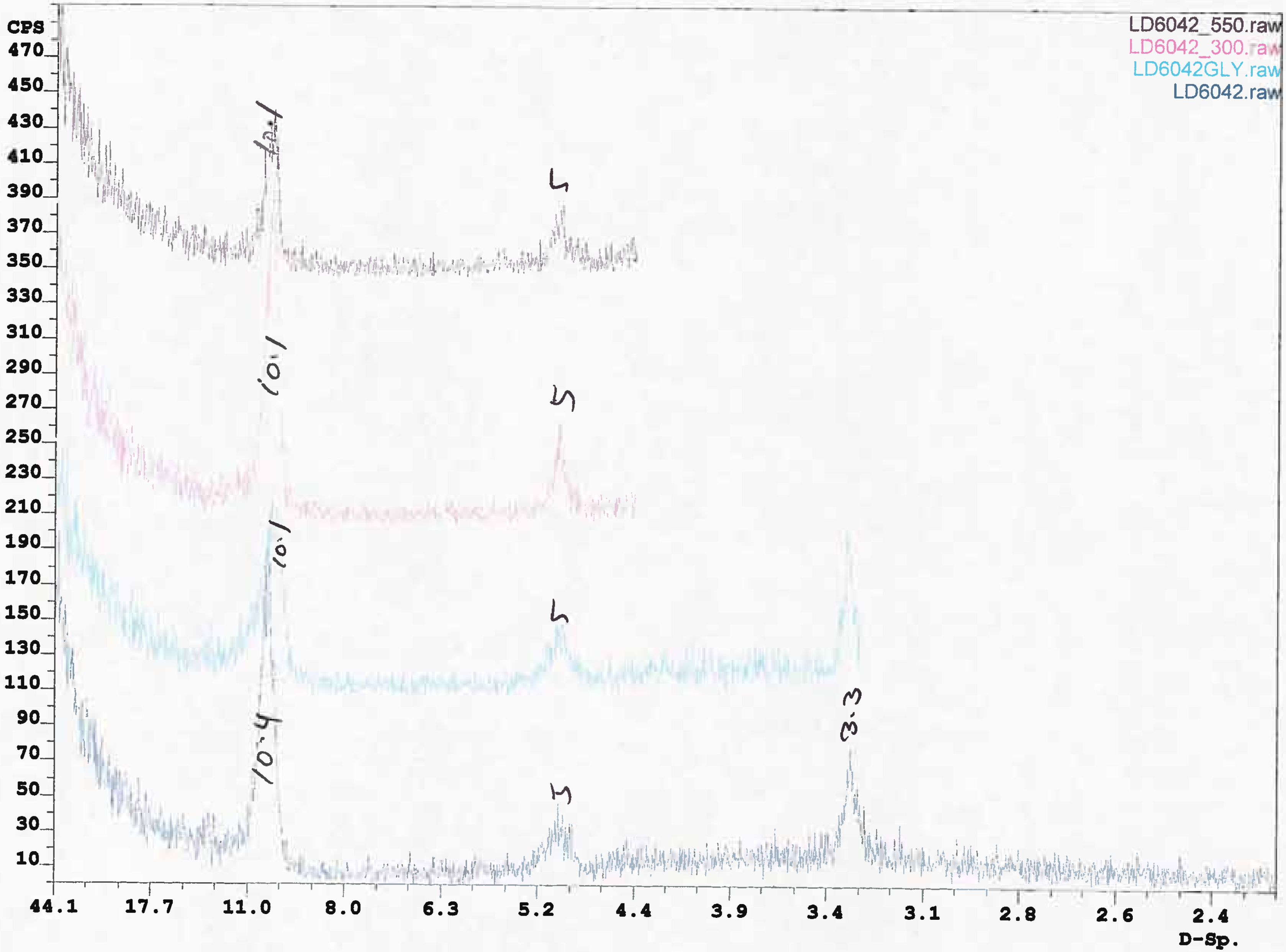
CPS
470
450
430
410
390
370
350
330
310
290
270
250
230
210
190
170
150
130
110
90
70
50
30
10
44.1
17.7
11.0
8.0
6.3
5.2
4.4
3.9
3.4
3.1
2.8
2.6
2.4
D-Sp.
LD6042_550.raw
LD6042_300.raw
LD6042GLY.raw
LD6042.raw
10.1
5
10.1
5
10.1
5
10.4
5
3.3

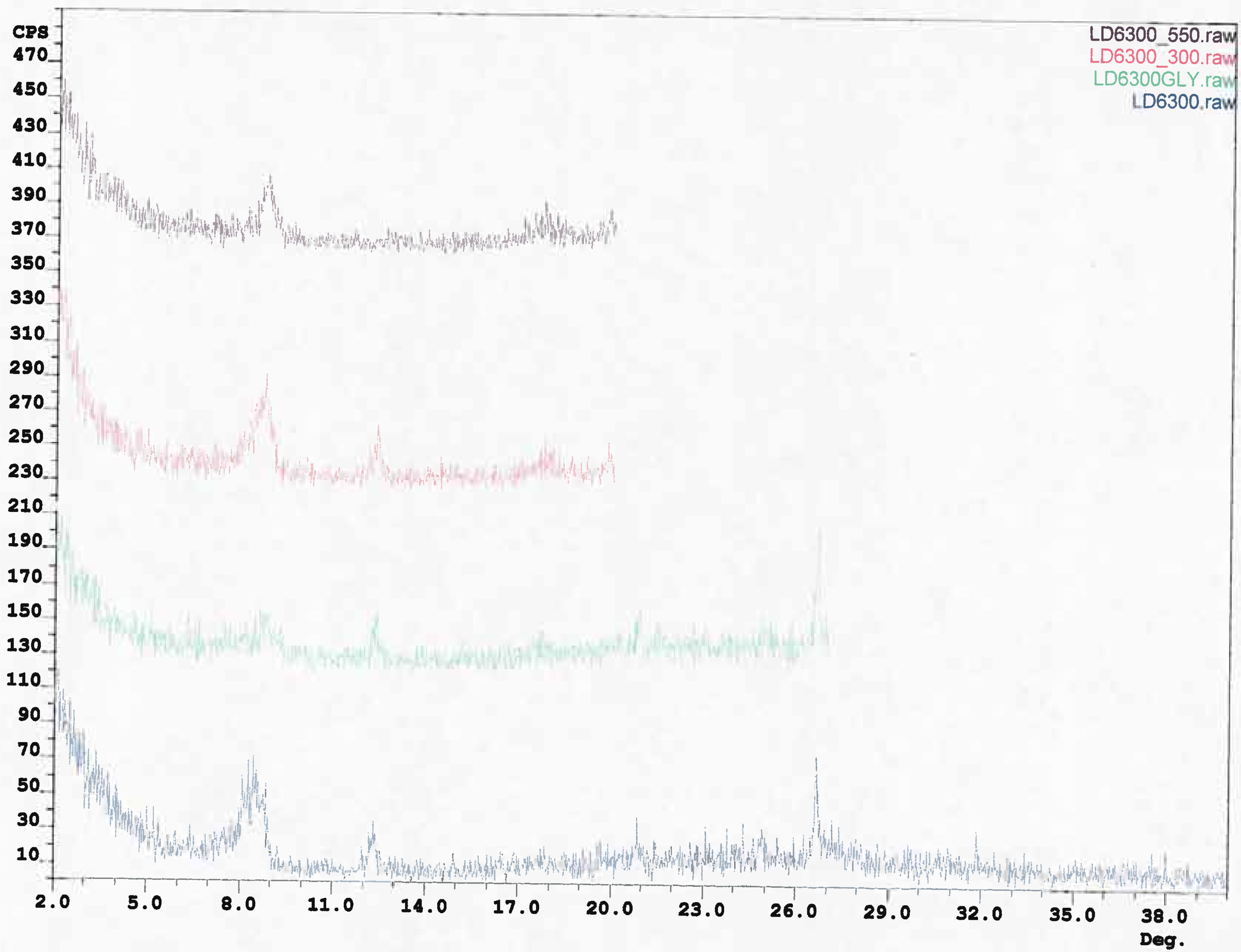
CPS
470
450
430
410
390
370
350
330
310
290
270
250
230
210
190
170
150
130
110
90
70
50
30
10
2.0
5.0
8.0
11.0
14.0
17.0
20.0
23.0
26.0
29.0
32.0
35.0
38.0
Deg.
LD6300_550.raw
LD6300_300.raw
LD6300GLY.raw
LD6300.raw

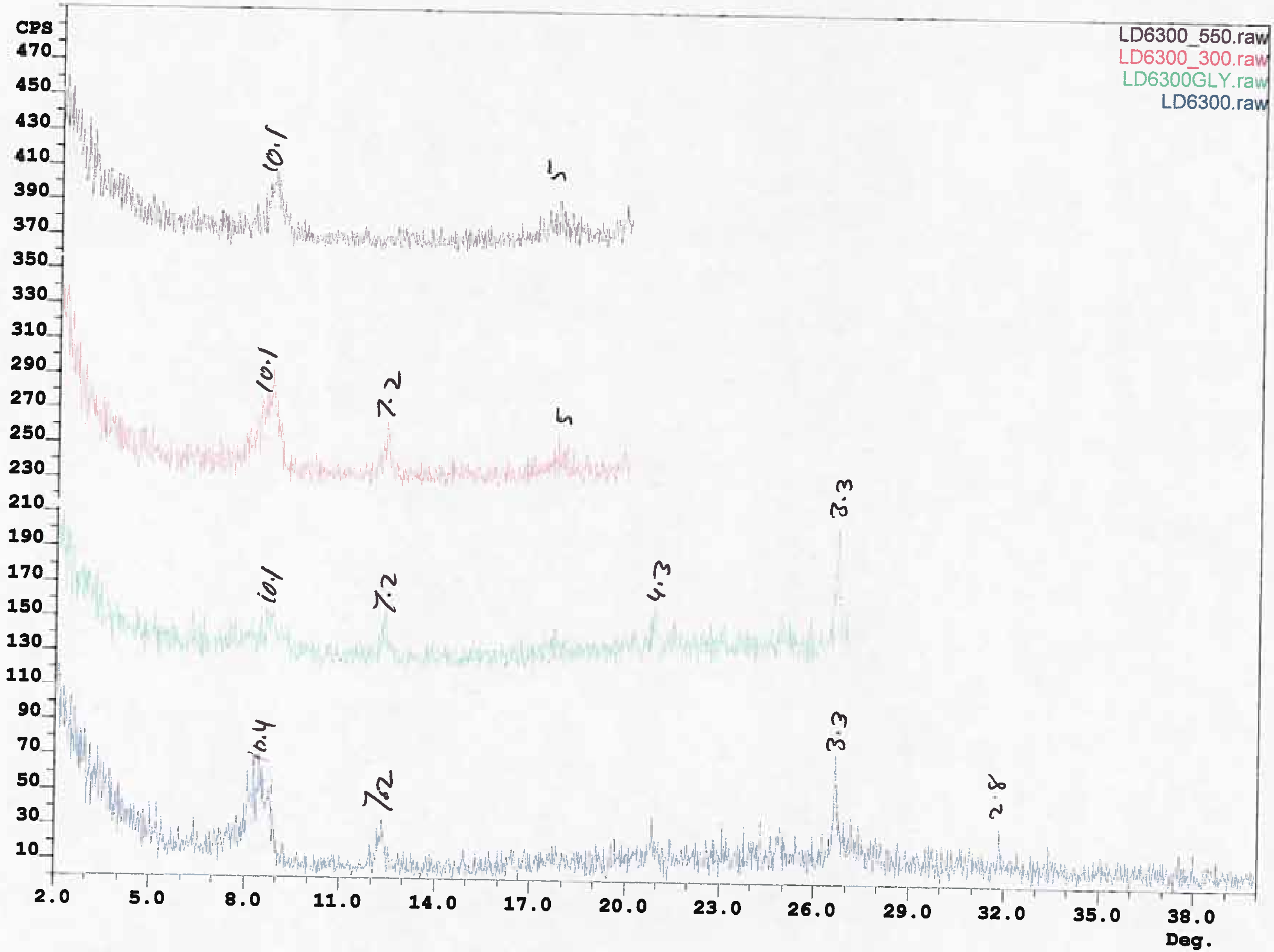
CPS
470
450
430
410
390
370
350
330
310
290
270
250
230
210
190
170
150
130
110
90
70
50
30
10
2.0
5.0
8.0
11.0
14.0
17.0
20.0
23.0
26.0
29.0
32.0
35.0
38.0
Deg.
LD6300_550.raw
LD6300_300.raw
LD6300GLY.raw
LD6300.raw
10.1
5
10.1
7.2
5
10.1
7.2
4.3
3.3
10.4
7.2
3.3
2.8

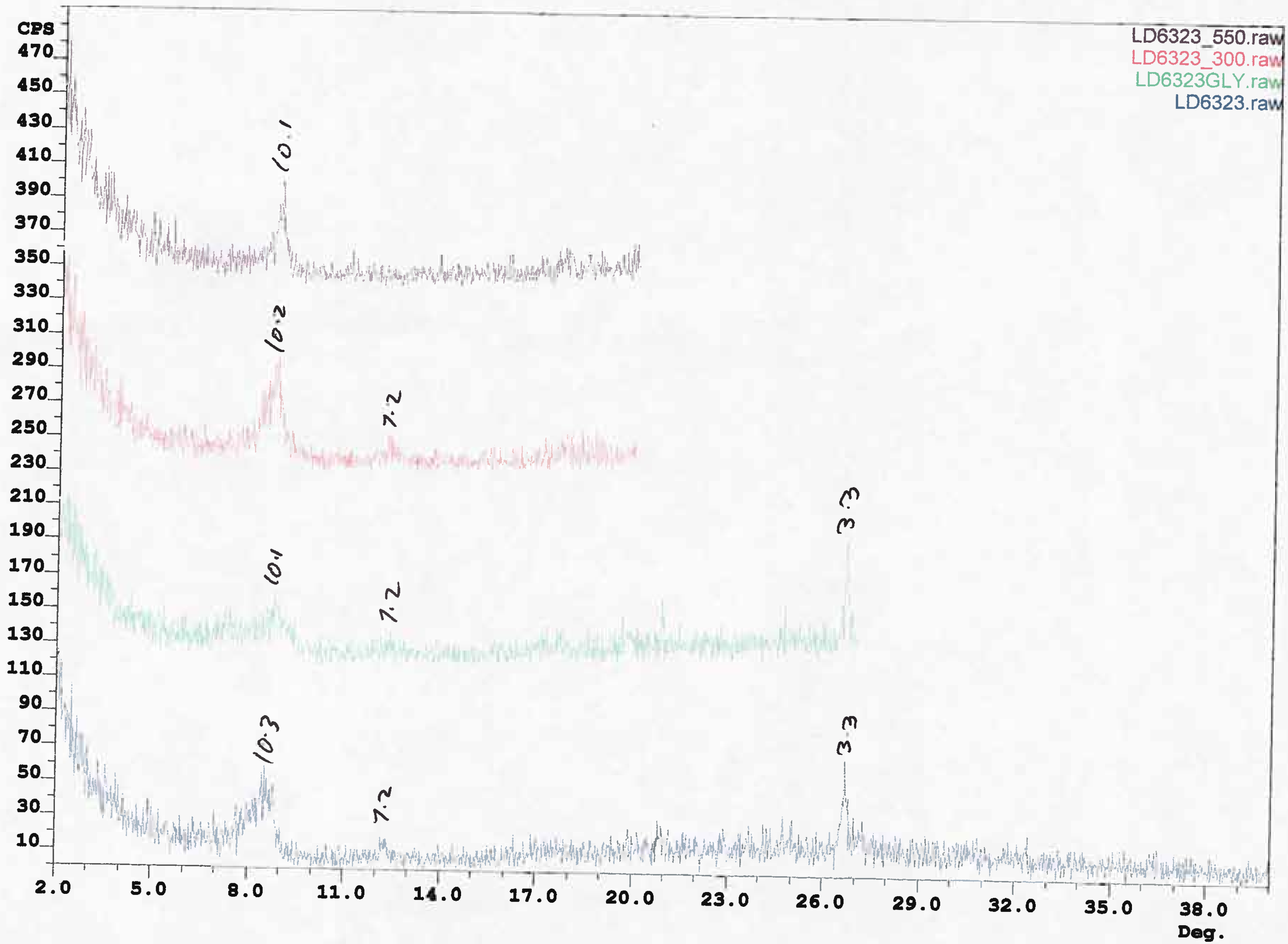

CPS
470
450
430
410
390
370
350
330
310
290
270
250
230
210
190
170
150
130
110
90
70
50
30
10
2.0
5.0
8.0
11.0
14.0
17.0
20.0
23.0
26.0
29.0
32.0
35.0
38.0
Deg.
LD6323_550.raw
LD6323_300.raw
LD6323GLY.raw
LD6323.raw
10.1
10.2
7.2
3.3
10.1
7.2
10.3
3.3
7.2

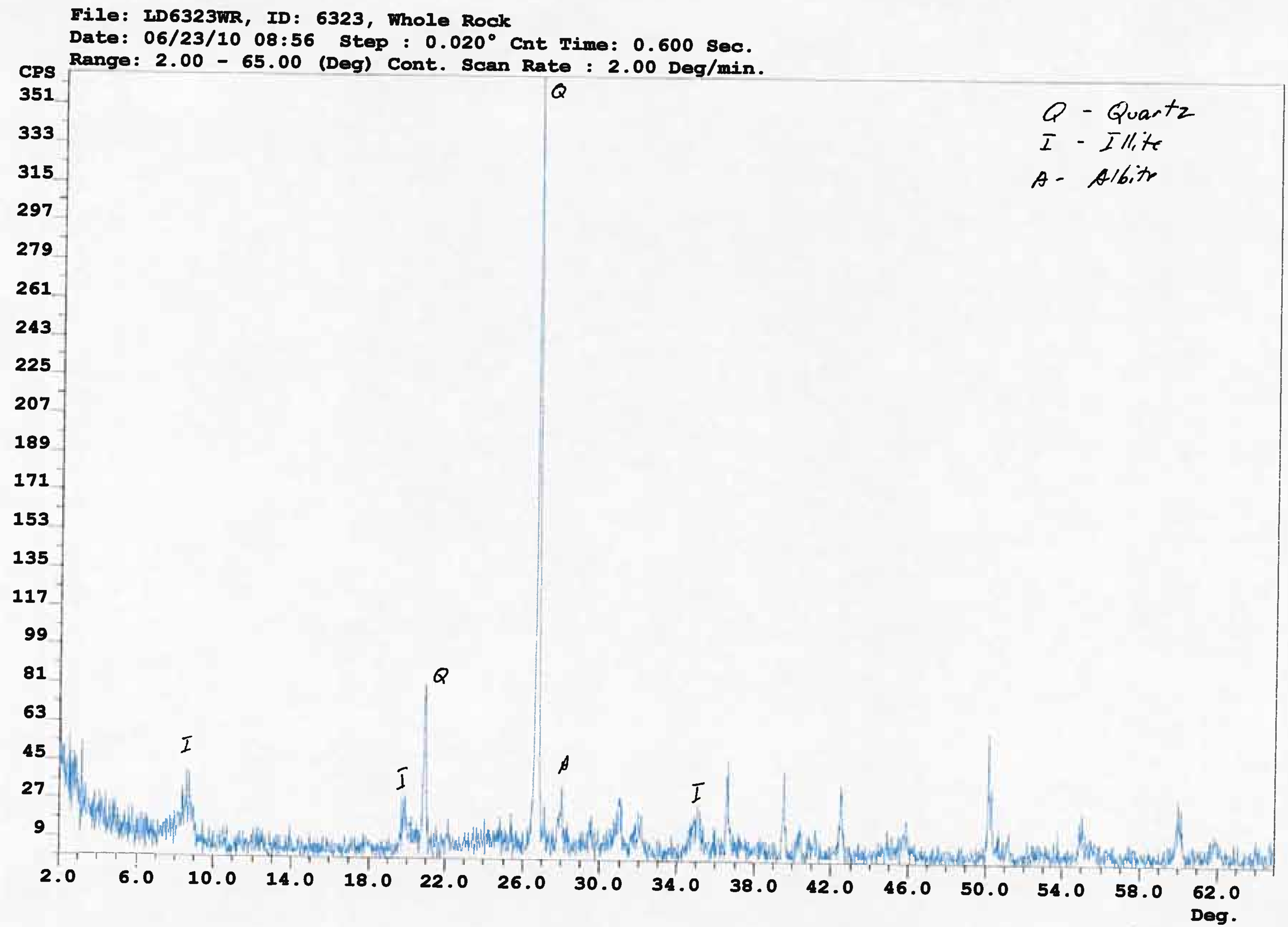
File: LD6323WR, ID: 6323, Whole Rock
Date: 06/23/10 08:56 Step : 0.020° Cnt Time: 0.600 Sec.
Range: 2.00 - 65.00 (Deg) Cont. Scan Rate : 2.00 Deg/min.
CPS
351
333
315
297
279
261
243
225
207
189
171
153
135
117
99
81
63
45
27
9
2.0
6.0
10.0
14.0
18.0
22.0
26.0
30.0
34.0
38.0
42.0
46.0
50.0
54.0
58.0
62.0
Deg.
Q - Quartz
I - Illite
A - Albite
Q
Q
I
I
A
I

277

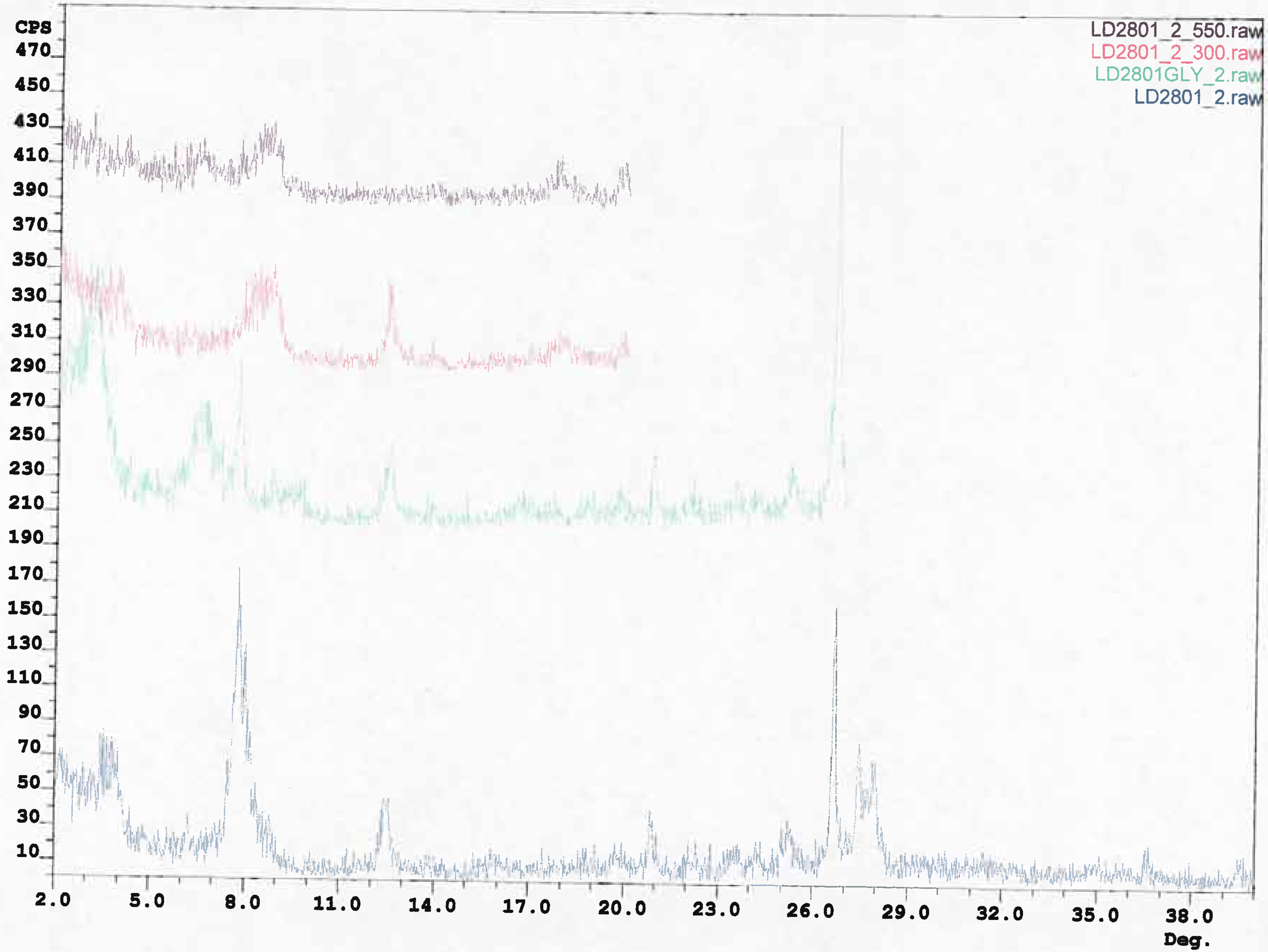

CPS
470
450
430
410
390
370
350
330
310
290
270
250
230
210
190
170
150
130
110
90
70
50
30
10
2.0
5.0
8.0
11.0
14.0
17.0
20.0
23.0
26.0
29.0
32.0
35.0
38.0
Deg.
LD2801_2_550.raw
LD2801_2_300.raw
LD2801GLY_2.raw
LD2801_2.raw